UNIVERSIDAD COMPLUTENSE DE MADRID

FACULTAD DE FARMACIA

TESIS DOCTORAL

Papel de C3G en la diseminación, tumorigénesis y señalización celular del glioblastoma // Role of C3G in glioblastoma dissemination, tumourigenesis and cell signalling

MEMORIA PARA OPTAR AL GRADO DE DOCTOR

PRESENTADA POR

Sara Manzano Figueroa

DIRECTORES

María Almudena Porras Gallo
Álvaro Gutiérrez-Uzquiza

UNIVERSIDAD COMPLUTENSE DE MADRID

FACULTAD DE FARMACIA

TESIS DOCTORAL

Papel de C3G en la diseminación, tumorigénesis y señalización celular del glioblastoma // Role of C3G in glioblastoma dissemination, tumourigenesis and cell signalling

MEMORIA PARA OPTAR AL GRADO DE DOCTOR

PRESENTADA POR

SARA MANZANO FIGUEROA

DIRECTOR

MARÍA ALMUDENA PORRAS GALLO

ÁLVARO GUTIÉRREZ-UZQUIZA

UNIVERSIDAD COMPLUTENSE DE MADRID

FACULTAD DE FARMACIA

DEPARTAMENTO DE BIOQUÍMICA Y BIOLOGÍA MOLECULAR

El presente trabajo ha sido realizado en el Departamento de Bioquímica y Biología Molecular de la Facultad de Farmacia de la Universidad Complutense de Madrid, bajo la dirección de la **Dra. María Almudena Porras Gallo** y el **Dr. Álvaro Gutiérrez Uzquiza**.

Este trabajo ha sido posible gracias a la financiación del Ministerio de Educación, Cultura y Deporte del Gobierno de España mediante la concesión de un contrato pre-doctoral FPU de la convocatoria de 2015 para realizar la Tesis Doctoral. Asimismo, el trabajo ha sido financiado a través de proyectos del Ministerio de Ciencia e Innovación del Gobierno de España (SAF2016-76588-C2-1-R y PID2019-104143RB-C22). Además, la estancia breve de más de 3 meses en el laboratorio dirigido por el Dr. Ignacio Rubio (Jena, Alemania) ha sido posible gracias a una Beca Erasmus^{+} de la Comisión Europea otorgada por la Universidad Complutense de Madrid.

OPTA AL GRADO DE DOCTOR CON MENCIÓN INTERNACIONAL:

Sara Manzano Figueroa

Acknowledgements/Agradecimientos

En primer lugar, un gracias muy especial a **Almudena** por su dedicación, su paciencia y su cercanía. Gracias por valorar mi entusiasmo desde el primer día y ayudarme a dejar a un lado los miedos. Gracias por enseñarme a ver la señalización celular a través de tus ojos y por mantener la puerta de tu despacho siempre abierta para mí. Por cada consejo y por no cansarte nunca de resumir mis infinitos textos.

Gracias también a **Álvaro** por valorarme tanto, por escucharme y por tener siempre claro el siguiente paso del camino. Voy a echar de menos tus infinitas llamadas por teléfono, al igual que tus despistes. Quiero que sepas que es un orgullo para mí salir de esta aventura habiendo aprendido tanto, sobre todo de biología molecular, de uno de los mejores investigadores que conozco (aunque haya quedado comprobado que trabajando junt@s tenemos toda la mala suerte del mundo).

Y, por supuesto, el tercer ‘‘gracias’’ tiene que ser para ti, **Paloma**. Gracias por los abrazos (que se han convertido en caricias en las manos en tiempos del coronavirus) en los momentos más difíciles. Gracias por haberme escuchado sin prisas y por tu manera tan resolutiva de afrontar los problemas. Eres la flipada con más energía de ese laboratorio, y, de verdad, ojalá nunca pierdas toda esa pasión por la ciencia.

Gracias también al resto de mi laboratorio, a quienes estuvieron al principio de los tiempos (*a María, Neibla y Celia por enseñarnos tantas cosas; a Isa porque hacer el TFG juntas fue una suerte enorme; a José Luis y Roberta por las risas*) y a quienes han ido viniendo después (*Cris Baquero, Cris Cruz, Fernando, Nerea, Elena, Óscar, Cristian, Sara, Adrián, Toni, Raúl, María, Claudia…*). Gracias a **Óscar**, mi coautor favorito, por el ‘Equipo GBM’. Por estar ahí en lo bueno y en lo malo, por ser la mar de agradable, por los abrazos, por valorarme, por no ponerse (ponernos) límites y por esos debates sin fin que tanta vida me han dado. Eres un gran científico, y un amigo todavía mejor. Ya sabes, como le dijo Stanley Cohen a Rita Levi Montalcini ‘*You and I are good, but together we are wonderful*’. Aprovecho para dar las gracias al grupo de **Carmen Guerrero y Chema**, con quienes siempre compartimos lo bueno y lo menos bueno de esta ‘‘maravillosa’’ proteína llamada C3G. Y también un ‘‘gracias’’ especial a mi bioinformática de referencia, **María R.**, porque no podría haber tenido una compañera mejor para estos últimos meses. Gracias por tu bondad, tus ganas de aprender y tu amistad. Eres una gran científica, así que créetelo y sal a comerte el mundo **gif de la niña musculosa**.

Además, quiero dar las gracias a nuestras vecinas del **laboratorio Hígado**, porque gracias a ellas nunca nos ha faltado ni una placa de cultivos, ni una multicanal, ni unas risas. Gracias a Arancha, Blanca, César y Marga; a María y Annalisa; a Laura, Nerea y Sara Baak; a Carlos y Carlos Jr; y, por supuesto, a los

innumerables alumn@s que han pasado por allí y nos han hecho la vida más amena. También aprovecho para agradecer su cariño al resto de la gente de la sección de Farmacia. Es imposible nombraros a tod@s, pero gracias tanto a l@s predocs, por compartir lamentos conmigo, como a l@s postdocs/IPs, por ser grandes referentes. Gracias, **Bea Chamorro**, por el ánimo y las risas, los desahogo en los ratos de saturación y los impulsos para mis señales de *western*. Muchas gracias, de verdad, a **Toñi, Mercedes, Paloma y Mariola**, por vuestro trabajo y vuestra cercanía. Hacer ciencia sería todavía más difícil sin vosotras.

Muchísimas gracias a **Isra V.** (y al resto del grupo de Guillermo Velasco, por compartir su conocimiento y sus células conmigo), a **Anaís** (por hacerme un huequito en su vida y por su ayuda en esos primeros CAMs) y a **Bea Linillos** (por volver después de tantos años con más fuerza que nunca; por entenderme, por transmitirme su luz y por intentar enseñarme que en esta vida la clave es ocuparse sin preocuparse).

Of course, I would like to thank all my friends from Jena (Germany), where I spent three amazing months. Especially thanks to **Ignacio, Steph and Iqra** for their attention, their help and their company during all that time. Thanks for keeping in touch with me these years by email and even postcard! I'm looking forward to working with you again in the future. Additionally, I would like to thank everybody who worked with me there: Joel, Franzi, Sharmila, Petra, Jorge, Friederika, Lea, Wanling, Jessi, Tobi, Elisa, Adrian, Michu, Max, Julia… We spent really nice moments together and I wish you all the best in your life! Gracias a **Manuela, Paula, Roxana, Chris y Pau**, entre muchas otras personas, por los bailes, los intercambios culturales, por Praga y por los kebabs. Sharing the apartment with Nadine was a great gift to me (as well as with Fernanda, Sahil, Felipe and Mona). **Nadine**, your enthusiasm, your vitality and your generosity were essential to me those months. I have never met a more open-minded person and I really miss our ''wine moments'' after dinner, chatting about life, science and travelling.

Fuera del mundo científico, quiero darle las gracias a **Álvaro A.** por ser mi mejor decisión del 2019 y por su forma de hablarme, tan directa, cercana y profesional. Gracias por vivir mi tesis desde la silla de enfrente, en esa sala que has convertido en un lugar seguro donde soltar carga y observar desde otros ángulos.

¿Y qué habría sido de mí estos años sin mi **Club de Lectura**? Muchísimas gracias a Blanca, Carmen, Amaya, Clara, Alexia, Arantza, Vanessa, Melina,… A todas las que fueron y a todas las que somos. Gracias por abrirme la mente y ayudarme siempre a pensar un poquito más allá. Sororidad como arma, y que la revolución nos pille leyendo.

Nunca estaré lo suficientemente agradecida a la bioquímica por cruzarme en la vida con *las bioqs*, junto a quienes llevo ya muchos años disfrutando, creciendo y viajando. Sois un seguro de risas, sueños cumplidos e historias exageradas al 200%. '*After all this time?*', '*Always*'. Que el mundo se nos siga quedando pequeño y los bares de Madrid insuficientes. Gracias a **Lara** por alegrarme los días grises a base de comidas juntas en la Facultad; por tu fuerza y determinación, y por no dejar nunca de bailar conmigo. Gracias a **Clara** por desprender tanta alegría vital y por no fallarnos nunca. Pero sobre todo gracias por haber estado siempre a un mensaje de distancia, incluso cuando estabas por ahí recorriendo el mundo. Y por volver todas las veces sin que nada hubiese cambiado entre nosotras. Gracias a **Alberto** por repensarse manteniéndonos a su lado, por vivir nuestras tesis como si fueran suyas, por escucharnos en silencio o a carcajadas, y por seguir nuestras locuras sin dudar.

¿*Y ahora qué les digo a las dos personas que al principio de esto decidieron aventurarse a sufrir conmigo el día a día del doctorado*? A Irene y a Cris quiero darles las gracias, de todo corazón, por haberme aguantado cuando no lo hacía ni yo y por hacer que la rutina valiese la pena cuando todo era tan complicado. Ay, si ese pasillo hablase… Gracias por recogerme cada vez que me caía (incluso literalmente, que algunas películas no están hechas para todos los públicos) y por los aperitivos, las cenas especiales, los bollitos y los bailes durante la cuarentena. **Irene**, gracias por tu apoyo incondicional, por tu fuerza, por tus cabezonerías (sólo algunas) y por intentar enseñarme a decir ''no''. Gracias por espantarme a l@s *monstruos de debajo de la cama* y por *hacerme grande cada vez que te tenía delante*. Ojalá el futuro nos disipe *las dudas infinitas* y nos dejemos llevar, que dicen que *suena demasiado bien*. Y aunque es posible que *ahora seamos peores* (versión mambo), espero que nos sirva para no volver a perder nuestra *pequeña sonrisa de Amelie*. **Cris**, muchísimas gracias a ti también, *wapa*. Mi chica de los pequeños gestos y las grandes gestas. Gracias por escucharme y por amenizarme la vida con tus canciones; por el gimnasio, los memes, las reflexiones en voz alta, los debates y las competiciones por decir la burrada más grande. Gracias por sentarte a mi lado aquel día de nervios infinitos, pero sobre todo por no dejar de cuidarme desde entonces. Eres una persona maravillosa, que no se te olvide, y ojalá sigas siempre manteniendo tus ganas de aprender. Moreover, thanks **Rick** for all your *'¿Qué pasa, tronca?'*. Our Pisito has always been glad to receive you and I'm sure that we will enjoy lots of *pintxos* in Bilbao and stroopwafels in The Netherlands together!!

Gracias, **Mon**, por conseguir siempre que me llegasen desde el otro lado del océano tanto tus ánimos como tu confianza en mí. *Amiga linda*, nos quedan muchos tacos y aguas de Jamaica por compartir todavía.

Altor, me encantaría poder explicar aquí todo lo que significas para mí y todo lo que has hecho por esta tesis, pero hay cosas que están por encima de las palabras.

Has sido un apoyo y ancla continuos (sí, ancla). Me has enseñado el valor de los viajes en Alsa y, sobre todo, has abrazado a mis fantasmas como nadie. Gracias por convertirme en una '*epic gamer*' y por acompañarme en mis sueños por el mundo. Gracias por tu naturalidad y tu capacidad de reírte de la vida (y de mí), por nunca darte por vencido, por pararte a conocer mis complejidades y por enseñarme que los problemas se solucionan mejor en compañía. Gracias por creer en los imposibles, aunque los kilómetros y las dudas dijesen lo contrario. Eres coautor de todo esto por derecho propio, por adaptarte con infinita paciencia a mis interminables jornadas de trabajo. Ten claro que es mejor trabajar a tu lado en el suelo, que en el mejor de los sillones lejos de ti. Por seguir quemando el mar juntas a fuego lento, entre perreos y animús. Como siempre, ggwp <3! (*PD: ¿te lo imaginabas así?*)

También quiero darle las gracias a mi segunda familia: **M. Luisa, Tatiana, Javi, Antonio, Betty, Saúl, Luisa, Antonia…** Gracias por todas las palabras y mensajes de ánimo durante este tiempo. Aunque no os lo suela decir, siempre he sabido que puedo contar con vosotr@s y vuestro apoyo ha sido muy importante estos años.

Los fines de semana en el Norte siempre han sido mis favoritos y en Bilbao he conocido a gente genial: Soraya, Jon, Humberto, Eva, Aitziber, Carlos, Leire,… Gracias por cuidar tanto de Aitor y por recibirme siempre con ese cariño incondicional. **Soraya**, gracias por las charletas infinitas en casa. Eres maravillosa y estoy segura de que podré contar contigo siempre que lo necesite. **Humberto y Eva**, gracias por todos los ratos y penas compartidas, sin olvidarnos de las caídas dignas en el Sella. Sois geniales y os merecéis todo lo bueno en esta vida.

Last but not least, un gracias infinito a otro de mis apoyos constantes: mi familia. A **Sergio y Carmen**, gracias por enseñarme que la realidad se encuentra más allá de los muros de nuestros privilegios y por hacer que los debates sean eternos si empiezan alrededor de nuestra mesa del salón. Sergio (mi tate!), no olvides que para mí siempre serás un referente, aunque tomemos caminos distintos. Carmen, gracias, de corazón, por tus cuidados, tu comprensión y tu apoyo. A **Francis y Paloma**, gracias por mirarme siempre con los mismos ojos llenos de orgullo y por quererme incondicionalmente. Por apoyarme en mis decisiones, por aguantar mis nervios, y por ayudarme a afrontar la vida a base de esa alegría infinita tan vuestra. Por entender que necesito espacio pero también cariños; por educarme en igualdad y por no dejar de ponerme libros a mi alcance desde muy pequeña. Por las tardes de chicas, las llamadas infinitas y los mensajes de ánimo al despertar. Gracias por ver una y otra vez las fotos antiguas conmigo, por dejaros ganar al *Rummikub* y por seguirme en los planes más imposibles. Sin todos los ratos preguntándome la lección, nada de esto se habría hecho realidad. Así que espero que tantas siestas al son de la biología hayan valido la pena. Sois geniales en todos los aspectos y nunca me voy a cansar de repetíroslo. Qué suerte tengo con vosotr@s.

Index

Abstract/Resumen

Role of C3G in glioblastoma dissemination, tumourigenesis and cell signalling

Introduction

GBMs (*glioblastomas*), or grade IV astrocytomas/gliomas, are the most frequent and aggressive brain tumours, whose diagnosis and treatment is still inefficient. RTKs (*receptor tyrosine-kinases*), mainly EGFR, and their downstream pathways are altered in almost 90% GBMs. RTKs, are relevant for the regulation of GBM tumourigenesis and dissemination and for GSCs (*GBM stem cells*), a GBM subpopulation that display stem-like and GBM-initiating properties. Dissemination is also linked to GBM aggressiveness. EMT (*epithelial-mesenchymal transition*)-like processes would facilitate the acquisition of a more mesenchymal and invasive phenotype. Both, stemness and disseminative capacity have been associated to GBM recurrence and therapy resistance.

C3G, encoded by *RAPGEF1* gene, is a GEF (*guanine-exchange factor*) for small GTPases, mainly Rap1. It participates in diverse signalling hubs through GEF-dependent and -independent mechanisms. Consequently, C3G plays diverse functions during the embryonic development and in adult cells, such as regulation of death/survival balance, cytoskeleton organization, adhesion and migration. In cancer, C3G plays a different role depending on tumour stage and cell context. For example, C3G is upregulated in primary HCCs (*hepatocellular carcinomas*), promoting proliferation, while its downregulation increases metastasis initiation. C3G is highly expressed in brain and it regulates neural precursors' proliferation, migration and differentiation. However, almost nothing is known about the role played by C3G in GBM.

Aims

The main objective of this research project is to analyse the role played by C3G in GBM dissemination and tumourigenesis, identifying the mechanisms involved and the crosstalk between C3G and different cell signalling pathways.

To achieve this, we propose three specific aims:

- To determine whether C3G expression is altered in GBM tumours from patients and human GBM cell lines compared to healthy brain, as well as to identify if C3G levels correlate with GBM molecular subtypes or aggressiveness markers.
- To analyse the function of C3G in GBM cells by *in vitro* and *in vivo* approaches, characterizing its role in the regulation of adhesion,

migration/invasion, tumourigenesis, GSC-like phenotype and glucose metabolism.

- To identify the molecular mechanisms involved in the actions of C3G in GBM and the interplay between C3G and cell signalling pathways associated to GBM progression.

Results

First, we found that *RAPGEF1* mRNA levels in patients' GBM samples and C3G protein levels in human GBM cell lines were downregulated as compared to their corresponding healthy controls. Second, using U87 cell line and two patient-derived cell lines (12Φ12D and HCO1D), we downregulated C3G levels by gene silencing. Additionally, C3G was depleted by CRISPR/Cas9 technology and transiently overexpressed C3G. We detected that C3G down-regulation enhanced migration/invasion of GBM cells (U87, 12Φ12D and HCO1D) using transwells and wound healing assays. As determined by western blot, gelatin zymography and RT-qPCR, this was accompanied by upregulation of mesenchymal markers such as Vimentin, MMP2 activity and *TWIST1* and *ZEB2* mRNA levels. Importantly, C3G overexpression decreased invasion and promoted adhesion. C3G-induced adhesion was independent of its GEF-activity, while inhibition of invasion depends on C3G GEF activity, as revealed by overexpressing a C3G mutant lacking CDC25H domain or Rap1A-wt/V12 proteins. Moreover, C3G-silenced GBM cells generated more foci in *in vitro* anchorage-dependent and independent growth assays (except in HCO1D cells) and larger tumours in *in vivo* xenograft and CAM assays, even though proliferation was decreased. Tumours originated by C3G-silenced cells in CAM assays presented higher levels of α-SMA and MECA32, pointing to an enrichment in stroma and blood vessels. C3G downregulation also favours the acquisition of stemness properties and an anaerobic glycolytic metabolism.

We also found that p38α/β MAPK inhibition decreases invasiveness and promotes adhesion in GBM through C3G-independent mechanisms. Moreover, C3G silencing promotes ERKs hyperactivation, whose inhibition decreased C3G knock-down-induced invasiveness and foci formation capacity. On the other hand, C3G silencing reduces EGFR signalling and functional effects (on invasion) by decreasing cell surface EGFR (detected by flow cytometry) through inhibition of recycling, as demonstrated by monensin treatment. According to results from an anti-phospho-RTKs array, C3G downregulation also regulate the activation of multiple RTKs, upregulating the phosphorylation of several RTKs, highlighting FGFR1. FGF-2, likely acting through FGFR1 promotes invasion in C3G-silenced GBM cells through ERKs hyperactivation.

Conclusions

1. *RAPGEF1* mRNA levels are decreased in patient GBM samples compared to healthy brain. Similarly, C3G protein levels are reduced in GBM cell lines compared to astrocytes.
2. C3G silencing reduces adhesion, while enhances migration and invasion of U87, 12Φ12D and HCO1D cells, by promoting the acquisition of a pro-mesenchymal phenotype. C3G depletion in U87 cells using CRISPR/Cas9 technology induces a pro-migratory phenotype, mimicking the effect observed by gene silencing.
3. Transient overexpression of C3G favours adhesion and decreases invasion. Its effect on invasiveness is dependent on C3G GEF catalytic domain, CDC25H.
4. Overexpression of a constitutively active Rap1AV12 mutant decreases C3G knock-down-induced invasion.
5. In U87 and 12Φ12D GBM cells, C3G silencing promotes *in vitro* foci formation and the generation of larger tumours in *in vivo* heterotopic xenografts and *in ovo* CAM inoculation assays with less cell density and proliferation.
6. In HCO1D GBM cells, C3G knock-down decreases foci formation and reduces cell density, generating multiple scattered cells and very small colonies
7. p38α/β MAPK inhibition with SB203580 promotes adhesion and inhibits invasion through a mechanism not dependent on C3G levels.
8. C3G downregulation induces ERKs hyperactivation in U87 and 12Φ12D cells.
9. C3G silencing-associated high motility and foci formation is impaired by ERKs inhibition with PD98059 in GBM cells. In contrast, PD98059 treatment only decreases proliferation in non-silenced cells.
10. C3G knock-down decreases EGFR activation and downstream signalling, as well as EGF-induced invasiveness by impairing EGFR localization at the plasma membrane through inhibition of its recycling. Contrary, C3G downregulation upregulates the activation of FGFR1 and other RTKs.
11. FGF-2, likely acting through FGFR1, promotes invasion via ERKs upregulation.
12. C3G silencing promotes the acquisition of GSC-like properties.
13. C3G knock-down promotes the use of glucose through anaerobic glycolysis by increasing the activity of the last steps of the pathway, including LDH activity and lactate release.

Papel de C3G en la diseminación, tumorigénesis y señalización celular del glioblastoma

Introducción

Los GBMs (*glioblastomas*), o astrocitomas/gliomas de grado IV, son los tumores cerebrales más frecuentes y agresivos, cuyo diagnóstico y tratamiento es ineficaz. Los RTKs (*receptores tirosina-quinasa*), principalmente EGFR, y sus vías de señalización están alteradas en casi el 90% de los GBMs. Los RTKs regulan la tumorigénesis, diseminación, y a las células madre de GBM (GSCs), una subpoblación con capacidad de auto-renovación e iniciación tumoral. La diseminación está asociada a su agresividad. La transición epitelio-mesénquima facilitaría la adquisición de un fenotipo mesenquimal e invasivo. Tanto la capacidad progenitora como invasiva, se asocian a recurrencias y resistencia a terapia.

C3G, proteína codificada por el gen *RAPGEF1*, es un factor activador del intercambio de nucleótidos de guanina (GEF) de proteínas G monoméricas, principalmente, Rap1. Mediante mecanismos dependientes e independientes de su actividad GEF, C3G regula múltiples funciones celulares durante el desarrollo embrionario y en adultos. Por ejemplo, el balance muerte/supervivencia, la organización del citoesqueleto, la adhesión y migración. En cáncer, C3G juega un papel diferente dependiendo del estadio y contexto tumoral. Por ejemplo, en hepatocarcinoma, C3G está sobre-expresado, promoviendo proliferación, mientras que su disminución favorece la metástasis. C3G está sobre-expresado en cerebro, regulando proliferación, migración y diferenciación de precursores neurales. Sin embargo, su papel en GBM es desconocido.

Objetivos

El objetivo principal de este proyecto es analizar el papel de C3G en la diseminación y tumorigénesis del GBM, identificando los mecanismos implicados y las posibles interacciones de C3G con otras vías de señalización.

Para conseguirlo, se plantean tres objetivos específicos:

- Determinar si la expresión de C3G está alterada en tumores de pacientes de GBM y líneas celulares en comparación con cerebro sano, estableciendo si los niveles de C3G se correlacionan con subtipos de GBM o indicadores de agresividad.
- Analizar *in vitro* e *in vivo* la función de C3G en adhesión, migración/invasión, tumorigénesis, fenotipo GSC y metabolismo glucídico en las células de GBM.

- Identificar los mecanismos moleculares implicados en las acciones de C3G en GBM y las vías de señalización asociadas a su progresión.

Resultados

Inicialmente, encontramos una bajada en los niveles de ARNm y proteína C3G en tumores y líneas celulares de GBM, comparando con sus controles sanos. Posteriormente, utilizando la línea celular U87 y dos líneas derivadas de pacientes de GBM (12Φ12D y HCO1D), se disminuyeron los niveles de C3G mediante silenciamiento génico. En células U87, también se usó la tecnología CRISPR/Cas9 para reducir totalmente los niveles de C3G, así como se sobre-expresó C3G transitoriamente. La bajada en los niveles de C3G aumentaba la migración/invasión de las células de glioblastoma utilizando *transwells* y ensayos de cierre de herida. Mediante *western blot*, zimografía y *RT-qPCR* se vio que estos cambios se asociaban al aumento de marcadores mesenquimales (Vimentina), actividad MMP2 y ARNm de *TWIST1* y *ZEB2*. La sobreexpresión de C3G promovió la adhesión y disminuyó la invasión, siendo esto último dependiente de su actividad GEF, como se demuestra al sobreexpresar el mutante de C3G sin dominio CDC25H o Rap1A-wt/V12. Además, las células de GBM con silenciamiento de C3G generaron más focos en ensayos de crecimiento dependiente e independiente de anclaje (excepto en HCO1D) y tumores de mayor tamaño en xenotransplantes e *in ovo*, aunque la proliferación celular disminuía. Estos tumores presentaban más células estromales y vasos sanguíneos, de acuerdo con los niveles de α-SMA y MECA32, respectivamente. Los niveles bajos de C3G favorecían la adquisición de propiedades progenitoras y un metabolismo glucolítico anaerobio.

La inhibición de p38α/β MAPK disminuía la invasividad y aumentaba la adhesividad independientemente de C3G. El silenciamiento de C3G inducía una hiper-activación de las ERKs, cuya inhibición impedía el aumento de invasión y formación de focos. Por otro lado, el silenciamiento de C3G atenuó la señalización del EGFR y sus efectos sobre la invasión, disminuyendo sus niveles en la superficie celular (detectado por citometría) mediante la inhibición de su reciclaje, demostrado mediante tratamiento con monensina. Sin embargo, según los resultados de un *array* anti-fosfo-RTKs, el silenciamiento de C3G también regulaba la activación de otros RTKs, incrementado la fosforilación de varios RTKs como FGFR1. El FGF-2 probablemente vía FGFR1 promovía la invasión a través de la hiper-activación de las ERKs.

Conclusiones

1. Los niveles del ARNm de *RAPGEF1* están disminuidos en muestras de GBM de pacientes comparado con cerebro sano, así como los niveles proteicos de C3G en líneas celulares de GBM en comparación con astrocitos.

2. El silenciamiento de C3G reduce la adhesión y aumenta la migración/invasión de células U87, 12Φ12D y HCO1D, promoviendo la adquisición de un fenotipo pro-mesenquimal. La pérdida de C3G en células U87 usando tecnología CRISPR/Cas9 induce un fenotipo pro-migratorio, semejante al inducido por silenciamiento.
3. La sobreexpresión transitoria de C3G promueve adhesión y disminuye la invasión, siendo esto último dependiente de su actividad GEF.
4. La sobreexpresión del mutante Rap1AV12, constitutivamente activo, disminuye la invasión inducida por el silenciamiento de C3G.
5. El silenciamiento de C3G en células U87 y 12Φ12D promueve la formación de focos y genera tumores de mayor tamaño en xenotransplantes y ensayos de inoculación *in ovo,* teniendo dichos tumores una menor densidad celular y proliferación.
6. En las células HCO1D, el silenciamiento de C3G disminuye la formación de focos, generando células dispersas y colonias pequeñas.
7. La inhibición de p38α/β MAPK con SB203580 promueve adhesión e inhibe la invasión, independientemente de C3G.
8. El silenciamiento de C3G induce una hiper-activación de ERKs en células U87 y 12Φ12D.
9. La alta capacidad de invadir y formar focos de células con silenciamiento de C3G se impide al inhibir las ERKs con PD98059. Sin embargo, el PD98059 sólo disminuye la proliferación de células no silenciadas.
10. El silenciamiento de C3G disminuye la activación y señalización de EGFR, así como la invasión inducida por EGF, impidiendo la localización de EGFR en la membrana plasmática mediante la inhibición de su reciclaje. Por el contrario, otros RTKs se sobreactivan.
11. El FGF-2, probablemente vía FGFR1, promueve la invasión incrementando la -activación de ERKs.
12. El silenciamiento de C3G promueve la adquisición de propiedades de tipo GSC.
13. El silenciamiento de C3G promueve el uso de glucosa mediante glucolisis anaerobia, incrementando la actividad de sus últimas etapas, incluyendo la actividad de LDH y liberación de lactato.

Abbreviations

12Φ12D	12Φ12 patient-derived cells with differentiated phenotype
2-HG	2-hydroxyglutarate
293T	HEK (*human embryonic kidney*) 293T cells
α-KG	α-ketoglutarate
α-SMA	α-Smooth muscle actin
ADAM(T)	A desintegrin and metalloproteinase (with thrombospondin motifs)
AIR	Autoinhibitory region
ALDO	Aldolase
ANLS	Astrocyte to neuron lactate shuttle
ATCC	American Type Culture Collection (*cell line repository*)
ATP	Adenosine tri-phosphate
BBB	Blood-brain barrier
BCA	Bicinchoninic acid (*protein quantification method*)
BSA	Bovine serum albumin
C3G	Crk SH3-domain-binding guanine-nucleotide-releasing factor
C3G-ΔCat	C3G mutant lacking CDC25H domain
C3G-FL	C3G full-length
CAM	Chicken chorioallantoic membrane cell inoculation assay
Cas9$^+$-NTC	Cas9$^+$ non-targeting lentiguide-puro cells
CBR	CDC25H binding region
CDC25H	CDC25 homology
CIE	Clathrin independent endocytosis
CME	Clathrin-mediated endocytosis
CML	Chronic myeloid leukaemia
CNB	Cyclic nucleotide binding domains
CNS	Central nervous system
CoA	Coenzyme A
CSCs	Cancer stem cells
CST	Cell Signalling Technology (*commercial trademark*)
C-terminal	Carboxi-terminal end (*protein structure*)
Ct	Cycle threshold
CTCs	Circulating tumour cells
DAG	Diacilglicerol
DAPI	4′,6-diamidino-2-phenylindole
DMEM	Dulbecco's modified Eagles Medium
DTCs	Disseminated tumour cells
EA	Enzymatic activity
ECM	Extracellular matrix
e.g.	*For example*
EGF(R)	Epidermal growth factor (receptor)
eIF3b	Eukaryotic translation initiation factor 3b
ELDA	Extreme limiting dilution assays
EMT	Epithelial to mesenchymal transition
ENM	Extra-neural metastasis
ENO	Enolase
ENU	Ethyl-nitrosourea
ERK	Extracellular signal-regulated kinases
EV	Empty vector
F-actin	Filamentous actin
FAD	Flavin adenine dinucleotide
FAK	Focal adhesion kinase

FBS	Fetal bovine serum
FBPase	Fructose-1,6-biphosphatase
FGF(R)	Fibroblast growth factor (receptor)
FH	Fumarate hydratase or fumarase
G6PDH	Glucose-6-phosphate dehydrogenase
GAP	GTPase-activating protein
GAPDH	Glyceraldehyde-3-phosphate dehydrogenase
GBM	Glioblastoma
gDNA	Genomic DNA
GEF	Guanine-nucleotide exchange factor
GF	Growth factor
GFAP	Glial fibrillary acidic protein
GIC	Glioblastoma initiating cell
GLS	Glutaminase
GLUD	Glutamate dehydrogenase
GLUT	Glucose transporter
GO	Gene ontology
GS	Glutamine synthase
GSC	Glioblastoma stem cell
HAs	Human Astrocytes
hC3G	Human C3G
HCC	Hepatocellular carcinoma
HCO1D	HCO1 patient-derived cells with differentiated phenotype
HDR	Homology-Directed Repair
HIF	Hypoxia-inducible factor
HK	Hexokinase
HRP	Horseradish peroxidase
IDH	Isocitrate dehydrogenase
IGF(R)	Insulin-like growth factor (receptor)
IL	Interleukin
InsR	Insulin receptor
IT	Inhibitory region
JNK	Jun N-terminal kinase
KO	Knock-out
LDH	Lactate dehydrogenase
LG	pLentiGuide-puro
LIF	Leukaemia-inhibitory factor
MAPK	Mitogen-activated protein kinase
MAPKK	MAPK kinase
MAPKKK	MAPKK kinase
MCS	Multi-cloning site
MCT	Monocarboxylate transporter
MDK	Midkine
MEF	Mouse embryonic fibroblasts
MET	Mesenchymal to epithelial transition
HGF	Hepatic growth factor
MGMT	O^6-methylguanine methyltransferase
miRNA	micro-RNA
MLC(K)	Myosin-light chain (kinase)
MMP	Matrix metalloproteinase
MOI	Multiplicity of infection

MTB transition	Multi-to-bipolar transition
Mw	Molecular weight
NBDG	2-(N-(7-nitrobenz-2-oxa-1,3-diazol-4-yl)amino)-2-deoxyglucose
NGS	Normal goat serum
NHEJ	Non-homologous DNA end joining
NOS	Not otherwise specified (*glioblastoma classification context*)
ns	Statistically not significant *p* value
NCS	Neural stem cell
NTC	Non-targeting control
N-terminal	Amino-terminal end (*protein structure*)
O.D.	Optic density
PBS	Dulbecco's phosphate buffered saline solution
PCR	Polymerase chain reaction
PDCs	Patient-derived cells
PDGF(R)	Platelet-derived growth factor (receptor)
PDH complex	Pyruvate dehydrogenase complex
PDK	Pyruvate dehydrogenase complex kinase
PDX	Patient-derived xenograft
PEI	Poly-ethyl-enimine
PEP	Phospho-enol pyruvate
PFA	Paraformaldehyde
PFK	Phosphofructokinase
PI3K	Phosphatidylinositol 3 kinase
PK	Pyruvate kinase
PNS	Peripheral nervous system
pRb	Protein of retinoblastoma
PMSF	Phenylmethylsulfonyl fluoride
PPP	Pentose-phosphate pathway
Rap	Ras-related protein
ROCK	Rho-associated serine/threonine kinase
ROS	Reactive oxygen species
RSEM	RNA-Seq by Expectation Maximization
RTK	Receptor tyrosine kinase
RQ	Relative quantity
SCB	Santa Cruz Biotechnology (*commercial trademark*)
SDH	Succinate dehydrogenase
sgRNA	Single guide RNA
SH2 domain	Src Homology 2 domain
SH3 domain	Src Homology 3 domain
shC3G	Short-hairpin RNA (shRNA) stable C3G-silenced cells
shNTC	Short-hairpin RNA (shRNA) NTC cells
SNP	Single nucleotide polymorphism
TCA	Tricarboxylix acid cycle (or Krebs' cycle)
TCGA	The Cancer Genome Atlas program
TGF-β(R)	Transforming growth factor-β (receptor)
TIMP	Tissue inhibitor of metalloproteinase
TMZ	Temozolomide
TTBS	Tween Tris-buffered saline solution
TyrK	Tyrosine kinase
U87	U87-MG cell line
V12	Rap1A mutant, constitutively active

VEGF(R)	Vascular endothelial growth factor (receptor)
vs.	*Versus*
WHO	World Health Organization
wt	Wildtype

Introduction

1. Cancer, central nervous system and glioblastoma

Cancer is nowadays understood as a generic term that includes a large group of genetic diseases characterized by the abnormal growth of cells beyond their usual boundaries with potential ability to disseminate through their adjoining tissues and/or spread to other organs (metastasis) (*WHO webpage*, 2020). Tumourigenesis in humans is considered a multistep process with progressive genetic and non-genetic (e.g. epigenetic) alterations that drive the gradual transformation of normal human cells into highly malignant derivatives with certain growth and disseminative advantages (Hanahan & Weinberg, 2000) (Hanahan & Weinberg, 2011).

Worldwide, all cancer-related diseases were responsible for more than 17 million new diagnoses and almost 10 million deaths in 2018 (*WHO) webpage*, 2020) (*World Cancer Research Fund webpage*, 2020) (*Figure I*). In general, men have higher cancer incidence and worse long-term prognosis. Lung cancer has the highest incidence index in men (15.5% of new diagnoses with around 1 million deaths in both genders/sexes in 2018), followed by prostate cancer (14.5% of new cases). In women, breast cancer presents the highest incidence (25.4% of new diagnoses), although its mortality has decreased in recent years. Unfortunately, all this is conditioned by health systems quality and country incomes (*World Cancer Research Fund webpage*, 2020).

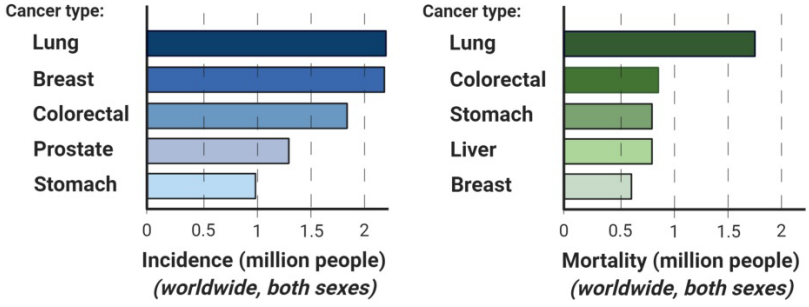

Figure I – **Cancer incidence and mortality worldwide (2019).** Data extracted from *WHO webpage* (2020) and *World Cancer Research Fund webpage* (2020).

Inherited genetic alterations as well as environmental factors and mutagens (e.g. radiation, chemicals and viruses) promote cancer onset and development through multi-stage genetic and epigenetic alterations. Hence, multi-omics analyses have revealed changes in expression and methylation patterns, point mutations and copy number alterations of genes in cancer. In spite of its molecular diversity, six main categories of essential functional alterations were described as hallmarks of cancer that allow the acquisition of a growth advantage to tumour cells: growth self-

sufficiency (or sustained proliferation), evasion of growth suppression, cell death inhibition, limitless replicative potential (immortality), sustained angiogenesis and tissue spreading capacity (invasiveness and metastasis) (Hanahan & Weinberg, 2000). More recently, two more hallmarks were added: metabolism reprogramming (and deregulated energetics) and immune system regulation (*Figure II*) (Hanahan & Weinberg, 2011). Tumourigenesis promotes these mechanisms through progressive genome instability tolerance and the inflammation activated during tumour onset and growth seems to accelerate the progression from a benign neoplasia to a malignant lesion.

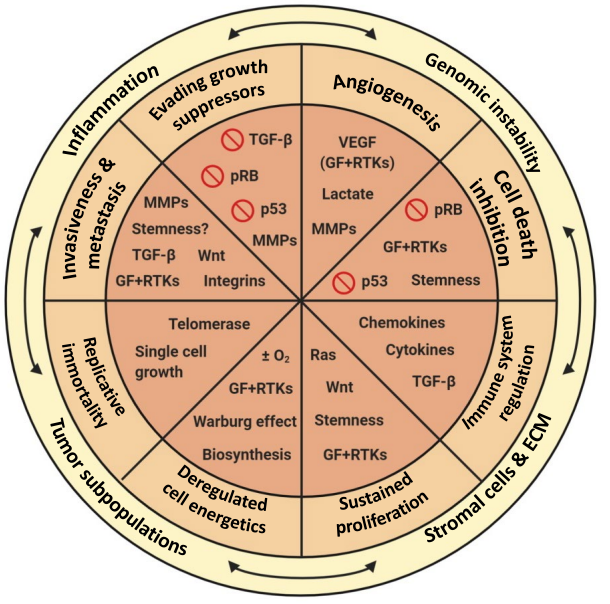

Figure II – **Hallmarks of cancer and mechanisms involved.** Eight functional alterations (growth self-sufficiency, insensitivity to growth suppression, cell death evasion, limitless replicative potential, sustained angiogenesis, tissue spreading capacity, metabolism reprogramming and immune evasion) have been described as essential for tumour growth. Importantly, all of them are promoted and influenced by cellular and extracellular processes (mainly, inflammation, cancer-associated genomic instability, the appearance of tumour subpopulations and the interaction with stromal cells and ECM components). Finally, each of these eight mentioned alterations is governed by varied signalling pathways, tightly regulated in non-tumour cells. Figure adapted from Hanahan & Weinberg, 2000 and Hanahan & Weinberg, 2011. *ECM: extracellular matrix; GF: growth factors; RTKs: receptor tyrosine-kinases; MMPs: matrix metalloproteinases.*

Although tumours are quite diverse (Campbell et al., 2020), some pathways are frequently altered (*Figure II*). These alterations are usually found in signalling pathways tightly regulated in non-tumour cells, which are exploited by cancer cells as a consequence of diverse loss/gain of function genetic alterations. Traditionally, pathways involved in tumour cell proliferation and survival have been the most studied. In non-tumour cells proliferation is tightly regulated by pRb and p53, although

both can be inactivated by diverse mechanisms in cancer cells (Burkhart, 2008) (Joerger & Fersht, 2016). Mitogens and pro-proliferative pathways, such as Ras/ERKs or PI3K/Akt, can also be overactivated in tumours, promoting growth, self-sufficiency and cell death inhibition (Hanahan & Weinberg, 2011). For example, *RAS* genes are mutated in approximately 25% of human cancers (Hobbs; Der; and Rossman, 2016). There are more factors that affect additional pathways that control the mentioned hallmarks (Hanahan & Weinberg, 2011). For example, Myc-mediated proliferative and anti-differentiation pathways, brake on telomere shortening through telomerase reactivation or TGF-β shift from cell cycle inhibitor to EMT (*epithelial to mesenchymal transition*) inducer function. Importantly, microenvironmental elements and stromal cells are also involved in cancer (*Figure II*). Unluckily, different factors reduce the potential use of these pathways as therapeutic targets such as redundant mechanisms for similar functions, unexpected negative feedback loops and cancer cell plasticity.

1.1. Central nervous system

Through nerve impulses, the nervous system controls a wide range of signals from individual's surrounding and body in order to adjust to them. From the anatomical point of view, nervous system can be divided into CNS (*central nervous system*), consisting of brain and spinal cord, and PNS (*peripheral nervous system*), which connects CNS with the organs and the limbs, transmitting information from/to CNS (Brodal, 2006). The cells that comprise the nervous system derive from neuroepithelial cells located in the ectoderm, displaying a NSC (*neural stem cell*) phenotype. During the first weeks of human embryonic development, these cells proliferate, leading to neural plate formation and, later on, this structure invaginates to generate the neural tube (Brodal, 2006). Further proliferation of these neuroepithelial cells in the neural tube is responsible for the generation of brain and spinal cord precursor structures.

Through asymmetric divisions, neuroepithelial cells give rise to the main cell types from CNS: neurons and glial cells (astrocytes, oligodendrocytes, ependymal cells and microglia) (*Figure III*) (Brodal, 2006). Depending on cell fate, neurogenesis or gliogenesis programs can be activated, leading to different cell populations, which coexist and cooperate to carry out the different nervous system functions. Nervous system is built up by neurons (nerve cells), diverse glial cells, mainly, astrocytes, oligodendrocytes in CNS and resident immune-like microglial cells. Neurons are composed by a cell body, where the nucleus is located, multiple dendrites and generally a single axon, with nerve terminals to form synaptic contacts. Neurons are connected into complex neural networks, accompanied by glial cells. Glial cells are essential for proper synaptic functioning. Astrocytes have extensions in all directions and possess a large surface suited for molecule exchange and capillary contact. They

act as neuronal homeostasis regulators and synapse controllers. Oligodendrocytes cover axons with a myelin sheath to accelerate impulse conduction. This cylinder structure is formed by numerous layers of cell membrane generated when oligodendrocytes wrap themselves around the axon.

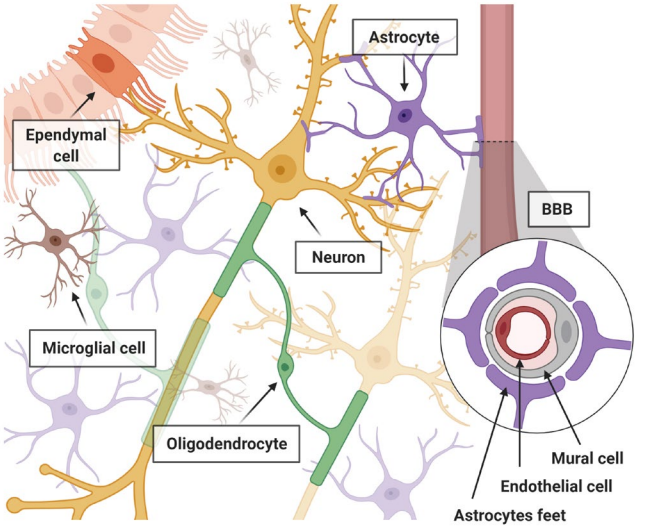

Figure III – Central nervous system (CNS) and brain: cell types and organization. In brain, different cell types (mainly, neurons, astrocytes, microglia and oligodendrocytes) coexist and interact with in order to coordinate signalling and metabolism, improving the synaptic functioning. Importantly, in brain, blood-brain barrier (BBB) regulates homeostasis and it is formed by endothelial and mural cells and interconnected with brain parenchyma through the astrocytes feet.

Blood vessels that vascularize the CNS have unique properties in order to tightly regulate the exchange of ions, nutrients and cells between blood and brain, precisely controlling CNS homeostasis (Daneman, 2015). CNS capillary structure forms the BBB (*blood-brain barrier*), which is compromised by endothelial cells covered by mural cells (mainly, pericytes), astrocyte foot processes and several basement membranes. Pericytes extend long cellular processes along the abluminal surface of the endothelium that can often span several endothelial bodies. During development, CNS pericytes are formed by differentiation of neural crest progenitors, although extra-CNS pericytes derive from mesoderm. Pericytes play important roles in angiogenesis, ECM (*extracellular matrix*) regulation and immune cell infiltration. They also regulate blood flow in response to neural activity. Importantly, astrocytes act as the cellular link between neurons and BBB, controlling pericytes contraction/dilation and, consequently, capillary diameter, blood flow and molecule exchange.

1.2. CNS tumours and glioblastoma generalities

As almost any other tissue, CNS is also subjected to develop tumours. Indeed, in 2019, around 300.000 tumours located in the CNS were diagnosed worldwide (ranked as the 17th cancer in incidence rate) and approximately 250.000 deaths were reported to be caused by them (ranked as the 12th cancer in mortality rate) (*WHO webpage*, 2020) (*World Cancer Research Fund webpage*, 2020). Following the general tendency in cancer, men have higher incidence of primary CNS tumours and secondary brain metastases (excluding sex-specific cancers), as well as worse prognosis compared to women (Sun et al., 2015). Several reasons have been suggested, such as sexual dimorphism in cancer-associated pathways or stromal differences. Understanding sex-related molecular mechanisms could improve personalized treatment and it could uncover hidden protective elements present in women.

In 2007, WHO classification of CNS primary tumours was established, based on histological grading (microscopic evaluation of tumour morphology) (*Figure IV*) (Louis et al., 2007). This scale defined grades I to IV as follows:

- **(i)** Grade I: lesions with low proliferative potential and the possibility of cure by surgical resection.
- **(ii)** Grade II: infiltrative neoplasms with low proliferative activity, but high level of recurrence and tendency to progress to higher grades of malignancy.
- **(iii)** Grade III: lesions with histological evidence of malignancy, including nuclear atypia and brisk mitotic activity.
- **(iv)** Grade IV: cytological malignant, mitotically active, necrosis-prone neoplasms, typically associated with rapid evolution, widespread infiltration in surrounding tissue and fatal outcome.

Other parameters (e.g. patient age, tumour location or genetic alterations) were taken into consideration for prognosis evaluation, but not for tumour definition. In this classification, gliomas were defined as neuroepithelial tumours that can be sub-organized depending on their cell type of origin: astrocytes (leading to astrocytomas), oligodendrocytes (oligodendrogliomas), and mixed astrocytic and oligodendrocytic (oligoastrocytomas), among others (*Figure IV*) (Louis et al., 2007).

In 2016, WHO classification of CNS tumours included molecular parameters, in addition to histology. Hence, gliomas were grouped according to their *IDH* (*isocitrate dehydrogenase*) mutation status, independently of their astrocytic or oligodendroglial origin (*Figure IV*) (*Box 1*) (Louis et al., 2016). Importantly, in the absence of proper genetic evaluation or alterations not matching the standard mutations, NOS (*not otherwise specified*) category was also included. 2007 WHO definition into I-IV grades

was also retained as complementary. Nowadays, 2016 WHO classification of CNS tumours is used in clinic and we will use it as a reference when necessary in this work.

BOX 1 – IDH mutations in glioblastoma

IDH-1, -2 and -3 isoforms catalyse the oxidative decarboxylation of isocitrate leading to α-KG (*α-ketoglutarate*) in TCA (*tricarboxylic acid*) cycle (Turner & Adamson, 2011). Whereas IDH-1 localizes within the cytoplasm, mitochondrial IDH-2 and IDH-3 isoforms generate NAD(P)H for oxidative phosphorylation and ATP production. IDH-1 and IDH-2 isoforms can reverse their catalysed reaction, using or generating NAD(P)H, according to cell needs. In astrocytes, this affects glucose and glutamate/glutamine metabolism and anti-oxidant reactions. Mutations in *IDH-1* and *IDH-2* are usually detected in secondary GBMs (*glioblastomas*); particularly, R132H mutation in *IDH-1* (leading to arginine replacement by histidine at residue 132 from the protein) is found in up to 90% of these GBM patients. Mutations decrease isocitrate binding to the enzyme, promoting abnormal α-KG conversion to 2-HG (*2-hydroxy-glutarate*) (considered an oncometabolite) coupled to NAD(P)H consumption. α-KG alters metabolism (e.g. glycolytic enzymes), protein stabilization/degradation (e.g. prolyl-hydroxylases) and epigenetic regulation. For example, α-KG is an essential co-factor for certain histone- and DNA-demethylases, while 2-HG is a competitive inhibitor. Thus, *IDH1/2* mutations result in hypermethylated histones and DNA, which in turn alters gene expression and drives cancer progression. Hence, low levels of α-KG lead to malignant progression through different mechanisms. An example is the upregulation HIF1α via prolyl-hydroxylases inactivation, which induces survival, metabolism reprogramming, invasion and angiogenesis. Moreover, IDH mutations are associated to a better glucose sensing adaptation, differentiation blockage, increased ROS (*reactive oxygen species*) or higher mutagenic rate, among others.

GBMs (*glioblastomas*) are grade IV astrocytomas/gliomas which are not only the most frequent brain tumours (4 new diagnosis per 100.000 population), but also the most aggressive ones (Ostrom et al., 2014). This is due to GBM intrinsic properties (such as high mitotic activity, low differentiation grade, high cell heterogeneity and infiltrative capacity with vascular hyperplasia) and the lack of effective treatments. Indeed, median survival rate of GBM patients is around 12-14 months and less than

10% patients show 5-year-survival (Ostrom et al., 2014). Recent data point out that females have a lower incidence and slightly better prognosis than males (Tian et al., 2018). Signs and symptoms associated to GBM depend on tumour location and size, since they are caused by pressure and impairment of nervous structures. Although they vary during malignant progression, several can be highlighted: headaches combined with nausea and vomiting, seizures, memory loss, behavioural changes, depression or focal neurologic deficits.

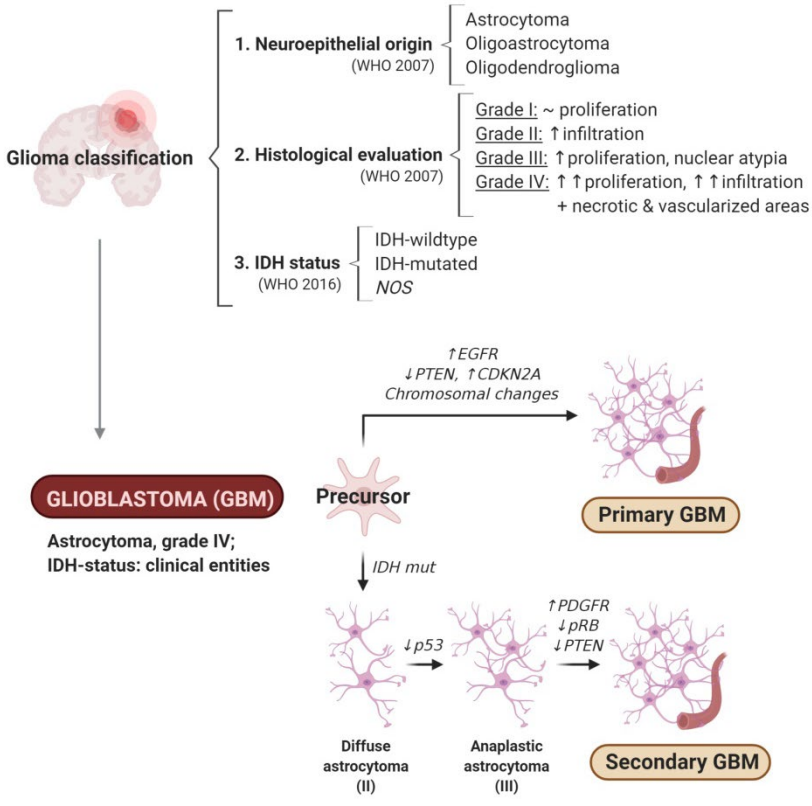

Figure IV – **Gliomas classification and glioblastoma subtypes.** From 2016, gliomas classification is focussed on IDH status, although other factors such as the neuroepithelial origin of the tumour and histological evaluation from previous classification system are also considered. Glioblastomas (GBMs), also known as grade IV astrocytomas, can be sub-classified into primary or secondary GBMs depending on their IDH status, progression and mutational profile.

Before CNS tumours classification reorganization by OMS in 2016, GBMs were subclassified as primary (almost 90%), generated *de novo* in elderly patients, or secondary (around 5-10%), resulting from grade II/III astrocytomas malignant progression (*Figure IV*) (Ohgaki & Kleihues, 2013). Nowadays, GBMs are defined as grade IV gliomas (astrocytic and oligodendroglial tumours) with three novel sub-types: *GBM-IDH-wildtype* (almost 90% of cases), *GBM-IDH-mutant* (around 10%) and *GBM-*

NOS (rare diagnosis) (Louis et al., 2016). Interestingly, the majority of primary GBMs do not present mutations in *IDH* gene, while progression from grade III to grade IV astrocytoma during secondary GBM formation has been linked to *IDH* mutations. The incidence ratio, diagnosis age, molecular alterations and prognosis also indicate that *GBM-IDH-wildtype* and *GBM-IDH-mutant* entities denoted by WHO, mostly coincide with previously described primary and secondary GBMs, respectively.

1.2.1 Molecular alterations and signatures of glioblastoma

In spite of GBM intra- and inter-patient heterogeneity, certain alterations are directly associated to this tumour, leading to the definition of diverse molecular signatures. RTKs (*receptor tyrosine-kinases*) and their downstream pathways are altered in almost 90% GBMs. The most commonly altered RTK in GBM is EGFR (mutated or amplified in 50-60% of cases), followed by PDGFRα (amplified in 13% cases), ErbB2 (mutated in 8% of cases), Met (amplified in 2-4% cases) and FGFR1 (amplified in 3.2% cases) (*Figure V*) (TCGA, 2008). Importantly, a truncated constitutively-active mutant EGFR variant (EGFRvIII) is frequently expressed in GBM, resulting in cell proliferation and survival, but not necessarily worse prognosis (J. R. D. Pearson & Regad, 2017). Moreover, RTK ligands (growth factors) are usually upregulated (e.g. FGFs) and non-mutated RTKs can be over-activated, such as VEGFR, which drives angiogenesis in growing GBMs (J. R. D. Pearson & Regad, 2017). Intracellular signalling pathways activated by growth factors through RTKs and other signals are usually altered in GBM, too (TCGA, 2008). For example, Ras is only mutated in 2% cases, but it is over-activated when NF1 (a Ras GAP) is mutated o deleted (18% cases). PI3K is also mutated in 15% cases and PTEN is inactivated or deleted in 36% cases. All these alterations are known to contribute to progression, dissemination and therapy resistance (J. R. D. Pearson & Regad, 2017). Alterations resulting in p53 pathway inactivation (including CDKN2A deletion, MDM2 amplification or p53 mutations) affect around 85% of patients and pRb is the third most altered pathway in GBM (78% of GBM patients) (TCGA, 2008) (J. R. D. Pearson & Regad, 2017). Interestingly, p53 and pRb sexual dimorphism affects GBM growth. Hence, upon p53 loss, NF1-deficient astrocytes display ten-fold higher tumourigenic potential, when derived from males as compared to females, although these differences disappear when pRb is also deleted (Sun et al., 2015).

Some of these alterations have been associated to GBM subtypes, too (Ohgaki & Kleihues, 2013). Besides IDH-wildtype status, primary GBMs are characterized by EGFR amplification, CDKN2A and pRb deletions, chromosome-10 loss and mutations in PTEN. Secondary GBMs present p53 mutations, important for progression from grade II to grade III astrocytomas, in addition to pRb promoter methylation, IDH mutation or PDGFR amplification, all involved in the last steps of progression from grade III astrocytoma (*Figure IV*).

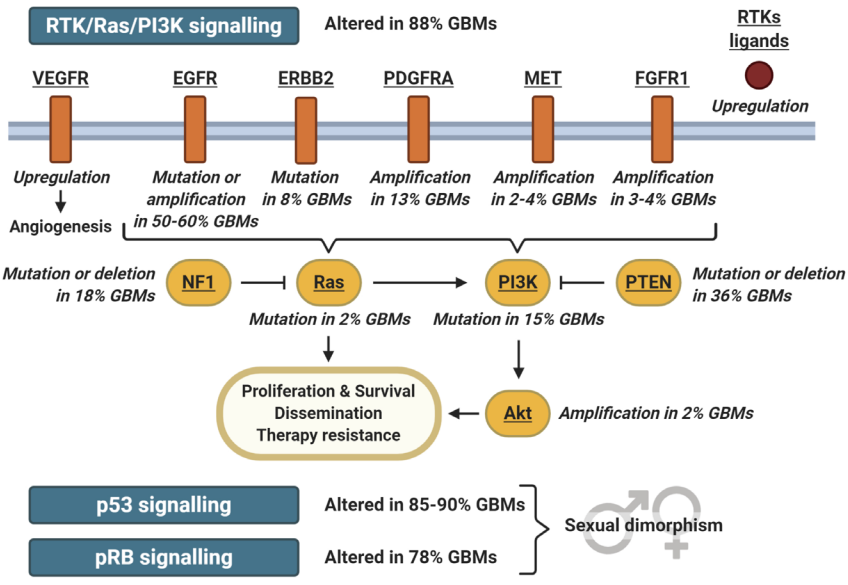

Figure V – **Most predominant molecular alterations in glioblastoma (GBM) samples.** Receptor tyrosine kinases (RTKs) (mainly EGFR), diverse RTK-activated signalling pathways, p53 pathway and pRb pathway are susceptible of being altered in GBM, being responsible for the aggressive characteristics of these tumours. Adapted from J. R. D. Pearson & Regad, 2017.

Integrated multidimensional genomic studies, including genome-wide DNA copy number correlations, sequence-based mutation detections and expression analyses, have allowed a sub-classification of GBMs into four robust molecular signatures: classical, mesenchymal, proneural and neural (Verhaak et al., 2010).

- Classical subtype constellates the most common aberrations detected in GBM, such as chromosome-7 amplification paired with chromosome-10 loss, EGFR amplification and EGFRvIII expression, p53 mutation and CDKN2A deletion. Moreover, neural stem markers (mainly, Nestin), Notch and Shh pathways are also upregulated.
- Mesenchymal subtype is characterized by NF1 alteration and PTEN mutations, in addition to overexpression of mesenchymal markers (e.g. CHI3LI), Met, astrocytic markers (e.g. CD44, MERTK) and inflammation-related genes that lead to large necrotic areas in these tumours.
- Proneural subtype displays PDGFRα upregulation, IDH mutations and p53 loss, all of which have been previously associated with secondary and IDH-mutant GBMs. These tumours express oligodendrocyte (e.g. NKX2-2, OLIG2) and proneural development (e.g. SOX, DCX, DLL3, ASCL1 or TCF4) genes.

- Neural subtype is the most similar to normal brain, although malignant transformation is unequivocal at histological level. Neuronal markers are upregulated in these samples (e.g. NEFL, GABRA1, SYT1 or SLC12A5).

Importantly, recurrences do not seem to involve class changes and the standard treatment used for GBM increases survival in classical, mesenchymal and neural subtypes, but not in proneural one. To finish with, mesenchymal subtype exhibits the most consistent disparity in male:female rates, followed by proneural and neural, while classical subtype occurs equally in both sexes (Sun et al., 2015).

All these complex subclassifications and molecular studies have widely tried to improve GBM patient clinical outcomes, but, unluckily, heterogeneity and plasticity are still tough issues to deal with in this pathology.

1.2.2 Diagnosis and treatment of glioblastoma

Currently, gliomas can be detected and diagnosed at an advanced stage using neuroimaging methods such as magnetic resonance imaging upon the appearance of neurological alterations. Initially, tumour advance is masked by brain adaptive mechanisms, leading to the absent of clinical manifestations, even when histological signs would be clear (Silantyev et al., 2019). New diagnosis tools are required to cover GBM heterogeneity and its infiltrative capacity and to be able to detect all tumour-associated subpopulations, patient-specific characteristics and infiltrated masses outside the main focus (Agarwal et al., 2016). Not only tumour tissue that is collected by invasive and risky methods, but also biological fluids could be used for GBM early diagnosis, such as cerebrospinal fluid, peripheral blood or urine. They can be collected by minimally invasive methods and they summarize tumour heterogeneity. Indeed, diverse biomarkers from different types of samples have been proposed, such as proteins, genetic alterations in circulating DNA, oncometabolites, CTCs (*circulating tumour cells*), extracellular vesicles or miRNAs (*micro RNAs*), among others, but they need to be further studied (Silantyev et al., 2019).

Regarding GBM treatment, the median survival after diagnosis is 12.1 months for patients undergoing resection followed by radiotherapy (Stupp et al., 2005). It is important to point out that resection is not innocuous, since it can couple neurological problems due to the rapid change in tumour-brain interactions and destabilization of brain adaptive responses. Resection plus radiotherapy as therapeutic strategy turned out to be insufficient and/or inefficient for patients in the long term due to inaccurate resection in disseminative tumours, high relapse rate and/or tumour resistance over time (Silantyev et al., 2019). Consequently, in spite of treatment, a two-year survival rate was observed in 10.4% of patients some years ago (Stupp et al., 2005). Nowadays, the first-line treatment, not only includes surgical resection of the main

tumour mass followed by adjuvant radiotherapy, but also chemotherapeutic treatment with TMZ (*temozolomide*), an alkylating agent (Stupp et al., 2005). This novel first-line approach has increased median survival up to 14.6 months and a two-year-survival rate rose up to 26.5% of patients. Nevertheless, TMZ did not report any benefit in proneural GBM subtype (Verhaak et al., 2010).

Great efforts are being made to improve GBM treatment at different levels, such as developing novel surgery techniques. For example, neuroendoscopy or fluorescence-guided resections, or introducing changes in therapy administration that can allow better distribution into the tumour without affecting healthy areas (Van Meir et al., 2010). Regarding molecular approaches, it is important to highlight:

- MGMT (O^6-*methylguanine methyltransferase*) inhibitors in order to avoid resistance to alkylating agents such as TMZ. This resistance is common in GBM patients, because of DNA repairing enzymes, mainly MGMT, are upregulated in these tumours (Hegi et al., 2008).
- RTK inhibitors, acting mainly on VEGFR and EGFR, but also on Met, FGFR or PDGFR (Van Meir et al., 2010) (J. R. D. Pearson & Regad, 2017).
  - **(i)** The most relevant anti-VEGFR therapy tested in GBM is Bevarizumab, a monoclonal antibody that binds VEGF, preventing its binding to VEGFR. It is used to impair increased vascularization, commonly found in GBMs. Although initial results indicated that it increased recurrent patient survival, later studies proved the generation of resistance by upregulating other pro-angiogenic signals such as FGF, PDGF or chemokines and increased invasiveness (Van Meir et al., 2010).
  - **(ii)** Multiple strategies have been used to impair EGFR activation in GBM (J. R. D. Pearson & Regad, 2017). Erlotinib, a small-molecule inhibitor, slightly increases survival in combination with TMZ, but it has no effect as monotherapy. Other EGFR inhibitors, also acting on other RTKs do not further increase clinical benefits, such as Gefitinib (anti-EGFR plus anti-VEGFR inhibitor) or Lapatinib (anti-EGFR plus anti-HER2/ErbB2 inhibitors). Finally, Cetuximab was tested in recurrent patients. It is an antibody against EGFR extracellular domain, which acts as an antagonist that prevents ligand binding. However, their benefits were minimal, partially due to problems to cross the BBB.
- Intracellular pathways inhibitors. For example, those using targets from mTOR or Ras pathways (Van Meir et al., 2010) (J. R. D. Pearson & Regad, 2017).
- Histone deacetylases inhibitors for a transcriptional-wide regulation (Van Meir et al., 2010) (J. R. D. Pearson & Regad, 2017).

Tumour adaptation to these molecular therapies leads to multi-target drugs or administration of multiple drugs, as well as BBB modulation to increase drug entry into the tumour, since BBB is disrupted in tumour core, but not necessarily in its periphery, where active drug efflux transport should be impaired.

1.3. Cell populations in glioblastoma and their interactions

1.3.1. Glioblastoma origin and glioblastoma stem cells

As mentioned above, GBM molecular subdivision reveals insights into GBM origin (Verhaak et al., 2010). Hence, proneural signature is enriched in oligodendrocytic markers, while classical GBMs display an enhanced astrocytic profile. Neural subtype expresses oligodendrocytic and astrocytic markers, although they are defined by a strong upregulation of neuron-associated genes. To finish with, mesenchymal GBMs are characterized by high inflammation and, consequently, they have an astroglial-like signature with upregulation of microglial markers. These potential linage reminiscences could be the result of diverse differentiation paths from a common original precursor, for example, NSCs (hierarchical model). They could also indicate the presence of multiple GBM-initiating populations in brain with diverse stem-like properties (stochastic model) (Lathia et al., 2015).

In general, CSCs (*cancer stem cells*) are defined as a small subpopulation of cancer cells with stem and initiating capability, which is considered to be responsible for tumour onset and therapy resistance. These cells have a stem-like phenotype with auto-renewal capacity and stem markers expression, such as OCT4, NANOG, SOX2 or CD44. In addition, they can differentiate into non-stem tumour cells and stromal cells to support tumour progression (Clarke et al., 2006). Their origin is controversial and several hypotheses have been suggested, such as the oncogenic transformation of tissue-specific adult stem cells and/or stem-like capacity associated to malignancy. These CSCs are resistant to classical chemotherapeutical agents and they undergo quiescence, although they can be later reactivated, originating recurrences in cured patients (Clarke et al., 2006).

As key mediators of tumour origin and onset, CSCs present in GBM, known as GSCs (*GBM stem cells*) or GICs (*GBM-initiating cells*), have also been studied. GSCs resemble NSCs in multiple properties, including self-renewal, ability to differentiate, although partially compromised, and *in vitro* formation of neurospheres upon non-adherent and serum-free culture conditions. In addition, GSCs are also capable of initiating tumourigenesis. They express specific markers and maintain basal proliferation and anti-apoptotic mechanisms without decreasing their stem-like phenotype (Liebelt et al., 2016). As mentioned for CSCs, in general, the origin of GSCs is also controversial. On one hand, the majority of studies suggest that GSCs

could appear when cancer driver mutations occur in NSCs (Y.Wang et al., 2009), a hypothesis supported by the higher tumour formation in brain areas surrounding the subventricular zone, where adult NSCs are located (Liebelt et al., 2016). On the other hand, other studies point out that non-stem tumour populations can generate GSCs during tumourigenesis (J.Wang et al., 2008), and neuronal/astrocytic dedifferentiation promotes pro-oncogenic mechanisms that induce gliomas (Friedmann-Morvinski et al., 2012).

Absence of proper dedifferentiation/differentiation signatures hinders distinguishing GSCs from NSCs or from GSC progeny. Thus, GSCs markers are common to NSCs: transcription factors (e.g. SOX-2, Olig2, NANOG, Mushashi or Bmi), the intermediate filament protein Nestin, or surface markers such as CD133, CD44, integrin α6 or L1CAM. All of them have been detected in partially stem-like tumour populations and/or stem cells-derived progeny (Lathia et al., 2015). The signalling pathways that govern GSC phenotype, mainly Notch, Shh, BMPs, Wnt, STAT3, NFκB or RTKs, such as EGFR, FGFR, Alk and Eph, are not specific for these cells and they are involved in multiple steps of both physiological and pathological processes, as described above (Liebelt et al., 2016). Moreover, their activation is coordinated through genetic/epigenetic changes combined with microenvironmental and metabolic factors, mainly hypoxia, so that, GSCs location within the tumour mass correlates with the hypoxic gradient.

Data indicate that GSC population is enriched upon anti-tumour treatment and it has been involved in tumour relapse (J. Chen et al., 2012) (Palanichamy et al., 2018). Diverse mechanisms explain why GSCs can survive therapy and mediate relapses (Lathia et al., 2015) (Liebelt et al., 2016), highlighting:

- **(i)** Relative quiescent or slow cycling phenotype combined with anti-apoptotic action.
- **(ii)** Alteration of DNA damage response machinery and MGMT upregulation.
- **(iii)** Drug uptake/efflux modification by upregulation of ABC transporters.
- **(iv)** Lineage plasticity and heterogeneity, mediating tumour adaptation.

GSC study has led to novel therapeutic approaches based on disruption of their paths and markers, inactivation of microenvironment-GSCs interactions or forced differentiation of GSCs to decrease their stem-associated potential. For example, it is known that MDK (*midkine*)-activated Alk signalling promotes cell death resistance and the acquisition of a GSC phenotype by GBM cells via autophagy inhibition and SOX9 stabilization (López-Valero et al., 2020). Indeed, Alk inhibitors (e.g. crizotinib or lorlatinib) administrated with TMZ, the benchmark agent for GBM treatment, induce a high decrease in tumour size in mice models, promoting apoptosis and reducing GSC population in the tumour.

1.3.2. Tumour microenvironment

Tumour microenvironment is defined as the different cells, signalling molecules, ECM (*extracellular matrix*) components, metabolites and other elements, which surround tumour cells. It is created and dominated by the tumour. Reductionist views of tumours, considering that cancer relies on a homogeneous tumour mass, are incomplete and far from the reality found in clinic. A change of paradigm beyond reductionism is necessary, especially taking into account that research points to the importance of tissue, microenvironment, ECM, carcinogenesis, cancer control and its progression. Mutagenesis and tumour progression drive subclonal populations, which are selected when carrying advantages in a particular context (intra-tumour heterogeneity) (Hanahan & Weinberg, 2011). Regions demarcated by various degrees of stemness/differentiation, proliferation, vascularity or inflammation, among others, have been revealed by histopathological analysis of human tumours. Moreover, new mutations may produce new adaptive traits for selection, and, conversely, contextual changes may modify the selective pressure, favouring pre-existing alterations.

ECM is the most important non-cellular component of tissues, which actively provides support for cells via its dynamic remodeling. In cancer, this remodeling is mediated by secretion of ECM components (collagen, laminin, proteoglycans and fibronectin) and regulators, such as MMPs (*matrix metalloproteinases*), secreted by cancer and stromal cells (Kessenbrock et al., 2010) (Walker et al., 2018). Cellular integrins interact with ECM, promoting intracellular signals that also lead to ECM rearrangement (synthesis, reorganization or degradation). Hence, ECM is involved in biochemical forces against movement as well as migration/invasion tracking, ligand presentation, cell-cell communication or signal reservoir for proliferation, angiogenesis, inflammation or spreading, among others.

Cancer-associated fibroblasts and myofibroblasts (activated fibroblasts in response to ILs or TGF-β) are tumour stromal cells directly implicated in ECM secretion and signals production (Hanahan & Weinberg, 2011) (Walker et al., 2018). These cells have some characteristics similar to tissue-associated fibroblasts (for example, α-SMA expression), but, they can promote tumour growth, proliferation, angiogenesis, metastasis and therapy resistance. For example, in $HER2^+$ breast cancer, cancer-associated fibroblasts secrete FGF-5, which activates FGFR2 in tumour cells leading to HER2 transactivation via c-Src and anti-HER2 therapy resistance (Fernández-Nogueira et al., 2020). Hence, anti-HER2 therapies should be combined with FGFR inhibitors and α-SMA (*α-smooth muscle actin*), FGF5, FGFR2 or c-Src could be used as predictive markers.

In the tumour microenvironment, several types of immune cells, stem cells and nervous cells have also been detected. Immune cells recruited to the tumour stroma lead to the activation of an inflammatory response that initially inhibits its malignant growth. However, tumours can evade the immune response through different mechanisms and the infiltrated inflammatory cells promote tumourigenesis by inducing ECM remodelling and signal secretion (Hanahan & Weinberg, 2011). Inflammation recruits mesenchymal stem cells from bone marrow and surrounding tissues and activates their differentiation to mature mesenchymal cells, such as cancer-associated fibroblasts, macrophages or endothelial cells (Guan & Chen, 2013). Mesenchymal stem cells have been involved in tumour stemness, migration, angiogenesis, immunosuppression and treatment resistance through secretion of different factors, such as TGF-β1, LIF (*leukaemia-inhibitory factor*), IL10 or CXCL12, among others. Moreover, infiltrated nerve cells are associated to cancer progression and dissemination (Jobling et al., 2015). Nerve and cancer cells crosstalk is reciprocal: nerve cells release neurotransmitters that stimulate cancer and stromal cells, for example, through β-adrenergic receptors, while cancer cells secrete neurotrophic factors, such as NGF, which promote neoneurogenesis.

Angiogenesis is a key element for tumour growth, not only for nutrients and oxygen support, but also for toxins withdrawal. Even though early-stage tumours do not usually have access to vasculature, tumour growth is accompanied by the upregulation of pro-angiogenic genes promoted by oncogenes, such as Ras and Myc, ECM remodelling and VEGF or FGF-1/2 release, among others (De Palma et al., 2017) (Walker et al., 2018). For example, inflammatory cells activate angiogenesis by increasing ECM-sequestered VEGF availability (Bergers et al., 2000). This continuous activation results in unbalanced endothelial proliferation/apoptosis and aberrant vasculature: convoluted and excessive vessel branching with enlarged vessels, erratic blood flow and leakiness (De Palma et al., 2017). This vascular hyperpermeability activates pro-platelets that secrete pro-agiogenic factors and chemoattractants for immune cells. Pericytes, which bind to and stabilize the vasculature, also play an important role in cancer. Their attachment to this aberrant vasculature favours endothelial differentiation via Ang-1/Tie-2 axis (Raza et al., 2010). Tumour-associated endothelial cells maintain the expression of endothelial markers, such as Tie-2 and MECA-32, but also display new expression patterns and surface molecules (De Palma et al., 2017).

GBM microenvironment includes stem cells niches, BBB and different cell types, which comprises not only host brain populations, but also infiltrated hematopoietic mesenchymal stem cells (Bi et al., 2020) (Klemm et al., 2020). Disturbances in BBB function linked with GBM tumour core are often observed, while peripheral areas present intact BBB and they support tumour spreading, and surgical resection does

not affect them (Agarwal et al., 2016). In GBM, angiogenesis contributes to the expansion and remodelling of the existing vasculature through universal mechanisms, mainly branching mediated by vessel sprouting or splitting of vessel lumens from interstitial tissue. In addition, GBM-specific mechanisms, such as vascular co-option and vasculogenic mimicry are also involved (Liebelt et al., 2016). Remarkably, GBM cells are able to transdifferentiate into endothelial-like and pericyte-like cells to support tumour-associated vasculature. Indeed, certain GSC subpopulations express endothelial markers, such as PECAM-1 (also known as CD31), Tie2, VEGFR-2, VE-cadherin (also known as CD144) or VEGF and they can form tubular networks under endothelial culture conditions (Liebelt et al., 2016). Interestingly, GBMs with EGFR alterations can undergo an EMT-like process that allows the acquisition of a pericyte-like phenotype, promoting angiogenesis and tumour growth (Gargini et al., 2019). The microtubule-associated protein, Tau, inhibits EGFR signalling, except when EGFR is constitutively activated, which correlates with lower expression of pericyte markers and decreased Ang-2/Ang-1 ratio, usually associated to bad prognosis.

1.3.3. Metabolism reprograming

Metabolism is the set of cellular regulated sequential biochemical reactions in charge of promoting proliferation, maintaining structures and adapting to environmental changes. Thus, cancer cells modify and reprogram their metabolism in response not only to a higher ATP need, but also to the increased demand of lipids, nucleotides and aminoacids synthesis required for proliferation (*Figure VI*). This adaptation also optimizes the use of resources available in their microenvironment, so that, it affects both tumour cells and tumour-associated stroma.

In tumour microenvironment, hypoxia induces the stabilization of HIF transcription factor, which is known to promote angiogenesis, survival, migration, tumour growth and glycolysis (Tennant et al., 2009). Cancer cells are known to preferentially use the anaerobic glycolytic metabolic pathway even in the presence of oxygen (Vander Heiden et al., 2009) (Liberti & Locasale, 2016). This is known as Warburg effect and there are multiple metabolic consequences derived from this adaptation in cancer cells.

Warburg effect could be considered an inefficient adaptation because anaerobic glycolysis has a low yield of ATP production, only 2 ATP per glucose molecule, while TCA followed by mitochondrial oxidative phosphorylation (aerobic glycolysis) can generate up to 36 molecules of ATP per glucose. However, anaerobic glycolysis has a faster rate, so that the amount of ATP synthesized in a given period of time could be comparable in both pathways (Liberti & Locasale, 2016). Importantly, some tumours acquire a high glycolytic phenotype, enhancing their glucose uptake, but maintaining an aerobic glycolytic rate similar to the surrounding normal tissue (Mathupala et al.,

2010). This, together with other observations, indicates that mitochondria would not be defective in cells displaying Warburg effect, although certain mitochondrial enzymes can be downregulated such as PDH (*pyruvate dehydrogenase*), FH (*fumarate hydratase*) or SDH (*succinate dehydrogenase*). The extra glucose intake is diverted by tumours to biosynthetic pathways, such as fatty acid and nucleotide synthesis, and NADH/NADPH generation to support their rapid proliferation (Vander Heiden et al., 2009) (Mathupala et al., 2010). Finally, subpopulations of cancer cells with complementary metabolic adaptations coexist within tumours. Hence, cells undergoing Warburg effect secrete lactate, which is imported and used as an energy source by other cells (Hoang-Minh et al., 2018) (Commander et al., 2020).

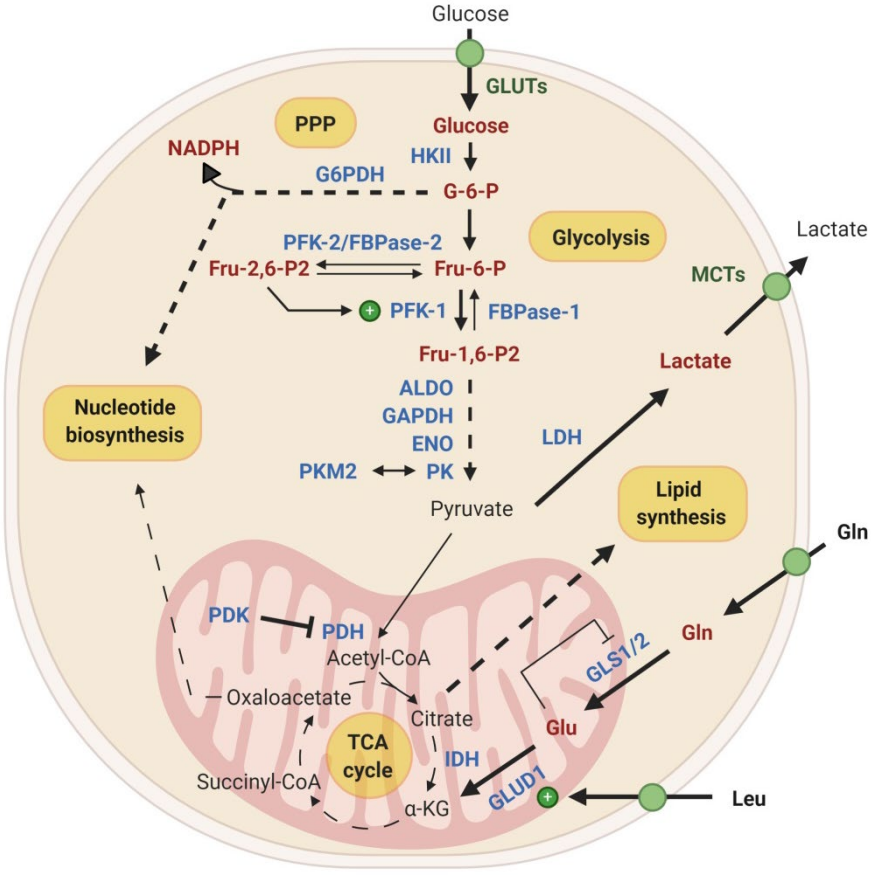

Figure VI – Schematic representation of cancer metabolism focused on glycolysis and Warburg effect, as well as their interactions with other routes. Cancer cells present an altered metabolism due to the high demand of ATP and nutrients (lipids, nucleotides and aminoacids) and the need of adaptation to novel microenvironmental conditions (e.g. via lactate secretion). *ALDO: Aldolase; ENO: Enolase; G: Glucose; Fru: fructose; P: phosphate; TCA: tricarboxylic acids; α-KG:α-ketoglutarate.*

In non-tumour cells, extracellular glucose enters into the cell via GLUTs (*glucose transporters*), specific glucose transporters that mediate its transport through the plasma membrane. Then, glucose is mainly metabolized by glycolysis, a multi-step pathway that includes reactions catalysed by HK (*hexokinase*), G6PDH (*glucose-6-phosphate dehydrogenase*), PFK (*phospho-fructokinase*), aldolase, enolase or PK (*pyruvate kinase*), among others (*Figure VI*) (Burns & Manda, 2017). The majority of these transporters and enzymes are upregulated in cancer in levels and/or activity, such as HKII (a HK isoform with the highest affinity for glucose), GAPDH or PFK1 (Tennant et al., 2009). For example, PFK1/FBPase1 (*fructose-1,6-biphosphatase*) activity depends on fructose-2,6-biphosphate, the product of the reaction catalysed by PFK2/FBPase2. Thus, PFK2/FBPase2 expression is increased in several tumours, leading to higher concentration of fructose-2,6-biphosphate. This increases PFK1 activity, while decreases FBPase1 activity, favouring tumour growth (Dayton et al., 2016). Importantly, cancer-associated PK isoform, PKM2, plays a relevant role in tumourigenesis. There are four PK isoforms encoded by two genes. The *PKLR* gene encodes PKL (liver form) and PKR, and the *PKM* gene encodes PKM1 and PKM2 isoforms generated by alternative splicing. While PKM1 is a constitutively active tetrameric enzyme, PKM2 is allosterically-regulated (Dayton et al., 2016). It requires the binding of fructose-1,6-bisphosphate to form an active tetrameric complex that favours glycolysis. In the absence of this molecule, PKM2 forms dimers with low enzymatic activity that slow down glycolysis, allowing intermediates from glucose metabolism to be derived to biosynthetic pathways such as PPP (*pentose-phosphate pathway*) (Kowalik et al., 2017). In addition, PKM2 can play pro-tumourigenic roles in the nucleus, where it acts as a protein kinase that phosphorylates different substrates, such as transcription factors or histones, contributing to genetic and epigenetic regulation of cancer cells (Dayton et al., 2016) (Zahra et al., 2020).

Pyruvate, the end-product of glycolysis, undergoes conversion to acetyl-CoA, followed by mitochondrial TCA and oxidative phosphorylation under normoxia or to lactate under anaerobic conditions via LDH (*lactate dehydrogenase*). Pyruvate mitochondrial processing is regulated by PDH complex (also named as PDC), formed by PDHE1, PDHE2, PDHE3 and PDHX subunits, which catalyses the irreversible mitochondrial conversion of pyruvate to acetyl-CoA (Burns & Manda, 2017). In cancer cells, pyruvate, the end-product of glycolysis, undergoes conversion to lactate instead of acetyl-CoA even under normoxia conditions. This can be regulated by PDH activity inhibition as a consequence of PDHE1α subunit phosphorylation by PDK (*PDH kinase*) enzymes or by genetic downregulation of PDH complex components (Michelakis et al., 2010) (Woolbright et al., 2019) (Commander et al., 2020). Therefore, pyruvate is converted into lactate by LDH. In particular, LDH-M isoform encoded by *LDHA* gene, is upregulated in cancer cells favouring the generation of lactate (Valvona et al., 2016). As a consequence, *LDHA*/*LDHB* ratio is increased and

often used as an indicator of anaerobic glycolysis *vs.* oxidative phosphorylation. Lactate is not a waste product of glycolysis. It contributes to tumour acidification, creating a hostile environment for the action of immune cells involved in tumour progression inhibition. Lactate also activates angiogenesis inducing VEGF secretion. In addition, it can be metabolically used by surrounding cells through, for example, Cori cycle or astrocyte-neuron lactate shuttle in specific tissues (Vander Heiden et al., 2009). Lactate secretion is mediated by the lactate transporters, MCTs (*monocarboxylate transporters*) that allow lactate exchange through plasma membrane. They are also upregulated in cancer cells (e.g. MCT-4).

Glycolysis is not the only metabolic pathway dysregulated in cancer (*Figure VI*). Glycolytic reprogramming has been linked to PPP activation in cancer cells and G6PDH, its rate-limiting enzyme, is upregulated in tumours (Kowalik et al., 2017). PPP is a key pathway that generates anabolic intermediates from glucose-6-phosphate, such as ribose-5-phosphate for nucleotide synthesis and reducing power (NADPH) by its oxidative branch (Burns & Manda, 2017). PPP also promotes TCA slowdown or reversion, contributing to fatty acid synthesis, β-oxidation inhibition and glutaminolysis activation. This last pathway is relevant in cancer due to the fact that glutamine is involved in feeding TCA and in the synthesis of aminoacids and nucleotides (Tennant et al., 2009). Glutamine is deaminated by GLS (*glutaminase*), generating glutamate that can be converted into α-KG by GLUD (*glutamate dehydrogenase*) enzyme. As α-KG can be used for fatty acids synthesis and NADPH generation via TCA and acetyl-CoA production, glutamine and GLS are essential for cancer cells (Villar et al., 2015). There are two GLS isoforms, GLS/GLS1/KGA (kidney isoform) and GLS2/LGA (liver type) encoded by *GLS* and *GLS2* genes, respectively (Villar et al., 2015). GLS1 is ubiquitously expressed, inhibited by glutamate and mainly responsible for the GLS activity of tumour cells. GLS2, mainly expressed in the liver, cannot be inhibited by glutamate. In tumours, leucine entry into cells is favoured, since it allosterically activates GLUD1, avoiding glutamate accumulation and GLS1 inhibition (Villar et al., 2015). Glutamine can be generated from glutamate by a reaction catalysed by GS (*glutamine synthase*).

All these metabolic enzymes and transporters can be controlled at the level of expression, activity and/or localization in cancer cells by different signals and signalling pathways, such as PI3K/Akt/mTORC1, growth factors, ROS, aminoacids or chromatin modifications (Vander Heiden et al., 2009) (Tennant et al., 2009) (Liberti & Locasale, 2016). Moreover, these changes in metabolism affect not only to tumour cells and CSCs, but also stromal cells and their microenvironment. Stromal cells need to face the lack of glucose, glutamine and other nutrients, mainly consumed by tumour cells, and the microenvironment acidification. This affects ECM remodelling, angiogenesis (De Palma et al., 2017), invasion (Commander et al., 2020) or

immunosuppression, among other tumour characteristics (Hanahan & Weinberg, 2011).

The understanding of GBM metabolic reprogramming is specially complicated, mainly due to the particularities of CNS and brain metabolism. In normal brain, there are complex metabolic interactions among astrocytes, neurons and BBB, such as ANLS (*astrocyte to neuron lactate shuttle*) (Turner & Adamson, 2011) (Bi et al., 2020). Astrocytes have direct access to vascular structures, and they display a more anaerobic glycolytic metabolism, in agreement with the presence of LDH isoforms that enhance lactate production and the overexpression of lactate transporters, MCT-1 and MCT-4, and the glucose transporter, GLUT-1. In contrast, neurons relay on highly oxidative conversions of astrocytes-released lactate, controlled by LDH isoforms that favour lactate to pyruvate conversion and MCT-2 and GLUT-3 upregulation. Mitochondrial TCA works in astrocytes as a source of intermediates, for example, for glutamine synthesis after glutamate uptake, or for anti-ROS response.

Many of the properties associated to GBMs depend on their metabolic adaptations, which promote tumour invasion, microenvironment remodelling and growth advantage over normal cells (Bi et al., 2020). The Warburg effect is evident in GBM, although GBM cells are also oxidative (Strickland & Stoll, 2017). The importance of GBM metabolism was highlighted by WHO classification in 2016, as mentioned before, when IDH mutational status was incorporated as the primary factor to sub-classify GBMs and other CNS tumours (Louis et al., 2016). The metabolic consequences of IDH mutations have been widely studied (see *Box 1* for additional information), but this is not the only relevant metabolic core in this pathology. For example, glutamine, an essential mediator of glutamate homeostasis in brain, also plays a role in GBMs. As explained before, in GBM cells, GLS activity leads to glutamate generation that enters TCA, contributing to anabolic metabolism. However, glutaminolysis inhibition does not affect GBM proliferation, since half of glutamate derived from glutamine does not enter TCA, but it is secreted. In contrast, in GBMs, glutamine generated from glutamate and GS activity from tumour cells and astrocytes, present in the microenvironment, has been associated to tumour progression and poor prognosis (Tardito et al., 2015).

Furthermore, recent studies indicate that GBM subpopulations with different metabolic profiles support each other and cooperate to globally address dissemination and drug resistance (Hoang-Minh et al., 2018) (Commander et al., 2020). Thus, these subpopulations can be differentiated into the same tumour according to their specific functions, such as fast cycling cells *vs*. slow cycling cells, or invasive cells *vs*. growing cells, or by using clinic-relevant markers, such as LDH, GLUT, MCTs or glycolic enzymes isoforms, PDK/PDH expression or GLS levels, among others (Valvona et al., 2016). For example, in GBMs, different populations of

tumour cells can cooperate each other or with cells from the microenvironment (e.g. astrocytes) in order to promote ANLS-like interactions (Turner & Adamson, 2011), mimicking normal brain homeostasis.

1.4. Spreading and dissemination

Cancer cells can disseminate from primary foci and generate secondary ones, and metastasis is the most common mechanism for this event. Metastasis increases cancer-associated death as a consequence of the generation of secondary tumours in vital organs. For example, about 70% of colorectal cancer patients develop metastasis, being these metastases associated to a decreased in 5-year survival rate (around 14%) compared to regional/localized tumours (70-90%) (*NIH - National Cancer Institute (Colorectal cancer) webpage*, 2020). However, not all tumours disseminate to distant organs. In particular, CNS tumours rarely generate ENMs (*extra-neural metastases*). Nevertheless, they have a high capacity to infiltrate into the surrounding areas and create secondary foci (Lun et al., 2011). Still, it remains controversial if this should be considered metastasis. Most authors refer to it as dissemination/spreading. Similarly, some other solid cancers, such as prostate (Datta et al., 2010) or salivary gland (Bhattacharyya & Fried, 2002) tumours, also display regional dissemination and nodal metastasis in surrounding tissues or lymphatic nodes, in addition to the generation of distant metastasis.

However, both dissemination and metastases are usually inefficient. It is required a high cell plasticity for local invasion and penetration, including attachment and adhesion, as well as ECM degradation and migration, intravasation into nearby vessels, transit of cells through the circulatory system (CTCs), extravasation into a novel parenchyma, and adaptation plus seeding by forming small nodules (micro-metastases), which grow leading to macroscopic tumours, reactivating all the mentioned hallmarks to be adapted to the new niche pressure (*Figure VII*) (Hanahan & Weinberg, 2011). This requires not only cell migration and invasion, but also cell fate control, quiescence/dormancy *vs*. proliferation.

1.4.1. Cell adhesion

Cell adhesion is important for both embryonic and adult physiology and in pathologies. In most cancers, cell-cell and cell-ECM interactions are mainly linked to survival, proliferation and motility. Epithelial cells, tightly packed in tissues, form layers with specific polarity and have different structures for cell adhesion, being of special relevance tight junctions, adherens junctions and focal adhesions (*Figure VII*).

Tight junctions regulate the selective transit of ions and solutes, cell polarity and signalling pathways via protein recruiting. Claudins, occludins and ZO-1/2/3 proteins

are their main components and mediate their interaction with the cytoskeleton and other proteins (Bhat et al., 2019). Cancer-associated disruption of tight junctions yields malignant transformation, proliferation and spreading (Bhat et al., 2019). For example, Claudin-1 overexpression has been linked to the repression of a pro-invasive mesenchymal phenotype in gliomas and ZO-1 upregulation.

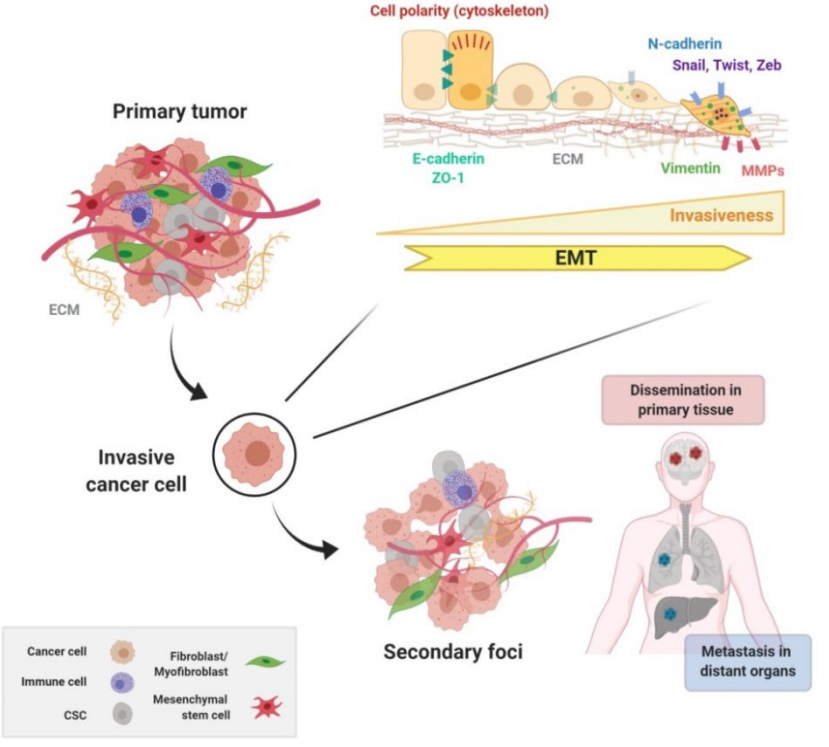

Figure VII – Cancer dissemination in primary tissue and/or metastasis to distant organs: role of epithelial to mesenchymal transition (EMT). For dissemination, cancer cells need to acquire specific features, such as invasive capacity, extracellular matrix degradative ability or adaptation to new microenvironments. The EMT process is the set of cellular changes that allow the conversion of epithelial cells to mesenchymal ones and, consequently, it plays a role in the disseminative process. *MMPs: matrix metalloproteinases; ECM: extracellular matrix; CSC: cancer stem cell.*

Adherens junctions are formed by cadherins (calcium-dependent hemophilic binding proteins). In particular, E-cadherin is the main coordinator of the epithelial phenotype. It accumulates in adherens juctions, forming macro-protein complexes that regulate actin cytoskeleton organization and cell polarity (Gloushankova et al., 2017). Non-phosphorylated β-catenin interacts with and stabilizes E-cadherin, while its phosphorylation or E-cadherin downregulation lead to β-catenin release (Wijnhoven et al., 2000). Free excess β-catenin is usually degraded, but Wnt and RTK pathways induce its nuclear translocation and β-catenin-mediated transcription. In cancer, β-catenin activation is associated with invasiveness and proliferation

(Wijnhoven et al., 2000). N-cadherin is the second most characterized cadherin in tumour cells. It is expressed in mesenchymal cells, promoting migration and invasion, for example, by interaction with RTKs (e.g. FGFR) (Gloushankova et al., 2017). The potential roles of other cadherins (for example, VE-cadherin) in cancer need to be further studied.

Finally, focal adhesions are integrin-containing, multi-protein structures that contain talin, paxillin, VASP, vinculin or α-actinin, among other proteins, which form mechanical links between intracellular actin bundles and the ECM (Nagano et al., 2012) (Horton et al., 2015). Upon integrin activation, Src and FAK are recruited to focal adhesions, which promote cytoskeletal rearrangements, adhesion/migration or proliferation via small GTPases, such as Rho, Rac, Cdc42 or Rap (Nagano et al., 2012). Deregulation of these proteins is linked to metastasis and decreased survival in cancer (Zhang et al., 2019). During movement, focal adhesions undergo progressive cycles of assembly-disassembly (Horton et al., 2015). The strength of cell-ECM interactions is dependent on integrin expression, ECM composition and density, and assembly-disassembly rate, which determines migration track and speed (Friedl & Wolf, 2003) (Walker et al., 2018). Under low interaction conditions, focal adhesions are immature and unstructured and migration is inhibited. Under high interaction conditions, focal adhesions cannot be disassembled and migration is impaired. Only under moderate interaction conditions, adhesion structures coordinate with motility programs.

In GBM, it is important to point out that nervous tissues do not have an epithelial organization and CNS tumours are considered disorganized and aberrant. In spite of this, astrocytes are polarized cells expressing high levels of the mentioned adhesion molecules and matrix receptors and they communicate through cell-cell junctions (Iser et al., 2017).

1.4.2. Cell migration and invasion

Cell migration is the directed movement of cells in response to chemical and/or mechanical signals, while cell invasiveness requires an extra ability of migratory cells to navigate through the extracellular matrix within a tissue or to infiltrate neighboring tissues (*Figure VII*). Mesenchymal motility entails directional and individual cell movement, but amoeboid or collective movements should be considered, too (Friedl & Wolf, 2003). In all cases, migration and invasion requires high plasticity and coordinated regulation of diverse signalling pathways. The diversity in the mechanisms promoting migration/invasion of cancer cells decreases effectiveness of anti-metastasis treatments (Thiery et al., 2009) (Nieto et al., 2016).

Focussing on mesenchymal migration/invasion, the most accepted model determines five essential steps that implicate cytoskeleton reorganization, focal adhesions dynamics and small GTPases pathways involvement (Friedl & Wolf, 2003).

(i) First, actin protrusions are generated in the leading edge of the migrating cell, including lamellipodia, filopodia, pseudopodia, invadopodia and podosomes. This cell polarization and elongation is induced by growth factors, cytokines, chemokines and microenvironmental signals that promote phosphatidyl-inositols generation via PI3K and PI45K, activation of small GTPases, such as Rac, Ras, Cdc42 or Rho, among others that leads to the regulation to several signalling cascades.

(ii) Second, cells interact with ECM, so that outside-in integrin signalling induces the establishment of focal adhesions and signalling activation.

(iii) Then, surface proteases are recruited to these cell-ECM contacts and cleave ECM components, as well as pro-MMPs to release active MMPs. ECM degradation provides the space required for cell expansion and displacement.

(iv) This is followed by myosin II interaction with actin filaments and these actomyosin fibers control contraction. Two kinases are mainly implicated in this step: MLCK (*myosin light chain kinase*) and ROCK (*Rho-associated serine/threonine kinase*). MLCK is a calcium-dependent kinase that phosphorylates the MLC (*myosin light chain*), activating myosin II and actinomyosin contraction. This can be avoided by MLC phosphatases, which are inhibited by ROCK-dependent phosphorylation via Rho.

(v) Finally, the trailing edge is detached by focal contacts disassembly and integrins are internalized by endocytic vesicles.

This is retained in tumour cells, even though cancer alterations lead to an increased pro-migratory capacity in the absence of sufficient stop signals. Hence, deregulation of migratory mediators, such as Rac, Rho, ROCK, MLCK or MMPs, is linked to progression and worse prognosis in different cancers (Friedl & Wolf, 2003) (Horiuchi et al., 2003) (Wertheimer et al., 2012).

1.4.3. Matrix metalloproteinases

Proteolysis is a key step during both local migration and invasion. Among other proteases, MMPs (*matrix metalloproteinases*) are highly relevant in cancer. They belong to zinc-protease family, as well as ADAMs (*a desintegrin and metalloproteinases*) or ADAMTs (*ADAMs with thrombospondin motifs*), and share a common general structure based on a pro-peptide, only present in the pro-MMP form, the catalytic domain and a hemopexin-like C-terminal domain (Sternlicht & Werb, 2001). Pro-MMPs are enzymatically inactive due to the interaction of a cysteine

residue from the pro-domain with the zinc ion situated in the catalytic site, but this pro-domain is susceptible of proteolytic processing by other proteases, such as furin or activated MMPs, leading to MMP activation. MMPs are regulated at different levels, such as gene expression, cell-ECM interactions, compartmentalization, proteolytic processing, specific inhibitors (TIMPs (*tissue inhibitor of metalloproteinases*)) in response to GFs, cytokines or microenvironmental conditions (e.g. ROS) (Sternlicht & Werb, 2001). MMPs can also carry out catalytic-independent functions.

Fluorogenic *in vivo* evaluation demonstrates that tumours have increased MMP activity compared to healthy tissues and overexpression of several MMPs, including MMP-3, -7, and -14, results in carcinogenesis (Kessenbrock et al., 2010). Moreover, in several epithelial cancer models, MMP downregulation impairs tumour migration and metastasis. MMPs mediate ECM cleavage for cell movement and contribute to the release of pro-invasive/metastatic signals (e.g. TGF-β or EGF) from ECM, solubilisation and/or proteolytic activation (Friedl & Wolf, 2003). They also facilitate the generation of other bioactive compounds upon ECM degradation (Kessenbrock et al., 2010), promoting proliferation, survival or pro-inflammatory effects, too. Importantly, MMPs are implicated in E-cadherin/β-catenin regulation. Infiltrating stromal cells are the major source of MMPs in tumours, mainly inflammatory cells, but also cancer-associated fibroblasts, bone marrow-derived stem cells and endothelial cells (Kessenbrock et al., 2010). Inflammatory cells secrete MMPs that promote not only invasiveness, but also angiogenesis (Bergers et al., 2000). In spite of this, metastasis and tumourigenesis are not universally promoted by MMPs. For example, MMP inhibitors do not impair migration of lymphoma or esophageal cells (Friedl & Wolf, 2003) and MMP-8 secreted by neutrophils contributes to tumour suppression in carcinogen-induced skin cancer (Balbín et al., 2003). Consequently, MMP inhibitors have yielded inconsistent outcomes in cancer clinic, likely due to plasticity: loss of a particular mechanism related to motility results in migratory scape through alternative strategies (Friedl & Wolf, 2003) (Kessenbrock et al., 2010).

1.4.4. Epithelial to mesenchymal transition and similar processes

EMT (*epithelial to mesenchymal transition*) process is the set of cellular events that control the conversion of an epithelial cell into a mesenchymal one (*Figure VII*). Epithelial cells form packed layers in different tissues and they are characterized by apicobasal polarity and close cell-cell and cell-matrix contacts. Conversely, mesenchymal cells display a fibroblastic-like phenotype with low cell-cell contacts, absence of polarity and increased ability to migrate/invade. Thus, EMT involves a morphogenetic program that includes adhesive structures rearrangement, cytoskeleton reorganization and pro-migratory structures activation, among others,

which is controlled transcriptionally by EMT-associated transcription factors (Thiery et al., 2009) (Lamouille et al., 2014) (Nieto et al., 2016). EMT can be reversed by MET (*mesenchymal to epithelial transition*), being both programmes essential for some physiological processes and pathologies (*Box 2*).

BOX 2 – EMT in embryonic development, physiological responses and non-tumourigenic pathologies

Complementary cycles of EMT/MET are crucial during embryonic development for cell differentiation and three-dimensional organization of organs (Thiery et al., 2009). Primary EMT occurs early during the embryonic development: before implantation to give rise to the parietal endoderm and immediately after implantation, during gastrulation, to generate the mesoderm and for neural crest delamination from the dorsal neural tube. Secondary EMT of early mesodermal cells, condensed into transient epithelial structures (e.g. somites), generates mesenchymal cells, which differentiate into specific cell types. Tertiary EMT takes place in more specialized structures. For example, during the formation of the cushion mesenchyme that will give rise to cardiac valves precursors. Although all these EMT programs have features in common such as Snail expression and E-cadherin down-regulation, they are modulated by specific signals. For example, neural crest formation depends on the coordinated action of complementary gradients of signals such as FGF, Wnt, Notch, retinoic acid or BMP4 (Nieto et al., 2016).

Another important physiological function of EMT is tissue repair in response to damage (Thiery et al., 2009).

The EMT process is implicated in pathologies, such as fibrosis (Thiery et al., 2009). The excessive amount of extracellular matrix (e.g. collagen) secreted by myofibroblasts in fibrosis can lead to organ failure. A significant portion of these myofibroblasts arise through EMT. Hepatic stellate cells and other hepatic cells undergoing EMT are key mediators of liver fibrosis (Zeisberg et al., 2007) (Nieto et al., 2016).

EMT program dysregulation has been involved in cancer progression. In animal models and cancer cell lines, it was early demonstrated that EMT promotes invasiveness and metastasis (Pearson, 2019). Tumour EMT is conditioned by an intricate counterbalance between the internal growth pressure exerted by the expanding main tumour nest and the free edge of the tumour periphery. According to this, attenuation of cell proliferation correlates with invasive capacity and EMT in

certain cell contexts (Biddle et al., 2011) (Hosseini et al., 2016) (Hoang-Minh et al., 2018). Moreover, analysis of tumour subpopulations has demonstrated that cells undergoing EMT secrete signals to drive invasion in sibling epithelial populations, through EMT-dependent and –independent mechanisms, and to modulate stromal cells (Pearson, 2019). Importantly, in cancer, the mesenchymal state is associated to a higher disseminative ability and metastasis, but colonization and secondary foci growth requires EMT reversion through MET (*Figure VII*) (Tsai et al., 2012) (Stankic et al., 2013).

Direct evidence of EMT in human cancers has been difficult to obtain and it remains controversial for some authors. This difficulty is due to various reasons: (i) EMT is a dynamic, transient process, usually located in some specific areas or subpopulations of the tumour, (ii) lack of specific EMT-related signals, regulators and markers for each cancer context, (iii) similarities between mesenchymal cells derived from epithelial cancer cells and stromal cells such as cancer-associated fibroblasts, and, (iv) the unexpected role of EMT in early stages of tumourigenesis, even before detection of primary tumour (Nieto et al., 2016) (Pearson, 2019). Related to the latest, breast cancer studies suggest that a subpopulation of cells disseminate to distant tissues through EMT, even before the primary tumour is detectable, and they could be responsible for up to 80% of later metastasis (Hosseini et al., 2016). In spite of this, morphological evidence of EMT at invasive fronts of human tumours was obtained and, more recently, EMT signatures have been developed to score prognosis and drug sensitivity in cancer patients (Meng et al., 2014) (George et al., 2017).

EMT programme in cancer displays an inherent flexibility due to cell plasticity, tumour clonal diversity and cell context variations. Moreover, EMT cannot be longer considered a transition between two states. There are studies demonstrating the existence of intermediate and reversible stages, partial transitions (Shamir et al., 2016) and EMT-related processes, such as epithelial to ameboid transition, endothelial to mesenchymal transition or epithelial-derived mesenchymal cells to myofibroblasts transition (Friedl & Wolf, 2003) (Lamouille et al., 2014). All this complexity impairs the clinical use of EMT for therapy (Thiery et al., 2009) (Nieto et al., 2016).

Similar to other cancers, GBM high invasive capacity has been linked to EMT by some authors, although GBM cells are not epithelial. In addition, there are similarities between astrogliosis (abnormal expansion and activation of astrocytes in response to damage) and EMT, such as the role of TGF-β as an inducer of both processes and common markers (e.g. MMPs, ECM components or Vimentin) (Iser et al., 2017). In fact, the role of EMT in GBM dissemination is controversial due to two main reasons. First, bioinformatic analyses determine that, in terms of epithelial *vs.* mesenchymal phenotype, the majority of GBM tumour samples and cell lines have a pronounced

mesenchymal phenotype (Tso et al., 2006) (Iser et al., 2017), although it can be shifted toward a more mesenchymal one through an EMT-like process. Second, the molecular changes that define EMT in other tissues and tumours, such as “cadherin switch” do not necessarily occur in GBM upon EMT (Mikheeva et al., 2010) (Iser et al., 2017). Consequently, different terms are used to describe EMT-related phenotypic changes that specifically occur in GBM. The most relevant is “glial to mesenchymal transition”, which correlates with the upregulation of mesenchymal markers (equivalent to that observed upon EMT) and the additional downregulation of astrocytic/glial markers, such as GFAP, Olig2 or PDGFR (Mahabir et al., 2013) (Matias et al., 2017) (C. Chen & Wang, 2019). To underline the relevance of GBM molecular subtypes (classical, mesenchymal, proneural and neural) and potential phenotypic changes between them, the term‘‘proneural to mesenchymal transition” is also being considered of value (Fedele et al., 2019). All this points out that the EMT-like process in GBM can be partial or incomplete, with a high heterogeneity and plasticity and it can take place and be reverted many times along the malignant dissemination (Nieto et al., 2016). Therefore, the ‘‘EMT-like’’ term is likely the most suitable to be used in order to include all these dynamic data.

1.4.4.a. EMT-activating factors and signalling pathways

Several signals are involved in the regulation of EMT and EMT-like processes: growth factors (e.g. FGF, HGF, PDGF, EGF and VEGF), hypoxia, Wnt, TGF-β, chemokines (e.g. CXCL family), cytokines, Notch, Shh, BMPs and oestrogens (Thiery et al., 2009) (Lamouille et al., 2014). These canonical signals are correlated with enhanced migration/invasion in GBM (Iser et al., 2017). TGF-β (Joseph et al., 2014), CXCL12 and other chemokines (Gravina et al., 2017), and growth factors such as EGF or FGF (X. Wang et al., 2017) (Gargini et al., 2019) (Kowalski-Chauvel et al., 2019) are known to promote EMT in GBM cells. These EMT-inducing factors trigger different signalling pathways, such as ERKs, p38 MAPKs, JNKs, NFκB, Smad, Notch or Hh. They cooperate to promote specific EMT programs. For example, TGF-β facilitates EGF- or FGF-induced EMT mediated by ERKs in different cancer models (Shirakihara et al., 2011) (Uttamsingh et al., 2008). In HCC (*hepatocellular carcinoma*), cells undergo EMT in response to TGF-β when expressing CXCR4 chemokine receptor (Bertran et al., 2009). Time, spatial and tissue-specific regulation of EMT is also controlled by epigenetic changes, alternative splicing mechanisms, post-translational modifications and miRNAs (Thiery et al., 2009) (Lamouille et al., 2014) (Nieto et al., 2016).

1.4.4.b. Transcription factors driving EMT

The key regulators of EMT and EMT-like processes are the transcription factors that control this phenotypic transition at a transcriptional level, mainly Snail1, Slug (or

Snail2), Zeb1/2 and Twist1/2, but also KLF8, FoxC2, Prrx1 and others (Peinado et al., 2007). As they have distinct timing and expression profiles, their contribution depends on cell/tissue type and availability of partners and regulators. For example, Zeb1 is associated to colon cancer progression, whereas Zeb2 activates invasion in ovarian, gastric and pancreatic tumours (Peinado et al., 2007). A switch from Snail2/Zeb2 to Zeb1/Twist may underlie melanoma progression, too. Importantly, these transcription factors are regulated by post-translational modifications (Nieto et al., 2016). For example, Snail1 is susceptible of phosphorylation by GSK3β, leading to its degradation, but, complementary, GSK3β is regulated by EMT-activating signalling pathways such as Wnt, PI3K/Akt or NFκB (Yadi Wu et al., 2009). There are also increasing evidences of hierarchical expression control between them (Peinado et al., 2007) (Thiery et al., 2009). For example, Zeb1 expression is usually expressed upon Snail activation, although Zeb1 can be activated in tumours lacking Snail, too. In addition, not all these transcription factors are equally potent in repressing the epithelial phenotype and inducing mesenchymal properties, with Snail factors being potent epithelial repressors, but weaker mesenchymal inducers. All these EMT-associated transcription factors also play a role in GBM, highlighting Snail (Caja et al., 2018), Zeb-1 (Joseph et al., 2014) (Siebzehnrubl et al., 2013), Zeb-2 (Feng et al., 2019) and Twist-1 (Mikheeva et al., 2010) (Lamballe et al., 2016).

1.4.4.c. EMT markers and molecular changes

E-cadherin repression is a key EMT event, which is directly or indirectly controlled by most EMT-mediating transcription factors, which leads to adherens junction breakdown and β-catenin release (Thiery et al., 2009) (Gloushankova et al., 2017). In general, cell-cell and cell-matrix contacts are destabilized during EMT and proteins from cell junctions are downregulated, as described in previous sections (*1.3.1 and 1.3.2*). Thus, E-cadherin, ZO-1/2/3, some cytokeratins, occludin, claudin and other epithelial proteins, as well as β-catenin are repressed or re-localized upon EMT (Lamouille et al., 2014). This is accompanied by activation of the expression of mesenchymal markers. Specifically, E-cadherin downregulation is compensated by N-cadherin upregulation (“cadherin switch”), which generates weaker cell-cell interactions and promotes cell motility (Wheelock et al., 2008). It is important to point out that E-cadherin expression is limited, not only in GBMs, as it is only present in some epithelial and differentiated subsets of GBMs, but also in healthy brain, which cannot be considered an epithelial tissue. Moreover, N-cadherin may not change its expression upon EMT-like induction in GBM, although it can modify its cell distribution (Siebzehnrubl et al., 2013). This is why EMT-like processes in GBM are independent of the ‘‘cadherin switch’’, although it is denoted as the main marker of EMT in other cell types (Wheelock et al., 2008). EMT drives actin cytoskeleton reorganization, leading the generation of lamellopodia or spike-like actin-rich projections and actin

stress fibers formation. In addition, changes in intermediate filaments composition involved in cell migration and intracellular vesicle trafficking are induced (Lamouille et al., 2014). In particular, Vimentin upregulation is considered essential for EMT in some cell contexts (Ivaska, 2011). MMPs are also considered EMT positive markers in cancer (Kessenbrock et al., 2010).

1.4.4.d. Relationship between EMT and stemness

Cells undergoing EMT are considered to be susceptible of acquiring stem-like properties, in addition to therapy resistance (Thiery et al., 2009) (Lamouille et al., 2014).

EMT/MET cycles are produced during embryonic development, as previously described, and cells maintained in culture under stem conditions display EMT markers and maintain pluripotency and stem cell markers. Defined CSCs isolated from tumours express EMT markers (Mani et al., 2008), as well as, for example, breast cancer CSCs (that grow as mammospheres) display epithelial phenotype repression (Shipitsin et al., 2007). Consistent with this EMT-stemness relationship, differentiated cancer cells may suffer a transition to pro-migratory CSCs, enabling clonal expansion of certain oncogenic mutations, dissemination and later differentiation through MET for colonization of secondary locations (Nieto et al., 2016). However, a number of works have demonstrated that EMT is not necessarily associated to the acquisition of stemness properties (Celià-Terrassa et al., 2012) (Lamballe et al., 2016).

In GBM, EMT was also matched to the acquisition of GSC-like phenotype and/or treatment resistance in the majority of studies (Mikheeva et al., 2010) (Siebzehnrubl et al., 2013) (Meng et al., 2014) (Caja et al., 2018) (Kowalski-Chauvel et al., 2019). However, EMT-stemness link cannot be considered universal in this tumour (Lamballe et al., 2016).

1.4.5. Final steps of cancer dissemination and glioblastoma spreading particularities

Invasive cells can disseminate to adjacent tissues or enter into surrounding vessels (extravasation) leading to circulating tumour cells (CTCs). CTCs can interact with non-tumour cells and platelets, and they display anti-shear and anti-immune mechanisms (Dasgupta et al., 2017). A fraction of these CTCs is capable of entering into distant sites (intravasation), where they can persist, generating DTCs (*disseminated tumour cells*). DTCs may enter into a dormant state, characterized by a reversible growth arrest (quiescence) with lack of clinical symptoms and treatment resistance (Bragado et al., 2013) (Sosa et al., 2014). Different cancer types exhibit

discrete tissue preferences for metastasis (organo-tropism) due to specific gene expression, signal secretion patterns, stromal structure and accessibility ("seed and soil" hypothesis) (Obenauf & Massagué, 2015). For example, cancer cells metastasising in brain can favour pro-tumourigenic astrocytic populations, while decreasing anti-tumourigenic ones (Priego et al., 2018).

GBM aggressiveness correlates with its infiltrative and disseminative capacity, even being considered a ''whole-brain disease'', because the tumour easily mixes with normal tissue. Hence, surgical resection of tumour-bearing hemisphere does not avoid recurrence and most GBMs easily spread to contralateral hemispheres (Agarwal et al., 2016). Invasion is mainly performed along nerve tracts and meninges, but also through cerebrospinal fluid and brain blood vessels (Van Meir et al., 2010). Disseminative cells hide in brain tumour-distant areas, where they cannot be removed by surgery, rather than in perivascular areas, as seen in brain metastatic cells, too. These niches are characterized by BBB integrity, which interferes with treatment delivery. A low proliferative rate, similar to that found in dormant phenotypes in other tumours (Tong et al., 2018), and GSC-related properties have been associated to these invasive GBM cells (Van Meir et al., 2010) (Agarwal et al., 2016). Consequently, upon specific signals, these resistant cells can reactivate proliferation and give rise to recurrent tumours.

Interestingly, GBM cells do not usually scape from brain parenchyma and ENMs (*extra-neural metastases*) rate is very low (around 0.5%), generally occurring after craniotomy/shunting (Lun et al., 2011). Brain environmental properties and BBB function condition this event. Fast progression of primary neural locations and patients' premature deaths after diagnosis also compromise ENM growth and detection. Importantly, CTCs in peripheral blood are detected in GBM and other gliomas, and they have been proposed as potential clinical tools for tumour monitoring (Gao et al., 2016).

1.5. Cell signalling pathways involved in glioblastoma

As seen above, cancer presents an altered signalling communication between and within cells. Aberrations in signalling pathways are pleiotropic and complex, but RTKs, MAPKs and small GTPases, included Rap, are particularly relevant.

1.5.1 Receptor Tyrosine-kinases

Humans have 58 known RTKs (*receptor tyrosine-kinases*), classified into twenty subfamilies: EGFR (or ErbB), IR, PDGFR, VEGFR, FGFR, PTK7, Trk, ROR, MusK, Met, Axl, Tie, Eph, Ret, Ryk, DDR, ROS, LMR, Alk and Styk (*Figure VIII*) (Lemmon & Schlessinger, 2010).

RTKs display a similar structure that includes a ligand-binding region in the extracellular domain, a single transmembrane helix and a cytoplasmic region that contains the tyrosine kinase domain and additional C-terminal regulatory regions. RTKs intracellular regions allow their interaction with a wide array of proteins through different protein-protein binding domains, leading to the activation of several signalling pathways such as Ras/ERK, p38 MAPK, PI3K/Akt or JAKs/STATs, among others. Thus, RTKs are essential signalling hubs for cells, both under physiological and pathological conditions. Here, we will focus on two important RTK families in cancer and, in particular, in GBM: EGFR and FGFR.

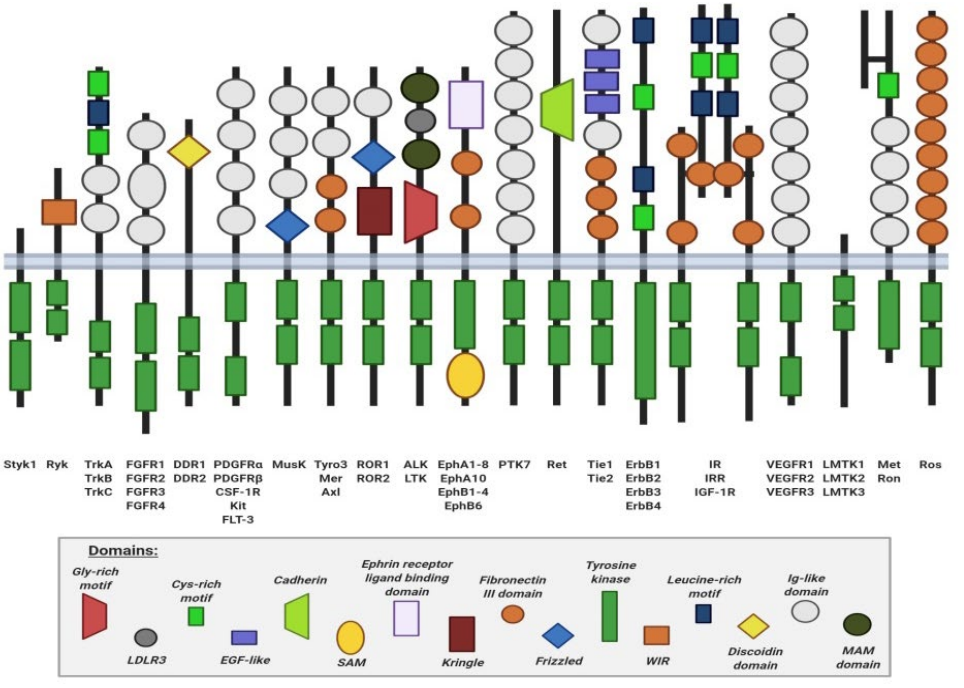

Figure VIII – Receptor tyrosine kinases (RTKs): subfamilies and domains. Twenty subfamilies of RTKs have been described. They all display auto-kinase activity, leading to the recruitment and/or activation of several downstream effectors. Adapted from Lemmon & Schlessinger, 2010. *LDLR3: low-density lipoprotein receptor repeat 3; SAM: sterile alpha motif.*

1.5.1.a. EGFR subfamily

EGFR subfamily encompasses four RTK members: EGFR (also known as ErbB1 or Her1), ErbB2 (Her2 or Neu), ErbB3 (Her3) and ErbB4 (Her4) (Zahonero & Sánchez-Gómez, 2014). EGFR is a transmembrane receptor for ligands from EGF family, which includes EGF, TGF-α (transforming growth factor-α) and HB-EGF (heparin-binding EGF). Ligand binding to the receptor induces its dimerization, auto-phosphorylation at intracellular residues Y992, Y1045, Y1068, Y1148 and Y1173,

leading to its activation. Then, adaptors and signalling molecules are recruited, triggering the activation of several downstream signalling cascades, such as ERKs, JNKs, p38 MAPKs, PI3K/Akt, JAKs/STATs, PLC/PKC or TyrKs (tyrosine kinases) such as Src (*Figure IX*). In this way, several cellular functions are regulated through the control of gene expression and the activity of different proteins.

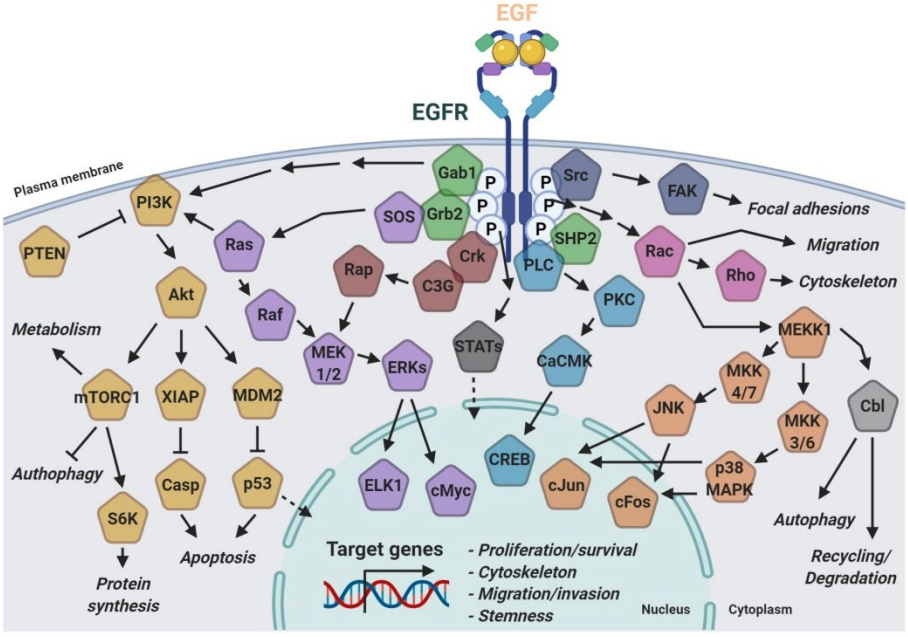

Figure IX – EGF/EGFR signalling: most relevant downstream pathways and functions. EGF binding to its receptor induces EGFR dimerization, auto-phosphorylation at intracellular residues and activation, promoting the recruiting of different signalling adaptors and macro-protein complexes. This leads to the activation of several signalling cascades (*indicated in different colours in the scheme*), which mediate a wide range of cellular functions (e.g. invasion/adhesion, proliferation or stemness), not only by regulating protein activity, but also through transcriptional regulation. *P: phosphorylated-tyrosine.*

EGFR compartmentalization allows its controlled localization in specific plasma membrane domains, such as lipid rafts, caveolae or clathrin-rich regions, as well as in intracellular membranes, determining the receptor exposure to different signalling platforms (signallosomes) (Tomas et al., 2014) (Zahonero & Sánchez-Gómez, 2014). EGFR signalling can be regulated by endocytosis followed by either receptor degradation or recycling. Upon ligand binding, plasma membrane EGFR is dimerized and autophosphorylated, leading to the binding of different adaptors and signalling molecules. In addition, E3 ubiquitin ligase Cbl is recruited by different EGFR-binding proteins, such as Grb2, which enables receptor ubiquitination. Ubiquitinization is a key post-translational modification involved in EGFR endocytosis, since ubiquitinated residues allow the interaction of EGFR with endosome-forming proteins from both

CME (*clathrin-mediated endocytosis*) and CIE (*clathrin-independent endocytosis*) pathways (Tomas et al., 2014). CME is the major endocytic pathway in mammalian cells and it occurs via the assembly and maturation of clathrin-coated pits that concentrate cargo as they invaginate and pinch off to form clathrin-coated vesicles. AP2 and dynamin are two key mediators of CME, while CIE pathways include dynamin-dependent (e.g. caveolae endocytosis) and dynamin-independent (e.g. macropinocytosis) mechanisms. CME is slower and favours cargo recycling to plasma membrane. In contrast, CIE acts faster and induces cargo degradation. In general, in the case of EGFR, strong stimuli, such as high ligand concentrations or potent ligands, induce CIE and signal attenuation, while CME promotes signal prolongation. Both mechanisms cooperate to maintain EGFR signal homeostasis (Tomas et al., 2014). Cancer-associated trafficking defects result in EGFR mislocalization and signalling deregulation. First, certain EGFR mutations are known to affect its trafficking, such as EGFRvv, mainly inhibiting Cbl capacity to ubiquitinate it. Second, trafficking controllers are regulated during tumourigenesis, such as Sprouty-2. Cancer-induced Sprouty-2 downregulation promotes EGFR endocytosis via CME and its recycling, prolonging its signal to induce cell proliferation and invasion. Finally, EGFR endocytosis is also regulated by certain anti-cancer treatments, being EGFR trafficking a novel target that could allow improvement of anti-EGFR treatments efficacy and avoid resistance.

EGFR is over-activated in many cancers, including GBM (Zahonero & Sánchez-Gómez, 2014). This is not only a consequence of *ERBB1* amplifications (found in around 30-40% of GBM patients), but it is also induced by overexpression of ligands and the receptor, alterations in downstream effectors and regulators, and mutations (e.g. EGFRvIII, a constitutively- active form of EGFR, or EGFRvv, an internalization-deficient EGFR truncated form). As it occurs in other cancers (Cowden Dahl et al., 2008) (Uttamsingh et al., 2008), EGFR upregulation has been associated to GBM initiation, GSC phenotype maintenance, tumour growth, invasion/dissemination, mainly through EMT induction, and chemo-/radio-therapy resistance (Zahonero & Sánchez-Gómez, 2014) (X. Wang et al., 2017). However, EGFR role in cancer seems to be more complex. This is why EGFR-targeted therapies had a promising potential in cancer, and in particular, in GBM, but their benefits are irregular. EGFR mutation status, ligand-independent activations, kinase-independent signalling mechanisms and alterations in downstream effectors or compartmentalization of regulators (e.g. Cbl, MIG-6 or Sprouty proteins) have been demonstrated to condition anti-EGFR therapies (Zahonero & Sánchez-Gómez, 2014). Moreover, EGFR-targeted treatments can also induce resistance due to RTK capacity to interact with and co-regulate other RTKs, leading to high signalling plasticity and compensatory mechanisms via alternative RTKs (Lemmon & Schlessinger, 2010) (P. A. Clark et al., 2012)

(Izumchenko et al., 2014) (Zahonero & Sánchez-Gómez, 2014). Synergistic approaches are being studied, although their clinical applications are complex.

1.5.1.b. FGFR family

Generally, in cancer, but particularly in GBM, the role of FGFRs has been widely studied. There are four transmembrane FGFRs, FGFGR1, FGFR2, FGFR3 and FGFR4, in addition to the soluble FGFRL1 (antagonist) (Jimenez-Pascual & Siebzehnrubl, 2019). All of them have different splicing forms associated to specific cell phenotypes, which differ in their intrinsic properties. For example, mesenchymal cells up-regulate FGFR1β, an isoform with a higher ligand sensitivity compared to FGFR1α. In humans, 22 members of the FGF ligand family have been identified so far. Their binding to FGFRs is regulated by ECM components, mainly heparin sulfate, and co-receptors. Upon FGF-FGFR interaction, the receptor dimerizes being activated by autophosphorylation. This triggers different signalling pathways, such as Crk/Rac/JNK, FRS2/Grb2/SHP2/ERKs, FRS2/Grb2/Gab1/PI3K/Akt or PLC/PKC, which activate proliferation, survival, cytoskeleton organization or migration, among others (*Figure X*). FGFR internalization and degradation are also important for the control of signal intensity and function, highlighting the role of Sprouty family proteins.

In GBM patients, somatic mutations, deletions or amplifications of *FGFR* genes can be found in some cases, although alterations of their expression and activity are more common. They mediate tumour onset and GSC phenotype, growth, migration, therapy resistance, angiogenesis and stromal regulation, as in other cancers (Watcharin Loilome, 2009) (Shirakihara et al., 2011) (Jimenez-Pascual & Siebzehnrubl, 2019). Indeed, FGFRs are essential in CNS development, and GBM cells employ these developmental mechanisms to their benefit. FGFR1 is highly associated to GBM progression, since its expression correlates with tumour grading (particularly, FGFR1β isoform), and it promotes dissemination, mainly in response to FGF-2 (Watcharin Loilome, 2009). Non-canonical FGFR activation by interaction with other RTKs such as EphA4 has been also demonstrated (Fukai et al., 2008). Moreover, FGFR1 is preferentially found in GSCs, leading to SOX2, Olig2 and Zeb1 expression (Kowalski-Chauvel et al., 2019). In contrast, FGFR2 loss correlates with bad prognosis and it is mainly caused by chromosome-10 deletion. Interestingly, FGFR3 levels are 5-fold higher in invading GBM cells than in the tumour core, while FGFR4 expression in GBM remains controversial (Jimenez-Pascual & Siebzehnrubl, 2019).

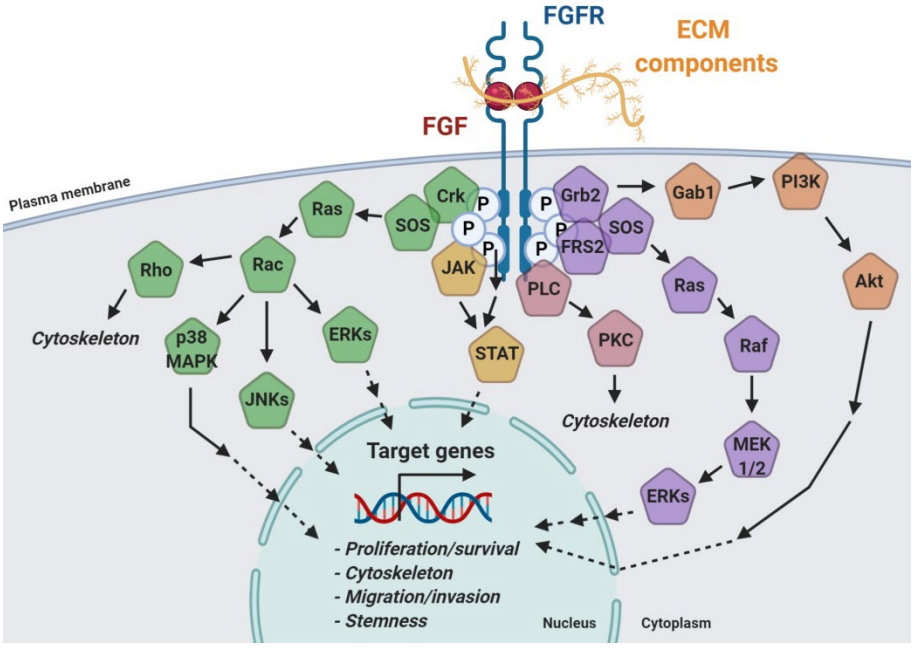

Figure X – **FGF/FGFR signalling: most relevant downstream pathways and functions.** FGF binding to its receptor, facilitated by diverse matrix components, induces FGFR dimerization, auto-phosphorylation at intracellular residues and activation. Through protein recruitment and protein macro-complexes formation, FGF/FGFR signalling induces the activation of several well-established cascades (*indicated in different colours in the scheme*). They are responsible for the regulation of several functions through modulating protein activity and/or transcription. *ECM: extracellular matrix; P: phosphorylated-tyrosine.*

As mentioned before, different studies have demonstrated the existence of complex interactions among RTKs in cancer cells. Thus, FGFR has been recently pointed out as an effective target for anti-EGFR and anti-Met resistant GBMs (Day et al., 2020).

1.5.2. MAPK superfamily

MAPK (*mitogen-activated protein kinase*) pathways are evolutionarily conserved three-step kinase cascades (MAPKKK, MAPKK and MAPK), regulated by scaffold proteins and phosphatases, which link extracellular signals to the machinery controlling different cellular functions (Cargnello & Roux, 2011). This is conditioned by cell type specifications, temporary and strength properties of each activating signal and cascade localization within the cell (cytosol, plasma membrane, endomembranes or even the nucleus).

MAPKs are activated upon dual phosphorylation of threonine and tyrosine residues in the activation loop by a MAP kinase kinase (MKK), which is activated when phosphorylated by a MAPK kinase kinase (MKKK) (Cargnello & Roux, 2011). In mammals, there are more than a dozen of MAPK genes codifying for different MAPKs. Classical MAPKs are the best known subfamilies, which includes: ERKs (ERK1/2), mainly activated by growth factors, and stress MAPKs that were initially described as kinases activated mainly by stress. The latest comprise JNKs (c-Jun N-terminal Kinases), JNK1/2/3, and p38 MAPKs with four isoforms: p38α, p38β, p38γ and p38δ (Cargnello & Roux, 2011).

1.5.2.a. ERKs

ERKs (ERK1/2) are ubiquitous serine/threonine MAPKs mainly activated by growth factors via RTKs, although they are also activated by integrins, G-coupled receptors, cytokines and other extracellular signals (Marampon et al., 2019). In a simplified model, ligand binding to RTKs promotes Raf (a MAPKKK) activation by Ras (via Grb2/SOS/Ras), which phosphorylates MEK1/2 (MAPKKs) in Thr residues. Then, MEK1/2 leads to ERKs dual phosphorylation, and active ERKs phosphorylate numerous cytoplasmic and nuclear targets, including kinases, phosphatases, transcription factors, pro-/anti-apoptotic factors or cytoskeletal proteins. ERKs are over-activated in the majority of cancers due to alterations at different steps of the pathway, such as RTK overexpression, Ras or Raf mutations or targets deregulation (Marampon et al., 2019). ERK signalling has been classically associated to survival and proliferation, although more recently it has also been linked to stemness maintenance, migration, angiogenesis, hypoxia response or therapy resistance, too. However, under certain conditions, ERKs activation is sustained, promoting anti-tumour functions, such as differentiation or senescence. In GBM, ERKs over-activation has been detected in both primary tumours (mainly in zones associated to vasculature) and in disseminative cells surrounding the peri-tumour area (Lama et al., 2007). Moreover, ERKs activation correlates with bad prognosis and therapy resistance (Day et al., 2020). Although ERKs inhibition decreases proliferation and migration in *in vitro* assays (G. Guo et al., 2013), it induces null or moderate benefits in clinic due to resistance elicited by different mechanisms. The sub-classification of tumours based on their Ras mutational status may increase clinical results (Sullivan et al., 2018).

1.5.2.b. p38 MAPKs

p38 MAPKs are serine/threonine MAPKs activated by dual phosphorylation in TGY motif (Cuadrado & Nebreda, 2010) (Martínez-Limón et al., 2020). p38 MAPKs subfamily comprises four isoforms: p38α and p38β, which are ubiquitously-expressed, and p38γ and p38δ, with a more restricted expression. They are strongly activated,

not only by environmental stress signals (e.g. oxidative stress, cytokines or DNA damaging agents), but also by mitogens. Each signal presents specific mechanisms to activate a huge range of MAPKKKs, highlighting ASK1, DLK1, TAK1, MLK3 or MEKK3/4, which are known to activate MKK6, MKK3 and MKK4 (MAPKKs) through phosphorylation. Then, MAPKKs phosphorylate and activate p38s, which can phosphorylate both cytoplasmic and nuclear proteins, leading to regulation of multiple functions (Cuadrado & Nebreda, 2010). On one hand, p38α was first described as a tumour suppressor, since its activation induces apoptosis in non-tumour and tumour cells (Porras et al., 2004) (Bragado et al., 2007), as well as senescence and cell differentiation. p38α positively regulates cell cycle inhibitors implicated in cancer such as p53 or pRb and many chemotherapeutic agents require p38α activity to induce apoptosis (Bragado et al., 2007). On the other hand, different studies have demonstrated that p38α acts as a multitasking kinase that also promotes survival, proliferation, migration and therapy resistance, among others (Martínez-Limón et al., 2020). For example, p38α promotes tumour growth and migration/invasion in coloncarcinoma (Arechederra et al., 2015) (Priego et al., 2016) and its inhibition prevents breast and prostate cancer metastasis in bone marrow. The role of p38α in response to stress and, in particular to ROS, would be responsible for p38α-induced apoptosis and tumourigenesis prevention at early stages, while highly aggressive cancer cells uncouple p38α activation from ROS sensing (Dolado et al., 2007). Additionally, dormant DTCs depend on p38α upregulation, while their awakening correlates with ERKs activation (Bragado et al., 2013) (Sosa et al., 2014). In GBM, p38α upregulation correlates with dissemination and bad prognosis (Demuth et al., 2007) and it has also been implicated in ROS-induced GSC differentiation (Sato et al., 2014). In summary, several evidences indicate that p38α activity could impair tumour onset, while more advanced tumours may benefit from its activation in order to grow, interact with the stroma and metastasise. Ralimetinib is a promising p38 inhibitor tested in clinical trials for ovarian cancer, GBM and metastatic breast cancer, in combination with standardized therapies (Martínez-Limón et al., 2020).

1.5.3. Rap GTPases

Rap (*Ras-related protein*) subfamily belongs to Ras superfamily of small G proteins and it includes two subtypes, Rap1 and Rap2 (with a 60% homology), and five isoforms: Rap1A, Rap1B, Rap2A, Rap2B and Rap2C (Guo et al., 2016). As a small GTPase, Rap activation is induced by a conformational change that allows GTP binding, facilitating GDP release (*Figure XI*). This is facilitated by GEFs (*guanine-nucleotide exchange factor*) (e.g. C3G), while GAPs (*GTPase-activating protein*) increase endogenous Rap GTPase activity, leading to the hydrolysis of bound GTP to GDP. Thus, GEFs and GAPs specifically modulate Rap activation, signal duration and localization in response to different stimuli (*Figure XI*). These regulators can

discriminate between Rap subtypes and their expression pattern and their regulation through distinct mechanisms such as cyclic nucleotides (e.g. cAMP), protein-protein interactions, phosphorylation or calcium are tightly controlled by different extracellular signals.

The function of Rap proteins as tumour promoters or suppressors is controversial, with different studies describing paradoxical results. This may be dependent on cell type and/or activation insights and different Rap isoforms may lead to opposite outcomes. For example, Rap1 promotes Hepatitis B virus-induced HCC growth, but it inhibits other types of HCC, while Rap2B is upregulated in some HCC cells enhancing proliferation and migration (Sequera et al., 2018). Rap1 activation has been associated to tumour invasion in colon carcinoma (Priego et al., 2016) or prostate cancer (Bailey et al., 2009). On the other hand, both blocking Rap1 activation and expressing an active form of Rap1 reduce melanoma cells ability to metastasise in lung (Freeman et al., 2010). In leukaemia cells, Rap1 promotes migration upon CXCL12 stimulation only when it is properly translocated from endosomes to plasma membrane (Pye et al., 2013). This demonstrates the importance of Rap1 activation/deactivation cycles and its intracellular localization for cell migration.

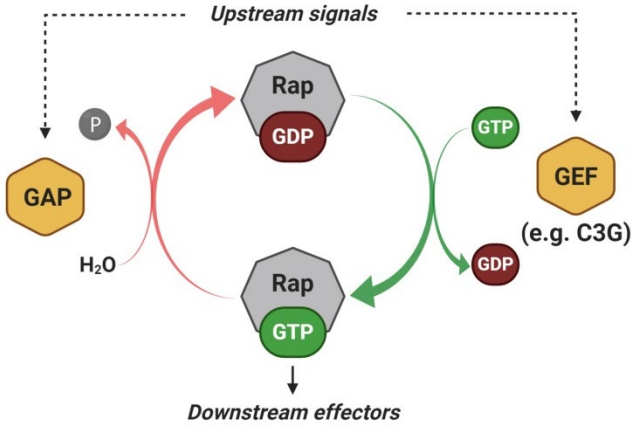

Figure XI – **Rap: activation/inactivation cycles and their regulation by GEFs and GAPs.** Activation of Rap is induced by GTP binding and GDP release. This process is facilitated by guanine-exchange factors (GEFs). Inactivation of these proteins is mediated by GTPase-activating factors (GAPs), which increase Rap endogenous GTPase, promoting the hydrolysis of GTP to GDP. *P: phosphate group*.

Not much is known about the role of Rap in GBM onset or progression. Rap1 has been involved in both GBM cell death (Moon et al., 2012) and proliferation (Sayyah et al., 2014). Rap1 also mediates PDGF-induced invasion via DOCK1 (Barrett et al., 2014), while Rap2A inhibits migration and invasion by down-regulating Akt activity (Lei Wang et al., 2014). Thus, the roles played by the different Rap family members in GBM are not clear, so further studies should be performed to clarify it.

2. C3G

C3G (*Crk SH3-domain-binding guanine-nucleotide-releasing factor*), also called RapGEF1, GRF2 and DKFZ p781P1719, is a GEF for small GTPases from Ras superfamily. It is ubiquitously expressed in mammalian cells and regulates important cellular functions (Tanaka et al., 1994) (V. Radha et al., 2011) . In humans, C3G is encoded by the *RAPGEF1* gene, which is located at chromosome 9 (position 9q34.3) and comprises 24 exons, spanning 163 kb (Takai et al., 1994).

BOX 3 – Crk beyond C3G: structure, signalling and function

Crk adaptor proteins (Crk and CrkL) are integral mediators of signal transduction, acting as convergence points of tyrosine kinase pathways and protein-protein interactions (Birge et al., 2009). *CRK* gene was discovered as a viral transforming gene encoding v-Crk protein, and, later, human *CRK* gene, encoding the alternative spliced CrkI and CrkII isoforms, and *CRKL* gene were identified. Crk modular structure is composed by a SH2 domain and SH3 domains (one in CrkI and two in CrkII and CrkL, named as SH3N and SH3C) separated by a flexible linker sequence containing a tyrosine residue that negatively regulates Crk function as an adaptor protein when phosphorylated. c-Abl is the main upstream kinase involved in CrkII phosphorylation. The lack of this negative regulatory mechanism in CrkI has been associated to its transforming capacity. When active, Crk proteins modulate multiple effectors, such as p130Cas, C3G, SOS, RTKs or c-Abl through interaction with them. The variety of Crk-interacting proteins, not only amplifies its signal, but also controls its subcellular localization and promotes the activation of specific signalling downstream pathways. Thus, Crk and CrkL play essential roles in proliferation, cytoskeleton organization, cell adhesion and migration, apoptosis or endocytosis of parasites. Importantly, Crk is known to be overexpressed in multiple carcinomas linked to an aggressive progression and increased motility, such as ovarian cancer or GBM.

C3G was originally discovered as a Crk-binding protein (*Box 3*) with potential GEF activity (Tanaka et al., 1994). C3G was first described as a 1077 residues protein with a 121 kDa predicted molecular weight, although *in vitro* translation resulted in a 130-140 kDa protein encoded by a nucleotide sequence containing a 3231 bp open-reading frame (Tanaka et al., 1994). Importantly the CDC25H (*CDC25 homology*)

domain was early detected in C3G protein (Tanaka et al., 1994) (Guo et al., 2016) and its GEF activity was confirmed. This domain was originally identified in the yeast CDC25 protein and it is conserved in Ras GEFs, such as SOS1/2 or Epac, being responsible for their GEF activity. C3G displays higher GEF activity over Rap1A/B proteins than over other members of Ras superfamily (T Gotoh et al., 1995). C3G also activates R-Ras (Takaya Gotoh et al., 1997) (Ohba et al., 2000) (Sasi Kumar et al., 2015), R-Ras2/TC21 (Ohba et al., 2000) or TC10 (Chiang et al., 2001), among others (V. Radha et al., 2011). C3G does not appears to regulate Rap2 (Van Den Berghe et al., 1997), H-Ras, K-Ras or R-Ras3/M-Ras (T Gotoh et al., 1995) (Van Den Berghe et al., 1997) (Ohba et al., 2000).

Due to this ability to regulate small GTPases, which are important signalling hubs, C3G has been implicated in different cellular functions, as it will be detailed below. However, C3G can also exert effects through mechanisms independent of its GEF activity (Guerrero et al., 1998) (Shivakrupa et al., 2003) (Guerrero et al., 2004) or even can have an opposite effect to that of Rap1 (Gutiérrez-Uzquiza et al., 2010). The contribution of the CDC25H region of C3G to its actions has been largely evaluated by comparing the functional effect of the overexpression of full length C3G (C3G-FL) and two deletion mutants of C3G: C3G-Cat that contains exclusively the catalytic CDC25H region of C3G and C3G-ΔCat, lacking CDC25H region (*Figure XII*) (Guerrero et al., 1998) (Shivakrupa et al., 2003). These studies revealed that C3G GEF activity is not always necessary for its actions and some effects rely on its ability to interact with other proteins (Shivakrupa et al., 2003) (Guerrero et al., 2004). Thus, the knowledge of C3G structure is essential to understand its functions and signal transduction mechanisms.

2.1. C3G modular structure and isoforms

As mentioned before, Ras GEFs have a modular structure with conserved domains responsible for their GEF activity, such as CDC25H, and complementary regions that allow their interaction with other proteins, such as proline rich domains and with small regulatory molecules such as DAG (*diacylglycerol*) that interacts with C1 domains or cyclic nucleotides with CNB (*cyclic-nucleotide binding*) domains (Guo et al., 2016). This allows a specific response to different extracellular signals. In particular, C3G structure can be divided into the following regions (*Figure XII*):

- **(i)** N-terminal region, which contains an E-cadherin binding domain (Hogan et al., 2004), auto-inhibitory sequences (Ichiba et al., 1999) (V. Radha et al., 2011) and the recently described novel GEF-activating domain (Carabias et al., 2020).
- **(ii)** Central region with several proline rich sequences, also named SH3-binding domains, (P0-P4) that allow interaction of C3G with SH3 domains from

other proteins such as Crk, p130Cas, Hck or c-Abl (Knudsen et al., 1994) (Shivakrupa et al., 2003) (V. Radha et al., 2011). There is also a tyrosine residue (Tyr504) susceptible of phosphorylation that regulates C3G activation (Ichiba et al., 1999). The central region of C3G also contains a region with an auto-inhibitory capacity, named AIR (*autoinhibitory region*) (Carabias et al., 2020). It is divided into CBR (*CDC25H binding region*)-AIR, located in P3 (residues 545-569), with the ability to interact with CDC25H module from C-terminal region, and IT (*inhibitory region*)-AIR, located in P4 (residues 570-646) and with the capacity to inhibit CDC25H activity.

(iii) C-terminal region, which is composed by the catalytic CDC25H domain and the REM module that together are responsible for the GEF activity of C3G (Tanaka et al., 1994) (Guo et al., 2016) (V. Radha et al., 2011).

C3G has been studied, both in humans and rodents, because its conservation degree among mammalian species is very high, having a 86% homology between *Homo sapiens* and *Rattus novergicus,* and 92% homology between *Homo sapiens* and *Mus muscules* (V. Radha et al., 2011).

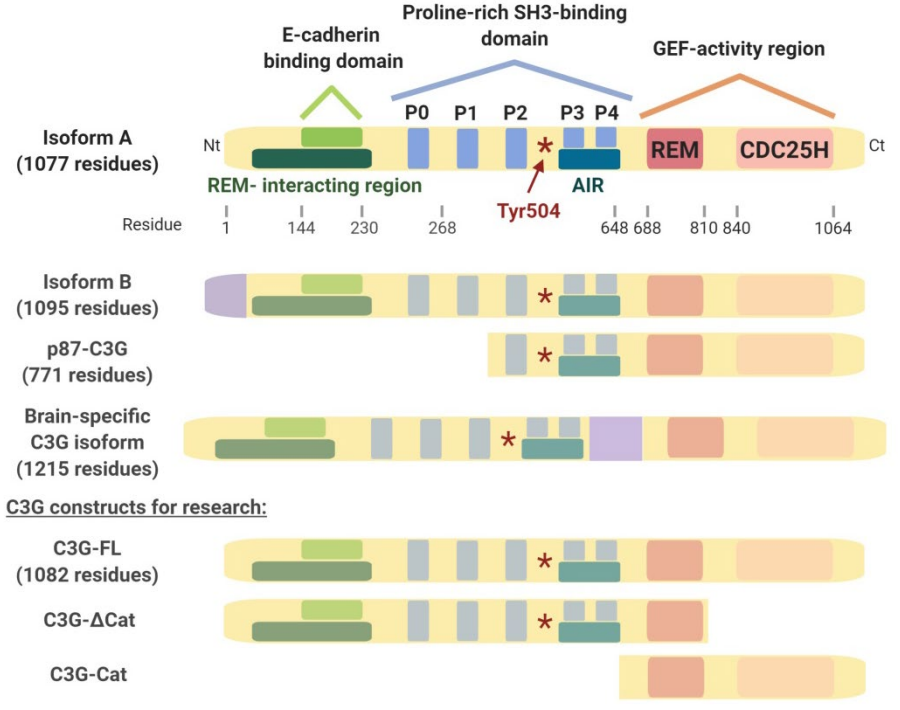

Figure XII – **Structure of C3G: isoforms and constructs used for research.** C3G domains from N-terminal to C-terminal: E-cadherin-binding domain and REM-interacting region; SH3-binding proline-riche domains (P0-P4) and autoinhibitory region (AIR); REM and CDC25H, both responsible for GEF activity of C3G. Red pin indicates the most well-established residue susceptible of phosphorylation: Tyr504. In isoforms with more aminoacids than isoform A, inserts are included in purple.

Since its discovery, the existence of C3G isoforms was described (Tanaka et al., 1994) (Guerrero et al., 1998). Two well-characterized isoforms that arise from C3G alternative splicing has been confirmed in humans. They differ in their N-terminal domain: 3 amino acids present in isoform A are replaced by 21 amino acids in isoform B (*Figure XII)* (V. Radha et al., 2011). They both generate polypeptides of around 140 kDa. Moreover, a CML (*chronic myeloid leukaemia*)-associated C3G isoform, known as p87C3G, has also been reported (Gutiérrez-Berzal et al., 2006). p87-C3G is a truncated isoform, whose sequence starts at Met306 residue, lacking the N-terminal region and the two first proline-rich sequences from the central region (*Figure XII*), but still able to interact with Brc-Abl oncogene through its third proline-rich sequence. Recently, a new brain-specific C3G isoform has been found in mouse and human tissues, but it remains undetectable in cell lines (Sriram et al., 2020). This isoform has an insert of 138 aminoacids in SH3-binding region (after P4, the fifth proline-rich sequence) due to alternative splicing, generating a polypeptide of 175 kDa. According to different protein databases and proteomic analyses (Cheerathodi et al., 2015), there are additional C3G isoforms that have not been characterized yet.

2.2. C3G regulation

C3G protein is ubiquitously expressed, but its levels vary in the different cell types and tissues. Even though little is known about C3G regulation in mammalian cells, it seems to be complex and context dependent.

At a transcriptional level, *in silico* analysis indicates that *RAPGEF1* promoter contains several binding sites for different transcription factors in the upstream and intergenic regions (*unpublished data from the group*). Although experimental validation is required for most of these sites, GATA-1 was demonstrated to induce C3G expression in megakaryocytes, promoting their differentiation (Ortiz-Rivero et al., 2018). Recent data also suggest that eIF3b, a translation initiation factor, could promote proliferation of CML cells through increasing C3G protein levels (Huang et al., 2020).

Although C3G expression is considered ubiquitous, there are important tissue and developmental specific differences. Hence, higher levels have been found in brain, skeletal muscle, fetal heart, lung and placenta (Tanaka et al., 1994) (Guerrero et al., 1998). According to databases, C3G expression is not directly affected by gender. However, C3G levels are regulated during several differentiation processes, such as neuroblastoma differentiation or monocytes differentiation to macrophages and in some pathologies, including cancer (V. Radha et al., 2011). As mentioned before, C3G transcripts are also regulated by alternative splicing, leading to different isoforms of the protein (Gutiérrez-Berzal et al., 2006) (V. Radha et al., 2011).

C3G does not present domains regulated by lipids, cyclic nucleotides or calcium, typically found in other Ras/Rap GEFs (Guo et al., 2016), but several regulatory sequences have been found. First, C3G GEF activity is negatively auto-regulated by a sequence located in the N-terminal region; as a consequence, C3G mutants lacking this sequence show a hyperactivation (Ichiba et al., 1999). However, a novel GEF activating domain from this N-terminal region has recently been described. It interacts with the REM module, but not with CDC25H, favouring C3G GEF activity (Carabias et al., 2020). Hence, point mutations in the REM residues mediating this interaction and C3G mutants lacking this N-terminal region, present decreased C3G-mediated Rap1 activation compared to wildtype C3G. In the central region of C3G there is also a GEF-regulating domain, named AIR. AIR interacts with and inhibits CDC25H, but Crk interaction with C3G breaks down this auto-inhibitory mechanism, facilitating the activation of C3G GEF activity (Carabias et al., 2020). Second, C3G is regulated by phosphorylation of, at least, Y504 residue by different upstream tyrosine kinases, such as Src, Hck or c-Abl, leading to an increase in C3G GEF activity (Ichiba et al., 1999) (Shivakrupa et al., 2003) (A. Mitra & Radha, 2010) (V. Radha et al., 2011). For example, Src-mediated C3G phosphorylation promotes C3G activation through alteration of the auto-inhibitory interaction between AIR and CDC25H domains (Carabias et al., 2020). Other tyrosine and serine residues of C3G are susceptible of being phosphorylated and they could be involved in its positive and/or negative regulation (Utreras et al., 2013) (*unpublished data from Guerrero's laboratory*). Finally, P0-P4 sequences from C3G central region mediate the interaction of C3G with proteins containing SH3 domains, such as p130Cas, Crk or c-Abl, leading to the formation of different protein complexes depending on stimuli and cell context (Wu et al., 2001) (Martín-Encabo et al., 2007) (Maia et al., 2013). For example, C3G is implicated in the formation of complexes that transduce RTK-activated signals and, therefore, C3G is regulated by growth factors (Lu et al., 2000) (Sakkab et al., 2000) (Chiang et al., 2001) (Kao et al., 2001). Other molecules that activate C3G are hormones (e.g. growth hormone), integrins, cytokines, chemokines or cadherins (V. Radha et al., 2011).

Both, Y504 phosphorylation and protein interaction, among other mechanisms, regulate C3G localization. C3G is usually located in the cytoplasm and its recruitment to the membrane is considered an activation mechanism (Guerrero et al., 1998). For example, Crk-C3G complex is preferentially located in the plasma membrane (Chiang et al., 2001), where C3G displays higher GEF activity (Ichiba et al., 1999). C3G has also been detected in cytoskeleton-related structures (V. Radha et al., 2004) (Martín-Encabo et al., 2007) (Sasi Kumar et al., 2015), Golgi (V. Radha et al., 2004) (Mitra et al., 2011) and, more recently, inside the nucleus (Shakyawar et al., 2017) (Shakyawar et al., 2018) (Nayak and Radha, 2019). Moreover, changes in location alters C3G access, not only to small GTPases and proteins containing SH3 domains, but also to

kinases and phosphatases that can act on it (V. Radha et al., 2004) (Martín-Encabo et al., 2007) (Mitra et al., 2011).

2.3. C3G physiological functions

According to its ubiquitous distribution within the organism, C3G regulates different functions both during embryonic development and in the adult stage through GEF-dependent and GEF-independent mechanisms (*Figure XIII*) (V. Radha et al., 2011).

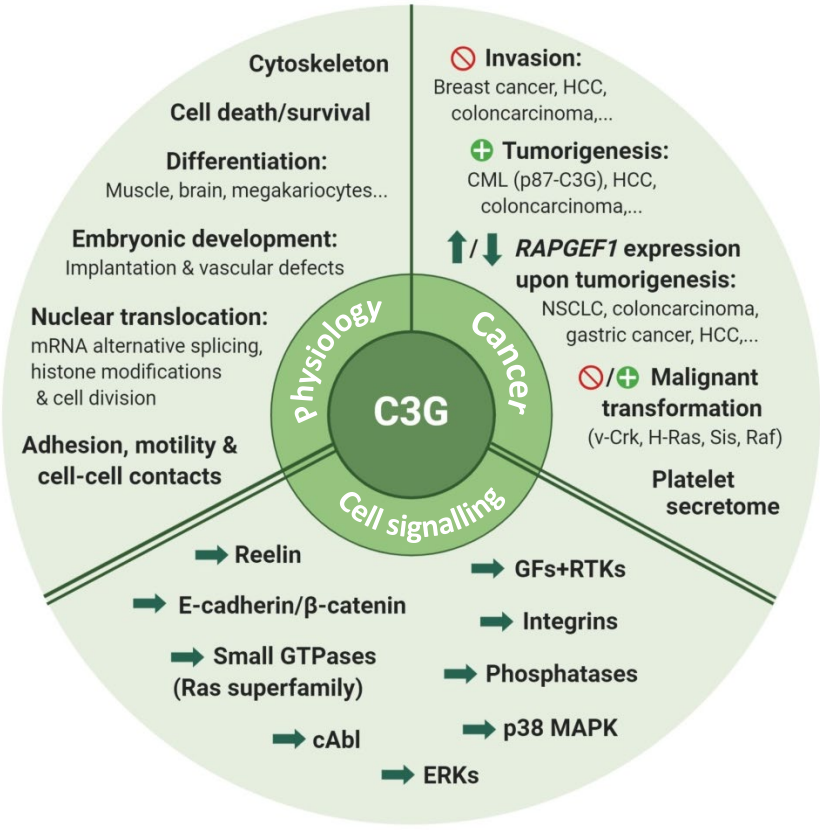

Figure XIII – **C3G functions: role in physiology and cancer. Cell signalling mechanisms controlled by C3G.** C3G is essential during the embryonic development and it plays diverse roles in cells under physiological conditions (e.g. cytoskeleton organization or cell-cell contacts promotion). Its role in tumourigenesis depends on cancer type and stage, although it has been described as an inhibitor of invasiveness and dissemination in several cancer types, such as breast cancer, hepatocellular carcinoma (HCC) or coloncarcinoma. C3G actions are mediated by different cell signalling pathways, whose activation/inactivation is controlled by C3G. *CML: chronic myeloid leukemia; NSCLC: non-small cell lung carcinoma; GFs: growth factors; RTKs: tyrosine-kinase receptors.*

C3G is essential for embryonic development, so that, C3G deficient (C3G-KO) mice die before embryonic day 7.5 (E7.5) due to problems in early implantation with

absence of typical fetal/placental structures likely caused by adhesion defects (Ohba et al., 2001). C3G-KO MEFs (*mouse embryonic fibroblasts*) isolated from these mice display Rap1-dependent impaired adhesion and accelerated migration. Moreover, hypomorphic $C3G^{gt/gt}$ mice, expressing less than 5% of total C3G, were also embryonic lethal, dying at E11.5-E14.5 due to defects in vascular supporting cells (Voss et al., 2003), even though other alterations in nervous system were also observed (Voss et al., 2006) (Voss et al., 2008) (Yip et al., 2012).

In the adult stage, C3G has also been involved in a wide range of cellular functions such as cell death/survival balance, control of adhesion and migration, proliferation and differentiation through interaction and/or regulation of different targets.

A reciprocal regulation between actin cytoskeleton and C3G has been shown. Hence, polymerized actin fibers enhance C3G effects and C3G regulates actin remodelling (V. Radha et al., 2004). Moreover, some proteins that interact with C3G are involved in the control of actin cytoskeleton, alone or in coordination with C3G, such as Crk (Birge et al., 2009) or c-Abl (V. Radha et al., 2007). These protein-protein interactions contribute to the regulation exerted by C3G on cell differentiation (V. Radha et al., 2008) (Dayma & Radha, 2011) (Sasi Kumar et al., 2015), vesicular trafficking (Chiang et al., 2001) or malignant transformation (Martín-Encabo et al., 2007). Moreover, C3G is a key regulator of adherens junctions and cell-cell interactions through regulation of the cytoskeleton, E-cadherin or Rap1 (Hogan et al., 2004) (Fukuyama et al., 2005) (Asuri et al., 2008) (V. Radha et al., 2011). For example, C3G can be located at focal adhesions, contributing to their stabilization (Voss et al., 2003). All this leads to an important role of C3G in integrin signalling, cell adhesion and migration under non-pathological cells. Hence, MEFs isolated from C3G-KO or $C3G^{gt/gt}$ mice show impaired adhesion, delayed spreading and accelerated migration (Ohba et al., 2001) (Voss et al., 2003). Accordingly, C3G knock-down in MEFs promotes migration and invasion through hyperactivation of p38α MAPK (Priego et al., 2016) and C3G overexpression in NIH3T3 fibroblasts increases adhesion (Guerrero et al., 2004). In some of these cases, Rap1 hyperactivation by other GEFs compensates C3G deficiency *in vitro*, but the tight regulation of small GTPases and their regulators may be responsible for avoiding these compensatory mechanisms *in vivo* (Ohba et al., 2001). C3G is also implicated in Lyn-activated integrin signalling and adhesion via Rap1 during chemotaxis of neutrophils (He et al., 2011). However, C3G cannot be considered a universal negative regulator of cell motility. For example, it has been involved in IGF1-induced cell migration (Guvakova et al., 2014) and in neuron migration during brain development (Voss et al., 2008) (Yip et al., 2012) (Shah et al., 2016).

C3G plays several cellular roles. It controls proliferation and survival/death balance in normal cells, displaying different functions that depend on the context and stimulus. Hence, in response to different stress stimuli, C3G knock-down in MEFs promotes either cell survival or cell death through enhancing p38α MAPK activity, independently of Rap1 (Gutiérrez-Uzquiza et al., 2010). C3G also promotes apoptosis through a mechanism dependent on Hck kinase activity (Shivakrupa et al., 2003) or c-Abl (A. Mitra & Radha, 2010). In injured cardiomyocytes, C3G silencing reduced survival through Bax regulation and ERKs inhibition (D. Yang et al., 2019).

C3G control of cell fate is important for some differentiation processes. For example, in neural progenitors, C3G induces p21 expression, an inhibitor of proliferation (V. Radha et al., 2008), so that, C3G-deficient mice present over-proliferation of some neural precursor populations, impairing their differentiation (Voss et al., 2006). In addition, C3G is involved in other steps of neural differentiation and bipolar morphology acquisition (Voss et al., 2008) (Yip et al., 2012) (Shah et al., 2016). C3G, upon its induction by GATA-1, also participates in mediating megakaryocytic differentiation (Ortiz-Rivero et al., 2018). Moreover, C3G is upregulated during skeletal muscle development, promoting myogenic differentiation and proliferation, and impairing cell death (Sasi Kumar et al., 2015).

Recently, new functions of C3G have been uncovered. Unexpectedly, endogenous C3G undergoes an exchange between cytoplasm and nucleus, which is involved in histone modifications repression associated with euchromatin (Shakyawar et al., 2017). Additionally, nuclear C3G binds to nuclear specs, regulating mRNA splicing (Shakyawar et al., 2018). It can also bind to mother centriole to control cell division (Nayak and Radha, 2019). All these new functions need to be further characterized in different cell types, as well as their functional relevance.

2.4. C3G in cancer and other pathologies

C3G widespread expression and its multiple physiological functions suggest the potential implication of C3G in different pathologies, such as cancer, although it needs to be confirmed for some of them. For example, SNPs (*single nucleotide polymorphism*) detected in the *RAPGEF1* gene sequence are associated to Diabetes type 2. C3G could also be involved in pathologies that arise upon chromosome-9 loss, where *RAPGEF1* gene is located. In addition, different experimental models indicate that C3G would be involved in glomerular nephritis and brain development disorders (Voss et al., 2003) (V. Radha et al., 2011).

Cancer is the pathology in which C3G involvement has been more widely studied. Nowadays, it is not possible to establish a common role for C3G in cancer, because it

seems to play different roles depending on the specific primary alterations, tumour stage and cell context, including microenvironment regulation (*Figure XIII*).

C3G is an important mediator of v-Crk-induced malignant transformation (V. Radha et al., 2011). In contrast, it inhibits malignant transformation induced by H-Ras, Sis, Raf or R-Ras oncogenes (Guerrero et al., 1998) (Guerrero et al., 2004) (Martín-Encabo et al., 2007). Hence, C3G overexpression results in inhibition of H-Ras-induced ERKs phosphorylation via phosphatase PP2A, p21 upregulation and cyclin A suppression, leading to a reduced anchorage-independent growth (Guerrero et al., 2004) (Martín-Encabo et al., 2007).

C3G can be upregulated or downregulated in tumours depending on tumour type and stage. For example, C3G levels increase in non-small cell lung cancer (Hirata et al., 2004). In addition, *RAPGEF1* gene presents a somatic demethylation associated to colon, gastric and ovarian cancers, which is usually associated to gene reactivation in cancer (Samuelsson et al., 2011). However, C3G has been shown to play a dual role in coloncarcinoma using *in vitro* and *in vivo* models (Priego et al., 2016). On one hand, C3G, in collaboration with p38α MAPK, promotes tumour growth, possibly by enhancing cell survival. On the other hand, C3G inhibits invasion, so that its down-regulation leads to a pro-migratory/pro-invasive phenotype mediated by p38α MAPK hyperactivation, characterized by MMP-2/9 upregulation, E-cadherin decrease and ZO-1 internalization. In cervical squamous cell carcinoma, C3G downregulation was initially linked to tumour growth (Okino et al., 2006), but later partially disproved (Samuelsson et al., 2011). In HCC, the analysis of public databases indicates that *RAPGEF1* mRNA levels increase in primary HCC patient samples as compared to healthy liver, and a high expression of *RAPGEF1* gene is associated with a reduced patient survival (Sequera et al., 2018). Moreover, C3G levels are increased in several human HCC cell lines and in mouse models of HCC, favouring tumour growth through the activation of survival and proliferation (Sequera et al., 2020). However, C3G inhibits invasion, so that, low levels of C3G enhance migration/invasion of HCC cells, facilitating cell dissemination and the generation of lung metastasis, although the growth of lung secondary tumours is associated to C3G upregulation, suggesting that C3G might be required for HCC proliferation and growth (Sequera et al., 2020). C3G also inhibits migration in breast carcinoma cells (Dayma & Radha, 2011), while it seems to promote metastatic spread of serous ovarian cancer via Rap1 (Che et al., 2015). Importantly, p87C3G isoform is overexpressed in CML cell lines and patient samples, being associated to CML development (Gutiérrez-Berzal et al., 2006). Bcr-Abl oncoprotein interacts with p87C3G and treatment with the Bcr-Abl kinase inhibitor, Imatinib, reverses p87C3G upregulation. In relation to this, C3G downregulation enhances Imatinib pro-apoptotic effect through the upregulation of p38 MAPK activity (Maia et al., 2009). C3G also regulates adhesion in K562 CML cells via p38α MAPK

regulation through the interaction with Bcr-Abl-containing complexes at focal adhesions (Maia et al., 2013). Recently, two missense mutations in AIR region of C3G have been found in non-Hodgkin's lymphoma patients (Y554H and M555K) that disrupt C3G auto-inhibitory mechanism, causing hyperactivation of Rap1 (Carabias et al., 2020), which might lead to lymphoma progression.

C3G is not only important in cancer cells, but also in the tumour stroma. In particular, C3G overexpression in platelets promotes angiogenesis and metastasis in a syngeneic model of melanoma by increasing the release of pro-angiogenic and pro-metastatic factors (Martín-Granado et al., 2017). This new function of platelet C3G in cancer is different from its role in platelet clotting previously described (Gutiérrez-Herrero et al., 2012).

Agonists and inhibitors of other GEFs have been tested in clinic, but C3G pharmacological regulation seems to be more complex due to its ubiquitous expression, its dual roles conditioned by cell context and its ability to display GEF-dependent and –independent functions (V. Radha et al., 2011). In spite of this, C3G cannot be totally discarded as a potential pharmacological target, although it is more plausible its potential value as a new cancer biomarker in clinic.

2.5. C3G in cell signalling

All physio-pathological functions of C3G mentioned above are coordinated by diverse complex signalling pathways, tightly regulated (*Figure XIII*). Some of them are more general, while others depend on cell context and microenvironment characteristics. Unfortunately, most of these signalling pathways and the mechanisms involved in their regulation have not been fully characterized yet.

Importantly, C3G is a mediator of RTK signal transduction. It has been involved in a wide range of functions elicited by RTKs such as EGFR (Okada & Pessin, 1997) (Lu et al., 2000) (Wu et al., 2001) (Kao et al., 2001), Met (Sakkab et al., 2000) (Sequera et al., 2020), Trk and TrkB (Lu et al., 2000) (Wu et al., 2001) (Kao et al., 2001) (Arévalo et al., 2006), FGFR (Lu et al., 2000), ALK (Schönherr et al., 2010), IGF1R (Guvakova et al., 2014), PDGFR (Voss et al., 2003) (Takahashi et al., 2008) or IR (Okada & Pessin, 1997) (Okada et al., 1998) (Chiang et al., 2001) pathways. In most of them, C3G is a Crk-interacting protein that connects RTKs to small GTPases activation and other signalling proteins. Depending on the stimuli and cell context, C3G can form different macro-protein complexes containing diverse proteins, including adaptors. Each complex can lead to the activation of specific pathways and/or functions. For example, in PC12 cells (embryonic rat neural cell line isolated from adrenal medulla), EGF, NGF and FGF-2 activate ERKs pathway, but the mechanisms and their effects differ notably (Lu et al., 2000) (Kao et al., 2001). EGF

promotes proliferation through transient activation of ERKs through SOS/Grb2/Ras and Crk/C3G/Rap1 pathways. Rap1 signal is downregulated by the interaction of EGFR with Crk/C3G/c-Cbl complex, promoting its ubiquitination, endocytosis and degradation. In contrast, NGF promotes neural differentiation through the initial activation of SOS/Grb2/Ras/ERKs pathway, followed by a sustained activation of Crk/C3G/Rap1/ERKs pathway. In this case, c-Cbl does not interact with Crk/C3G and Trk is not rapidly degraded. Finally, FGF-2 activates neural differentiation of PC12 cells inducing a sustained ERKs activation through a mechanism independent of C3G and Rap1. Therefore, it is not only important C3G involvement in each pathway, but also the proteins accompanying C3G in each case.

C3G is also important for Reelin/Dab1 pathway activation via Rap1. Hence, Reelin stimulation leads to C3G activation, so that C3G deficiency impairs Reelin signal transduction and function (Voss et al., 2008) (Yip et al., 2012). This pathway is essential for nervous system development, which will be further explained below.

C3G reciprocally regulates diverse kinases implicated in cell signalling, although some of the molecular mechanisms involved remain unclear. c-Abl is a SH3-containing cytoplasmic kinase that interacts with and regulates C3G at different levels, including phosphorylation, being both involved in common pathways (V. Radha et al., 2007) (A. Mitra & Radha, 2010). C3G also downregulates p38α MAPK activity, both under non-pathological (Gutiérrez-Uzquiza et al., 2010) and pathological conditions (e. g. CML and coloncarcinoma) (Maia et al., 2009) (Maia et al., 2013) (Priego et al., 2016). However, a direct interaction between C3G and p38 MAPK, forming complexes with paxillin and FAK in focal adhesions, has only been demonstrated in CML cells (Maia et al., 2013). Therefore, C3G/p38 MAPK relationship might be indirect in most cases and the function of C3G/p38 MAPK axis may depend on cell context and environment. Finally, different studies demonstrate that C3G inhibits ERKs activation. For example, this occurs upon its activation by Ras oncogene (Guerrero et al., 2004), likely through a mechanism dependent on PP2A activation and its recruitment to MEK/ERKs (Martín-Encabo et al., 2007), or upon stimulation with serum (Priego et al., 2016). In agreement with this, C3G knock-down reverses the inhibitory effect of Imatinib on ERKs (Maia et al., 2009). However, C3G promotes ERKs activation in injured cardiomyocytes (D. Yang et al., 2019). Thus, C3G/ERKs relationship might depend on the context. New studies in different cell types and with different stimuli are required to further characterize it.

As mentioned before, C3G interacts with E-cadherin through a specific domain present in its N-terminal region, leading to C3G relocalization, Rap1 activation and β-catenin degradation (Hogan et al., 2004) (Asuri et al., 2008) (V. Radha et al., 2011). β-catenin regulation by C3G is important for cerebral cortex development (Voss et al., 2006) and the enhanced migration observed in C3G-knock-down colon carcinoma

cells is associated with a reduction in E-cadherin levels (Priego et al., 2016). Moreover, a reciprocal negative regulation between C3G and β-catenin has been shown in highly invasive breast cancer cells (Dayma et al., 2012).

C3G is also a regulator of integrins, focal adhesions and filopodia, similarly to C3G interacting proteins (e.g. p130Cas or Crk) (V. Radha et al., 2011). Thus, C3G deficient cells lack integrin β1-positive focal adhesions, present a poor adhesion to certain extracellular matrixes (e.g. laminin) and a reduced spreading (Voss et al., 2003). Interestingly, the phenotype of C3G knock-out mice (Ohba et al., 2001) is similar to that of integrin β1 null mutants, so that KO-C3G mice embryonic lethality could be due to the absence of mature and stabilized focal adhesions.

C3G is also implicated in the regulation of phosphatases, so that C3G location regulates the recruitment of some phosphatases to a particular compartment and the substrate access. For example, the suppression of Ras-induced transformation by C3G is dependent on PP2A recruitment to the subcortical actin cytoskeleton, which is facilitated by its interaction with C3G, favouring ERKs dephosphorylation (Martín-Encabo et al., 2007). However, little is known about the phosphatases involved in C3G dephosphorylation. In the IMR-32 neuroblastoma cell line, C3G interacts with TC48, an alternative spliced isoform of tyrosine phosphatase TC-PTP, leading to C3G dephosphorylation in the Golgi (Mitra et al., 2011), but no further data are available.

2.6. C3G in the nervous system and brain

Even though C3G expression is ubiquitous in humans, differences are found among tissues. According to different studies (*Tanaka et al. (1994*), *Radha et al. (2011)*, *Cheerathodi et al. (2015))* and *ProteinAtlas database*, C3G levels are higher in fetal and adult brain compared to other tissues, both in humans and mice. However, C3G expression in specific areas or regions of adult brain has not been studied. Different databases (e.g. *GTExPortal* or *BioGPS* databases) point to slight differences among areas, but results are neither coincident nor conclusive. On the other hand, there is little information about C3G isoforms in the brain. In a Crk-binding proteome analysis, different C3G proteins were identified in murine embryonic (E16.5) brain as a result of RNA processing (Cheerathodi et al., 2015). Interestingly, by comparing C3G protein isoforms from embryonic brain and liver, it was determined that brain is more enriched in C3G isoforms that include the N-terminal region from isoform A of C3G (E-cadherin binding domain), suggesting that C3G could be involved in cell-cell and cell-matrix interactions in brain. Recently, a new brain-specific C3G isoform generated by alternative splicing has been described (Sriram et al., 2020). On the other hand, C3G in brain is susceptible of being regulated by different miRNAs, depending on particular SNPs found in the *RAPGEF1* sequence (Ramachandran et al., 2016).

C3G has been associated to important functions in the nervous system, mainly during embryonic development (*Figure XIII*). C3G$^{gt/gt}$ embryos display abnormalities in brain and nervous system development starting at E10.5 day. C3G is implicated in the regulation of the neural precursor population in the cortex. Hence, C3G depletion promotes proliferation via Akt/GSK3β/β-catenin axis deregulation and inhibits differentiation-associated migration in this area (Voss et al., 2006). In addition, in cortical neurons, C3G deficiency impairs precursors´ migration and cortical plate formation, as well as radial glial proper organization and attachment (Voss et al., 2008). In sympathetic ganglionic neurons, it regulates their positioning. C3G is highly expressed in the development of spinal cord, coordinating Reelin-promoted neural precursor's migration to the central channel (Yip et al., 2012). Moreover, conditional C3G-KO mice confirmed the role of C3G in different steps of cortical structure formation: migration of precursors from the ventricular zone for cortical plate formation, multi- to bi-polar transition and axon specification (Shah et al., 2016). Interestingly, recent studies point out that 140kDa C3G isoforms could be more relevant in embryonic mouse brain, while brain-specific 175kDa C3G isoform could be predominant in post-natal brain (Sriram et al., 2020). This work also describes differences in C3G levels between brain cells: higher in NeuN-positive cells (neurons) and lower in GFAP-positive cells (astrocytes), although this should be further characterized.

Some of the above mentioned processes are regulated by Reelin pathway. Reelin is a secreted glycoprotein essential for neurodevelopment that binds to ApoER2 and VLDLR receptors, leading to Dab1 activation (Bock & May, 2016). Reelin/Dab1 pathway coordinates several steps of cerebral cortex development, such as postmitotic arrangement of cortical precursors. Rap1 has been identified as one of the main targets of Reelin/Dab1 pathway to control cadherin, integrin, cytoskeleton and PI3K/Akt pathway. Rap1 activation is induced by Crk/C3G and, in fact, Crk-KO and C3G$^{gt/gt}$ mice display the set of alterations present in Reelin-KO mice (Park & Curran, 2008) (Voss et al., 2008) (Yip et al., 2012) (Bock & May, 2016). Interestingly, C3G deficiency did not alter Reelin levels, but blocked its signal transduction *in vivo* (Yip et al., 2012) and *in vitro* in Reelin-stimulated primary neurons (Ballif et al., 2004).

C3G is also important for Reelin-independent neural differentiation processes. As explained above, C3G participates in EGF-induced proliferation and NGF-promoted differentiation of neural precursors (Lu et al., 2000) (Kao et al., 2001). The differences between these pathways rely on the proteins interacting with C3G, which form different complexes that regulate signal transduction downstream each RTK. Moreover, Crk/C3G complex can modify Trk location in response to NGF during differentiation. A complex containing Crk, C3G, SHP2 and Gab2 interacts with and induces Trk translocation to EAAT1-positive early endosomes, where it colocalizes

with Rap1 and ERKs (Wu et al., 2001). Complementary, C3G promotes neural differentiation upon stimulation with BDNF (Arévalo et al., 2006), the monoclonal antibody that activates Alk (denoted as mAb46), (Schönherr et al., 2010), forskolin (V. Radha et al., 2008) (Mitra et al., 2011) or sildenafil (a phosphodiesterase-5 inhibitor) (Dar et al., 2020).

Nevertheless, almost nothing is known about the role played by C3G in the nervous system under pathological conditions, although its high expression suggests an important role. For example, C3G and Rap1 are implicated in neuroblastoma cells proliferation induced by Alk activation, a RTK commonly mutated in these tumours (Schönherr et al., 2010). However, C3G functions in neurodegenerative diseases or in CNS tumours remain totally undetermined.

3. Models for glioblastoma research

In spite of the increasing efforts made in cancer research, tumours propel us to develop dynamic and encloses-to-clinic models and GBM is not an exception. Its lack of homogeneity and the existence of overlapping pathological entities make difficult to set ‘‘perfect’’ models. On one hand, heterotopic and orthotopic inoculation of human cancer cells in nude mice and genetically-engineered mice recapitulate hallmarks of human GBMs and they would allow answering to questions related to GBM onset and progression (Lenting et al., 2017). On the other hand, at present, there are few carcinogen-induced GBM-like models: (i) GL261 model, generated by intracranial inoculation of methylcholanthrene, inducing ependymoblastomas with GBM-like characteristics, and (ii) ENU (*ethyl-nitrosourea*) model, induced by intravenously injection of ENU in pregnant animals, leading to mutations in NSCs from the progeny that generate diffuse astrocytomas (Lenting et al., 2017). Interestingly, it has been demonstrated that *in ovo* CAM assays are suitable to recapitulate the most characteristic features of human GBM onset and development (Hagedorn, 2005). In CAM assays, cells are inoculated in the chorioallantoic membrane of chicken embryos and they can be used to study tumour onset, dissemination/metastasis, angiogenesis, tumour-stroma interactions or drug effectiveness.

As mentioned above, the cellular models used for *in vitro* GBM research have a pronounced mesenchymal and stem-like phenotype under basal conditions (Iser et al., 2017), similarly to what is found in patient-derived samples, PDXs (*patient-derived xenografts*) and PDCs (*patient-derived cells*) (Tso et al., 2006). The most used GBM and GBM-like established human cell lines are U87 and U251 cells, followed by U118, T98G, LN18, LN229 and A172 cell lines (*ATCC (glioblastoma cell lines) webpage*, 2020). U87 cell line has been widely used during the last years as a proper

GBM-like model isolated from a male of undetermined age, displaying adherent properties and tumourigenic capacity. These cells present cell cycle control alterations (e.g. mutations in *CDKN2A*/*C* genes) and tumour suppressors' inactivation (mainly PTEN mutations) (*ATCC (U87MG) webpage*, 2020). Further genomic studies also indicated a highly aberrant genomic structure and a huge range of alterations, commonly found in GBM patients (M. J. Clark et al., 2010). However, experimental reproducibility of U87 studies is affected by the large number of sub-clones available worldwide and the alterations induced under serum culture conditions. In general, two main controversies have been found in *in vitro* GBM models: lack of gender variability, as among all previously mentioned cell lines, for instance, only LN229 cells derived from a female patient, and the difficulties to maintain in culture IDH-mutant cells.

GSC-like culture as neurospheres has enriched GBM research and its approach to clinic. Although not all GBM cells have a complete GSC phenotype, different studies pointed out that neurospheres cultures have more similarities to patient tumours than adherent cell cultures maintained in the presence of serum (Lee et al., 2006). Moreover, new techniques have been developed to isolate GSC populations directly from patients (López-Valero et al., 2018) (López-Valero et al., 2020) and to study GSC-associated properties (Hu & Smyth, 2009).

Due to close relationship between mutagenesis and tumourigenesis, CRISPR/Cas9 system is a promising tool for cancer research. It is based on the specific design of a sgRNA against a gene target and sgRNA-dependent double-strand DNA break by Cas9 enzyme, what is later repaired by diverse cell repair mechanisms (non-homologous DNA end joining or homology-directed repair, mainly). This leads to small deletions/insertions that deplete (knock-out) gene expression or to specific mutations in the expressed genes (knock-in) (Kaushik et al., 2019). CRISPR/Cas9 is used to uncover the function of single genes in different cancers as well as to characterize tumour onset and progression (Kaushik et al., 2019) or to look for new candidates implicated in drug resistance or dissemination using whole-genome sgRNA libraries, for example, in GBM (Prolo et al., 2019).

Group background

1. Function of C3G as a regulator of cell death/survival and adhesion/migration in non-tumour and tumour cells. Crosstalk with p38α MAPK.

For years, our group worked on the characterization of p38α MAPK role on cell death and survival in different cell types and contexts (Porras et al., 2004) (Zuluaga et al., 2007) (Bragado et al., 2007) (Gutiérrez-Uzquiza et al., 2012). Moreover, in collaboration with Dr. Guerrero's group, a crosstalk between p38α MAPK and C3G in apoptosis was uncovered. Thus, in CML K562 cells, C3G down-regulation enhances Imatinib-induced apoptosis through the up-regulation of p38α activity mediated by a Rap1-dependent mechanism (Maia et al., 2009). In MEFs, C3G knock-down also increases p38α activation, inducing either survival or cell death depending on the stimuli, but through a Rap1-independent mechanism (Gutiérrez-Uzquiza et al., 2010). Later on, it was found that the functional interaction between C3G and p38α MAPK also plays a role controlling cell adhesion and migration. In CML K562 cell line, C3G and p38α interact and collaborate to promote cell adhesion through a common regulatory pathway, although they display antagonistic effects in the regulation of focal adhesion proteins (Maia et al., 2013). It was also demonstrated that, in MEFs, C3G inhibits cell migration and invasion via down-regulation of p38α activity, through a mechanism not mediated by Rap1 (Priego et al., 2016). Similarly, in coloncarcinoma HCT116 cells, C3G downregulation promotes migration and invasion, decreases invasion and upregulates p38α MAPK via Rap1, likely activated by other GEFs as a compensatory mechanism (Priego et al., 2016). Moreover, the inverse correlation between C3G protein levels with the invasive capacity of different human coloncarcinoma cell lines also supports the role of C3G as a negative regulator of migration in coloncarcinoma.

2. Role of C3G in coloncarcinoma

The above referred previous data obtained in HCT116 coloncarcinoma cells led to the study of C3G role at different levels. Both *in vitro* and *in vivo* studies revealed that C3G promotes tumour growth through p38α MAPK-independent mechanisms, so that silencing of both C3G and p38α has an additive effect decreasing tumour growth in xenograft assays (Priego et al., 2016). The pro-tumourigenic action of C3G is most likely dependent on an increased survival and adhesion, and it is not mediated by Rap1. As mentioned above, C3G also has an inhibitory effect on migration and invasion in HCT116 cells and its silencing provokes ZO-1 internalization, E-cadherin loss and re-organization of F-actin (*filamentous*-actin) cytoskeleton (Priego et al., 2016). Thus, C3G plays a dual role in coloncarcinoma actin through different mechanisms.

3. C3G function in HCC

More recently, our group has established a role for C3G in HCC progression, uncovering the requirement of C3G to fully activate HGF/Met signalling. *RAPGEF1* expression is higher in HCC samples compared to healthy livers according to bioinformatic databases. C3G levels also increase in human cell lines and different mouse models (Sequera et al., 2018) (Sequera et al., 2020). This high *RAPGEF1* expression correlates with HCC progression and poor prognosis in patients. Moreover, in HCC cells, C3G downregulation decreases *in vitro* and *in vivo* tumourigenic capacity, while migratory and invasive properties are enhanced, accompanied by upregulation of mesenchymal markers. On the other hand, *in vivo* studies with mouse HCC cells overexpressing Met revealed that C3G downregulation promotes the generation of lung metastasis, although C3G re-expression correlated with the growth of these secondary tumours. Furthermore, a defective activation of HGF/Met signalling upon C3G silencing was found in HCC cells, likely due to a deficient formation of Met/C3G/Gab1complex in the absence of C3G (Sequera et al., 2020).

.

Aims

General aim:

The main objective of this research project is to analyse the role played by C3G (encoded by *RAPGEF1* gene) in glioblastoma (GBM) dissemination and tumourigenesis, identifying the mechanisms involved and the crosstalk between C3G and different cell signalling pathways.

Specific aims:

1. To determine whether C3G expression is altered in GBM tumours from patients and human GBM cell lines compared to healthy brain, as well as to identify if C3G levels correlate with GBM molecular subtypes or aggressiveness markers.
2. To analyse the function of C3G in GBM cells by *in vitro* and *in vivo* approaches, characterizing its role in the regulation of adhesion, migration/invasion, tumourigenesis, GSC-like phenotype and glucose metabolism.
3. To identify the molecular mechanisms involved in the actions of C3G in GBM and the interplay between C3G and cell signalling pathways associated to GBM progression.

Materials and methods

1. Cell culture, cell lines and gene expression modifications

1.1. Cell lines

1.1.1. Glioblastoma cell lines

The following GBM cell lines were used:

(i) Human GBM U-87-MG (ATCC HTB-14TM) cell line (abbreviated as U87) was purchased from ATCC (Manassas, Virginia, USA). This cell line derives from a male GBM patient of unknown age and displays mutations related to cell cycle control (CDKN2A and CDKN2C) and tumour suppressors' inactivation (PTEN), among others (*American Type Culture Collection (ATCC) (U87MG) webpage*, consulted in June-2020, and *COSMIC Cell Lines webpage*, consulted in June-2020).

(ii) Non-commercial cell lines derived from GBM patients (PDCs) with a stem-like phenotype, named 12Φ12 and HCO1 cells. They were kindly supplied by Dr. G. Velasco (Complutense University of Madrid, Spain) and cell isolation protocol is detailed in *López-Valero et al., 2018*. PDCs were differentiated *in vitro* using DMEM (*Dulbecco's modified Eagles medium*) supplemented with 10% FBS (*fetal bovine serum*) (later described) and adherent plates, as previously described (López-Valero et al., 2020), generating 12Φ12D and HCO1D cell lines, respectively. Morphology was evaluated during the process and differentiation was considered completed after 5 passages (coincident with the lack of cell death after re-plating).

1.1.2. Non-tumourigenic human astrocytes

HAs (*human astrocytes*) were nicely provided by Dr. M. Valiente's laboratory (CNIO, Madrid, Spain) that originally purchased them from ScienCell (catalog #1800). This cell line was isolated from human cerebral cortex and their astrocytic phenotype was confirmed by detection of different astrocyte markers such as GFAP. Importantly, HA cell line is a suitable healthy control for this study since it does not display tumourigenic capacity (Bejarano et al., 2017).

1.1.3. HEK-293T cells

For virus production, viral particles titration and transfection testing, HEK (*human embryonic kidney*)-293T (ATCC CRL-3216™, abbreviated as 293T) cell line was used. This is a highly transfectable derivative of HEK-293 cell line that contains the

SV40 T-antigen. This makes this cell line suitable to replicate vectors carrying SV40 replication region, generating high titers of retroviruses. These cells display an epithelial morphology and adherent properties.

1.2. Cell culture conditions

1.2.1. Culture conditions and mycoplasma detection by PCR

U87, 12Φ12D, HCO1D and 293T cells were grown at 37ºC and 5% CO_2 in a humidified atmosphere in DMEM medium (4.5 g/L glucose) (Lonza, #12-604F) supplemented with FBS (10%) (Gibco, #10270106), streptomycin (10 µg/ml) (Sigma, S9137), penicillin G (12 µg/ml) (Sigma, #13752) and amphotericin B (0.25 µg/ml) (Sigma Aldrich, A2942-100ML). pH at 7.4 was maintained using Hepes (20 mM) (Fisher Scientific, BP310-1). Puromycin and/or blasticidine-resistant cells were grown in the presence of puromicyn (1 µg/ml) (Panreac, A2856) and/or blasticidine (10 µg/ml) (Sigma Aldrich, #15205). Both antibiotics were removed from cell media, at least, 48h prior to experiments.

HAs were grown in astrocyte medium (ScienCell, #1801) supplemented with antibiotics (ScienCell, #0503), FBS (ScienCell, #0010) and astrocyte growth supplement (AGS) (ScienCell, #1852) at 37ºC, 5% CO_2 in a humidified atmosphere.

Cells were trypsinized using Trypsin 0.25%-EDTA 0.02% (Hyclone, SH30042.02) and splitted into new plates when they reached 90% confluence or for doing experiments. Trypsin action was stopped with 10% FBS supplemented medium. The cellular suspension was counted using a Neubauer chamber after Trypan blue (Merck, #111732) staining to seed the required number of cells for each experiment.

The absence of mycoplasma in the cell cultures was checked periodically by PCR (*polymerase chain reaction*) using medium from cells as sample and specific primers for mycoplasma DNA amplification (*forward primer*: 5'-GTGGGGAGCAAACAGGATTAGA-3'; *reverse primer*: 5'-GGCATGATGATTTGACGTCGT-3').

Cellular morphology was periodically evaluated in all cell lines using a phase-contrast Eclipse TE300 Nikon Microscope coupled to a digital DS-U2 camera.

1.2.2. Cryopreservation and thawing of cells

For cryopreservation, cells were trypsinized, centrifuged (1.200 rpm/1157g, 5 min), resuspended in 10% DMSO in FBS and transferred to a cryopreservation vial that was progressively frozen: (i) at -20ºC for 30 min, (ii) at -80ºC for 24h and (iii) stored at -170ºC at the vapour phase of liquid nitrogen.

Thawing of cells was performed by quickly immersing the vial in a 37ºC water bath. Cells were directly seeded in a plate with complete cell culture medium. In the case of HAs, after quickly defrosting at 37ºC, cells were centrifuged (800 rpm/770g, 5 min) and the cellular pellet was seeded in a gelatine-covered dish containing fresh HA-complete medium.

1.2.3. Cell treatments

When indicated, cells were serum-starved using DMEM medium (4.5 g/L glucose, with L-glutamine) (Lonza, #12604F) with Hepes, streptomycin, penicillin G and amphotericin B without FBS (0%) for U87 cells and 0.5% FBS for 12Φ12D and HCO1D cells, for different time periods depending on the experiment.

In order to study cell signalling, cells at 70% confluence were serum-starved for 16h. Then, they were stimulated for different time periods with FBS or the indicated growth factor (*Table 1*). Chemical inhibitors of cell signalling pathways were also used for different experiments (*Table 2*). Factors and inhibitors included in *Tables 1 and 2* were used for the cell signalling and functional assays explained below.

Table 1 – Stimulation factors used in signalling experiments and/or functional assays

Stimulation factor	Use concentration	Reference
FBS	10%	Gibco, #10270106
EGF	10 ng/ml	R&D, #236-EG-200
FGF-2	50 ng/ml	Preprotech, AF-100-18B
MDK	100 ng/ml	Cellmid/LYRAMID

Table 2 – Chemical inhibitors used in signalling experiments and/or functional assays

Chemical inhibitor	Target	Use concentration	Reference
PD98059	MEK	20 µM	Calbiochem, #513000
SB203580	p38α/β	5 µM for p38α 10 µM for p38α/β	Calbiochem, #559389
Sodium azide (NaN_3)	Cytochrome oxidase (non-specific)	10 mM	Panreac, A1430
Infigratinib (BGJ398)	FGFR1	1 µM	NVP-BGJ398
Monensin	Recycling	10 µM	Sigma Aldrich, M5273

1.3. Gene expression modification in glioblastoma cell lines

1.3.1. Permanent C3G gene silencing

C3G was stably knocked-down (shC3G) in U87, 12Φ12D and HCO1D cells by infection with Lentiviral Particles containing a mixture of human C3G shRNAs (SCB, sc-29863-V) (*Table 3*). Additionally, shRNAs NTC (*short-hairpin RNA non-targeting control*) lentiviral particles (SCB, sc-108080) were used to generate shNTC U87 cells as a control.

Table 3 – shRNA sequences used for C3G knock-down using lentiviral particles (*colour legend*: sense siRNA; *hairpin*; antisense siRNA)

#1: sc-29863-VA (SCB)	
Sequence (5'→3'): GATCCGTTCTCATCTCTCTTCCTT*TTCAAGAGA*AAGGAAGAGAGATGAGAACTTTTT	
Targeted exon (*RAPGEF1*): 2	Off-targets in human genome: Chromosome 5 (non-coding region)
#2: sc-29863-VB (SCB)	
Sequence (5'→3'): GATCCGCATTCGGGTGGTTGATAA*TTCAAGAGA*TTATCAACCACCCGAATGCTTTTT	
Targeted exon (*RAPGEF1*): 7	Off-targets in human genome: None
#3: sc-29863-VC (SCB)	
Sequence (5'→3'): GATCCCCACTATGATCCCGACTAT*TTCAAGAGA*ATAGTCGGGATCATAGTGGTTTTT	
Targeted exon (*RAPGEF1*): 10	Off-targets in human genome: None

Cells were seeded 24 h prior to the viral infection at a density that guaranteed 50-60% confluence the next day. Then, the medium was replaced and cells were incubated overnight with fresh medium containing 75.000 infectious units of lentiviral particles and polybrene (10 µg/ml) (SCB, sc-134220) (MOI (*multiplicity of infection*)=5-10). Next day, the medium was replaced by a fresh one and, after 48h, cells were selected with puromycin (1 µg/ml) (Panreac, A2856), being concentration determined by a previous dose curve in non-infected cells. Several clones were obtained and a pool of them was used to perform the experiments. C3G silencing in stably knocked-down cells was verified by western blot and/or immunofluorescence analysis using anti-C3G antibody (Genosphere, custom-made against 4-245 aminoacids).

1.3.2. C3G knock-out using CRISPR/Cas9

C3G was stably knocked-out (KO-C3G) in U87 cells by CRISPR/Cas9 technology using the doble lentiviral system designed by Zhang laboratory (*Figure XIV*) (Shalem et al., 2014). It uses two lentiviral vectors: lentiCas9-blast plasmid (Addgene, #52962, PMID 25075903) and pLentiGuide-puro (carrying the sgRNAs (*single guide RNA*) of interest) (Addgene, #52963, PMID 25075903). pLentiGuide-puro plasmid was modified in our laboratory to generate viruses carrying sgRNA targeting human C3G (hC3G) (pLentiguide-hC3G-KO-1/2/3/5) (for further details, see section 2.1.1.).

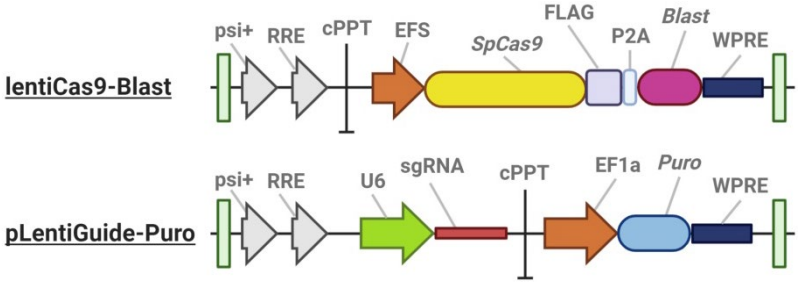

Figure XIV – Schematic representation of CRISPR/Cas9 double-virus system, developed in Zhang's laboratory. Main elements of lentiCas9-Blast (*upper*) and plentiGuide-Puro (*lower*) plasmids are represented. Lentiviral particles carrying lentiCas9-Blast plasmid induced the expression of *CAS9* gene (indicated as *SpCas9*) in U87 cells, generating U87+Cas9$^+$ cells. For that, blasticidine resistance (indicated as *Blast*) was used. Then, U87-Cas9$^+$ cells were infected with lentiviruses with different plentiGuide-Puro plasmids, which had incorporated the anti-*RAPGEF1* sgRNAs designed. For pool selection, puromycin resistance (*indicated as Puro*) was used. These plasmids present typical viral vector elements, such as: Psi+ (RNA target site for packaging by nucleocapsid), RRE (*Rev Response Element*; sequence to which the Rev protein binds), cPPT (*central polypurine tract*; recognition site for proviral DNA synthesis that increases transduction efficiency and transgene expression) or WPRE (*woodchuck hepatitis virus post-transcriptional regulatory element*; sequence that stimulates the expression of transgenes via increased nuclear export). *Adapted from Shalem et al., 2014.*

LentiCas9-Blast lentiviral particles were generated in 293T cells (for further details, see section 2.1.2.). U87 parental cells were first infected with these lentiviral particles to induce the expression of Cas9, following the infection protocol previously described. U87-Cas9$^+$ cells were selected with blasticidine (10 µg/ml) (Sigma Aldrich, #15205), whose concentration was determined by a previous dose curve in non-infected cells. *CAS9* genetic integration in U87-Cas9$^+$ cells genome was checked by gDNA (*genomic* DNA) isolation (using NK protocol, described in *Table 4*) and PCR amplification with specific primers (forward primer: 5'-CCAAAGAGGTGCTGGACG-3'; reverse primer: 5'-GCTCTTTCAATGAGGGTGGA-3') (see *Appendix 1*). Cas9 protein levels in U87-Cas9$^+$ cell pool were also verified by western blot using anti-Cas9 antibody (CST, #14697) (see *Appendix 1*).

Second, U87-Cas9$^+$ cells were independently infected with four different lentiviral particles containing sgRNAs targeting C3G: pLentiguide-hC3G-KO-1/2/3/5 plasmids (see details in section 2.1.1). Infection and puromycin selection (1 µg/ml) protocols were performed as previously described. Each pool of cells (U87-Cas9$^+$-KO-C3G-1/2/3/5) was expanded and gDNA was extracted using NK protocol (*Table 4*). Each targeted region was amplified by PCR using specific primers (*Table 5*) and Sanger sequencing was performed (in Genomics CAI from Complutense University of Madrid, Spain) to detect the genomic gaps generated by Cas9 action (see *Appendix 1*). Positive gaps in more than 50% of the cells from the pool were only found in U87-Cas9$^+$-KO-C3G-3 sample, therefore, the other infected cell lines were discarded. Single-cell cloning of U87-Cas9$^+$-KO-C3G-3 cells was carried out in 96 multiwell plates obtaining KO-C3G-# clones and C3G levels were checked by western blot and/or immunofluorescence analysis using anti-C3G antibody (Genosphere, custom-made anti 4-245 aminoacids) in each clone. Additionally, viral particles carrying non-targeting pLentiGuide-puro-NTC (*non-targeting control*) were used to infect U87-Cas9$^+$ cells, generating U87-Cas9-NTC cells as a control.

Table 4 – Genomic DNA (gDNA) extraction from cells using NK protocol

Step	Description	Reagents
1	Cell pellet overnight incubation at 55ºC with NK buffer	NK buffer composition: Tris-HCl (50 mM, pH 8), EDTA (50 mM), SDS (1%) and Proteinase K (100 µg/ml; Qiagen, #19131)
2	Incubation with RNAse A (30 min, at 37ºC)	RNAse A (50 µg/ml; Qiagen, #19101)
3	Protein precipitation with ammonium acetate, centrifugation, supernatant collection, gDNA precipitation with isopropanol and centrifugation	Ammonium acetate (Sigma, A1542) Isopropanol (Panreac, #141090.1211)
4	gDNA wash with Ethanol (70%), dry and suspension in Nuclease-free water	Ethanol (Panreac, #141086.1211)

Table 5 – Primers for PCR amplification of the targeted genomic regions in hC3G-KO CRISPR/Cas9 experiments

Amplified region of *RAPGEF1*	Forward primer (5'→3')	Reverse primer (5'→3')	sgRNAs targeting this region
Exon 2	CCGCCCATGGAATGCTACG	GAACCATCGCTTCTTCCCAC	sgRNA-1 sgRNA-2
Exon 5	CACCCTTGTCACCGAGAAG	TTTGAAGGTCAGGAGCAAGC	sgRNA-5
Exon 7	TGACAGACCGCGAGGTAGA	ACAGCTCCAGAGTCAGCCT	sgRNA-3

1.3.3. Overexpression of full-length C3G and C3G lacking the GEF catalytic domain

For transient C3G overexpression in U87 parental cells, pCDNA3-C3G-FL (carrying C3G-full length) and pCDNA3-C3G-ΔCat (carrying C3G lacking the GEF catalytic domain) constructs were generated (*see details in section 2.2.*). pCDNA3-EV (*empty vector*) was used as a control.

For plasmid transfection, cells were seeded 24 h prior transfection at a density that guaranteed 50-60% confluence next day (50000 cells/well in 6 multiwell plates). Then, antibiotics were removed from the culture medium to increase transfection rate. Each plasmid (2 µg) was independently diluted in Optimem medium (Life technologies, #31985062) and mixed with Metafectene (T040, Biontex) (1:3 ratio). After 15-30 min of incubation at room temperature, each transfection mix was transferred to the cells. Experiments were carried out in the next 72h period. Transfection efficiency was checked by western blot using anti-flag (F3785-2MG, Sigma Aldrich) and anti-C3G (Genosphere, custom-made against 4-245 aminoacids) antibodies.

1.3.4. Transient overexpression of Rap1A

In collaboration with Dr. Rubio's laboratory (University Hospital of Jena, Germany), different transfections were performed to determine the role of Rap1A in GBM. Rap1A-WT and Rap1AV12 (constitutively active Rap1A mutant) inserted in pmCherry-C1 plasmid were transiently expressed in U87 parental and U87shC3G cells. pmCherry-C1-EV was also transfected in U87 parental and U87shC3G cells as a control. This constructs were previously described by (Augsten et al., 2006).

Cells were seeded 24 h prior transfection at a density that guaranteed 50-60% confluence next day (50000 cells/well in 6 multiwell plates). Then, antibiotics were removed from the culture medium to increase transfection rate. Each plasmid (2 µg) was independently diluted in Optimem medium (Life technologies, #31985062) and

mixed with PEI (*polyethylenimine*) (PolySciences, #23966) (1:3 ratio). After 15-30 min of incubation at room temperature, each transfection mix was transferred to the cells. Transfection rate was evaluated 24h later by quantification of $mCherry^+$ fluorescent cells in the cell culture and rates lower than 30% were considered insufficient and cells discarded. Transfection rate ranged between 40-60%. If transfection was appropriate, culture medium was replaced by a fresh one and experiments were carried out in the next 72h period. Transfection efficiency was also checked by western blot using anti-mCherry antibody (custom made, kind gift of Dr. I. P. Prior (Liverpool)).

2. Generation of plasmid constructs and viral particles

2.1. Plasmids and viruses for C3G knock-out using CRISPR/Cas9 technology

2.1.1. sgRNA design and pLentiguide-Puro-C3G-knock-out plasmids production

Different sgRNAs sequences (*Table 6*) were selected to knock-out human C3G (hC3G-KO) in GBM cells. Each paired sgRNA was annealed by 5 min incubation at 95ºC and slow cooling down at room temperature. sgRNA-1 and sgRNA-2 were designed in our laboratory using CRISPR/Cas9 tool from Benchling software. sgRNA-3, sgRNA-4 and sgRNA-5 sequences were designed based on similarity to sequences previously described and validated (SCB, sc-401616). pLentiGuide-puro plasmid (Addgene, #52963, PMID 25075903) was digested with BsmBI (Esp3I) (Fisher Scientific, #10374280) and agarose-gel extracted (Qiagen, #28704) (*see Appendix 2*). All sgRNAs were designed to contain BsmBI-compatible sites. Each annealed sgRNA was independently incubated with purified digested pLentiGuide-puro plasmid and Ligase T4 (ThermoScientific, EL0011) for 1h at room temperature. XL-Gold UltraCompetent cells (Agilent, #200315) were transformed with each ligation mix, following the manufacturer's protocol. Bacteria were grown overnight in LB-agar plates (bactotriptone 10g/L, yeast extract 5g/L, NaCl 10g/L and agarose 1.5%) containing ampicillin (100 µg/ml) (Sigma Aldrich, A9518) at 37ºC. Five colonies were picked from each different plasmid transformation. Minipreps (Macherey-Nagel, #22740588) followed by Sanger sequencing using hU6F.LKO.1_5 primer (5'-GACTATCATATGCTTACCGT-3') were used to determine the correct incorporation of the inserts into each plasmid (*see Appendix 2*). At least, one positive plasmid was obtained for each sgRNA pair (except for sgRNA-4), generating the corresponding

pLentiGuide-puro-hC3G-KO-1/2/3/5 plasmids that were amplified and purified by Midiprep (Macherey-Nagel, # 22740410).

Table 6 – Primers designed for sgRNA sequences cloning in pLentiGuide-puro plasmids and human C3G-KO using CRISPR/Cas9

sgRNA	Forward primer (5'→3')	Reverse primer (5'→3')	pLentiGuide-puro-hC3G-KO-#
#1	CACCGTTCTCTTGA--TTTTGGGTGAG	AAACCTCACCCA--AAATCAAGAGAAC	#1
#2	CACCGAAAGAAGGG--AAAACCAGCTG	AAACCAGCTGGT--TTTCCCTTCTTTC	#2
#3	AAACCGGATGAAGA--GGTCGCGCCC	CACCGGGCGCG--ACCTCTTCATCCG	#3
#4	AAACGGCATTCGGG--TGGTTGATAAC	CACCGTTATCAA--CCACCCGAATGCC	-
#5	AAACGCGAATGAGG--TTGGCGAGGC	CACCGCCTCGC--CAACCTCATTCGC	#5

2.1.2. Virus generation for CRISPR/Cas9 experiments

Both LentiCas9-Blast and pLentiGuide-puro-hC3G-KO-1/2/3/5 plasmid packaging in lentiviral particles was carried out in 293T cells. For each plasmid, 4×10^5 293T cells were seeded into 10 cm tissue culture plates coated with gelatine (2%) (Sigma, G9391) to reach a 40-50% confluence the next day. Then, antibiotics were removed from the culture medium to increase transfection rate. In order to generate the mentioned lentiviral particles, three plasmids were co-transfected:

(i) Lentiviral packaging psPAX2 plasmid (Addgene, #12260) (2 µg) (common for all lentiviral productions). This plasmid induces the expression of lentiviral packaging genes *GAG* and *POL*.

(ii) Lentiviral enveloping pMD2-VSVg plasmid (Addgene, #12259) (1.5 µg) (common for all lentiviral productions). This plasmid induces the expression of lentiviral enveloping glycoprotein from VSV virus.

(iii) LentiCas9-Blast plasmid (2.5 µg) or one of the pLentiGuide-puro-hC3G-KO-1/2/3/5 plasmids generated (2.5 µg each). This third plasmid included in the mixture carries the sequence that will be inserted in the genome of the infected cells and it specifically determines the lentivirus generated in each plate. LentiCas9-Blast plasmid expresses human codon-optimized *Streptococcus pyogenes* Cas9 protein and blasticidin resistance under EFS promoter. pLentiGuide-puro- induces the expression of the specific sgRNA inserted under U6 promoter and puromycin resistance under EF-1a promoter.

Each mixture of three plasmids was resuspended in Optimem medium and mixed with PEI (1:3 ratio). After 15-30 min of incubation at room temperature, transfection mixes were transferred to 293T cells. Next day, the media were replaced by fresh standard media to remove the excess of plasmids and PEI. After 72h, each culture medium was independently collected, centrifuged (2000 rpm/1930g, 5 min) and passed through a 0.45 µm-pore filter (Cultek, #15431231). Samples containing the different lentiviruses were stored at -80ºC.

Virus generation was always checked by dose-response virus titration curves. 293T cells were seeded in 6 multiwell plates at 30% confluence. Cells from different wells were incubated overnight with fresh medium containing increasing volumes of samples with the lentiviral particles (from 0 µl to 1000 µl) and polybrene (10 µg/ml). After 48h, cells were treated for 7 days with blasticidine (10 µg/ml) (for lentiCas9-Blast titration) or puromycin (1 µg/ml) (for pLentiGuide-puro-hC3G-KO-1/2/3/5 titration). Finally, cells were washed with PBS (*Dulbecco's phosphate buffered saline solution;* Cultek, #91X0520), fixed and stained with violet crystal (0.2%) (Sigma Aldrich, C-0775)- ethanol (2%) solution. Antibiotic-resistant coloured colonies were counted and the number of lentiviral infectious units per ml in each sample was estimated. Only viral productions over 10^4 viruses/ml were used.

2.2. Plasmids for C3G overexpression

2.2.1. *RAPGEF1* cDNA subcloning into pCDNA3 plasmid

For C3G overexpression in GBM cells, *RAPGEF1* (C3G-encoding gene) cDNA sequence was subcloned from PLTR2-C3G-FL (*full length*) plasmid (generated by *Guerrero et al., 1998*) into pCDNA3 plasmid (described in *Zhou et al., 2019*) for C3G transient overexpression.

PLTR2- C3G-FL plasmid contains a *RAPGEF1* sequence obtained from human placenta, identical to that identified by *Tanaka et al., 1994* (considered *RAPGEF1* consensus sequence and included in NCBI CCDS Database, Q13905-1) except for the 5' end. PLTR2-C3G-FL sequence encoded M-S-G-K-I-E-K-A amino acid sequence instead of the M-D-T sequence described by Tanaka, 1994.

RAPGEF1 sequence from PLTR2-C3G-FL plasmid was amplified using specific primers designed in our laboratory (*forward primer*: 5'-CGCGGATCCGACACAGACTCTCAGCGTTCTC-3'; *reverse primer*: 5'-CGCCTCGAGCTAGGTCTTCTCTTCCCGGTCTGTTTTTC-3'). These primers were designed to amplify *RAPGEF1* consensus sequence and they included BamHI (5'-G^GATCC-3') and XhoI (5'-C^TCGAG-3') restriction sequences (underlined), necessary for its cloning into pCDNA3 plasmid. PCR amplification was performed with

High Fidelity Herculase II Fusion DNA Polymerase kit (Agilent, #600675) using the mentioned primers (1.25 µl each from 10 mM stocks), dNTPs (1.25 µl from 40 mM stock solution) and PLTR2-C3G-FL plasmid (1.25 µl of 1.2 µg/µl stock solution). PCR reaction was set up according to manufacturer's instructions (1 – 2 min at 95ºC; 2-(X30 cycles) 20 sec at 95ºC, 20 sec at 55ºC and 90 sec at 72ºC; 3- 3 min at 72ºC). PCR product was electrophoresed in an agarose (0.75%) gel in the presence of GelRed (VWR, #41003) and visualized in a VWR Imager Chemi Premium documentation system (*see Appendix 3*). The band of interest (3 kb) was extracted from the gel using a kit (Qiagen, #28704) and the product correspondence with *RAPGEF1* cDNA was determined by Sanger sequencing (Genomics CAI from Complutense University of Madrid, Spain). Once validated, the PCR product was digested with BamHI (ThermoFisher, FD0054) and XhoI (ThermoFisher, FD0694) by overnight incubation at 37ºC. In parallel, a modified version of pCDNA3 plasmid was digested with the same restriction enzymes (*see Appendix 3*). This modified version contains the sequences of 2 tags (*Flag* and *Strep*) after the initiation codon (ATG) and prior to the restriction enzyme site for BamHI. This modification has been made to include these sequences in the N-Terminal region of the protein. Digested, purified PCR product containing *RAPGEF1* cDNA sequence was ligated to plasmid using Ligase T4 protocol (ThermoScientific, EL0011). XL-Gold UltraCompetent Cells (Agilent, #200315) were transformed with the ligation mix, following the manufacturer's protocol. Bacteria grew overnight in LB-agar plates (bactotriptone 10g/L, yeast extract 5g/L, NaCl 10g/L and agarose 1.5%) containing ampicillin (100 µg/ml) (Sigma Aldrich, A9518) at 37ºC. Five colonies were picked from each different original plasmid and minipreps (Macherey-Nagel, #22740588) were performed. Sanger sequencing was used to check the correct incorporation of *RAPGEF1* in each plasmid, using T7 primer (5'- TAATACGACTCACTATAGGG-3') (*see Appendix 3*). Positive plasmids were obtained, generating the corresponding pCDNA-C3G-FL plasmid that was amplified and purified by Midiprep (Macherey-Nagel, #22740410). C3G-FL (130-140 kDa) expression was validated by western blot (C3G antibody; Genosphere, custom-made against 4-245 aminoacids) by transfection of 293T cells with Metafectene, following the protocol detailed in *section 1.3.3.* (*see Appendix 3*).

2.2.2. Mutagenesis to generate a pCDNA3-C3G construct carrying a C3G mutant lacking the GEF catalytic domain

In order to obtain pCDNA3-C3G-ΔCat plasmid, a pCDNA3 derivative carrying a C3G mutant lacking the GEF catalytic domain (specifically, CDC25H region), *in vitro* site-directed mutagenesis was performed over pCDNA3-C3G-FL plasmid. For this, QuickChange Site-Directed Mutagenesis Kit (#200519, Agilent) was used, following manufacturer's instructions. PCR mix included primers designed to introduce L815Stop mutation in pCDNA-C3G-FL plasmid (*forward primer*: 5'-

AGGTGGCACACCTCTATAGCTTCTTCTGGTCCACCTTGTCC-3'; *reverse primer*: 5'-GGACAAGGTGGACCAGAAGAAGCTATAGAGGTGTGCCA-CCT-3'), designed in our laboratory using Agilent Quickchange online software. Mutagenesis protocol included incubation with DpnI to eliminate all non-mutated methylated plasmid after PCR. Then, XL-Gold UltraCompetent Cells (Agilent, #200315) were transformed with the mix, following the manufacturer's protocol. Bacteria were grown overnight in LB-agar plates (bactotriptone 10g/L, yeast extract 5g/L, NaCl 10g/L and agarose 1.5%) containing ampicillin (100 µg/ml) (Sigma Aldrich, A9518) at 37ºC. Five colonies were picked and minipreps (Macherey-Nagel, #22740588) were performed. Sanger sequencing was used to check the correct incorporation of L815Stop mutation in the plasmid, using hC3G-695 primer (5'- GGATCTGGGGACATCTTACTG-3') (*see Appendix 4*). Positive plasmids were obtained, generating the corresponding pCDNA-C3G-ΔCat plasmid that was amplified and purified by Midiprep (Macherey-Nagel, #22740410). C3G-ΔCat (100-105 kDa) expression was validated by western blot (C3G antibody; Genosphere, custom-made against 4-245 aminoacids) after transfection of 293T cells with Metafectene, following the protocol detailed in *section 1.3.3.* (*see Appendix 4*).

Restriction maps of pCDNA3-FFSS plasmids used in this thesis (pCDNA3-EV, pCDNA3-C3G-FL and pCDNA3-C3G-ΔCat) are shown in *Appendix 5*.

3. Analyses of public databases information from glioblastoma patients

3.1. C3G expression analysis

C3G (*RAPGEF1*) mRNA expression in GBM patients was analysed using 171 samples from TCGA RNAseq studies, grouped into control (5 samples) and primary GBM tumour (153 samples). Clinical data for the corresponding samples were downloaded from *FireBrowse database* (consulted in June-2020). This allowed us to divide samples according to patient sex/gender and age. Original data also included 13 recurrent tumours, but they were discarded due to lack of clinical information. *RAPGEF1* expression was normalized for each sample using different housekeeping genes: *GUSB*, *ACTB* (β-actin) and *UBC* (Ubiquitin C). RNAseq data was expressed as log2 RSEM (*RNA-seq by Expectation Maximization*). As far as data did not present a normal distribution, Mann-Whitney statistical test was used to check significance and *p* value for each analysis was included in the graph. Data were represented using R/ggplot2 environment bioinformatic data analysis.

3.2. Heatmap

Using data from the mentioned TCGA cohort, each sample was grouped in a molecular GBM subtype according to the expression of markers defined in *Verhaak et al., 2010* and explained in the *Introduction* section. Then, C3G (*RAPGEF1*) expression was also included in the analysis. All this information was represented as a heatmap using R/pheatmap statistical-bioinformatic package.

4. Protein analysis by western blot

4.1. Protein extraction and quantification

Once culture medium was removed (or collected if necessary), cells were washed with PBS, and usually lysed with IP^{++} buffer (*Table 7, left panel*), or $RIPA^{++}$ buffer for nuclear proteins (such as Cas9) (*Table 7, right panel*). Cells were maintained on ice for 20 min, vortexing for 20 sec every 5 min. Then, lysates were centrifuged (13.000 rpm/15.000g, 10 min, 4ºC) and the supernatant (containing the extracted proteins) was collected and stored at -80ºC. Protein concentration was measured either by Bradford (for IP^{++} lysates) or BCA (*bicinchoninic acid*) method (for $RIPA^{++}$ lysates). A blank and a standard curve of known concentrations of BSA (*bovine serum albumin*) (Panreac, A1391) was prepared. Then, Bradford reagent (Sigma Aldrich, B6916) was added 5-10 min prior absorbance measurement at 595 nm. Alternatively, BCA reagents (ThermoFisher, #10341664/ #10495944/ #10753505) were used. First, reagents A and B were mixed in a 1:1 proportion and, then, reagent C was added in a 50:1 proportion. Absorbance was measured at 562 nm.

4.2. Protein electrophoresis

Protein electrophoresis conditions were specifically established according to the proteins of interest in each case. First, either SDS-PAGE gels (*Table 8A, upper panel*) or non-SDS-PAGE gels (Anderson gels) (*Table 8B, lower panel*) were used to separate proteins depending on the required separation. Second, the target protein size determined the concentration of acrylamide:bisacrylamide in the separation gel (from 7.5% to 15%) (*Table 8*). Samples were prepared by adding Laemmli buffer 4X (Tris-HCl 40 mM, pH 7.6; Glycerol 10%; SDS 1%; Bromophenol blue 0.002%, β-mercaptoethanol 2 mM; DTT 0.1 mM). They were boiled 10 min at 95ºC and loaded into the gel, as well as a molecular weight marker (ThermoFisher, #11832124). Electrophoresis was developed at 80-120V using the appropriate running buffer for each gel (*Table 8*).

4.3. Protein transfer and immunodetection

Electrophoresed proteins were transferred to nitrocellulose membranes (Amersham, #15259794) activated with H_2O using a semidry-transfer equipment (Biorad, #170394). Whatmann papers, gel and membrane were previously soaked in transfer buffer (Tris-HCl 50 mM, Glycine 400 mM, methanol 20% and SDS 0.1%). Transfer was performed at 15V for different time periods depending on gel and protein size (20-45 min/gel). Protein transfer was confirmed by staining with Ponceau S (0.5%, diluted in Trichoroacetic acid 1%).

Table 7 – Lysis buffers for protein extraction

IP^{++} buffer composition	
Tris-HCl pH 7.5	50 mM
NaCl	150 mM
NP-40	1%
EGTA	5 mM
EDTA	5 mM
PMSF	1 mM
Aprotinin	10 µg/ml
Leupeptin	10 µg/ml
Na_3VO_4	1 mM
NaF	20 mM

$RIPA^{++}$ buffer composition	
Tris-HCl pH 7.5	10 mM
NaCl	150 mM
NP-40	1%
SDS	0.1%
Triton X-100	1 mM
Sodium deoxycholate	1%
EDTA	2mM
PMSF	1 mM
Aprotinin	10 µg/ml
Leupeptin	10 µg/ml
Na_3VO_4	1 mM
NaF	20 mM

Phosphatase/protease-inhibitors references:
PMSF (phenyl-methyl-sulfonyl fluoride) → Sigma Aldrich, P-7626;
Aprotinin → Panreac, A2132; Leupeptin → Sigma Aldrich, L2884;
Na_3VO_4 → Sigma, S-6508; NaF → Sigma Aldrich, S-6776

After membrane washing with TTBS (*Tween Tris-buffered saline solution*) (Tris-HCl 10 mM, pH 7.4; NaCl 150 mM; Tween 0.05%), it was blocked with 5% skimmed milk or BSA in TTBS for 1h at room temperature. Primary antibodies were usually prepared in 0.5% BSA or skimmed milk-TTBS solution (1:500-1:2500 dilution, depending on antibody) (*Table 9*) and incubated overnight at 4ºC. Next day, membrane was washed with TTBS (3 washings, 10 min/each) and incubated with the appropriate secondary antibody conjugated with HRP (*horseradish peroxidase*) (anti-rabbit antibody (CST, #7074), anti-mouse antibody (CST, #7076) or anti-sheep antibody (SCB, sc-2473)). Secondary antibodies were prepared in 1% BSA-TTBS or 0.5% milk -TTBS at 1:5000 dilution. After washing with TTBS (3 washings, 10 min/each), membrane was incubated with Enhancer-Chemiluminescent Luminol

(ECL) solution (standard sensitivity: Thermo Fisher, #32106; high sensitivity: BioRad, #170-5061) and protein signal was developed using X-Ray films (Thermo Fisher, #34089) or digitally detected with VWR Imager Chemi Premium documentation system. Signal intensity (proportional to protein quantity) was determined by densitometric analysis of each band with ImageJ software and referred to the signal of a housekeeping control (β-actin or α-tubulin). Data were represented as the fold-increase of control sample in each experiment.

Table 8 –Protein electrophoresis: gel mixtures (final volume of each mix = 10 ml) and running buffers compositions

(A) SDS-PAGE GELS				
Reagent	**Reference**	**Separating gel 8%**	**Separating gel 15%**	**Stacking gel**
Acrylamide/ Bisacrylamide mixture	Panreac, A0951	2.65 ml	5 ml	1.64 ml
H_2O	-	4.65 ml	2.3 ml	6.8 ml
Tris-HCl 1.5 M, pH 8.8	Panreac, A1086	2.5 ml		-
Tris-HCl 1 M, pH 6.8	Panreac, A1086	-		1.26 ml
SDS 10%	Panreac, A0951	100 µl		100 µl
Ammonium persulfate (10%)	Fisher Scientific, #10396503	100 µl		100 µl
TEMED	Sigma Aldrich, T9281	4 µl		10 µl
Running buffer: Tris-HCl 25 mM, pH 8.3; Glycine 200 mM; SDS 0.1%				

(B) ANDERSON GELS				
Reagent	**Reference**	**Separating gel 7.5%**	**Separating gel 15%**	**Stacking gel**
Acrylamide 30%	Panreac, A1090	2.52 ml	5.03 ml	1.66 ml
Bisacrylamide 1%	Panreac, A1095	1.95 ml	0.87 ml	1.33 ml
H_2O	-	3.02 ml	1.59 ml	5.75 ml
Tris-HCl 1.5 M, pH 8.8	Panreac, A1086	2.52 ml		-
Tris-HCl 1 M, pH 6.8	Panreac, A1086	-		1.25 ml
Ammonium persulfate (10%)	Fisher Scientific, #10396503	50 µl		50 µl
TEMED	Sigma Aldrich, T9281	5 µl		10 µl
Running buffer: Tris-HCl 50 mM, pH 8.3; Glycine 400 mM; SDS 0.1%				

Table 9 – Primary antibodies for protein analysis by western blot (*Mw: Molecular weight*) (*ref: reference*)

Target	Ref#	Mw (kDa)	Dilution	Target	Ref#	Mw (kDa)	Dilution
C3G (1-300 aminoacids)	SCB, sc-15359	130	1:1000	P-EGFR (Tyr1068)	CST, #3777	130	1:500
C3G (4-245 aminoacids)	Genos-phere, *custom made*	130	1:500	EGFR	CST, #4267	130	1:1000
Vimentin	BD, #550513	57	1:1000	P-p38MAPK (Thr180/ Tyr182)	CST, #9211	38	1:5000
E-cadherin	BD, #610182	130	1:1000	p38αMAPK	SCB, #9211	38	1:1000
Cas9	CST, #14697	140	1:1000	P-ERKs (Thr202/ Tyr204)	CST, #9101	42/44	1:1000
β-actin	CST, #3700	45	1:2500	ERKs	CST, #9102	42/44	1:1000
α-Tubulin	CST, #2146	55	1:2500	P-Akt (Ser473)	CST, #9271	60	1:1000
mCherry	*Custom made*	25	1:1000	Akt	CST, #9272	60	1:1000
Flag	Sigma Aldrich, F3785-2MG	-	1:1000	P-MK2 (Thr334)	CST, #3007	75	1:500
Cas9	CST, #14697	140	1:1000	GFAP	Dako, Z033429-2	50	1:1000

5. Analysis of Tyrosine Kinase Receptors phosphorylation profile using an array

To evaluate the activation state (phosphorylation) of several RTKs, a Human Phospho-RTK Array Kit (R&D, #ARY001B) was used, following the manufacturer's protocol.

Cell culture conditions were previously established by checking several RTKs and downstream effectors phosphorylation (e.g. EGFR and Gab1) by western blot in a time-course analysis upon treatment of serum-starved cells with 10% serum for 0h, 4h or 24h.

For the analysis with the P-RTKs array, parental U87and U87shC3G cells (60-70% confluence) were serum-starved overnight and treated with 10% FBS for 4h. Then, culture medium was removed and cells were washed with cold PBS, keeping plates and samples on ice. Lysates were prepared as previously described, but using Lysis Buffer 17^{++}: Lysis buffer 17 (supplied with the kit) supplemented with aprotinin (10 µg/ml) and leupeptin (10 µg/ml). Protein concentration was determined by Bradford and BCA methods, both detailed above.

Membranes were activated and blocked using Array Buffer 2 from kit for 1h at room temperature. Then, membranes were incubated overnight at 4ºC with cell lysates, previously prepared (300 µg proteins diluted in Array Buffer 1 up to 1.5 ml of final volume per membrane). Next day, membranes were washed and incubated with anti-phospho-Tyrosine-HRP detection antibody from kit for 2h at room temperature. Then, after washing, membranes were incubated with Chemi Reagent from kit and the result was visualized using VWR Imager Chemi Premium documentation system. Signal intensity for each spot was determined by densitometric analysis using ImageJ software. To confirm that membranes were incubated with the same amount of protein sample, the intensity of positive control spots included in the array was determined and no differences were found.

6. Proteome-wide analysis

Proteome-wide analysis was carried out in the Proteomics Scientific and Technical Service from IACS (Zaragoza, Spain) in collaboration with Dr. Mª Angeles Álava.

Cells were seeded and grown in 10 cm plates until 80% confluence. Then, they were serum-starved for 24h. Cells were washed twice with PBS and lysed with Urea (6M)- SDS (0.1%) solution. To increase cell fragmentation, lysates were sonicated (4 cycles of 30 sec followed by 10 sec rest per cycle), maintained on ice for 1h (vortexing 20 sec every 10 min) and finally, 30 min at room temperature. Then, they were centrifuged at 13.000 rpm/15.000g for 20 min and supernatants were collected. Proteins were quantified by Lowry method using a standard curve of known concentrations of BSA (Panreac, A1391) and three solutions: (A) Na_2CO_3 (2%) - NaOH (0.1 M), (B_1) $CuSO_4 \cdot 5H_2O$ (1%) and (B_2) Sodium and potassium tartrate (2%). They were mixed in 50:0.5:0.5 proportion at the time of use and added to each

sample. Then, Folin C reagent was added. After 30 min incubation (in a darkness chamber at room temperature), absorbance was measured at 580 nm. Samples were stored at -80ºC until proteomic analysis.

The differential expression of proteins in parental *vs.* C3G-silenced U87 cells were analyzed by DIGE (differential in-gel electrophoresis). To do it, proteins were separated by two-dimension electrophoresis (2D). Protein spots of interest were excised, stained with coomasie blue followed by fluorescent and non-fluorescent scanning. Then, the selected spots were submitted to enzymatic digestion and they were analyzed by mass spectrometry (MALDITOF y TOF/TOF), followed by the identification of proteins isolated by mass spectrometry LC-ESI-MS/MS in the proteomic facility at Zaragoza University (Spain).

Data obtained after proteomic-wide analysis were processed through several bioinformatic GO analyses. When detected, keratins were considered sample contaminants and they were not taken into account for further analyses. The detected deregulated proteins were divided into two subgroups according to their overrepresention in U87 parental or U87shC3G cells. Using the uniprot ID number for each of them, several enrichment analyses of GO (*Gene Ontology*) terms were carried out by using *Panther software* (consulted in December 2019), *Cancertool software* (consulted in December 2019) and *DAVID software* (consulted in December 2019) software. In particular, we analysed GOBP (*GO biological processes*), GOCC (*GO cellular component*), GOMF (*GO molecular function*), Reactome (only in Cancertool software) and KEGG Pathway (only in DAVID software). They all were used under default settings. Statistically significant GOs were represented and compared taking into account their adjusted *p* value.

7. Fluorescence analysis in cells

7.1. Immunofluoresce staining

Cells were seeded on gelatine (2%)-coated (Sigma Aldrich, G9391) glass coverslips in 24 multiwell plates and grown as indicated for each experiment up to 50%-70% confluence. Then, cells were washed twice with PBS and fixed with 4% PFA (*paraformaldehyde*) (Sigma Aldrich, #158127) (20 min, at room temperature). Cells were permeabilized using 0.5% Triton X-100 in PBS for 10 min and blocked by incubation with 3% BSA - 1.5% NGS (*normal goat serum*)-PBS solution for 1h at room temperature. For nuclear staining (e.g. Ki67), permeabilization solution additionally contained 0.1% SDS. Then, coverslips were incubated overnight with the primary antibody diluted in 3% BSA - 1.5% NGS-PBS (*Table 10*) at 4ºC. They were

washed with PBS and incubated with secondary antibody diluted in BSA 3%- NGS 1.5%-PBS (*Table 10*) for 2h at room temperature. Nuclei were stained with DAPI (*4',6-diamidino-2-phenylindole*) (Panreac, #A4099) (1:1000 dilution). After washing with PBS, coverslips were mounted using mowiol reagent (Thermofisher, P36930) and visualized in either a Nikon Eclipse TE300 epifluorescence microscope or a Leica TCS-SL confocal microscope (Microscopy and Flow Cytometry CAI, Complutense University of Madrid, Spain). For localization analysis and quantification, ImageJ software was used. Fluorescence intensity was usually represented by the Integrity Density (ID) parameter (fluorescence intensity mean value multiplied by the percentage of positive area for each image) referred to DAPI staining (total positive area).

Table 10 – Antibodies used for protein analysis by immunofluorescence in cells

Primary antibodies		
Target	**Reference #**	**Dilution**
C3G (4-245 aminoacids)	Genosphere, *custom made*	1:100
Ki67	Abcam, ab15580	1:200
ZO-1	Invitrogen, 617300	1:50
β-catenin	BD, #610154	1:100

Secondary antibodies			
Isotype	**Emission wavelength**	**Reference #**	**Dilution**
Goat anti-rabbit	555 nm	Invitrogen, A32732	1:500
Goat anti-mouse	555 nm	Invitrogen, A32727	1:500
Goat anti-rabbit	488 nm	Invitrogen, A32731	1:500
Goat anti-mouse	488 nm	Invitrogen, A32723	1:500

7.2. F-actin cytoskeleton staining

For F-actin staining, the same fixation and permeabilization protocol was used. Then, coverslips were incubated with rhodamine-conjugated phalloidin (1:500 dilution)

(Sigma Aldrich, P1951) for 1h at room temperature. Nuclei were stained with DAPI (Panreac, #A4099) (1:1000 dilution).

7.3. Evaluation of EGF-induced EGFR trafficking by fluorescence microscopy

EGF-mediated EGFR endocytosis was evaluated by *in situ* fluorescence microscopy in living cells at different time points in Dr. I. Rubio's laboratory (Jena, Germany). Cells were seeded on gelatine (2%)-coated glass culture dishes and cells grown until 70-80% confluence. Then, they were incubated with binding-medium (phenol red free DMEM medium supplemented with BSA (0.1%) and HEPES (20mM)) for 30 min and stimulated with Alexa Fluor 488-labelled EGF (50 ng/ml) (Invitrogen, E13345) directly in the heating plate placed in LSM microscope at 37ºC. Images were taken at different time points (0-15 min after stimulation) to visualize EGF-EGFR interaction and EGF-mediated EGFR endocytosis. Fluorescence intensity was measured in all images with ImageJ Software and represented by the Integrity Density (ID) parameter.

8. Flow cytometry analysis of EGFR localized on the plasma membrane

The levels of EGFR on plasma membrane were determined by flow cytometry in non-permeabilized cells maintained in 10% or 0% FBS-DMEM medium. When indicated, serum starved cells were treated with EGF (10 ng/ml) for 2h to induce a long term EGF-mediated EGFR endocytosis as a control. To analyse EGFR recycling, cells were treated with the inhibitor of recycling monensin (10 μM) (Nishimura et al., 2015) (Nishimura & Itoh, 2019) for 1h, in the absence or presence of EGF. Then, cells were scrapped using PBS and centrifuged at 1500 rpm/1445g for 5 min. The pellet was resuspended in PBS and incubated with EGFR affibody conjugated with FITC (Abcam #ab81872) (1:200 dilution) for 30 min. FITC intensity was analysed in an Accuri BD FACS Flow Cytometer (Jena, Germany).

9. Analysis of mRNA levels

9.1. RNA extraction and quantification

Total RNA was extracted from cells using NucleoSpin RNA kit (Macherey-Nagel, 22740955) following the manufacturer instructions including DNAse treatment to

prevent DNA contamination. Total RNA was eluted with nuclease-free water and stored at -80ºC until use. For RNA quantification, absorbance at 260 nm (A_{260}) was measured in a spectrophotometer taking into account that RNA at 40 µg/ml concentration displays 1 unit of A_{260}. RNA purity was considered acceptable when A_{260}/A_{280} ratio = 1.7-2.

9.2. cDNA synthesis

Reverse transcription was performed using SuperScript III RT kit (Invitrogen, #18080-040) following the manufacturer's indications and using 1-3 µg RNA. First, RNA was denaturated by incubation at 95ºC for 5 min in the presence of Oligo(dT) (0.5 mM) and dNTPs (10 mM each). Then, samples were incubated at 50ºC for 1h with RNase Inhibitor (Promega, N2115), DTT (5 mM) and SuperScript III (retro-transcriptase) (200 U) in cDNA synthesis buffer. Reaction was stopped inactivating the enzyme by incubation at 70ºC for 15 min. Synthetized cDNA was stored at -20ºC until its use.

9.3. Real time PCR and data analysis

The cDNAs of interest were specifically amplified by quantitative PCR (qPCR) using specific primers (*Table 11*) and SYBR Green (Roche, #04 913 914 001) to monitor amplified DNA. Primers amplification efficiency was previously determined and ranged between 85%-115%. During the exponential amplification phase, a signal threshold is established over the background fluorescence. The Ct (*cycle threshold*) value for each target gene is determined as the fractional number of cycles required to reach this threshold. Then, Ct values are used to calculate changes in gene expression as a relative fold change between an experimental and the control sample, which is finally represented by RQ (*relative quantity*) factor. First, sample Ct is normalized with housekeeping gene Ct (*GUSB*), obtaining ΔCt value ($\Delta Ct_{sample} = Ct_{sample} - Ct_{housekeeping}$). Then, ΔCt for each sample is referred to ΔCt value of the control sample, and ΔΔCt value is calculated ($\Delta\Delta Ct_{sample} = \Delta Ct_{sample} - \Delta Ct_{control}$ and, as a consequence, $\Delta\Delta Ct_{control} = 0$). Finally, the RQ value is determined by formula $RQ_{sample} = 2^{(-\Delta\Delta Ct\ sample)}$ (and $RQ_{control} = 1$).

Sample in triplicate were used, and negative controls: RT- (RNA sample) and non-sample control (water). The reaction was performed in a 7900 Fast Real Time System (Life Technologies) from Genomics CAI at Complutense University of Madrid, Spain.

Some qPCRs were performed using the Taqman method. Specific Taqman probes (*Table 12*) for each gene with a reporter fluorescent dye at 5′-end and a quencher dye at 3′-end were used. Signal emission is due to DNA polymerase exonuclease activity

over the fluorescent dye at 5'-end. Data analysis and experiments were similarly performed, but *ACTB* gene was used as housekeeping.

Table 11 – Specific primers designed for RT-qPCR using SYBR Green method

Target gene	Forward primer (5'→3')	Reverse primer (5'→3')	Efficiency (%)
TWIST1	CAAAGAAACAGGGCGTGGGG	CAGAGGTGTGAGGATGGTGCC	106.7
ZEB2	AATGCACAGAGTGTGGCAAGGC	ATCTGGCGTTCCAGGGACTCAT	108.5
GAPDH	ATGTTCGTCATGGGTGTGAA	GGTGCTAAGCAGTTGGTGGT	90
MCT1	TGCGTGGGTACTGGAACAAG	TGCAGGTCAAATCCAAATATCGTT	92.6
PDHK1	CTTCTCAGGACACCATCCGT	AACCATGTTCTTCTAGGCCTTTCAT	92.8
PKM	GGCTCATCAAGGGCAGCG	AGATCTTGCTGCCCACTTCC	110
GUSB	ATCACCGTCACCACCAGCGT	GTCCCATTCGCCACGACTTTG	107

Table 12 – Reference number (Hs) of Taqman probes used in RT-qPCR assays

Target gene	Hs
DLAT	Hs00898876_m1
DLD	Hs00164401_m1
GLUT1	Hs00892681_m1
GLUT3	Hs00359840_m1
LDHB	Hs00929956_m1
SDHA	Hs00188166_m1
SDHC	Hs01698067_s1

Target gene	Hs
MCT4	Hs00358829_m1
PDHA1	Hs01049345_g1
PDHAB	Hs00168650_m1
PDHX	Hs00185790_m1
ACTB	Hs01060665_g1
SDHB	Hs00268117_m1

10. Adhesion, migration, invasion and cell cycle evaluation

10.1. Adhesion assay

For adhesion evaluation, 30000 trypsinized cells were seeded per well in 12 multiwell plates (uncoated or coated with Matrigel (5 μg/cm^2; Corning, #356234)) in medium containing FBS (10%). They were maintained at 37ºC and 5% CO_2 for 15

min or 30 min. When indicated, SB203580 was added during the experiment to inhibit p38(α) MAPK pathway (following indications included in *Table 2*). Then, adhered cells were fixed and stained with violet crystal (0.2%)-ethanol (2%) or DAPI (1:1000 in 0.5% Triton X100-3% BSA in PBS) for 20 min at room temperature. Excess of staining solutions was removed with water or PBS, respectively. Stained cells were quantified using ImageJ software.

10.2. Wound healing assay

Confluent cells in 60 cm plate were treated with Mitomycin C (6.25 µg/ml) (DNA alkylating agent) (Sigma Aldrich, M0503) for 30 min to inhibit cell proliferation. Then, a straight scratch was performed, cells were washed with PBS and fresh FBS-free cell culture medium was added. Cells were maintained in culture (in the absence of FBS) and migration was monitored at different time points (0h, 6h and 24h) using a phase-contrast Eclipse TE300 Nikon microscope to take images of the scratch. When indicated, PD98059 was added during the experiment to inhibit ERKs pathway (following indications in included *Table 2*). After 48h, the scratch was totally closed by cells of all the analysed cell lines. The percentage of wound healing closure was measured by processing images using TScratch software, referring data to 0h time value.

10.3. Invasion assay

Invasive capacity was analysed using 8 µm-pore transwells (Falcon, #353097) coated with Matrigel (333 µg/cm2) (Corning, #356234) (Figure XV). 25000 cells were seeded in the upper chamber in serum-free medium. When indicated, 10% FBS medium was added into the lower chamber to act as chemoattractant.

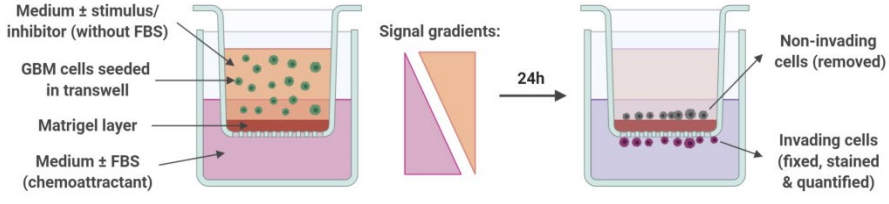

Figure XV – **Invasion assay through Matrigel**. Cells are seeded in the upper chamber of the transwells in the absence or presence of exogenous stimuli. In the lower chamber, medium supplemented with 10% serum (FBS, *fetal bovine serum*) is added for some experiments to act as chemoattractant. After 24h, invasive cells are fixed, stained and quantified.

To evaluate invasion in response to a specific ligand stimulation, cells in the upper chamber were treated with EGF, MDK or FGF-2 (as indicated in *Table 1*) or maintained untreated and no serum was added into the lower chamber. To inhibit

MEK/ERKs and p38 MAPK, cells in the upper chamber were treated with PD98059 or SB203580, respectively (according to *Table 2* indications). When indicated, 10% FBS-medium was added into the lower chamber to act as chemoattractant.

In all cases, cells were maintained 24h at 37ºC and 5% CO_2. Then, cells from the lower chamber were fixed with 4% PFA for 20 min, washed twice with PBS and stained with violet crystal (0.2%) or DAPI (1:1000 in 0.5% Triton X100-3%BSA in PBS) for 20 min at room temperature. Then, they were counted using a phase-contrast Eclipse TE300 Nikon microscope coupled to a digital camera and ImageJ software.

10.4. Analysis of the activity of secreted MMP2 by gelatine zimography

Both MMP2 (gelatinase A) and MMP9 (gelatinase B) activities were determined by gelatin-zymography, although MMP9 activity in GBM cells was very low to be determined. Confluent cells were serum-starved for 24h. Cell culture medium was collected and analysed by electrophoresis in 8% SDS-PAGE gel (*Table 8A*) containing gelatine (0.1%) (Sigma, G9391), under non-reducing conditions. To normalize the volume of medium loaded, the amount of total proteins in cell extract was quantified and mediums were loaded according to that quantification. Samples were prepared in β-mercaptoethanol-free and DTT-free Laemmli buffer 4X (Tris-HCl 40 mM, pH 7.6; Glycerol 10%; SDS 1%; Bromophenol blue 0.002%) and they were not boiled. Electrophoreses were carried out at constant voltage (80 V). Next, gels were washed with Triton X-100 (2.5%) for 30 min and incubated overnight in Substrate buffer (Tris 50 mM pH 7.5, NaCl 0.2M, $CaCl_2$ 5 mM, Triton X-100 1%, NaN_3 0.02%) at 37ºC. MMP2 enzymatic activity was proportional to gelatine degradation in the gel, which was visualized by gel staining with Coomassie Brilliant Blue (BioRad, 161-0400) as clear bands over dark background. Band intensity was determined using ImageJ software and data were referred to control sample in each experiment.

10.5. Cell cycle analysis by flow cytometry

To study proliferation and apoptosis, cell cycle analysis was carried out by flow cytometry in attached and non-attached cells. Cells were maintained attached (80% confluence) or detached (in suspension under soft shaking to prevent adhesion) for 6 h, in either complete or serum-free medium. Then, cells in suspension were centrifuged, washed with PBS and the pellet was fixed. On the other hand, attached cells were trypsinized, pelleted by centrifugation, washed with PBS and fixed.

Cell pellet fixation was performed with cold ethanol (70%) for 1 min. Fixed cells were centrifuged (2000 rpm/1930g, 5 min), washed and resuspended in PBS.

Samples were incubated with RNase (0.1 µg/ml) (Qiagen, #19101) at 37ºC for 30 min to eliminate RNA. To stain DNA, propidium iodine (50 ng/µl) (Panreac, A2261) was added 5 min before cell cycle analysis at the cytometer. Cells with DNA content less than 2N were considered apoptotic. Cells with DNA content higher than 2N were considered proliferative: 4N for G_2/M phase of cell cycle and in between 4N and 2N for S phase of cell cycle. DNA content and cell populations were analysed using MODFIT mathematical model by Microscopy and Flow Cytometry CAI (Complutense University of Madrid, Spain).

11. *In vitro* analysis of tumourigenic capacity

11.1. Anchorage-dependent growth assay

To assess anchorage-dependent growth, 300 cells were seeded in a 6 cm plate with complete DMEM medium and were grown for 21 days at 37ºC and 5% CO_2. When indicated, plates were additionally treated with PD98059 every 3 days according to *Table 2*. Then, cell culture medium was removed, cells washed with PBS twice and foci were stained with violet crystal (0.2%)-ethanol (2%) solution for 15 min at room temperature. Excess of staining was washed with water and the number of foci was quantified macroscopically. Finally, cell organization into each focus was evaluated and quantified (number of cells per focus) using a phase-contrast Eclipse TE300 Nikon Microscope and Image J software.

11.2. Anchorage-independent growth assay

Anchorage-independent growth capacity was measured in soft-agar-cultures. First, a layer of agar (0.5% for U87 cells or 0.75% for PDCs) (Sigma Aldrich, A9414) diluted in complete DMEM medium was added per well in a 24multiwell plate. Then, cells (3.000 per well for U87 cell line and 6.000 per well for PDCs) were seeded in a new layer of agar (0.35%) diluted in complete DMEM medium. Cells were incubated for 14 days at 37ºC and 5% CO_2, adding fresh complete medium every 3 days. When indicated, cells were additionally treated with PD98059 every 3 days according to *Table 2*. Foci formation capacity was quantified by quantification of the total number of foci per field and foci diameter using a phase-contrast Eclipse TE300 Nikon microscope coupled to a digital camera and ImageJ software. Isolated cells were not considered foci and they were not quantified. For the quantification of the number of cells per focus, foci were stained with DAPI (1:1000 in 0.5% Triton X100, 0.1% SDS, 3% BSA, 1.5% NGS, PBS solution) (Panreac, A4099) and each fluorescent nucleus was counted as a cell in a manual way using ImageJ software.

12. *In vivo* tumour growth assays and sample analysis

12.1. Tumour xenograft assays in mice

All mice experiments were carried out in compliance with the institution's guidelines. For *in vivo* tumour growth evaluation, parental U87 and U87shC3G cells were used. Cells resuspended in PBS ($1x10^6$ cells in 100 µl) were subcutaneously injected into both flanks of seven-week old female nude mice (Envigo, #6903F) (4 animals for parental U87 cells and 5 animals for U87shC3G cells). PBS was injected in one control animal as a vehicle control. Tumour size was monitored twice a week. On day 15 after inoculation, mice were sacrificed and tumours excised, weighed and measured. Tumour area (A) (mm^2) was calculated by the formula $A=\pi*(D/2)*(d/2)$ and tumour volume (V) (mm^3) by $V=(4/3)*\pi*(D/2)*(D/2)*(d/2)$.

12.2. *In ovo* assay by cell inoculation into chicken embryo chorioallantoic membrane

The chicken chorioallantoic membrane (CAM) assays were performed as previously described (*Figure XVI*) (Hagedorn, 2005) (Fernández-Nogueira et al., 2020). Briefly, we used premium specific pathogen-free, fertile, 9-day-incubated embryo chicken eggs (supplied by Gibert farmers and Santa Isabel farmers). Cells ($1x10^6$ for U87/U87shC3G or $2x10^6$ for 12Φ12D/12Φ12DshC3G cells) diluted in PBS-Matrigel solution (1:1 ratio) were inoculated per egg in chicken embryo CAMs under sterile conditions. Then, chicken embryos were incubated at 37ºC for 7 days. Finally, tumours were excised, weighed, measured and fixed in 4%PFA (overnight at 4ºC in rotation) to be paraffin-embedded and analysed by immunostaining. Tumour volume was calculated with the above mentioned formula.

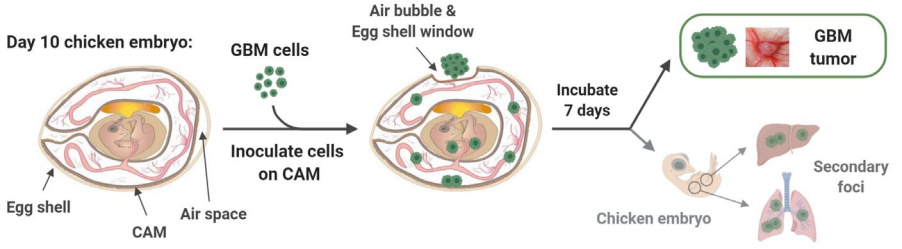

Figure XVI – ***In ovo* tumour growth assays (CAM assays)**. GBM cells were inoculated in the chorioallantoic membrane (CAM) of 9-day-incubated chicken embryos. After 7 days, tumours were extracted, measured and fixed.

12.3. Tumours processing and analysis

12.3.1. Tissue paraffin-embedding and slide preparation

Fixed tumours were washed twice with PBS, dehydrate and embedded in paraffin (Merck, #1.07157) following the protocol described in *Table 13*. Paraffin blocks containing tumour samples were stored at 4ºC until its use. They were cut in 8 µm sections using a microtome, placed on slides and incubated overnight at 37ºC. Prior to immunofluorescence staining, slides were dewaxed and rehydrated following the protocol described in *Table 14*.

Table 13 – Tumour paraffin-embedding protocol

Stage	Step repeats	Reagent	Time (each)	Temperature
1 Dehydration	1	Ethanol 30%	20 min	4ºC
	1	Ethanol 50%	20 min	4ºC
	1	Ethanol 70%	20 min	4ºC
	1	Ethanol 90%	Overnight	4ºC
	3	Ethanol 100%	20 min	Room temperature
2 Clearing with xylene	3	Xylene (Panreac, #251769.2711)	15 min	Room temperature
3 Paraffin-embedding	3	Paraffin-xylene (1:1 ratio)	30 min	62ºC
	3	Paraffin	1h	62ºC
4 Paraffin-blocking	(i) Place tissues in the molds with fresh paraffin (at 62ºC)			
	(ii) Place plastic cassettes on the top of tissue-containing molds (at 62ºC)			
	(iii) Remove air bubbles			
	(iv) Harden overnight at room temperature and demold carefully			

12.3.2. Immunofluorescence staining of paraffin sections

After antigen retrieval and washing, samples were permeabilized by incubation with 0.5% Triton X-100-PBS for 5 min, washed with PBS and blocked with 3%BSA-1.5%NGS-PBS solution for 30 min at room temperature. Then, they were washed with PBS and incubated overnight with the primary antibody at 4ºC in a humid box. Primary antibodies were prepared in blocking solution (*Table 15*). Next day, slides were washed with PBS, treated with 0.01% Tween- PBS for 5 min and incubated for 1h with the secondary antibody (*Table 15*) and DAPI (1:1000) (Panreac, A4099) in blocking solution. Finally, slides were washed with PBS and water, and mounted with mowiol (Thermofisher, P36930). Fluorescent staining was visualized in a Nikon

Eclipse TE300 epifluorescence microscope coupled to a digital camera and for immunoflorescence quantification, ImageJ software was used. Integrity Density (ID) referred to DAPI staining (positive total area) was determined.

Table 14 – Protocol for immunofluorescence staining of paraffin sections

Stage	Step repeats	Reagent	Time (each)
1 Wax removal	Incubation at 55ºC for 30-45 min		
2 Re-hydration	2	Xylene	5 min
	2	Ethanol 100%	5 min
	1	Ethanol 90%	3 min
	1	Ethanol 80%	3 min
	1	Ethanol 70%	3 min
	2	Water	3 min
3 Antigen retrieval	Heat slides in Citrate buffer (10 mM, pH 6) using a microwave (800 W, 12 min) and let them cool down at room temperature		
4 Washing	1	Water	5 min
	1	PBS	5 min

12.3.2. Hematoxylin-eosine staining of paraffin sections

Hematoxylin/eosin staining of CAM tumour-paraffin sections was performed as follows. After deparaffinization, sections were rehydrated by successive washes with limonene/xylene (3 min, twice), ethanol 100% (3 min, twice), ethanol 95% (3 min), ethanol 70% (3 min) and water (3 min). Then, sections were incubated with hematoxylin (Carazzi's Hematoxylin (Panreac #255298.1610)) for 17 min, washed with water (3 min, twice), incubated with eosin (eosin Yellowish (1%), (Panreac #251301.1611)) for 9 min and washed with water (3 min, twice). After this, sections were dehydrated by successive washes with ethanol 70% (3 min), ethanol 95% (3 min), ethanol 100% (3 min, twice) and limonene/xylene (3 min, twice). Then, they were mounted using Eukitt (Fluka).

Table 15 – Antibodies for protein analysis by immunofluorescence in tumour sample

Primary antibodies		
Target	**Reference #**	**Dilution**
C3G (4-245 aminoacids)	Genosphere, custom made	1:50
Cleaved-Caspase 3	CST, #9661	1:100
Ki67	CST, # 9449	1:100
Vimentin	BD, #550513	1:100
αSMA	Dako, M0851	1:100
MECA32	Pharmingen, #550563	1:50
PKM2	CST, #3198S	1:100
Nestin	Abcam, ab105389	1:100
GFAP	Dako, Z033429-2	1:200
NeuN	Merck, MAB377	1:200

Secondary antibodies			
Isotype	**Emission wavelength**	**Reference #**	**Dilution**
Goat anti-rabbit	555 nm	Invitrogen, A32732	1:200
Goat anti-mouse	555 nm	Invitrogen, A32727	1:200
Goat anti-rabbit	488 nm	Invitrogen, A32731	1:200
Goat anti-mouse	488 nm	Invitrogen, A32723	1:200

13. Analysis of cell metabolism

13.1. Enzymatic activity analysis

EA (*enzymatic activity*) assays were adapted from *Teslaa & Teitell, 2014*. All enzymatic activities are expressed as U/µg of protein (specific enzymatic activity)

being proteins measured by BCA method. All reactions were coupled to NAD(P)H changes which were analysed spectrophotometrically by quantification of absorbance at 340 nm per min (ΔA/min). This corresponded to the speed of the reaction (slope of the linear part of reaction curve). Then, using Lambert-Beer equation, $A = \varepsilon * C * l$, where $\varepsilon_{NAD(P)H} = 6.22 * 10^3\ cm^{-1}M^{-1}$ and l=1 cm, it is calculated the concentration units per minute (U).

In all experiments, cells were seeded in 6 multiwell plates (500.000 cells per well) and next day, cell culture medium was replaced by a fresh one supplemented or not with 10%FBS. In some experiments, cells were additionally treated with sodium azide as indicated in Table 4. Cells maintained 24h in culture were washed twice with PBS and then protein was extracted with Standard enzymatic activity buffer (SEA buffer; Tris-HCl 50 mM pH 7.5, NaCl 150 mM, NP40 1%, EDTA 1 mM, DTT 1mM, aprotinin 10 μg/ml, leupeptin 10 μg/ml, Na_3VO_4 1 mM y NaF 20 mM), except when the use of other buffer is indicated.

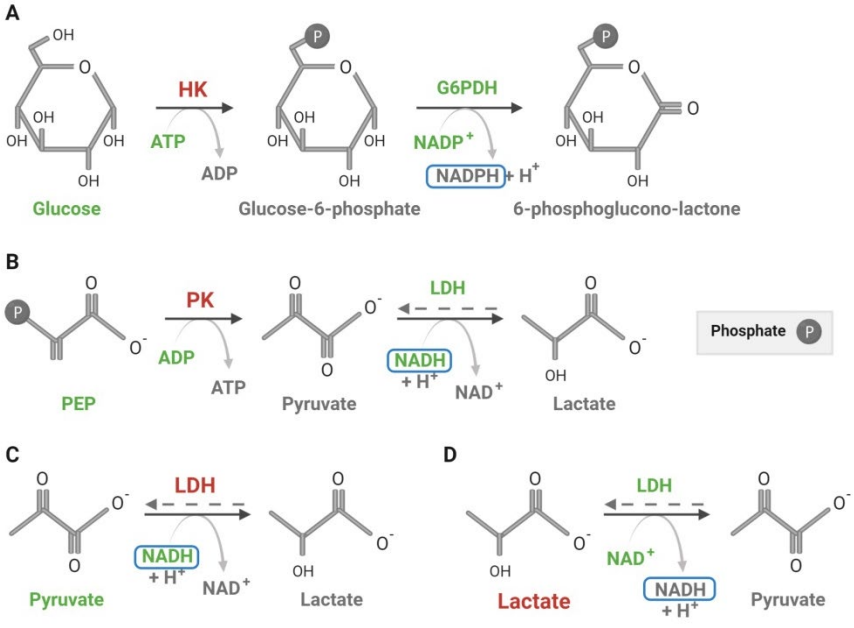

Figure XVII – ***In vitro*** **reactions used to measure enzymatic activities or metabolites: hexokinase (HK) (*A*), pyruvate kinase (PK) (*B*), lactate dehydrogenase (LDH) (*C*) and lactate (*D*)**. The enzyme/metabolite measured is indicated in red. Reagents (including exogenous enzymes) supplemented in the reaction mix are indicated in green. Molecules used for spectrophotometric measurement are surrounded by a blue square.

13.1.1. Hexokinase

For HK activity determination, glucose conversion to glucose-6-phosphate was coupled to the reaction catalysed by G6PDH (glucose-6-phosphate conversion to 6-phosphoglucono-lactone, consuming NADP+ that leads to NADPH production) (*Figure XVIIA*). For the reaction, 5 µg of proteins extracted using SEA buffer were diluted in 250 µl HK reaction buffer (Tris-HCl 50 mM pH 7.5, $MgCl_2$ 10 mM, ATP 0.6 mM (Sigma Aldrich, A2383), glucose 100 mM (Panreac, A3730), $NADP^+$ 0.2 mM (Sigma Aldrich, N0505) and G6PDH 0.1 U/ml (Sigma Aldrich, G4134)). Absorbance at 340 nm was determined for up to 20 min (one measurement per minute) at 37ºC.

13.1.2. Piruvate kinase

For PK activity determination, PEP (*phospho-enol pyruvate*) conversion to pyruvate in the presence of ATP was coupled to the reaction catalysed by LDH (pyruvate conversion to lactate and NADH consumption) (*Figure XVIIB*). For the reaction, 1 µg of proteins extracted using the SEA buffer was diluted in 250 µl PK reaction buffer (Tris-HCl 50 mM pH 7.5, KCl 100 mM, $MgCl_2$ 5mM, ADP 0.6 mM (Sigma Aldrich, A2754), PEP 0.5 mM (Sigma Aldrich, #860077), NADH 0.5 mM (Sigma Aldrich, N7004), FBP 10 µM (Sigma Aldrich, F6803) and LDH 10 U/ml (Sigma Aldrich, #59747)). Absorbance at 340 nm was determined for up to 20 min (one measurement per 30 sec) at 37ºC.

13.1.3. Lactate dehydrogenase

For LDH activity determination, NADH consumption during pyruvate conversion to lactate was measured (*Figure XVIIC*). Protein samples were extracted using phosphate-Triton lysis buffer (K_2HPO_4 0.1 M pH 7.4 and Triton X-100 0.5%). For the reaction, 25 µl of protein extract was diluted in 75 µl of phosphate-Triton buffer. Then, pyruvate (20 mM) (Sigma Aldrich, P8574) and NADH (0.5 mg/ml) (Sigma Aldrich, N7004) were added. Absorbance at 340 nm was determined for up to 20 min (one measurement per minute) at 37ºC.

13.2. Glucose uptake assay

Cells were seeded in 6 multiwell plates (500.000 cells per well) and next day cell culture media were replaced by glucose-free DMEM medium (Gibco, #11966025), supplemented or not with 10%FBS, as indicated. Cells were incubated 1h under these conditions. Then, NBDG (*2-(N-(7-nitrobenz-2-oxa-1,3-diazol-4-yl)amino)-2-deoxyglucose*) a fluorescent glucose analogue (excitation peak at 465-490 nm and emission peak at 535-550 nm) (Thermo Fisher, N13195) was added to cell medium at different concentrations (0-100 µM). After 1h incubation, culture medium was collected and stored, and cells were scrapped using PBS. Then, they were

centrifuged at 1200 rpm/1157g for 5 min, washed and resuspended in PBS. Cells were maintained on ice and propidium iodide (50 ng/µl) (Panreac, A2261) was added 5 min before their analysis in the cytometer (Microscopy and Flow Cytometry CAI (Complutense University of Madrid, Spain)).

13.3. Quantification of lactate in the culture medium

Cells were seeded in 6 multiwell plates (50000 cells per well) in complete DMEM medium and grew for 3 days. Then, cell culture medium was replaced by fresh medium supplemented or not with 10% FBS, as indicated. At different time points, cell culture medium was collected.

Lactate present in the culture medium was determined by spectrophotometry using the reaction catalysed by exogenous LDH (lactate conversion to pyruvate coupled to NAD^+ reduction) (*Figure XVIID*). A standard curve of known lactate concentrations (0-4 mM) (Fluka, 69775) in serum-free medium was used to extrapolate data from cell samples. The reaction was prepared by adding cell culture medium sample (16 µl) to a buffer solution containing hydrazine (0.335 mM), glycine (0.42 mM) and NAD^+ (1.6 mM) up to 260 µl. The mixture absorbance at 340 nm was used as the blank (A_1). Then, exogenous LDH (2U per well) (Roche, #10127876001) was added and samples were incubated at 25ºC for 1h. Absorbance at 340 nm was measured again (A_2). Absorbance change due to LDH action was calculated as $\Delta A = A_2-A_1$ and interpolated in lactate curve. Since FBS contains lactate, for media supplemented with FBS, an additional control with 10% FBS-DMEM, in the absence of cells, was included. To obtain the amount of lactate produced and released by these cells, the concentration of this control was subtracted.

Total proteins from cells was extracted for each sample using phosphate-Triton buffer and quantified by BCA method to refer the amount of lactate in cell culture medium to total protein.

14. Evaluation of stemness

14.1. Stem-like cell culture

Stem-like GBM spheres cultures were generated by maintaining GBM cells in a stem/GSC phenotype-promoting cell culture medium (*Table 16*) as previously described (Lee et al., 2006) (López-Valero et al., 2018) (López-Valero et al., 2020). For this, differentiated parental U87 and U87shC3G cells were diluted in stem-promoting sphere medium (10^6 cells in 10 ml), seeded in non-adherent 10 cm dishes (Cultek, #351029) and maintained in the incubator for 24h. Cells in suspension were

collected (passage 0 (p+0)), centrifuged and re-seeded in a new non-adherent dish. Attached cells were discarded. Cells in suspension were maintained in the sphere medium and, approximately every 10 days, when sphere diameter reached 50-150 µm, they were subcultured (p+1, p+2, p+3…). Spheres present in the culture medium were disaggregated with trypsin (dilution 1:3), centrifuged at 1.200 rpm/1157g, counted and re-plated as individual cells ($5x10^5$ cells per plate) in new non-adherent cell culture dishes. Standard protocols determine that stem-like phenotype is stable from passage (indicated as p+) 2-3.

Table 16 - Stem-promoting sphere culture medium composition

Reagent	Reference	Final concentration
DMEM:Ham's F12 medium (1:1 mixture)	DMEM → Lonza, #12-604F Ham's F12 → Lonza, #12-615F	1X (*commercial*)
Streptomycin	Sigma, S9137	10 µg/ml
Penicillin G	Sigma, #13752	12 µg/ml
HEPES	Fisher Scientific, BP310-1	20 mM
EGF	R&D, #236-EG-200	20 ng/ml
FGF-2	Preprotech, AF-100-18B	20 ng/ml
Sodium heparin	Sigma Aldrich, H3149-25KU	2 µg/ml
B27	Gibco, #17504-044	1X (*commercial*)
LIF	Millipore, LIF1010	1 µg/ml

Since FBS and DMSO can interfere with stemness and promote GSC (*GBM stem cell*) differentiation, sphere cryopreservation was performed with STEM-CELLBANKER product (Zenoaq), following manufacturer's indications for cryopreservation as well as thawing.

14.2. Analysis of stemness properties

To evaluate stemness properties, the number of spheres and their size were analysed in every passage. For that, in every GSC-like culture, images were taken at every passage using a phase-contrast Eclipse TE300 Nikon Microscope coupled to a digital DS-U2 camera. Then, the number of spheres and their diameter was measured using ImageJ software. These parameters are not specific for stemness and can be influenced by other factors. Hence, the expression levels of different stem-cell markers and ELDAs (*extreme limiting dilution assays*) are also required.

14.3. Extreme limiting dilution assays

To evaluate self-renewal capacity of stem-like cultured cells, ELDAs (*extreme limiting dilution assays*) were performed at different culture passages. Spheres were disaggregated with diluted trypsin and individual cells were counted. Then, they were seeded in 96 multiwell plates at different cell densities: from 10 to 100 cells per well. In all wells, complete cell culture medium was added. Two weeks later, sphere formation capacity was evaluated using a phase-contrast Nikon Eclipse TE300 microscope. All seeded wells were evaluated according to the following criteria: (i) Negative well: total absence of spheres; (ii) Positive well: appearance of at least one sphere, independently of its size. No differences were established among wells depending on the number of spheres found.

These data were processed using ELDA software taking into account all considerations previously described (Hu & Smyth, 2009). Data were visualized by a dose-response graph (number of cells seeded per well in axis X *vs.* logarithm of the fraction of negative wells in axis Y), where slope of the continuous line is proportional to the self-renewal capacity of the cells. If the slope is higher, cells have more stem-like phenotype and higher GBM-initiating capacity. Discontinuous lines indicate the 95% confidence interval, also calculated by ELDA software.

15. Statistical analysis

Data were represented as the mean values of, at least, 3 independent experiments ± S.E.M. All statistical analyses were carried out with GraphPad Prism Software version 6.01. Unpaired Student's t-test was used to compare two experimental groups under normal distribution of the data. To compare more than two groups, ANOVA analysis was performed. One-way ANOVA was used for one variable and two-way ANOVA for two variables, followed by either Tukey or Bonferroni test. Statistical significance was considered when p value <0.05 (*p<0.05, **p<0.01 and *** p<0.001)

Results

1. C3G is downregulated in glioblastoma samples, independently of patient gender and age

As mentioned in the introduction, GBMs (*glioblastomas*) are a great challenge in clinic due to their aggressive phenotype (with high proliferation, disseminative capacity and plasticity) and the lack of effective treatments. Although it is known that C3G regulates invasion and growth in other tumours (e.g. coloncarcinoma or HCC), and it controls different functions in brain, the role of C3G in GBM remains unknown.

Therefore, we first studied the expression of *RAPGEF1* gene (encoding C3G) in human GBM samples (166 samples) compared to healthy brain (5 samples) from RNAseq cohort obtained from TCGA database. *RAPGEF1* mRNA expression was normalized with *GUSB* (*Figure 1A*), *ACTB* (*Figure 1B*) and *UBC* (*Figure 1C*). In all cases, it was significantly downregulated in GBM samples compared to healthy brain. Moreover, *RAPGEF1* downregulation was not dependent on patient sex/gender (*Figure 2A*) or age (*Figure 2B*), suggesting that C3G may play a role on GBM onset and/or development.

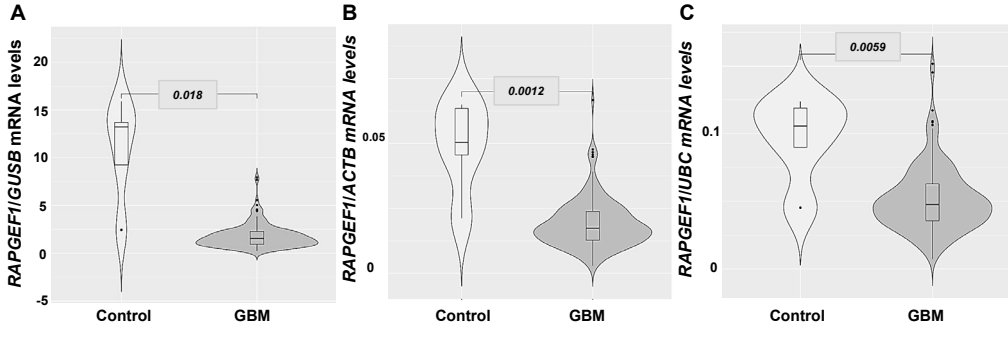

Figure 1 – *RAPGEF1* mRNA expression is down-regulated in GBM samples compared to non-tumour controls. *RAPGEF1* (gene encoding C3G) mRNA levels in healthy brain (control) (5 samples) and GBM samples from patients (153 samples) obtained from TCGA database normalized to *GUSB* **(*A*)**, *ACTB* (β-actin) **(*B*)** and *UBC* (Ubiquitin C) **(*C*)**. *p* value for each comparison is shown (Mann-Whitney statistical test).

Integrated multidimensional genomic studies have allowed GBM subclassification into four molecular signatures: classical, mesenchymal, proneural and neural (Verhaak et al., 2010). Using expression data available from RNAseq-TCGA cohort, GBM samples were clustered according to the expression of GBM molecular subtype markers and *RAPGEF1* expression was analysed in each subtype (*Figure 3*). Although the results were not statistically significant, GBM samples with high *RAPGEF1* expression preferentially clustered as proneural GBMs, while classical and mesenchymal GBMs presented low *RAPGEF1* expression. These data would be

important in clinic. Hence, C3G levels could be used as predictors of GBM subtypes, patient outcome and tumour response to treatment, among others.

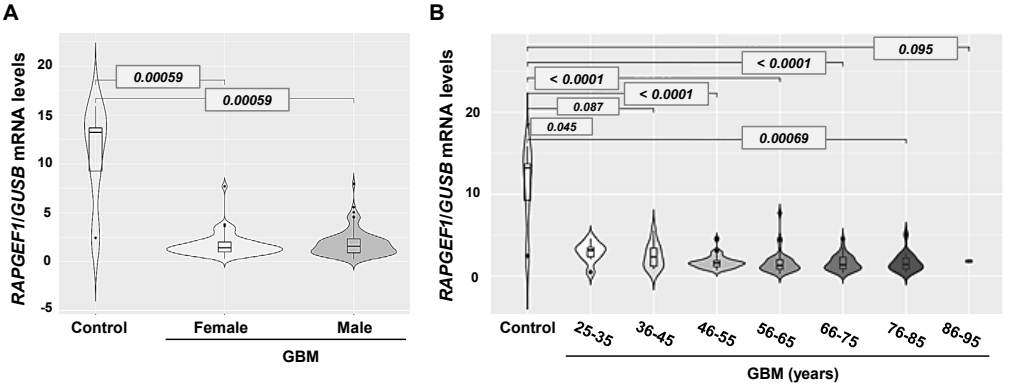

Figure 2 – ***RAPGEF1* mRNA levels downregulation in GBM tumours from patients is not sex/gender- or age-dependent.** Clinical data for RNAseq TCGA cohort were downloaded from FIREBROWSE and C3G (*RAPGEF1*) expression, normalized to *GUSB*, was analysed in GBM samples according to patient sex/gender (5 samples in control, 52 in female and 92 in male) **(*A*)** and diagnosis age (5 samples in control, and 9, 12, 35, 48, 35, 16 and 2, respectively in mentioned age groups) **(*B*)**. *p* value for each comparison is shown (Mann-Whitney statistical test).

Unluckily, the correlation between *RAPGEF1* expression and patient survival using Kaplan-Meier test did not reveal any significant change due to the low therapeutic window and life expectancy of GBM patients upon diagnosis (*not shown*). New analyses are also required to study the role of mutations in C3G function in GBM onset and/or progression.

To further confirm C3G downregulation in GBM, C3G protein levels were determined by western blot in a panel of human GBM cell lines compared to non-tumourigenic glial cells from brain (human astrocytes). C3G levels were decreased in all GBM cell lines analysed (U87, U118, T98, U251 and A172 cells) compared to GFAP (*glial fibrillary acidic protein*)$^{+}$ HAs (*human astrocytes*) (*Figure 4*). Moreover, it was found an inverse correlation between C3G and Vimentin, a mesenchymal marker widely associated with GBM aggressiveness (Lin et al., 2016) (Zhao et al., 2018) (Nowicki et al., 2019). Indeed, Vimentin was absent in HAs while upregulated in all GBM cell lines analysed. Interestingly, GBM cell lines presenting lower levels of C3G (U87, U118, U251 and A172) had also higher GFAP levels than HAs and the opposite occurs in GBM cells with higher levels of C3G (T98), suggesting an inverse correlation between C3G and GFAP that should be further confirmed.

Therefore, C3G downregulation in GBM samples and cell lines suggests a promising role for this protein in GBM onset and/or progression. Hence, further studies were performed to establish the role played by C3G in this tumour, as well as the mechanisms involved.

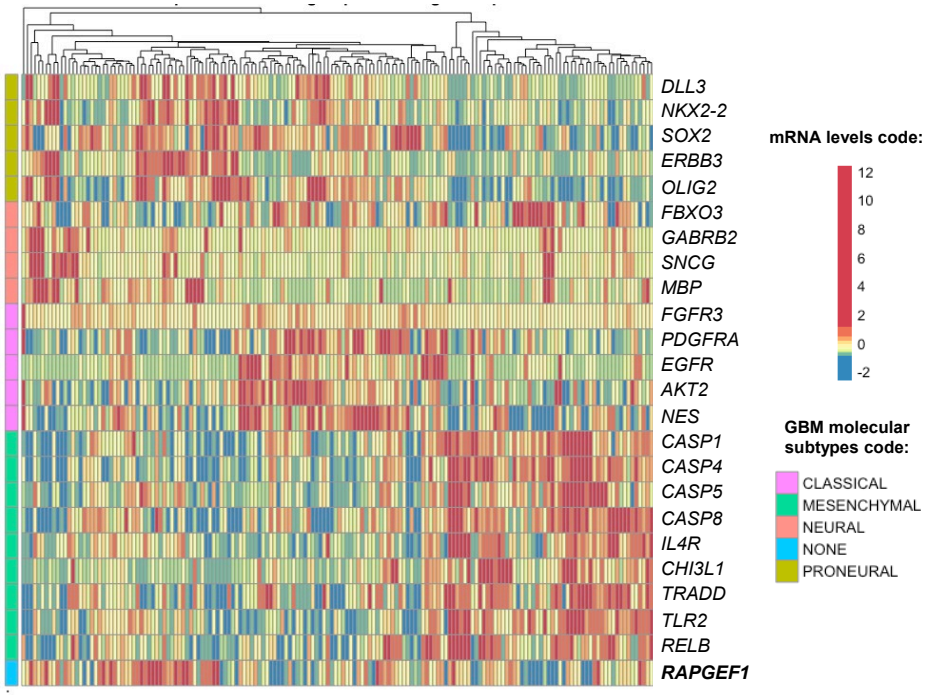

Figure 3 – ***RAPGEF1* downregulation appears to be associated to classical and mesenchymal GBM molecular signatures.** Heatmap representation of TCGA cohort expression data from GBM samples (horizontally) clustered by expression of genes associated to GBM molecular signatures (Verhaak et al., 2010) (vertically). C3G (*RAPGEF1*) expression is included at the bottom line (NONE category).

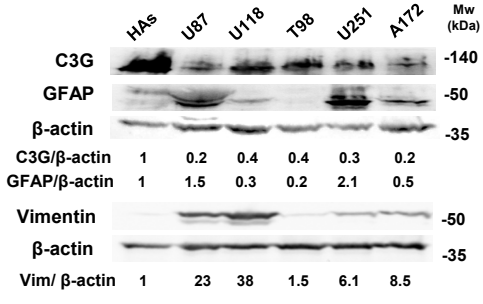

Figure 4 – **C3G is downregulated in GBM cell lines compared to GFAP$^+$ human astrocytes. Inverse correlation between C3G and Vimentin levels.** Western blot analysis of C3G, GFAP and Vimentin protein levels in HAs (human astrocytes) and the indicated GBM cell lines, normalized to β-actin. Densitometric quantification of C3G/β-actin, GFAP/β-actin and Vimentin/β-actin ratios are shown.

2. C3G inhibits invasion of glioblastoma cells through induction of an epithelial to mesenchymal-like process

2.1. C3G regulates glioblastoma cell morphology and F-actin organization

2.1.1. C3G silencing increases the number of migratory structures, while decreases cell-cell contacts in GBM cells

Taking into account that C3G levels are decreased in GBM compared to healthy brain and astrocytes, next step was to analyse the repercussions of this downregulation on tumour onset and/or development. To do it, we used several *in vitro* GBM cell models, as well as different approaches to modify C3G expression.

First, we started by using U87 cells, a well-established GBM cell line previously employed in multiple studies. We permanently silenced C3G in U87 cells using a mixture of shRNAs specifically designed against human *RAPGEF1* mRNA (shC3G). C3G downregulation was verified by western blot, which showed a decrease of approximately 60-70% both in the presence or absence of serum (*Figure 5A, upper-left panel*). Complementary, C3G silencing was also demonstrated by immunofluorescence staining (*Figure 5A, lower panel*). U87 non-targeting shRNA (shNTC) cells were also generated as a control, which have similar C3G levels to those detected in parental U87 cells (*Figure 5A, upper-right panel*). Regarding cell morphology, U87shC3G cells adopted a striking phenotype with fewer cell to cell contacts (*Figure 5B, upper panel*). These changes were more pronounced in the presence of serum. Importantly, at similar confluence, parental U87 cells were organized as a monolayer, although irregular, while U87shC3G accumulated in some places, extended long cell protrusions to another cells and left empty gaps along the plates. No qualitative differences in cell morphology and organization were observed between parental and shNTC U87 cells (*Figure 5B, lower panel*). The lack of cell-cell contacts was also evidenced by immunofluorescence analysis of β-catenin, which interacts to cadherins forming adherens junctions, and ZO-1 (a tight junction marker) (*Figure 5C*). This clearly showed a higher presence of β-catenin in cell-cell contacts in parental than in C3G-silenced U87 cells. A similar tendency was observed in ZO-1 staining, although to a lesser extent.

Next, we analysed F-actin (*filamentous-actin*) organization by staining with rhodamine-conjugated phalloidin. As observed in *Figure 6A*, parental U87 cells display some lamellipodia and F-actin accumulation around cells, close to the plasma membrane. In contrast, in U87shC3G cells, F-actin was more disorganized, being highly present in cell extensions. Hence, the number of migratory structures,

quantified following criteria described by Jeong et al. (2008), was significantly higher in U87shC3G than in parental cells (*Figure 6B*).

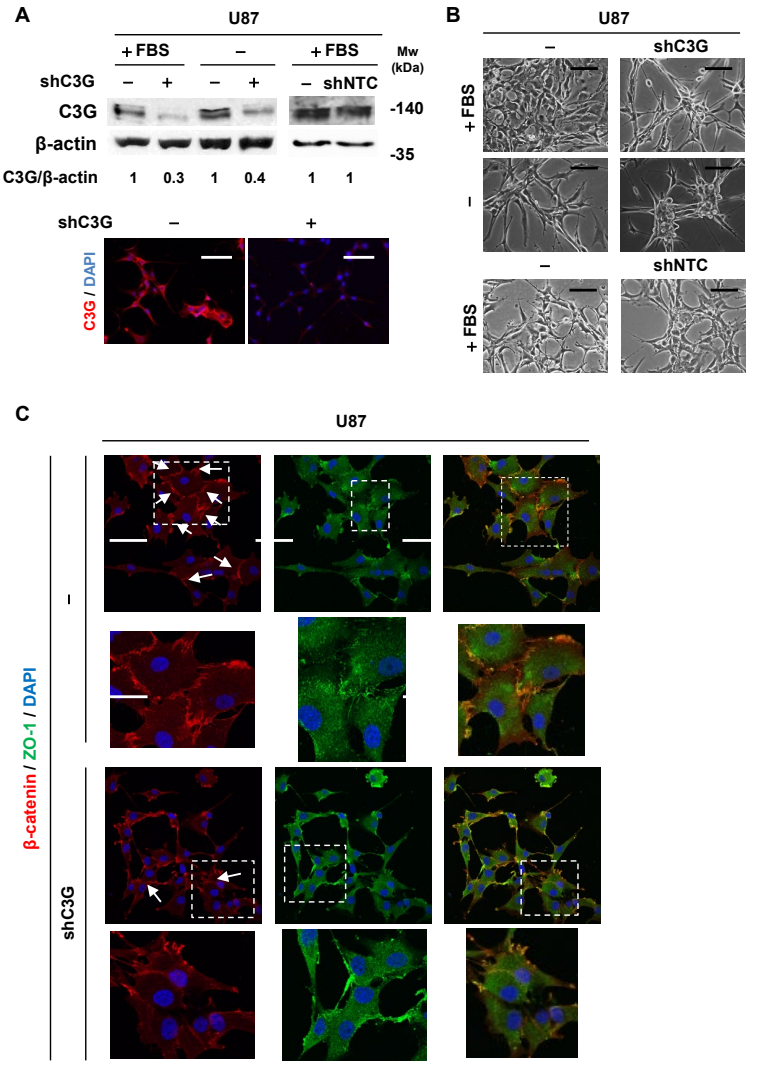

Figure 5 - C3G silencing promotes changes in cell morphology and decreases the presence of β-catenin- and ZO-1 in cell-cell contacts. **(*A-upper panel*).** Western blot analysis of C3G normalized to β-actin to demonstrate C3G silencing (*left*) and the lack of effect of shNTC (*right*) in U87 cells, in the presence (+) and absence (-) of serum (FBS) for 24h. Densitometric quantification of C3G/β-actin ratio are shown. **(*A-lower panel*)** Qualitative immunofluorescence analysis of C3G (red) in parental and C3G-silenced U87 cells. Nuclei were stained with DAPI (blue). Scale bars: 50 μm. **(*B*)** Phase-contrast microscopy images of parental U87, U87shNTC and U87shC3G cells maintained either in the presence (+) or absence (-) of serum (FBS) for 24h. Scale bars: 50 μm. **(*C*)** Representative images of β-catenin (red) and ZO-1 (green) staining analysed by confocal microscopy. Nuclei were stained with DAPI (blue). An amplification of cells inside the square is also shown. Scale bars: 25 μm.

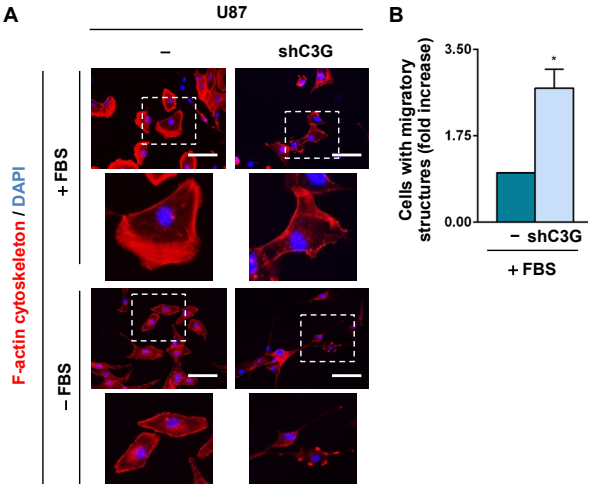

Figure 6 – C3G knock-down induces the reorganization of actin cytoskeleton of U87 cells, increasing the number of pro-migratory structures. **(*A*)** Fluorescence microscopy images of rodhamine-labelled phalloidin staining (red) in parental and C3G-silenced U87 cells, maintained as indicated (+/- FBS for 24h). Nuclei were stained with DAPI (blue). An amplification of cells inside the square is also shown. Scale bars: 50 µm. **(*B*)** Histograms showing the quantification of the number of cells presenting migratory structures (following criteria determined by Jeong et al. (2008)), expresses as the fold increase mean value ± S.E.M. (at least, n=3). **p* value <0.05, versus parental cells.

Next, in an attempt to approach to clinics we analysed the effect of C3G silencing in two non-commercial PDCs (*patient-derived cells*), named 12Φ12(D) and HCO1(D) cells. These PDCs were initially isolated from different patient tumours and maintained as neurospheres, favouring the maintenance of their GSC-like phenotype (12Φ12 and HCO1 cells) (López-Valero et al., 2018). The tumourigenic capacity and GSC-like phenotype of these cell lines were previously studied by Dr. G. Velasco's group (López-Valero et al., 2018) (López-Valero et al., 2020). We induced the *in vitro* differentiation of these cells in presence of serum, generating 12Φ12D and HCO1D cell lines (*Figure 7A*). This differentiation process was required for a number of studies carried out in 2D cultures. Total serum deprivation induced cell death in both differentiated cell lines, so that, when required, it was performed by maintaining them in the presence of 0.5% serum.

Efficient C3G knock-down was obtained using the above described shRNAs, generating 12Φ12DshC3G (*Figure 7B, left*) and HCO1DshC3G (*Figure 7B, right*) cells. Parental 12Φ12D cells displayed an epithelial-like morphology, generating well-structured monolayers in culture, while 12Φ12DshC3G cells presented reduced cell-cell contacts and increased neurite-like extensions (*Figure 7C*). Similarly, morphological changes were observed in HCO1D cells upon C3G silencing, such as loss of cell-cell contacts, although to a lesser extent than in U87 or 12Φ12D cells (*Figure 7D*). As shown for U87 cells, C3G silencing in PDCs induced F-actin

reorganization. F-actin was present at focal adhesions in parental 12Φ12D cells, while in 12Φ12DshC3G cells formed stress fibers and filopodia-like extensions (*Figure 7E*). According to this, more pro-migratory structures were detected in C3G-silenced than in parental 12Φ12D cells (*Figure 7F*). In HCO1DshC3G cells, actin was also disorganized and forming migratory structures, in contrast to HCO1D parental cells (*Figure 7G*).

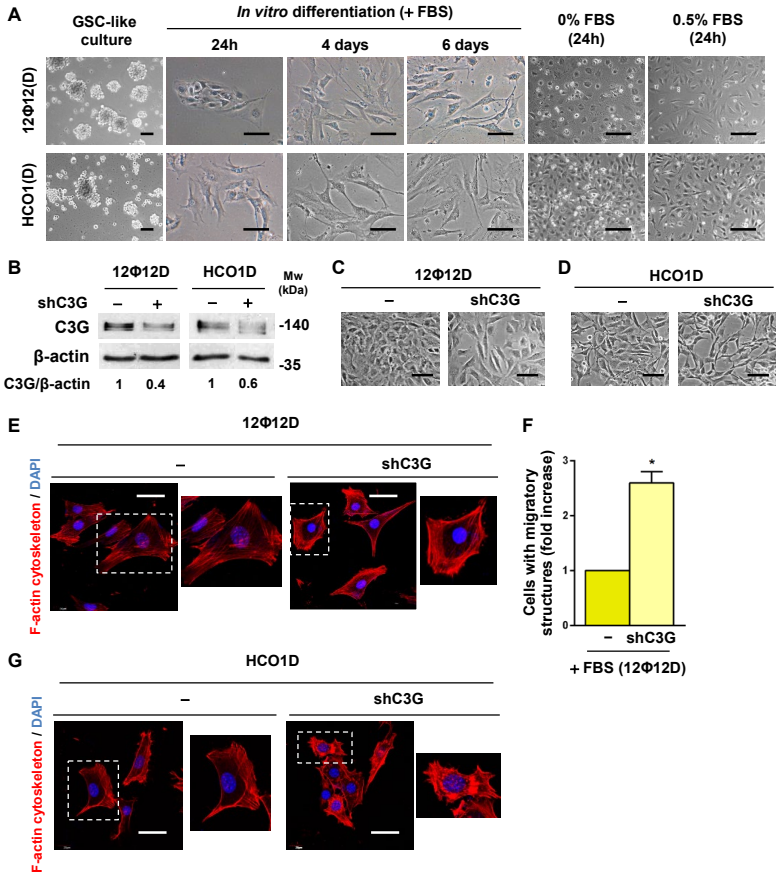

Figure 7 – GSC-like patient-derived cells can be differentiated *in vitro* using serum. C3G downregulation induces changes in the morphology and F-actin cytoskeleton organization in the differentiated cells. (*A*) Phase-contrast microscopy images of 12Φ12(D) and HCO1(D) cells maintained either under GSC-promoting culture conditions, or in the presence of serum (+FBS) to induce differentiation, or in the total (-FBS) or partial absence of serum (0.5% FBS) for 24h. Scale bars: 50 μm. **(*B*)** Western blot analysis of C3G normalized to β-actin to demonstrate C3G silencing in 12Φ12D (*left*) and HCO1D (*right*) cells, in the presence of serum. Densitometric quantification of C3G/β-actin ratio is shown. **(*C-D*)** Phase-contrast microscopy images of parental and C3G-silenced 12Φ12D (*C*) and HCO1D (*D*) cells maintained in the presence of serum. Scale bars: 50 μm. **(*E and G*)** Fluorescence microscopy images of rodhamine-labelled phalloidin staining (red) in parental and C3G-silenced 12Φ12D (*E*) and HCO1D (*G*) cells. Nuclei were stained with DAPI (blue). An amplification of cells inside the square is also shown. Scale bars: 50 μm. **(*F*)** Histograms showing the quantification of the number of 12Φ12D cells presenting migratory structures (following criteria determined by Jeong et al. (2008)), expressed as the fold increase of mean value ± S.E.M. (at least, n=3). **p* value <0.05, versus parental cells.

2.1.2. C3G knock-out in U87 cells mimics the changes induced by C3G silencing in cell morphology

In order to verify the results generated by gene silencing, C3G was stably knocked-out (KO-C3G) in U87 cells by using CRISPR/Cas9 technology. In particular, we employed a system based on that designed by Zhang laboratory (Shalem, 2014) with two lentiviral vectors: lentiCas9-blast plasmid, for Cas9 expression, and LentiGuide-hC3G-KO plasmids, carrying the anti-C3G sgRNAs. Although we generated diverse Lentiguide-hC3G-KO plasmids against different *RAPGEF1* gene regions, Cas9-mediated genome alteration was considered sufficient only for Lentiguide-hC3G-KO-3 constructs. Thus, these cells were single-cell cloned and C3G levels were checked by western blot in different clones (*Figure 8A, upper panel*). C3G knock-out was detected in two of them (KO-C3G-#1 and KO-C3G-#2 cells) and further confirmed by immunofluorescence (*Figure 8B*). On the other hand, U87-Cas9^{+} were infected with lentiviral particles carrying LentiGuide-puro-Non-Targeting plasmids, generating U87 Cas9-NTC cells as a control. In these cells, C3G levels were similar to those observed in parental U87 cells (*Figure 8A*).

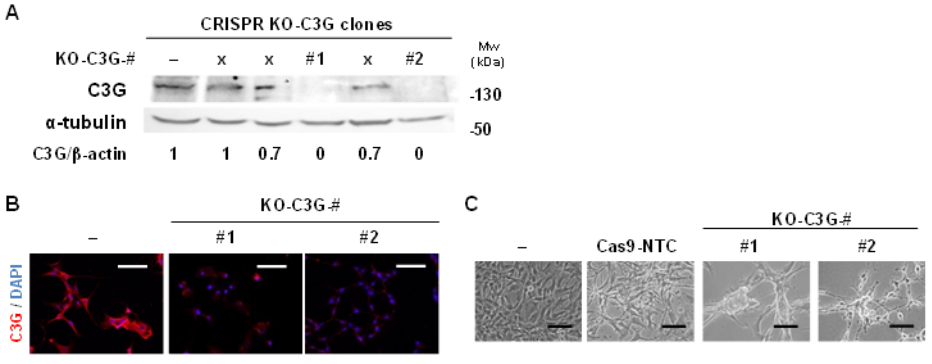

Figure 8 – **Effect of C3G knock-out, generated by CRISPR/Cas9 technology, in the morphology of U87 cells. (*A*)** Western blot analysis of C3G normalized to β-actin to check C3G depletion in C3G-KO clones of U87 cells, in the presence of serum. Densitometric quantification of C3G/β-actin ratio is shown. ''x'' indicates discarded clones. **(*B*)** Qualitative immunofluorescence analysis of C3G (red) and DAPI (cell nuclei, blue) in parental and C3G-silenced U87 cells. Scale bars: 50 μm. **(*C*)** Phase-contrast microscopy images of parental, Cas9-NTC and KO-C3G-#1/2 U87 cells, maintained in the presence of serum. Scale bars: 50 μm.

Interestingly, it was detected an accentuated morphological change upon C3G deletion in U87 cells. Hence, cells adopted a striking phenotype in the presence of serum (*Figure 8C*), resembling that of U87shC3G cells. Thus, KO-C3G-#1 and KO-C3G-#2 cells did not cover the plates as a monolayer even at high confluence, cell-cell contacts were decreased and they presented an increased number of cell

extensions. As expected, no differences in cell morphology were observed between parental and Cas9-NTC U87 cells (*Figure 8C*).

2.1.3. Full-length C3G or a C3G mutant lacking CDC25H domain are efficiently overexpressed in U87 cells, not modifying their morphology

Once we had used two different approaches to downregulate C3G that lead to similar changes in morphology and cytoskeleton organization, we decided to upregulate C3G levels as a complementary approach. Thus, we induced a transient overexpression of C3G in U87 cells using pCDNA3 constructs generated in our laboratory. We used pCDNA3-C3G-FL to overexpress C3G full length protein and pCDNA3-C3G-ΔCat for overexpressing a C3G mutant protein lacking the CDC25H region and, consequently, unable to act as a GEF, as previously demonstrated by *Guerrero et al. (1998)*). Overexpression of both proteins in parallel allowed us to study the involvement of GEF activity of C3G in its functions. pCDNA3-EV (pCDNA3 empty vector) was also transfected as a control. Transfection efficiency was checked by western blot, using anti-C3G (*Figure 9A, upper panel*) and anti-Flag (anti-DYKDDDDK) (*Figure 9A, lower panel*) antibodies. As expected, C3G-ΔCat protein presented a lower molecular weight (around 105 kDa) than C3G-FL and endogenous C3G proteins (around 140 kDa). Importantly, C3G-FL and C3G-ΔCat overexpression levels were equivalent and comparable. Morphology evaluation did not reveal clear changes upon C3G-FL and C3G-ΔCat overexpression under our research conditions (*Figure 9B*).

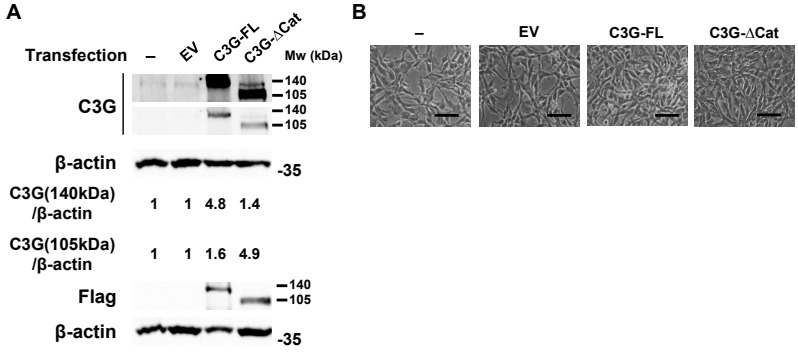

Figure 9 – **Effect on cell morphology of overexpression of C3G full-length or a C3G mutant lacking the CDC25H domain) in U87 cells using pCDNA plasmids. (*A*)** Western blot analysis of C3G (high exposure, *upper*; low exposure, *lower*) and Flag normalized to β-actin to check C3G-FL (~140 kDa) and C3G-ΔCat (~105 kDa) overexpression in U87 cells, in the presence of serum. Densitometric quantification of C3G/β-actin ratio is shown. **(*B*)** Phase-contrast microscopy images of U87 cells untransfected or transfected with pCDNA3-EV, -C3G-FL or –C3G-ΔCat constructs, maintained in the presence of serum. Scale bars: 50 μm.

Collectively, all these findings indicate that C3G controls GBM cell morphology, cytoskeleton organization and cell-cell contacts, suggesting that it could also play a role in migration/invasion and adhesion in these cells.

2.2. C3G negatively regulates the migratory and invasive capacity of glioblastoma cells, while promotes their adhesion

Previous data showed that C3G downregulation promoted migration and invasion of coloncarcinoma (Priego et al., 2016) and HCC (*hepatocellular carcinoma*) cells (Sequera et al., 2020) and that C3G overexpression inhibited migration of breast carcinoma cells (Dayma & Radha, 2011), being the increased invasiveness usually associated to a lower adhesion capacity. GBMs present a high invasive capacity, which is essential for the aggressive dissemination of these cancer cells to the surrounding tissue, correlating with patient worse prognosis. Importantly, the mentioned changes observed in GBM cells morphology and actin cytoskeleton organization upon C3G downregulation could be compatible with increased cell motility. Hence, we decided to assess the role played by C3G in migration, invasion and adhesion of GBM cells using *in vitro* functional assays.

2.2.1. C3G downregulation promotes cell invasion and migration of glioblastoma cells

First, invasion was evaluated *in vitro* using Matrigel-coated transwells and serum as chemoattractant. Invasiveness of C3G-silenced cells was highly increased as compared to their corresponding parental in U87 (*Figure 10A*), 12Φ12D (*Figure 10B*) and HCO1D (*Figure 10C*) cells. As described in the introduction, MMPs (*matrix metalloproteinases*) are essential for matrix degradation during invasion and cancer dissemination. Gelatin zymography assays showed that secreted MMP-2 activity was higher in U87shC3G than in parental U87 cells, in agreement with their pro-invasive phenotype (*Figure 10D*). Similarly, lack of C3G in the two U87-KO-C3G clones increased more than twice their invasive capacity as compared to that of C3G-expressing U87 cells (*Figure 11*), while U87shNTC (*Figure 10A*) and U87-Cas9-NTC (*Figure 11*) cells did not alter the invasive capacity. Importantly, basal invasion in the absence of chemoattractant was not detected in any case under our experimental conditions.

We also analysed migration in GBM 12Φ12D cells using wound-healing assays. In U87 and HCO1D cells, this analysis was not reliable due to the cell organization displayed by U87shC3G cells, with empty gaps along the plates, and the high sensitivity of HCO1D cells to Mitomycin C treatment. 12Φ12DshC3G cells showed a higher wound closure at 24h than parental 12Φ12D cells (*Figure 12*), confirming that C3G acts as a repressor of cell motility in GBM cells.

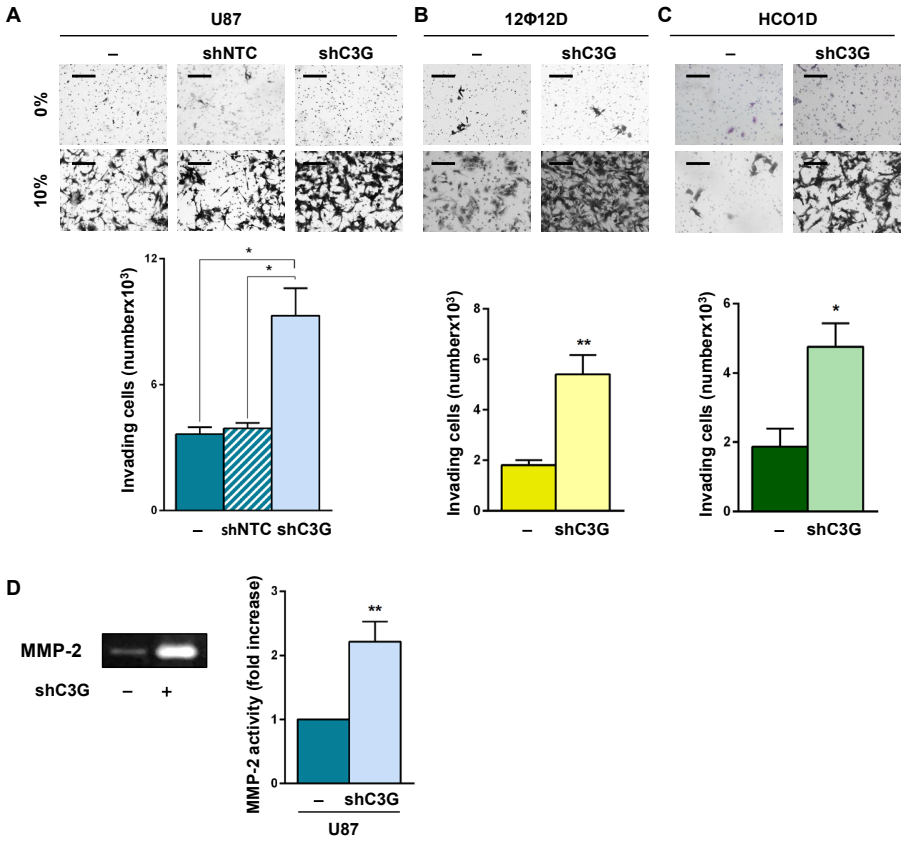

Figure 10 – **C3G-knock-down enhances invasion of GBM cells and increased secreted MMP-2 activity in U87 cells.** Non-silenced or C3G-silenced (shC3G) U87, 12Φ12D and HCO1D cells, as well as U87shNTC cells used as a control, have been used. **(*A-C*)** Invasion through Matrigel of U87 (*A*), 12Φ12D (*B*) and HCO1D (*C*) cells in the absence of chemoattractant (0%) or using serum as chemoattractant (10%). Representative images of invading cells (*upper panel*) and histograms showing the mean value ± S.E.M. of the number of invading cells when using serum as chemoattractant (at least, n=3) (*lower panel*). Scale bars: 100 μm. **(*D*)** MMP-2 activity of U87 cells: representative zymogram (*left*) and histogram showing the fold increase of MMP-2 activity (mean value ± S.E.M., at least n=3) (*right*). **p* value <0.05, ***p* value <0.01, versus parental cells or as indicated.

Based on these data, C3G downregulation promotes invasion and migration in GBM cell lines, as demonstrated through gene silencing and gene knock-out using CRISPR/Cas9 technology.

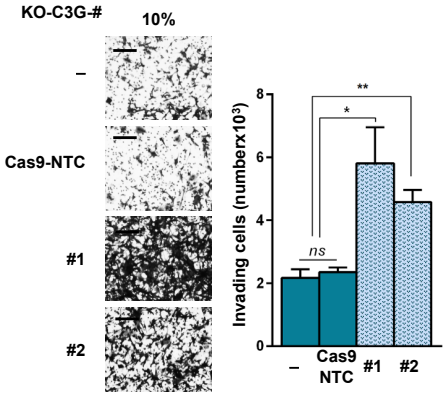

Figure 11 – C3G knock-out in U87 cells promotes invasion. Invasion through Matrigel of parental, Cas9-NTC and KO-C3G-#1/2 clones of U87 cells using serum as chemoattractant. Representative images of invading cells (*left*) and histograms showing the mean value ± S.E.M. of the number of invading cells (at least, n=3) (*right*). Scale bars: 100 µm. **p* value <0.05, ***p* value <0.01, as indicated.

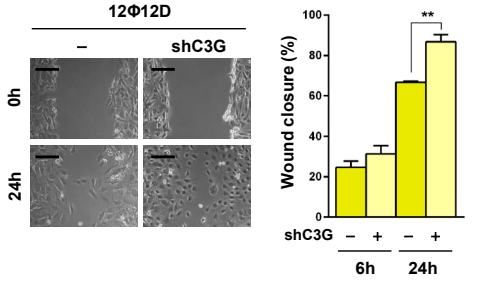

Figure 12 – C3G downregulation promotes migration in 12Φ12D cells. Wound healing assay in serum-starved non-silenced and C3G-silenced 12Φ12D cells. Representative phase contrast microscopy images at 0h and 24h of migration (*left*) and histogram representing the mean value of wound closure percentage ± S.E.M. at 6h and 24h (at least, n=3) (*right*). Scale bars: 100 µm. ***p* value <0.01, as indicated.

2.2.2. Effect of C3G and Rap1A overexpression on U87 invasiveness

Invasion was also evaluated in U87 cells transiently overexpressing C3G (*Figure 13*). In agreement with the above referred results, C3G-FL overexpression resulted in decreased invasion. Interestingly, C3G-ΔCat overexpression had no effect on invasion compared to control cells, suggesting that the GEF activity of C3G was involved in C3G-induced invasion inhibition in GBM cells. U87 cells transfected with the empty vector and parental cells presented a similar higher invasiveness.

To further understand if GEF activity of C3G was implicated in the regulation of GBM invasiveness, the role of Rap1A, the main C3G target, was also studied in U87 cells. Rap proteins have been described both as tumour promoters or suppressors

and it has been widely established that their activation/deactivation cycles and their intracellular localization played a key role in their regulation and function. Previous studies determined that different Rap isoforms could play different roles on GBM onset, growth and dissemination and each Rap isoform can act differently depending on cell context (Moon et al., 2012) (Barrett et al., 2014) (Sayyah et al., 2014) (Lei Wang et al., 2014).

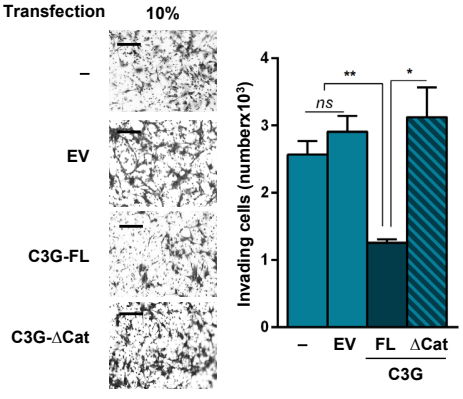

Figure 13 – C3G overexpression in U87 cells decreases invasion through a mechanism dependent on its GEF capacity. Invasion through Matrigel of U87 cells, untransfected or transfected with pCDNA3-EV, -C3G-FL or –C3G-ΔCat constructs, using serum as chemoattractant. Representative images of invading cells (*left*) and histograms showing the mean value ± S.E.M. of the number of invading cells (at least, n=3) (*right*). Scale bars: 100 μm.

There are five Rap isoforms, Rap1A, Rap1B, Rap2A, Rap2B and Rap2C (Guo et al., 2016), but C3G preferentially acts on Rap1A (T Gotoh et al., 1995). However, we were unable to detect significant changes in Rap1A activation (Rap1A-GTP levels) between parental and C3G-silenced U87 cells (not shown), probably due to the low levels of endogenous Rap1A present in U87 cells. Therefore, we studied the effect of the transient overexpression of Rap1Awt and a constitutively active mutant, Rap1AV12, using pmCherry-C1 constructs in parental and C3G-silenced U87 cells. As a control, cells were also transfected with the corresponding empty vector (pmCherry-C1-EV). As seen in *Figure 14A*, transfection efficiency was confirmed by western blot, detecting mCherry-EV (28.8 kDa) and mCherry-Rap1Awt/V12 (28.8 kDa plus 22 kDa, 50.8 kDa in total) bands (underlined in *Figure 14A* quantification). In non-transfected and Rap1Awt/V12 transfected cells, an unspecific band was found at around 30 kDa in anti-mCherry western blot. Thus, transfection efficiency was also confirmed by fluorescence microscopy mCherry detection (*Figure 14B*). Importantly, Rap1Awt and Rap1AV12 overexpression levels were equivalent in both, C3G-silenced and parental cells.

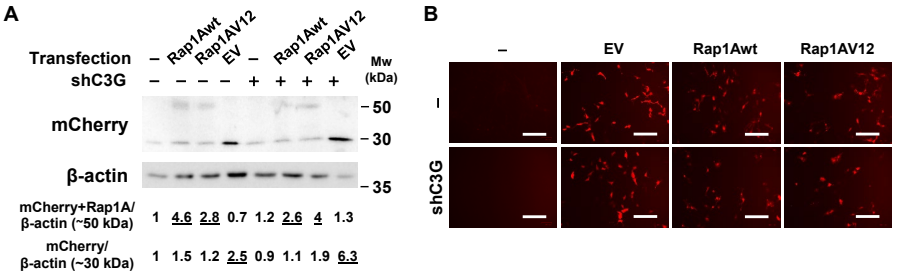

Figure 14 – mCherry-Rap1Awt and mCherry-Rap1AV12 were efficiently overexpressed in parental U87 and U87shC3G. (*A*) Western blot analysis of mCherry normalized to β-actin to check Rap1Awt/V12 (~50 kDa) overexpression by comparison of untransfected and transfected parental and C3G-silenced U87 cells with EV (*empty vector*) (~30 kDa). Densitometric quantification of mCherry/β-actin ratio is shown. **(*B*)** EV or Rap1Awt/V12 transfection efficiency confirmation through mCherry (red) fluorescence qualitative analysis. Scale bars: 100 μm.

We also evaluated the role of Rap1A on invasion (*Figure 15*). Rap1Awt had no significant effect on invasiveness of either parental or C3G-silenced U87 cells. Rap1AV12 overexpression did not either alter the invasive capacity of parental U87 cells. In contrast, the enhanced invasiveness of C3G-knock-down U87 cells was significantly reduced by Rap1AV12 overexpression.

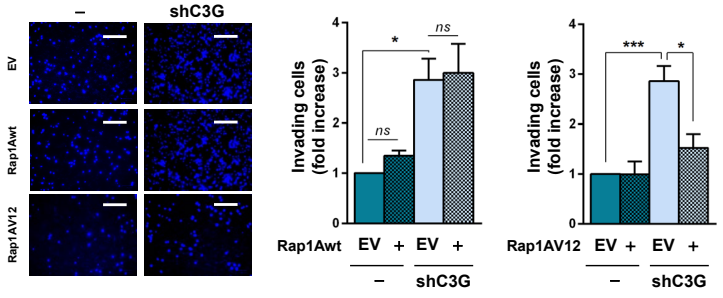

Figure 15 – Rap1AV12, but not Rap1Awt, decreases invasion of U87shC3G cells. Parental and C3G-silenced U87 cells, untransfected or transfected with pmCherry-EV/Rap1Awt/Rap1Av12 constructs were used in invasion through Matrigel assays, using serum as chemoattractant. Representative images of nuclei (stained with DAPI) of invading cells (*left*). Histograms showing the mean value ± S.E.M. of invading cells expressed as the fold increase of the value of cells transfected with EV (*empty vector*) (at least, n=3) (*right*). Scale bars: 100 μm. **p* value <0.05, ****p* value <0.001, as indicated.

Therefore, the role of C3G as an inhibitor of invasiveness in GBM cells might be dependent on its GEF activity, being Rap1A a potential mediator. However, we cannot exclude that other small G proteins might be implicated, specifically in GBM cell context.

2.2.3. C3G downregulation decreases adhesion of glioblastoma cells

Next, we studied C3G function in the regulation of adhesion of U87, 12Φ12D and HCO1D cells. As shown in *Figure 16A*, C3G knock-down decreased adhesion of U87 cells and PDCs to uncoated culture plates at different time points (mainly, at 30 min). C3G downregulation displayed a similar effect on adhesion of U87 cells to Matrigel-coated plates (*Figure 16B*).

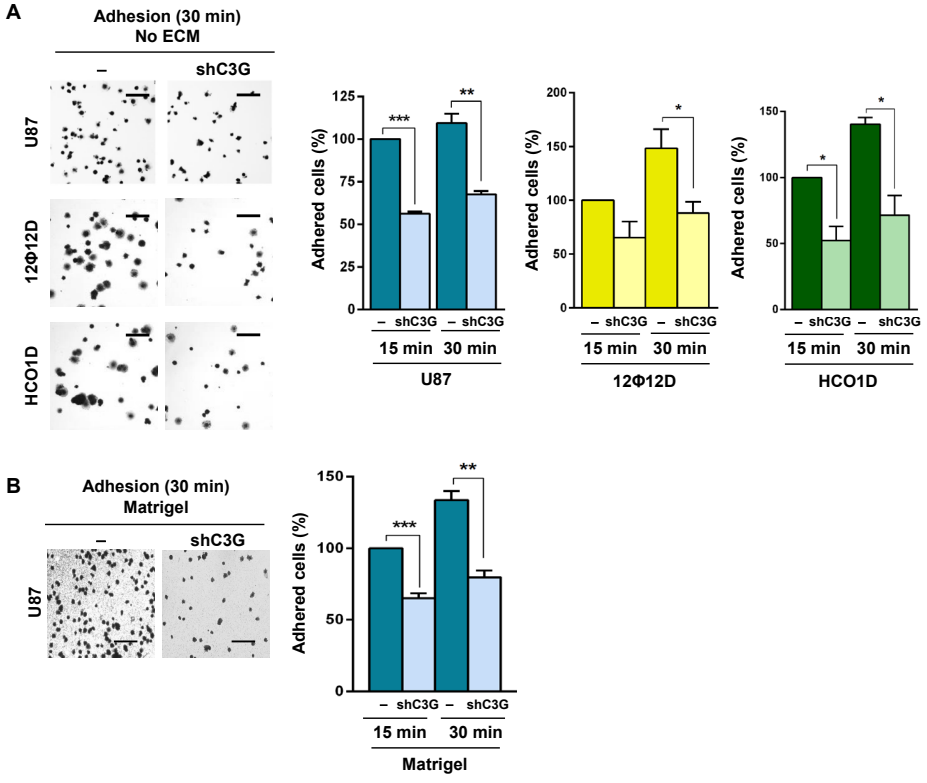

Figure 16 – **C3G silencing reduces cell adhesion of GBM cells.** Non-silenced or C3G-silenced (shC3G) cells have been used. **(*A-B*)** Adhesion analyses at 15 or 30 min in the absence of ECM for U87, 12Φ12D and HCO1D cells (*A*) or on Matrigel-coated plates for U87 cells. (*B*) Phase contrast microscopy images of adhered cells stained with crystal violet (*left*) and histograms showing mean value ± S.E.M. of the percentage of adhered cells referred to non-silenced cells at 15 min (at least, n=3) (*right*). Scale bars: 100 μm. **p* value <0.05, ***p* value <0.01, ****p* value <0.001, as indicated.

As expected, C3G depletion in U87 cells (C3G-KO) also impaired adhesion to uncoated plates at 15 min and 30 min, confirming the results obtained by gene silencing (*Figure 17*). U87-Cas9-NTC cells did not display differences in adhesiveness as compared to U87 parental cells.

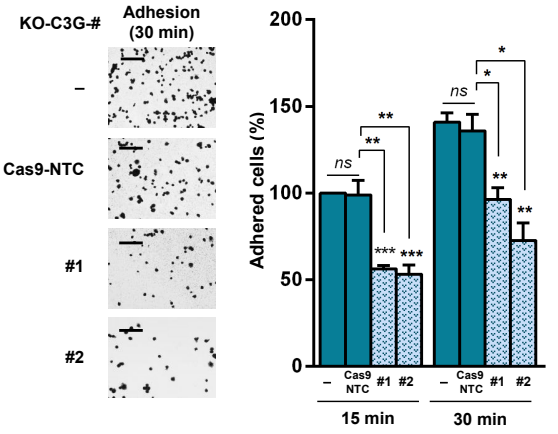

Figure 17 – C3G knock-out decreases adhesion in U87 cells. Adhesion analysis at 15 or 30 min of parental, Cas9-NTC and KO-C3G-#1/2 clones of U87 cells in the absence of ECM. Phase contrast microscopy representative images of adhered cells stained with crystal violet (*left*) and histogram showing the mean value ± S.E.M. of the percentage of adhered cells referred to parental cells at 15 min (at least, n=3) (*right*). Scale bars: 100 µm. **p* value <0.05, ***p* value <0.01, ****p* value <0.001, versus parental cells or as indicated.

These experiments indicate that C3G knock-down or knock-out reduces adhesion. This is in agreement with the changes in actin cytoskeleton previously observed and the pro-invasive phenotype acquired by GBM cells upon C3G downregulation.

2.2.4. C3G overexpression promotes adhesion of U87 cells, independently of its GEF activity

Next, we studied whether the effect of C3G on adhesion of GBM cells was dependent on its GEF activity by comparing the adhesiveness of U87 cells overexpressing C3G-FL or C3G-ΔCat (*Figure 18*). Overexpression of C3G-FL or C3G-ΔCat promoted adhesion to uncoated plates, while the empty vector had no effect. This is agreement with the results obtained by C3G downregulation. In addition, these data suggest that its GEF activity is not required for C3G-mediated adhesion in U87 cells. C3G-ΔCat mutant overexpression promoted adhesion in a similar way to C3G-FL. Transfection of U87 cells with pCDNA3 empty vector did not alter its adhesive capacity compared to parental cells.

We also determined the effect of Rap1Awt and Rap1AV12 overexpression on adhesion (*Figure 19*). Although Rap1AV12 overexpression promoted adhesion of U87shC3G cells at short times (15 min), either Rap1Awt or Rap1AV12 overexpression had no effect on adhesion of parental U87 or U87shC3G cells at 1h.

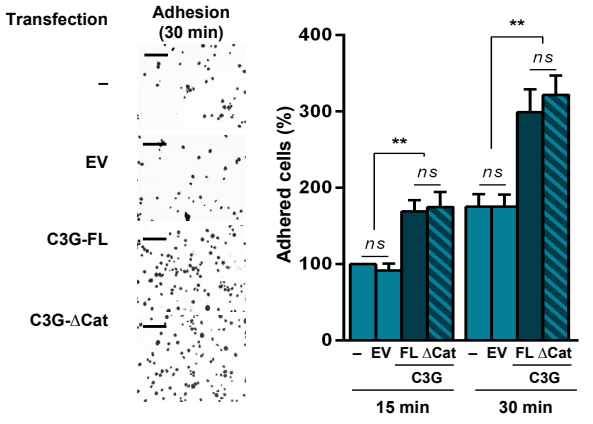

Figure 18 – Overexpression of C3G full length or a mutant lacking its catalytic domain promotes adhesion of U87 cells. Adhesion at 15 or 30 min of untransfected and pCDNA3-EV/-FL/-ΔCat U87 cells in the absence of ECM. Representative phase contrast microscopy images of adhered cells stained with crystal violet (*left*) and histogram showing mean value ± S.E.M. of the percentage of adhered cells referred to untransfected cells at 15 min (at least, n=3) (*right*). Scale bars: 100 μm. **p* value <0.05, ***p* value <0.01, ****p* value <0.001, versus parental cells or as indicated.

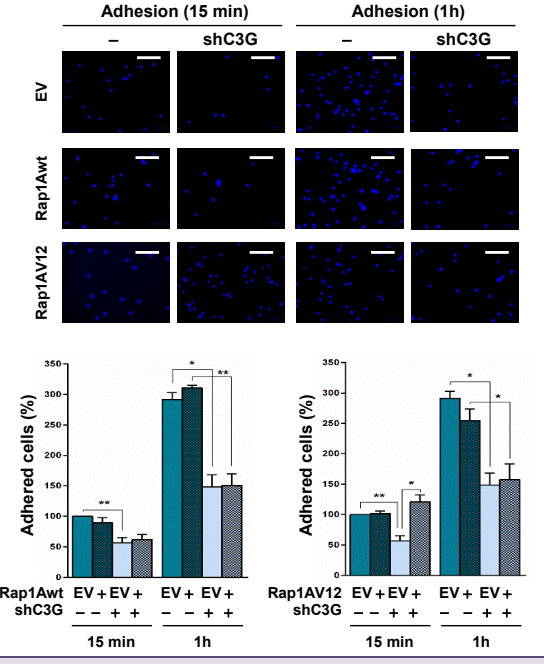

Figure 19 – Neither Rap1Awt nor Rap1AV12 overexpression induce major changes in U87 cell adhesiveness. Parental and C3G-silenced U87 cells, untransfected or transfected with pmCherry-EV/Rap1Awt/Rap1Av12 constructs, were used. ***(A)*** Adhesion at 15 min or 1h in the absence of ECM. Representative phase contrast microscopy images of adhered cells stained with DAPI (*upper*) and histograms showing mean value ± S.E.M. of the percentage of adhered cells referred to cells transfected with EV (*empty vector*) at 15 min (at least, n=3) (*lower*). Scale bars: 100 μm. **p* value <0.05, ***p* value <0.01, as indicated.

Taken together, all data shown in this section indicates that C3G downregulation promotes migration and invasion, while C3G induces cell adhesion. Nevertheless, the mechanisms by which C3G controls these different functions might be different, since its GEF activity is likely implicated in its capacity to inhibit invasion, while it might not be involved in the action of C3G on adhesion of GBM cells.

2.3. C3G downregulation enhances the invasive capacity of glioblastoma cells by promoting the acquisition of a more mesenchymal phenotype

As explained in the *Introduction* section, the role of EMT (*epithelial to mesenchymal transition*) in GBM remains controversial. GBM cells are not epithelial and usually display pro-mesenchymal phenotypes. Hence, canonical EMT-associated changes at molecular level are rarely observed in GBM tumours, such as the cadherin switch. Nevertheless, EMT-like processes have been demonstrated to be relevant for GBM tumourigenesis and dissemination. Thus, we analysed the effect of C3G downregulation on the levels of EMT markers in order to obtain further insights into the mechanisms by which C3G regulates invasion in GBM.

Parental U87 cells present an intermediate phenotype, expressing both epithelial and mesenchymal markers (Lamballe et al., 2016). We found that C3G silencing increased Vimentin protein levels, a well-established mesenchymal marker, upon serum starvation (*Figure 20A*). Similarly, Vimentin levels were also higher in HCO1DshC3G cells than in parental HCO1D cells (*Figure 20B*). 12Φ12D cells display a more epithelial-like phenotype. Hence, we observed that E-cadherin, the epithelial marker, was downregulated upon C3G knock-down in 12Φ12D cells, and Vimentin was upregulated (*Figure 20C*).

These results suggested that C3G may act as an inhibitor of the EMT-like process in GBM cells, reducing their invasiveness, while promoting their adhesiveness. Due to the key role of EMT-associated transcription factors, we evaluated if C3G controlled their mRNA expression in U87 cells. Interestingly, *TWIST1* (*Figure 20D*) expression was 2-fold higher in U87shC3G cells than in parental cells, both in the presence or absence of serum. *ZEB2* (*Figure 20E*) was also upregulated in C3G-silenced cells, but to a lesser extent.

This demonstrates that C3G downregulation in human GBM cells correlates with an accentuated mesenchymal phenotype, enhanced invasiveness and reduced adhesion likely associated to an EMT-like process.

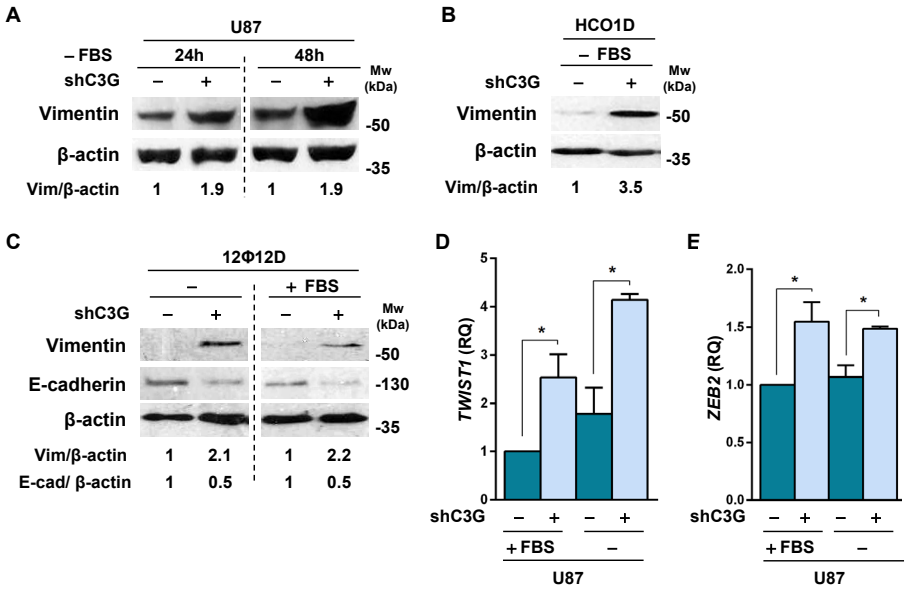

Figure 20 – **C3G downregulation induces EMT-like-associated changes in GBM cells.** Non-silenced or C3G-silenced (shC3G) cells have been used. **(*A-C*)** Western blot analyses of Vimentin and E-cadherin levels normalized to β-actin in U87 (*A*), 12Φ12D (*B*) and HCO1D (*C*) cells, in the presence (+) or absence (-) of serum (FBS) (representative images; at least, n=3). **(*D-E*)** *TWIST1* (*D*) and *ZEB2* (*E*) mRNA levels in U87 cells maintained either in the presence (+) or absence (-) (6h) of serum (FBS). Histograms represent RQ mean value ± S.E.M. referred to parental cells maintained in the presence of 10% serum (at least, n=3). **p* value <0.05, as indicated.

3. C3G downregulation in glioblastoma cells alters *in vitro* tumourigenic properties and reduces proliferation

The role of C3G in tumourigenesis has been already studied in some cancer types, highlighting coloncarcinoma and HCC. In order to determine the function of C3G in the tumourigenic capacity of human GBM cells, we first performed anchorage-dependent growth assays using all GBM cells previously described. The number of foci was increased upon C3G downregulation in U87 (*Figure 21A*) and 12Φ12D (*Figure 21B*) cells, while U87shNTC control cells did not presented differences as compared to parental U87cells. However, we found a significant decrease in the number of cells per focus in U87shC3G cells (*Figure 21A, right panel*). In contrast, HCO1DshC3G cells presented fewer and smaller foci as compared to those from parental HCO1D cells (*Figure 21C*). Nevertheless, a microscopic analysis allowed us to detect increased independent, scattered cells along the plate in C3G-silenced compared to parental HCO1D cells.

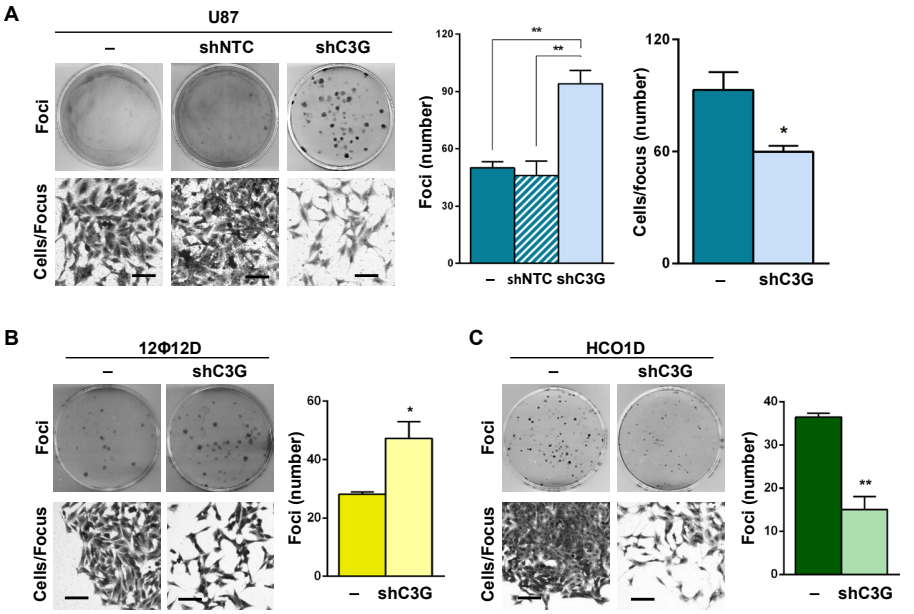

Figure 21 – C3G downregulation promotes foci formation in anchorage-dependent growth assays in U87 and 12Φ12D cells, but not in HCO1D cells. Non-silenced or C3G-silenced (shC3G) cells, as well as U87shNTC cells as a control, have been used. **(*A-C*)** Anchorage-dependent growth assays in U87 (*A*), 12Φ12D (*B*) and HCO1D (*C*) cells. Representative images of a macroscopic view of foci (*upper images*) and an individual focus (*lower-left images*). Histograms show the mean value ± S.E.M. of the total foci number and, for U87 cells, number of cells per focus (at least, n=3). Scale bars: 100 μm. **p* value <0.05, ***p* value <0.01, versus parental cells or as indicated.

To further characterize the role of C3G in GBM tumourigenesis, we also performed anchorage-independent growth assays. We measured the ability of GBM cells to form foci in soft-agar and we found that U87shC3G (*Figure 22A*) and 12Φ12DshC3G (*Figure 22C*) cells formed more foci than their respective parental cells. As a control, U87shNTC cells were used, but they did not show differences as compared to parental U87 cells. In contrast, HCO1DshC3G cells formed fewer foci than parental HCO1D cells (*Figure 22C*) and these C3G-silenced cells also showed a more scattered phenotype with multiple independent cells and small colonies, formed by less than 5 cells, along the plate. In general, foci formed by C3G-silenced cells contained fewer and more disseminated cells and cell-cell interactions were reduced, leading to a scattered phenotype (*Figure 22B in detail, plus lower panels from Figures 22C and 22D*). This reduced cell density of C3G-silenced GBM cells is likely a consequence of the increased cell scattering facilitated by their higher motility. However, foci diameter remained unchanged.

Proliferation is also important to control cell density within the foci. Parental U87 cells showed higher proliferation than U87shC3G cells, as determined by flow cytometry cell cycle analysis (*Figure 23A*), both under adherent and non-adherent

conditions. However, no differences were found in apoptosis (*data not shown*). These proliferation data were confirmed by Ki67 staining. Hence, the number of Ki67-positive (Ki67^{+}) cells was significantly higher in parental than in C3G silenced U87 cells (*Figure 23B*).

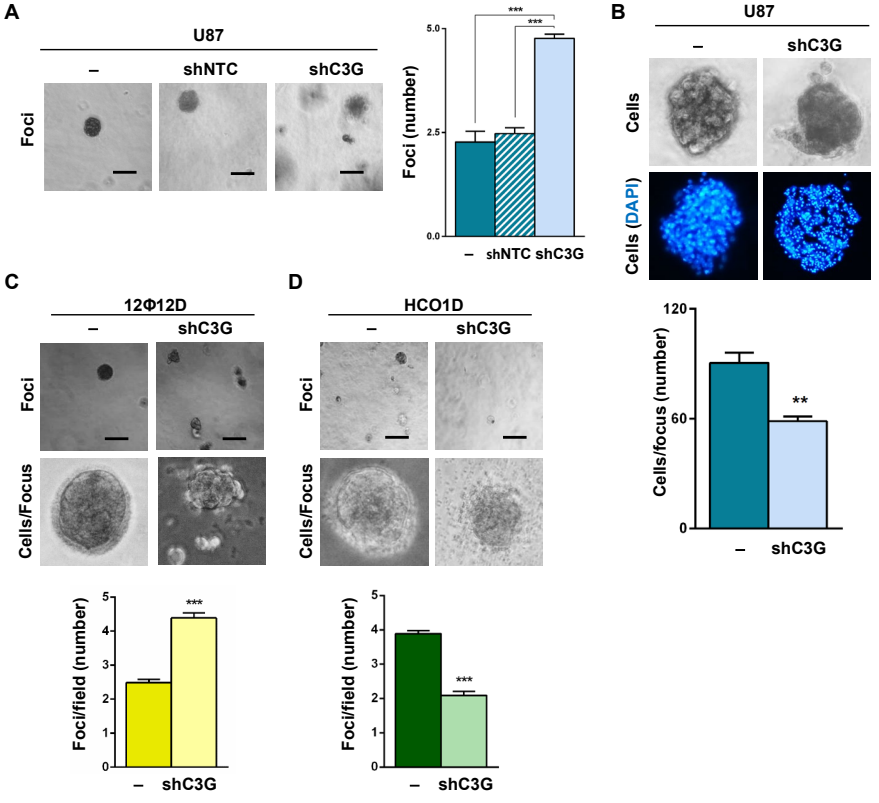

Figure 22 – C3G knock-down increases the number of foci in anchorage-independent growth assays in U87 and 12Φ12D cells, but not in HCO1D cells. Non-silenced or C3G-silenced (shC3G) cells have been used, as well as U87shNTC cells as a control. **(*A, C and D*)** Anchorage-independent growth assays in U87 (*A*), 12Φ12D (*B*) and HCO1D (*C*) cells. Representative images of foci (*left (in A) or upper (in C and D) images*) and zoom of individual foci organization (*lower images in 12Φ12D and HCO1D cells*). Histograms (*right (in A) or lower (in C and D) panels*) showing the mean value ± S.E.M. of the foci number per field (at least, n=3). Scale bars: 100 μm. **(*B*)** Zoom of individual foci organization of non-stained U87 cells (*upper images*) and DAPI stained nuclei (*lower images*). Histogram representing the mean value ± S.E.M. of the number of cells per focus (at least, n=3). ***p* value <0.01, ****p* value <0.001, versus parental cells or as indicated.

Taking together, all the results indicate that C3G downregulation in GBM cells promotes foci formation, while reduces cell density and modifies foci morphology. The decreased proliferation would explain the lower number of cells per focus. The increased foci formation could be a consequence of cell scattering, which is also observed in C3G-silenced HCO1D cells, even though they formed fewer foci.

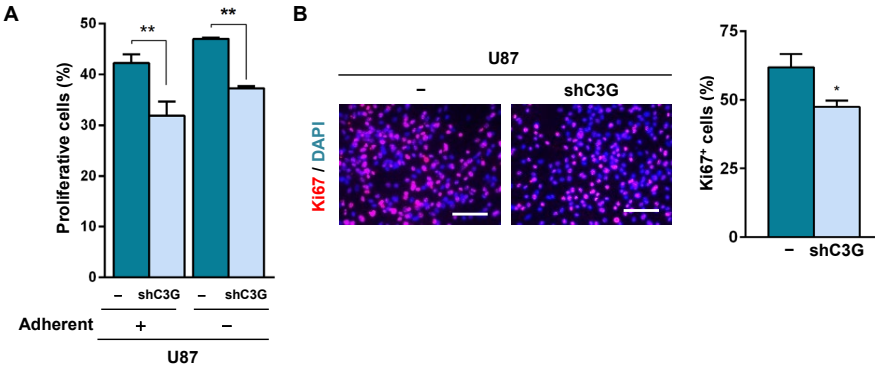

Figure 23 – C3G silencing is associated to decreased proliferation. (*A*) Cell cycle analysis by cytometry of C3G-silenced as compared to non-silenced U87 cells, maintained in the presence of serum under adherent or non-adherent conditions (6h). Histogram represents the percentage of cells in S and G_2/M phases of the cell cycle ± S.E.M. (at least, n=3). **(*B*)** Ki67 (red) staining in C3G-silenced and parental U87 cells maintained in the presence of serum and under adherent conditions. Nuclei were stained with DAPI (blue). Representative microscope images (*left*) and histogram showing the mean value ± S.E.M. of the percentage of Ki67 positive cells (at least, n=3) (*right*). Scale bars: 50 μm. **p* value <0.05, ***p* value <0.01, versus parental cells or as indicated.

4. Effect of C3G downregulation on *in vivo* glioblastoma tumour growth

As seen in the previous sections, *in vitro* assays revealed that C3G regulates the tumourigenic properties of GBM cells by controlling invasiveness, adhesion, foci formation capacity and proliferation. Therefore, to further characterize the role of C3G in GBM tumourigenesis, we analysed *in vivo* tumour growth by performing xenograft assays in nude mice. C3G knock-down and non-silenced U87 cells were injected into the flanks of nude mice and tumour size was monitored along the time. We found that tumours generated by U87shC3G cells showed a significant increased area (*Figure 24A*) and volume (*Figure 24B*) at experiment end point (10 days).

To further understand the role played by C3G and to characterize the intrinsic differences of GBM tumours generated by non-silenced and C3G-silenced GBM cells, we performed *in ovo* CAM (*chicken chorioallantoic membrane*) inoculation assays. This model is useful to study primary tumour growth, the presence of stromal cells and tumour angiogenesis. This model has been previously validated for human gliomas (Hagedorn, 2005). In agreement with xenograft results, C3G-silenced U87 and 12Φ12D cells generated larger tumours than non-silenced cells (*Figures 24C and 24D,* respectively). Moreover, the histological analysis of CAM-derived tumours

formed by non-silenced and C3G-silenced U87 cells, discarded the presence of necrotic areas in tumour cores (*Figure 25A*).

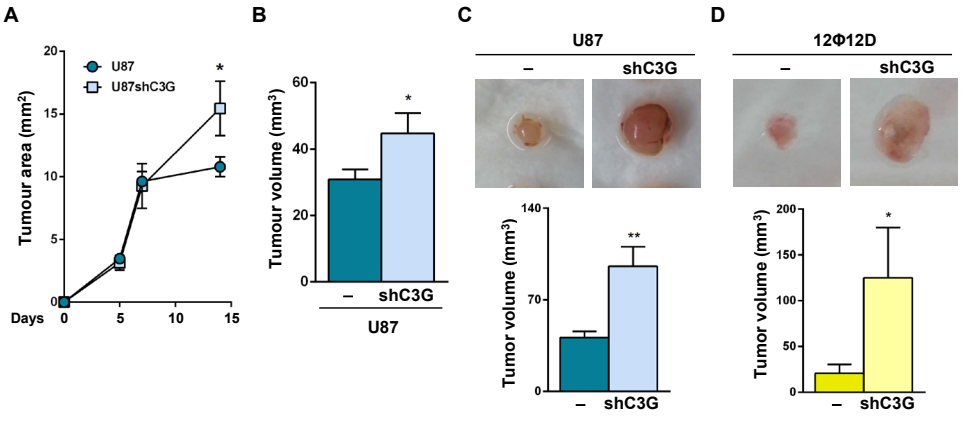

Figure 24 – C3G downregulation in glioblastoma (GBM) cells induces the formation of larger tumours in mice xenografts and CAM assays. Non-silenced and C3G-silenced cells were used. **(*A-B*)** Xenograft assay using U87 cells. Graphic showing the mean value of tumour area along the time (0-15 days) ± S.E.M. (two independent experiments, each: 5 mice and 2 flanks per mouse) (*A*) and histogram representing the mean value of tumour volume ± S.E.M. at the end-point (15 days) (*B*). **(*C-D*)** CAM assays using U87 (*C*) and 12Φ12D (*D*) cells. Representative tumours at the end point (7 days) (*upper*). Histograms represent the mean value of the tumour volume ± S.E.M. (3 independent experiments, total number of chick embryos 13) at the end point (*lower*). **p* value <0.05, ***p* value <0.01, versus parental cells.

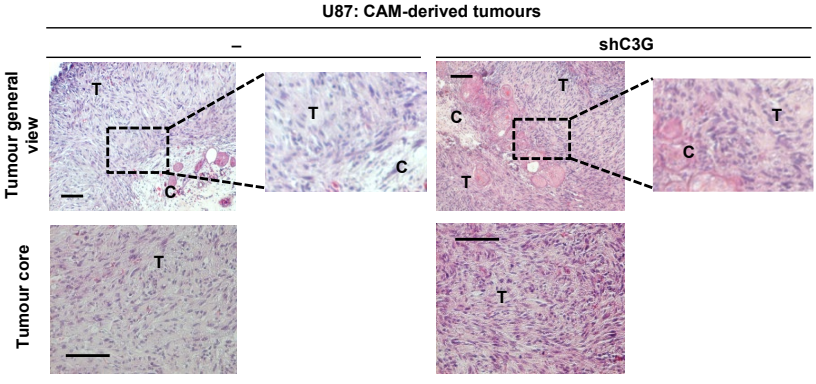

Figure 25 – CAM-derived tumours formed by non-silenced and C3G-silenced U87 cells do not present necrotic areas in the tumour core independently of C3G levels. Hematoxylin/eosin staining of sections from CAM-derived tumours formed by non-silenced and C3G silenced U87 cells. Phase contrast microscopy images: general view, where the tumour (T) and the CAM tissue (C) can be visualized (*upper-left panels*); magnification of the rectangle area (*upper-right panels*) or tumour core (*lower panels*). Scale bars: 50 μm.

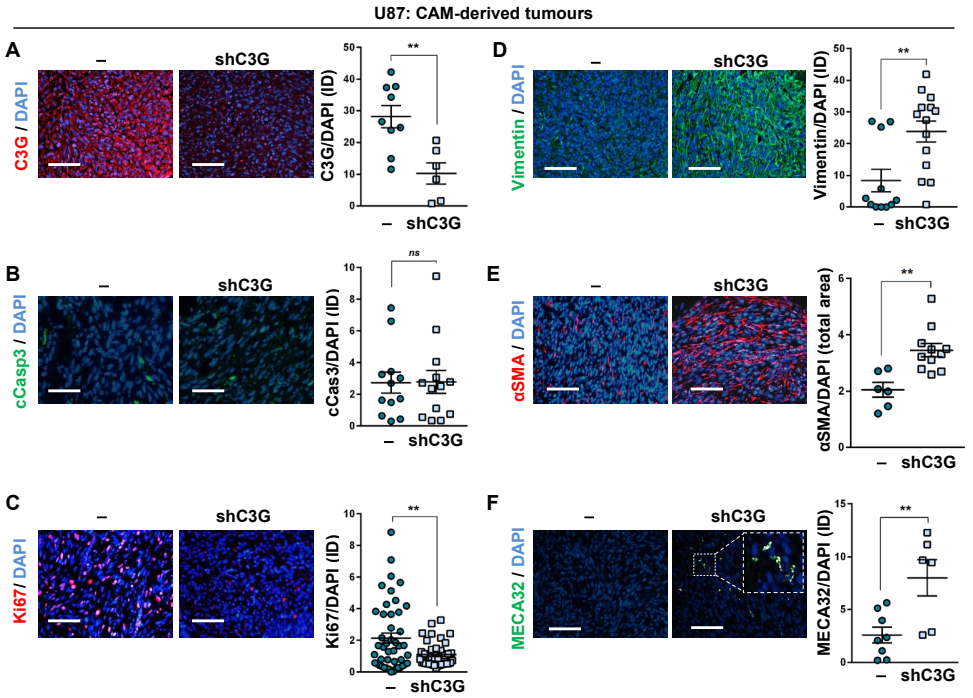

Figure 26 – Tumours formed by C3G-silenced cells show a more mesenchymal phenotype and a higher presence of stroma and blood cells, but a lower proliferation rate. (*A-F*) Immunofluorescence microscopy analysis in tumours generated by U87 cells without or with C3G silencing in CAM assays. The following staining was performed: C3G (red) (*A*), cleaved Caspase 3 (cCasp3) (green) (*B*), Ki67 (red), (*C*), Vimentin (green) (*D*), α-Smooth muscle actin (α-SMA) (red) (*E*) and MECA32 (green) (*F*). In all, cell nuclei were stained with DAPI (blue). Representative images (*left panels*) and graphs (*right panels*) showing fluorescence intensity normalized to DAPI-positive area (Integrated Density, *ID*) or total area mean values ± S.E.M. Several sections per tumour, from a total of 3 staining reactions were used . Scale bars: 100 μm. ***p* value <0.01, versus parental cells.

Next, we evaluated some of the characteristics of the tumours using tumour sections. First, we confirmed that C3G downregulation was maintained in U87shC3G-derived tumours (*Figure 26A*). In agreement with *in vitro* experiments, C3G knock-down had no effect on apoptosis (measured by cleaved caspase-3 staining; *Figure 26B*), while it reduced proliferation (measured by Ki67 staining; *Figure 26C*) and up-regulated the levels of the mesenchymal marker, Vimentin (*Figure 26D*). Moreover, we evaluated the impact of C3G on tumour stroma regulation. Interestingly, we also found that tumours generated by U87shC3G cells presented increased staining for α-SMA (*α-smooth muscle actin*), a marker of activated fibroblasts or myofibroblasts (*Figure 26E*). Tumours formed by U87shC3G cells also showed a higher density of blood vessels, detected by the marker MECA-32, (*Figure 26F*). This suggests that tumours generated by GBM cells with low levels of C3G might facilitate their enrichment in stroma and blood vessels, leading to larger tumours. Of course, GBM

stroma strongly differs from CAM-derived tumours stroma and more studies should be carried out to confirm this.

These results indicate that C3G downregulation alters *in vivo* GBM growth, validating the *in vitro* results. Hence, low levels of C3G induce a more mesenchymal phenotype in GBM tumours accompanied by downregulation of proliferation and increased stroma presence.

5. Regulation of cell signalling by C3G: implication in the regulation of p38α MAPK, ERKs and receptor tyrosine-kinases

As explained in the introduction and group background sections, C3G regulates diverse cell signal transduction pathways in different cell types. It regulates a wide range of proteins, such as Rap1 (and other small GTPases), phosphatases, integrins, RTKs (*receptor tyrosine-kinases*) or MAPKs (p38α MAPK and ERKs) (Gutiérrez-Uzquiza et al., 2010) (V. Radha et al., 2011) (Priego et al., 2016). In particular, published data from our group showed that C3G downregulation enhances p38α MAPK and ERKs activation in MEFs and coloncarcinoma cells (Gutiérrez-Uzquiza et al., 2010) (Priego et al., 2016). Based on this, we analysed the effect of C3G silencing on cell signalling and its function in C3G-induced effects on GBM.

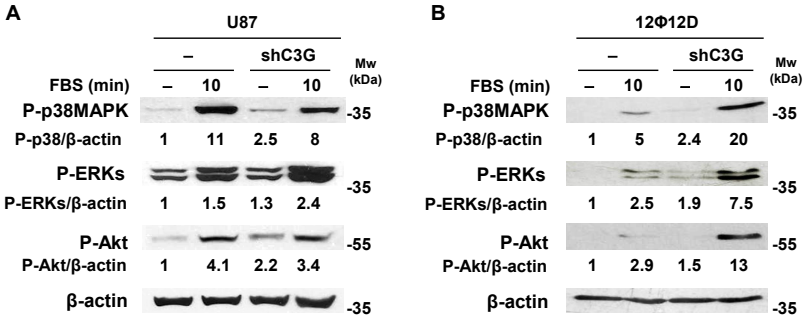

Figure 27 – Effect of C3G knock-down on different signalling pathways in GBM cells in response to serum. (*A-B*) Representative images of western blot analysis of phosphorylated (P) p38 MAPK, ERKs and Akt levels normalized to β-actin in U87/U87shC3G cells (*A*) and 12Φ12D/12Φ12DshC3G cells (*B*). Serum -deprived cells were maintained untreated (-) or treated for 10 min with 10% serum (FBS). Densitometric analysis of P-*protein*/β-actin ratio is included, expressed as the fold increase of the value of untreated parental cells.

We first measured the activation of different cell signalling pathways upon serum stimulation at 10 min. In stimulated cells, we detected lower levels of P-p38 MAPK,

higher levels of P-ERKs and similar levels of P-Akt in U87shC3G as compared to parental cells (*Figure 27A*). However, in 12Φ12D cells, C3G knock-down increased the phosphorylation levels of p38 MAPK, ERKs and Akt induced by serum (*Figure 27B*). In addition, C3G silencing in U87 and 12Φ12D cells seems to slightly increase basal levels of P-p38 MAPK, P-ERKs and P-Akt (Ser473) (*Figure 27A and 27B)*.

Therefore, C3G controls the activation of different signalling pathways in GBM in response to serum, but this seems not be homogenous for all cell lines and could be time and/or growth factor-dependent. Therefore, a more detailed study is required.

5.1. Role of p38 MAPK in C3G-mediated effects on adhesion and migration of glioblastoma cells

C3G-p38α MAPK crosstalk has been previously reported in other cell types, uncovering important signalling mechanisms regulating different cell funtions. Hence, we decided to study it in GBM. p38 MAPK activation upon serum stimulation in GBM cell lines did not reveal any homogeneous result in U87 and 12Φ12D cells, demonstrating a non-universal role (as activator or inhibitor) of C3G on p38 MAPK activity in GBM (*Figure 27*). Nevertheless, we further studied this crosstalk being aware of its relevance in other cell types, uncovering new regulatory signalling mechanisms for GBM cells. For example, as previously explained, we demonstrated that C3G negatively controls p38α MAPK activity in HCT116 coloncarcinoma cells, being this interplay between both proteins the mechanism responsible for the pro-invasive phenotype of HCT116 cells induced by C3G silencing (Priego et al., 2016). Moreover, p38α MAPK has also been involved in the upregulation of migration and dissemination of GBM (Demuth et al., 2007), among other cancer types (Martínez-Limón et al., 2020).

Taking into account all this, we evaluated the potential contribution of p38 MAPK to the effects of C3G in GBM cells. To do it, parental and C3G-silenced U87 cells were treated with the p38α/β MAPK inhibitor, SB203580. The dose used (5 μM) predominantly inhibits p38α isoform, although we cannot discard effects over p38β. As shown in *Figure 28A,* SB203580 prevented serum-induced phosphorylation of MK2, confirming p38 inhibition. SB203580 treatment also reduced invasiveness of parental and U87shC3G cells (*Figure 28B)*. On the other hand, p38 MAPK inhibition significantly increased adhesion (*Figure 28C*) at different time points in both parental U87 cells (at 15 min) and U87shC3G cells (at 30 min). However, since C3G silenced cells have a reduced adhesion, the effect of SB203580 treatment was stronger, at least, at 30 min.

These results indicate that p38α/β MAPK promotes GBM invasion, as previously shown by other groups (Demuth et al., 2007), being this effect independent of C3G

levels. This might explain why C3G downregulation did not induce the same changes in p38 MAPK activation in U87 and 12Φ12D cells (*Figure 27)*.

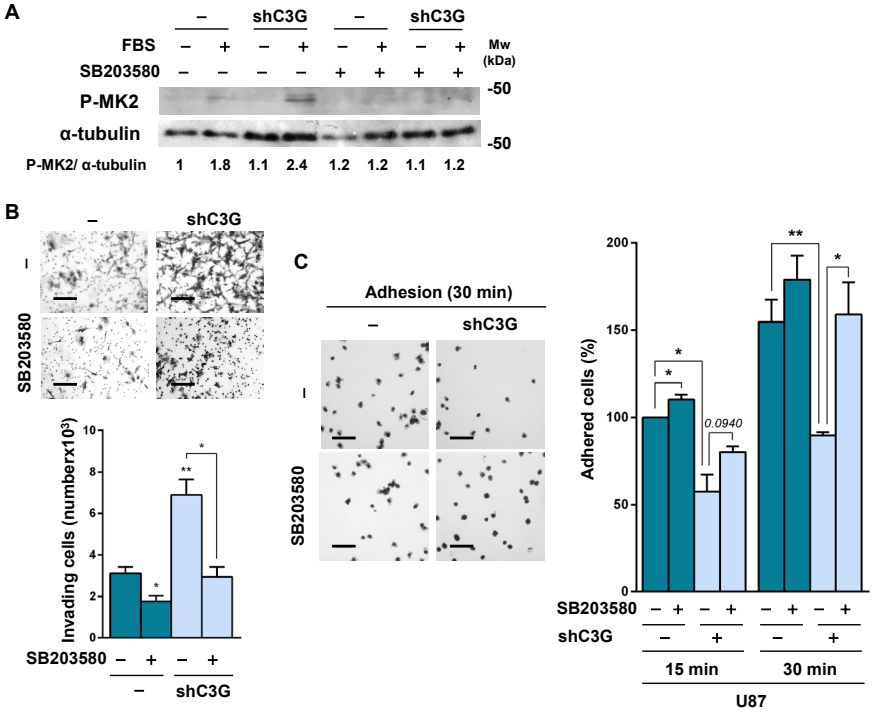

Figure 28 – p38α/β inhibition decreases invasion and enhances adhesion, independently of C3G levels in U87 cells. U87/U87shC3G cells, either in the presence or absence of SB203580 (5 μM), as indicated, were used. **(*A*)** Western blot analysis of phosphorylated (P) MK2 levels normalized to α-tubulin. Serum -deprived cells were maintained untreated (-) or treated (+) with 10% serum (FBS) for 10 min. Densitometric analysis of P-MK2/ α-tubulin ratio is included, expressed as the fold increase of the value of untreated parental cells. **(*B*)** Invasion through Matrigel in the presence of 10% serum as chemoattractant. Representative images of invading cells (*upper panels*) and histogram (*lower panel*) showing the mean value ± S.E.M. of the number of invading cells (at least, n=3). Scale bars: 100 μm. **(*C*)** Adhesion analysis at 15 or 30 min in the absence of ECM. Representative phase contrast microscopy images of adhered cells stained with crystal violet (*left*) and histogram showing the mean value ± S.E.M. of the percentage of adhered cells referred to non-silenced cells at 15 min (at least, n=3) (*right*). Scale bars: 100 μm. *p value <0.05, **p value <0.01, versus parental cells or as indicated.

5.2. ERKs upregulation induced by C3G silencing promotes invasion and foci formation in glioblastoma cells

Previous published data showed that C3G inhibits ERKs activation (Guerrero et al., 2004) (Martín-Encabo et al., 2007) (Maia et al., 2009) (Priego et al., 2016). However, the functional relevance of C3G-ERKs crosstalk in cancer cells has not been characterized. As seen in *Figure 27*, ERKs phosphorylation was upregulated in C3G silenced U87 and 12Φ12D cells under basal conditions and in response to

serum, as compared to parental cells. Importantly, both cell lines display a similar behaviour in all functions analysed, so that the implication of ERKs in C3G-regulated functions may be relevant.

To assess whether C3G effects were mediated by ERKs, we inhibited MEK/ERKs pathway with using a selective MEK inhibitor, PD98059, in U87 cells. PD98059 treatment decreased P-ERKs levels in parental and U87shC3G cells (*Figure 29A*). Next, we evaluated if ERKs inhibition differently controlled U87 invasiveness and foci formation depending on C3G levels.

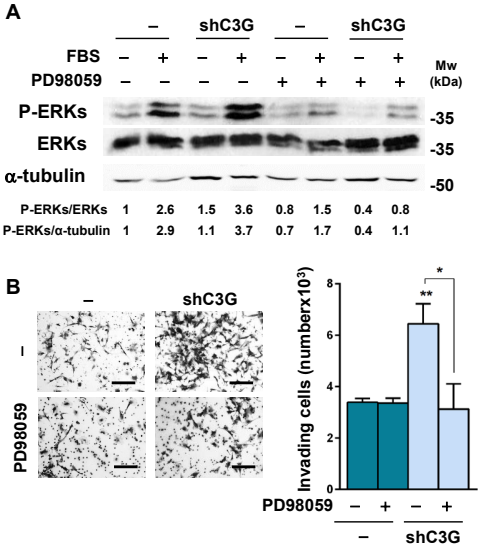

Figure 29 – ERKs inhibition by PD98059 treatment decreased invasiveness of U87shC3G cells. U87/U87shC3G cells maintained either in the presence or absence of PD98059 (20 μM), as indicated, were used. **(*A*)** Western blot images of phosphorylated (P) ERKs levels normalized to ERKs and α-tubulin. Serum -deprived cells were maintained untreated (-) or treated (+) with 10% serum (FBS) for 10 min. Densitometric analysis of P-ERKs/ERKs and P-ERKs/α-tubulin ratios are included, expressed as the fold increase of the value of untreated parental cells. **(*B*)** Invasion through Matrigel in the presence of chemoattractant (10% serum). Representative images of invading cells (*left panel*) and histogram (*right panel*) showing the mean value ± S.E.M. of the number of invading cells (at least, n=3). Scale bars: 100 μm. **p* value <0.05, ***p* value <0.01, versus parental cells or as indicated.

PD98059 treatment significantly reduced invasion of U87shC3G cells to the levels of parental cells (*Figure 29B*). In addition, migration of C3G-silenced 12Φ12D cells decreased upon treatment with PD98059, while having no effect on parental 12Φ12D cells (*Figure 30A*).

The effect of C3G downregulation on anchorage-dependent (*Figure 31A*) and -independent (*Figure 31B*) foci formation was also prevented by ERKs inhibition. In all these functional assays, U87 parental cells were not affected by PD98059 treatment.

Interestingly, cell proliferation in non-silenced U87 cells was reduced by PD98059, while remained unchanged in U87shC3G cells (*Figure 31C*). This was further confirmed by Ki67 staining (*Figure 31D*). These data indicate that ERKs inhibition decreases proliferation in non-silenced GBM cells, but not in C3G-silenced cells.

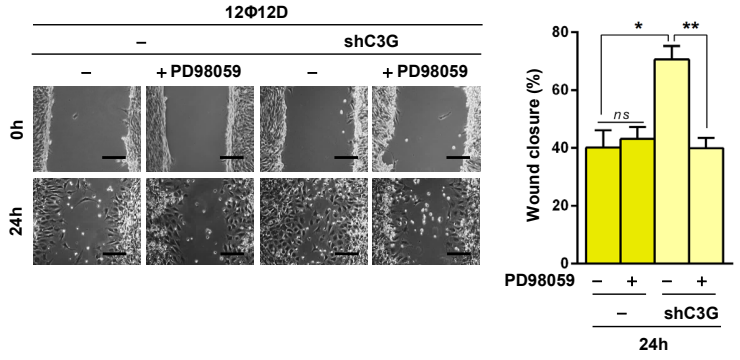

Figure 30 – ERKs inhibition with PD98059 decreases the migratory capacity of C3G-silenced 12Φ12D cells. 12Φ12D/12Φ12DshC3G cells maintained, either in the presence or absence of PD98059 (20 μM), as indicated, were used. Wound healing assay in serum-starved cells. Representative phase contrast microscopy images at 0h and 24h of migration (*left panels*) and histogram (*right panel*) representing the mean value of wound closure percentage ± S.E.M. at 6h and 24h (at least, n=3). Scale bars: 100 μm. **p* value <0.05, ***p* value <0.01, as indicated.

Altogether, these results indicate the existence of a C3G-mediated ERKs negative regulation in GBM with repercussions on invasiveness and tumourigenesis. Thus, C3G downregulation promotes ERKs activation, which promote increased invasiveness and foci formation capacity in anchorage-dependent and –independent growth assays.

5.3. C3G differentially regulates tyrosine-kinase receptors

Signalling by RTKs is broadly implicated in driving GBM onset and development. As mentioned in the introduction, EGFR mutations, amplification and/or overexpression of the gene are frequent in tumours from GBM patients (TCGA, 2008) (J. R. D. Pearson & Regad, 2017). In fact, due to EGFR importance in GBM, a number of strategies to treat GBM patients has been based on the impairment of EGFR activation in these tumours (J. R. D. Pearson & Regad, 2017), although their benefits in patients have been quite limited. This can be explained by the fact that EGFR activation and function are governed by a complex network of signalling regulators and mediators. Hence, when EGFR is inhibited, other RTKs display compensatory mechanisms (Lemmon & Schlessinger, 2010) (P. A. Clark et al., 2012) (Izumchenko et al., 2014) (Zahonero & Sánchez-Gómez, 2014) (Day et al., 2020).

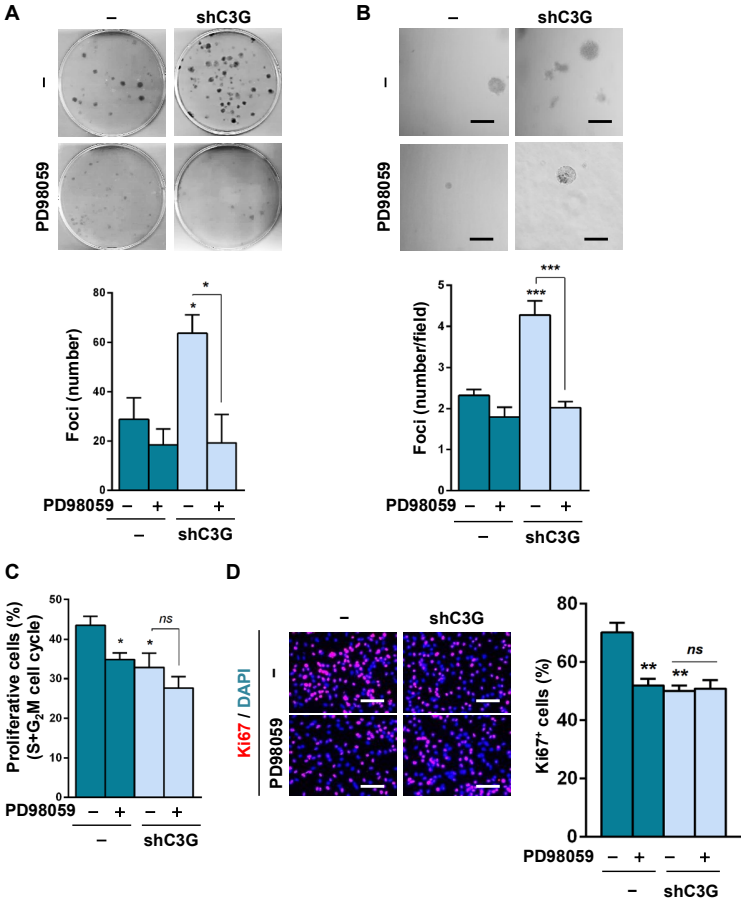

Figure 31 – Inhibition of ERKs activity with PD98059 decreases foci formation capacity of C3G-silenced U87 cells and proliferation in parental cells. U87/U87shC3G cells, maintained either in the presence or absence of PD98059 (20 μM), as indicated, were used. **(*A-B*)** Anchorage-dependent (*A*) and –independent (*B*) growth assays. Representative images of foci (*upper panels*) and histograms (*lower panels*) showing the mean value ± S.E.M. of the total foci number (at least, n=3). Scale bars: 100 μm. **(*C*)** Cytometric cell cycle analysis of adhered cells. Histogram represents the percentage of cells in S and G_2/M phases of cell cycle ± S.E.M. (at least, n=3). **(*B*)** Ki67 staining (red) of cells maintained in the presence of serum and under adherent conditions. Nuclei were stained with DAPI (blue). Representative microscope images (*left panel*) and histogram (*right panel*) showing the mean value ± S.E.M. of the percentage of Ki67 positive cells (at least, n=3). Scale bars: 50 μm. **p* value <0.05, ***p* value <0.01, ****p* value <0.001, versus parental cells or as indicated.

On the other hand, C3G has been widely linked to RTK-elicited functions (Okada et al., 1998) (Lu et al., 2000) (Sakkab et al., 2000) (Chiang et al., 2001) (Kao et al., 2001) (Voss et al., 2003) (Takahashi et al., 2008) (Schönherr et al., 2010) (Guvakova et al., 2014) (Sequera et al., 2020). Taking into account all this and the observed effect of C3G downregulation on cell signalling in response to serum in GBM cells, C3G might play a relevant function regulating RTKs in GBM cells.

5.3.1. C3G facilitates the activation of EGFR signalling by favouring its membrane localization

Based on the relevance of EGFR alterations and/or overexpression in GBM patient tumours (J. R. D. Pearson & Regad, 2017), we analysed if C3G regulated EGFR signalling in U87 cells upon EGF stimulation. C3G silencing reduced ligand-induced EGFR phosphorylation, but not total EGFR levels (*Figure 32A*). In addition, p38 MAPK, ERKs and Akt phosphorylation levels decreased in response to EGF in C3G-silenced U87 cells (*Figure 32A*). These results indicate that EGF/EGFR signalling is defective in GBM cells when C3G is downregulated.

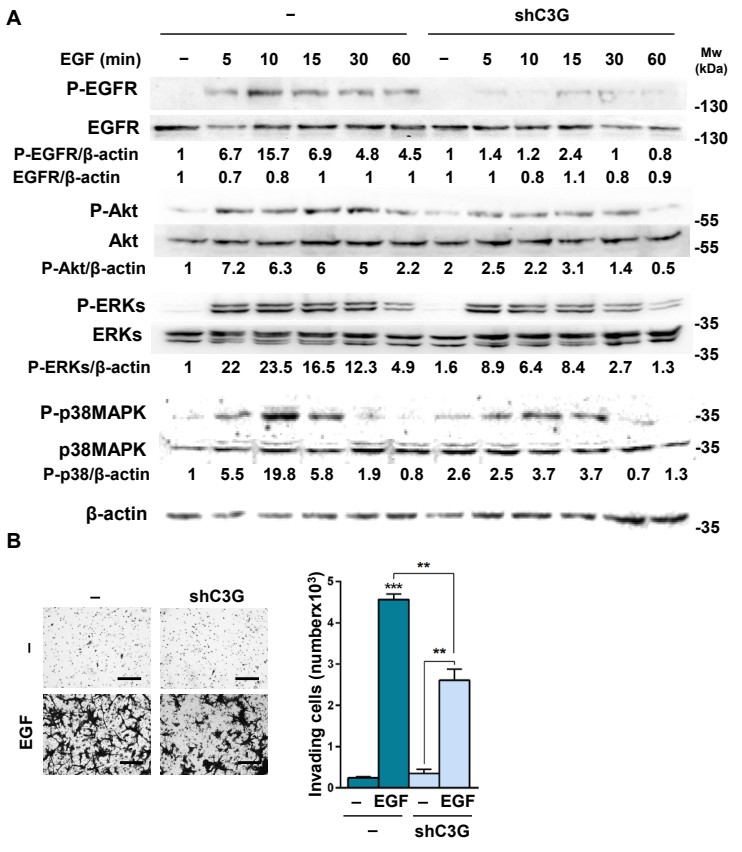

Figure 32 – C3G downregulation attenuates EGFR signalling and EGF-induced invasion. U87 and U87shC3G cells were used. **(*A*)** Western blot analysis of phosphorylated (P) and total levels of EGFR, Akt, ERKs and p38 MAPK proteins normalized to β-actin. Densitometric quantification of *proteins*/β-actin ratio expressed as the fold increase of the value of untreated cells (n=3). Serum-starved cells (for 16h) were stimulated with EGF (10 ng/ml) for 5-60 min or maintained untreated. **(*B*)** Invasion through Matrigel in response to EGF. Cells seeded in the upper chamber of transwells were maintained in the absence of serum and treated with EGF, when indicated. Representative microscopy images of invading cells (*left*) and histogram showing the mean value ± S.E.M. of the total number of invading cells (n=3) (*right*). Scale bars: 100 μm. ***p* value <0.01, ****p* value <0.001, versus parental cells or as indicated.

Next, we studied the functional consequences of the defective EGF/EGFR signalling in GBM cells. We observed a significant decrease in EGF-induced invasion upon C3G silencing in the absence of chemoattractant (*Figure 32B*).

C3G controls the exocytosis of angiogenic factors by platelets and interacts with VAMP7 (Martín-Granado et al., 2017) and it has been previously involved in vesicle trafficking (Chiang et al., 2001). Therefore, we studied if the alterations in EGFR signalling and functionality could be a consequence of changes in its endocytosis and/or recycling. We performed *in situ* EGF-induced EGFR endocytosis visualization assays using EGF labelled with Alexa Fluor 488. We detected a reduction in ligand-induced EGFR internalization in C3G knock-down cells (*Figure 33A*).

This suggested that C3G is involved in EGF-induced EGFR endocytosis and/or recycling. Therefore, we measured the amount of EGFR in the plasma membrane of U87 cells based on C3G levels, knowing that the total amount of EGFR in the cell remained unchanged (*Figure 32A*). Using flow cytometry as a complementary approach, we found that EGFR levels on cell surface were higher in parental U87 than in U87shC3G cells, both in the presence and absence of serum (*Figure 33B*). As a positive control of EGFR endocytosis, serum-deprived cells were treated with EGF for 2h. In parental U87 cells, the presence of EGFR in the membrane was highly reduced upon EGF treatment (*Figure 33C*), according to the rapid internalization observed by microscopy (*Figure 33A*). However, in U87shC3G cells, the low levels of EGFR at cell surface remained unchanged in response to EGF (*Figure 33C*). This also confirms the results observed by microscopy (*Figure 33A*). Moreover, inhibition of recycling by monensin (Nishimura et al., 2015) (Nishimura & Itoh, 2019) treatment significantly reduced EGFR levels at cell surface in non-silenced cells, while it had no effect on C3G-silenced cells (*Figure 33D*). These findings indicate that C3G would be required for EGFR membrane localization in GBM cells, mainly by favouring receptor recycling.

Taken together, these data indicate that C3G promotes EGFR plasma membrane localization, facilitating its activation by EGF and the subsequent activation of downstream signalling pathways. This leads to functional cellular effects such as invasion promotion. In U87shC3G cells, a high amount of EGFR remains internalized and therefore, unable to be activated by EGF, which results in a defective functional response.

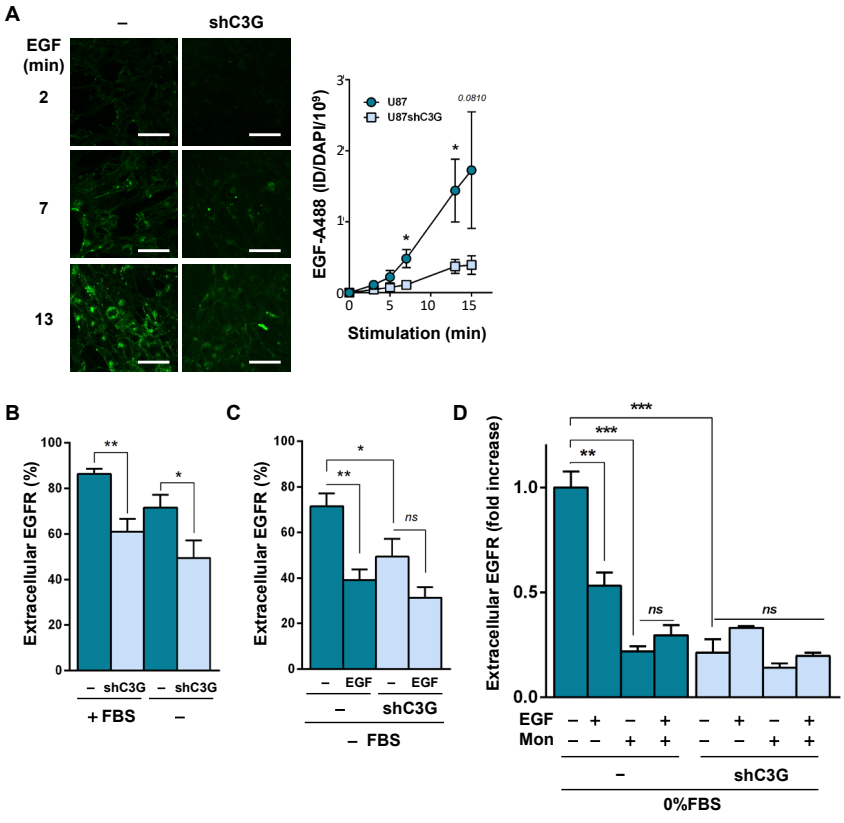

Figure 33 – EGFR endocytosis and plasma membrane localization are decreased in C3G-silenced U87 cells due to its reduced recycling. U87 and U87shC3G cells were used. **(*A*)** Representative fluorescence microscopy images of EGFR endocytosis induced by EGF labeled with Alexa 488 (EGF-A488, green) at different time points (*left panel*) and graph (*right panel*) represents fluorescence integrated density (ID) mean values ± S.E.M. (n=5-6). Scale bars: 50 μm. **(*B-D*)** Flow cytometric analysis of cell surface EGFR levels. Cells were maintained in medium supplemented with 10% serum (+ FBS) (*B*) or without serum (- FBS) (*B,C,D*). In *C and D*, cells were treated with EGF for 2h to induce endocytosis or maintained untreated. Additionally, in *D*, cells were maintained untreated or treated with monensin (10 μM) for 1h. Histograms show the percentage of cells presenting EGFR in the membrane (mean value ± S.E.M. (at least, n=3). **p* value <0.05, ***p* value <0.01, ****p* value <0.001, versus parental cells or as indicated.

5.3.2. C3G downregulation enhances the activation of several tyrosine kinase receptors in GBM cells. Effect on FGFR1 regulation and functionality

Although invasion was enhanced in U87shC3G cells using serum as chemoattractant, EGF driven invasion was decreased. Therefore, we evaluated the differential phosphorylation of RTKs using a proteome profiler human phospho-RTK array, searching for potential mediators of the increased invasion induced by C3G downregulation in response to serum.

In response to stimulation with serum (4h), the phospho-RTK array analysis revealed multiple changes induced by C3G knock-down in U87 cells (*Figures 34A and 34B, more detailed in Appendix 6*) and confirmed EGFR downregulation in U87shC3G cells as compared to parental cells. Other RTKs such as FGFR3, c-RET, ROR1 and MUSK also presented significant a lower phosphorylation in U87shC3G cells than in parental cells. Importantly, we found a significant upregulation in the phosphorylation of FGFR1, ErbB2, Eph family members (e.g. EphA6, EphB1, EphB2 and EphB4) and Tie-1/2. Several of these RTKs have been associated with cell migration and invasiveness. On the other hand, other RTKs presented the same activation status, independently of C3G levels, such as erbB4, FGFR4, Alk or RYK.

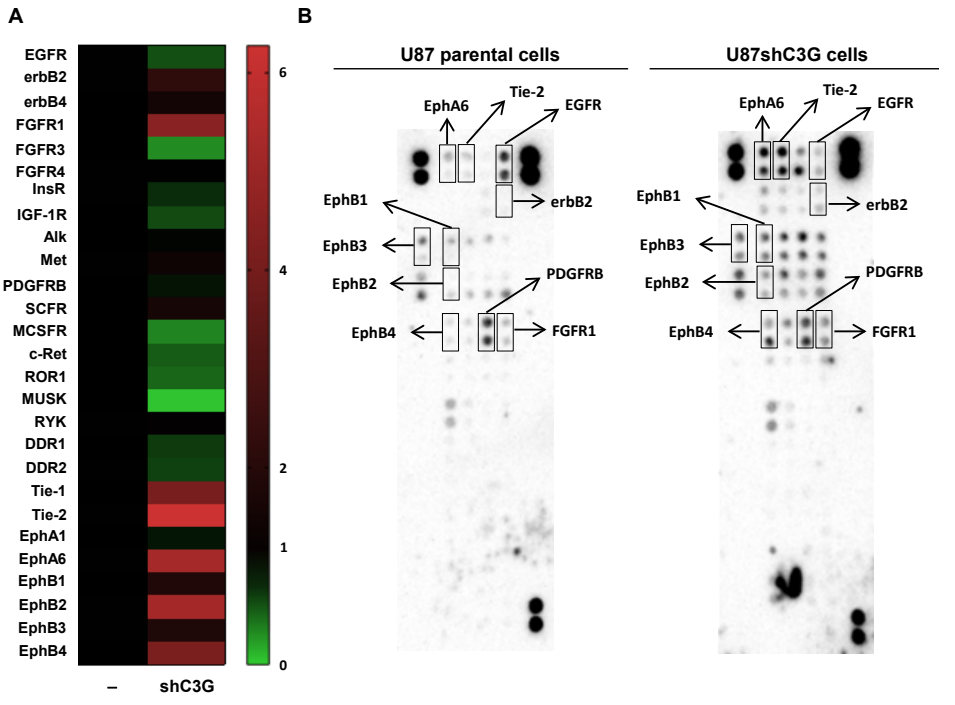

Figure 34 – C3G levels regulate the activation of diverse receptor tyrosine kinases in GBM cells. (***A***) Heatmap represents the relative phosphorylation levels of 27 RTKs present in the proteome profiler human phospho-RTK array. For each receptor, the mean value of the densitometric quantification of values of C3G-silenced cells as compared to parental cells, normalized to array positive controls (n=2). (***B***) Representative images of the membranes, where most relevant RTK spots are indicated.

Taking into account the relevance of FGFR1 in GBM (Watcharin Loilome, 2009) (Shirakihara et al., 2011) (Jimenez-Pascual & Siebzehnrubl, 2019), we evaluated the effect of its ligand, FGF-2, on invasion. U87shC3G cells stimulated with FGF-2 showed higher invasiveness than parental cells (*Figure 35A*). To further characterize the implication of FGFR1 signalling in the pro-invasive capacity of U87shC3G cells, we performed invasion assays using serum as chemoattractant in the presence of

Infigratinib, a FGFR1 inhibitor that can also act on FGFR2 and FGFR3, although to a lesser extent. We found that Infigratinib prevented invasion of C3G silenced U87 cells, while it had no effect on parental cells (*Figure 35B*). This confirms that FGFR1 over-activation is involved in the pro-invasive properties of GBM cells with C3G downregulation. To further validate the results obtained in the array and the invasive capacity of GBM cells upon activation of other RTKs, we measured midkine (MDK)-induced invasiveness. MDK acts as a ligand for Alk, an important RTK for GBM (López-Valero et al., 2020). According to the results derived from the array, its activation is independent of C3G levels. As expected, MDK-promoted invasion in both parental and C3G knock-down U87 cells regardless of C3G levels (*Figure 36)*. Therefore, these results validate data from the array and demonstrate their functional relevance in GBM cells, at least, in terms of invasion.

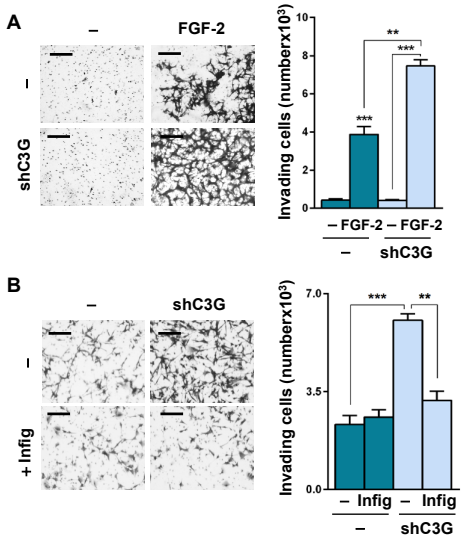

Figure 35 – Overactivation of FGFR1 upon C3G silencing plays a key role in the pro-invasive phenotype of C3G-silenced U87 cells. (*A*) FGF-2-induced invasion. Cells seeded in the upper chamber of transwells were maintained in the absence of serum and treated with FGF-2, when indicated. Representative phase contrast microscopy images of invading cells (*left panels*) and histogram (*right panel*) showing the mean value ± S.E.M. of the total number of invading cells (n=3). **(*B*)** Effect of Infigratinib (Infig) on invasion using serum (10%) as chemoattractant. Representative phase contrast microscopy images of invading cells (*left panels*) and histogram showing the mean value ± S.E.M. of the total number of invading cells (n=3) (*right panels*). Scale bars: 100 µm. ***p* value <0.01, ****p* value <0.001, versus parental cells or as indicated.

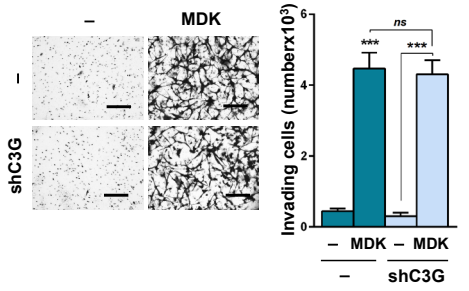

Figure 36 – MDK-mediated Alk activation does not mediate C3G silencing-associated pro-invasive effect observed in U87 cells. Cells seeded in the upper chamber of transwells were maintained in the absence of serum and treated with MDK when indicated. Representative images of invading cells (*left panels*) and histogram (*right panel*) showing the mean value ± S.E.M. of the total number of invading cells (n=3). Scale bars: 100 μm. ****p* value <0.001, versus parental cells or as indicated.

Altogether, these results indicate that C3G differentially regulates the activation and functionality of selected RTKs in GBM cells, decreasing EGFR activation, while increasing the activation of FGFR1 and other RTKs. This results in an overall enhanced invasiveness in GBM cells with C3G downregulation, in part mediated by FGFR1.

5.3.3. ERKs overactivation promoted by C3G silencing in U87 cells is responsible for FGF-2-induced invasiveness

As previously shown, C3G silencing up-regulated P-ERKs levels in U87 and 12Φ12D cells in response to serum (*Figure 27*). Moreover, we demonstrated that ERKs were involved in C3G knock-down-induced increased invasion (*Figures 29 and 30*) and foci formation (*Figure 31*).

On the other hand, FGF2-induced invasion was enhanced in U87shC3G cells. Therefore, we measured ERKs activation in response to FGF-2 in non-silenced and C3G silenced U87 cells. We also found increased P-ERKs levels when C3G was downregulated (*Figure 37A*), and ERKs inhibition by PD98059 prevented FGF-2-induced invasion (*Figure 37B*). Therefore, the increased FGFR1 activation upon C3G downregulation in GBM cells might enhance invasion by upregulating ERKs activation.

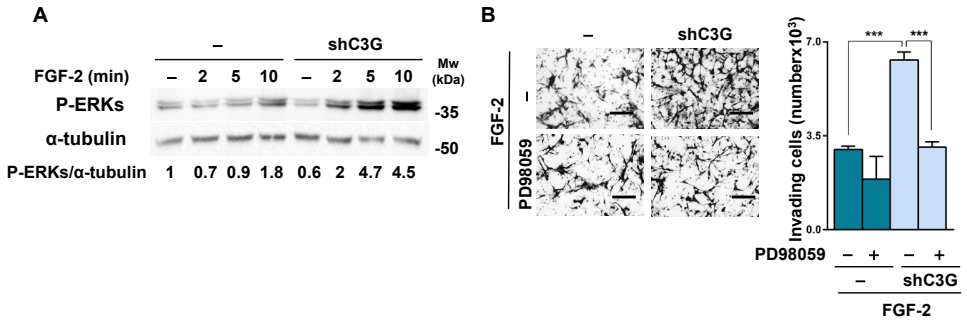

Figure 37 – FGF-2 induced ERKs upregulation mediates its pro-invasive effect on U87shC3G cells. U87 and U87shC3G cells were used. **(*A*)** Representative western blot analysis of phosphorylated (P) ERKs normalized to α-tubulin. Densitometric quantification of P-ERKs/α-tubulin ratio expressed as the fold increase of the value of untreated cells. Serum-starved cells (for 16h) were stimulated with FGF-2 (50 ng/ml) for 2-10 min or maintained untreated. **(*B*)** Invasion through Matrigel in response to FGF-2. Cells seeded in the upper chamber of transwells were maintained in the absence of serum and stimulated with FGF-2, and untreated or treated with PD09859. Representative phase contrast microscopy images of invading cells (*left panels*) and histogram (*right panel*) showing the mean value ± S.E.M. of the total number of invading cells (n=3). Scale bars: 100 μm. ****p* value <0.001, as indicated.

Taking altogether these results about C3G-mediated RTK regulation, we can conclude that C3G levels condition the activation status of different RTKs in GBM and, consequently, their functionality (e.g. their capacity to promote invasiveness). Specifically, in U87 cells, we have demonstrated that high levels of C3G allow EGFR activation and signalling, promoting invasion. In contrast, low levels of C3G provoke attenuation of EGFR activation by decreasing its presence in the plasma membrane and the overactivation of FGFR1. This upregulation of FGFR1 activity is in part responsible for the enhanced pro-invasive phenotype of U87shC3G cells through a mechanism dependent on ERKs activation.

6. C3G negatively regulates glioblastoma stem cell-associated properties

6.1. C3G knock-down increases sphere formation capacity in glioblastoma cells

As explained in the Introduction section, available treatments for GBM patients do not efficiently increase their survival. Among other reasons, GSCs may be responsible for resistance to treatment and can lead to tumour relapse in patients who initially respond to therapy (Liebelt et al., 2016). GSCs are also considered to be responsible for tumour initiation. Therefore, it is essential to characterize the

mechanisms governing GSCs appearance and their regulation to improve GBM patient outcomes. It is well-established that GSCs display self-renewal capacity and are able to form spheres *in vitro* under non-adherent and stem-cell promoting culture conditions.

Taking this into account, we evaluated whether C3G could be acting as a regulator of a GSC like phenotype in U87 cells. For that, we maintained parental and C3G silenced U87 cells under culture conditions that promoted a GSC phenotype using a medium containing EGF, FGF-2, B27 factors and LIF (*leukaemia-inhibitory factor*), among others. The sphere-forming capacity (number of spheres and their size) of these cells was analysed along the different subculture passages. As seen in *Figure 38A*, both, parental and U87shC3G cells showed sphere-forming capacity from p+1. Nevertheless, C3G-silenced cells generate more spheres from p+2 (*Figure 38B*), which indicates they could display an accentuated GSC-like phenotype. Sphere diameter was not affected by C3G knock-down (*Figure 38C*).

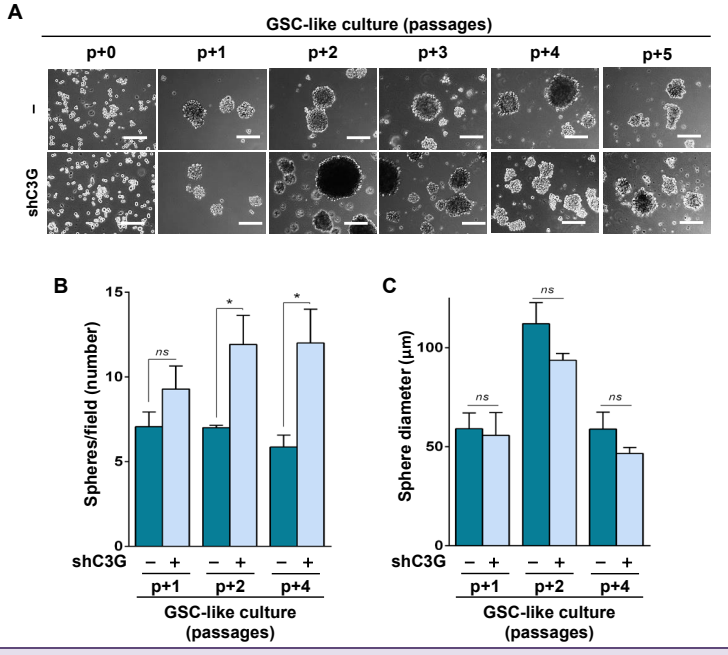

Figure 38 – C3G downregulation increases the capacity of U87 cells to form GSC-like spheres. U87 and U87shC3G cells were maintained under culture conditions promoting GSC phenotype. **(*A*)** Phase-contrast microscopy images of GSC-like spheres along the passages (*p+*). Scale bars: 100 µm. **(*B-C*)** Histograms showing number of spheres per field (*B*) or sphere diameter (*C*) measured with ImageJ software along culture passages ± S.E.M. (n=3). **p* value <0.05, as indicated.

To further investigate the potential function of C3G as a regulator of the GSC-phenotype and auto-renewal capacity of GBM cells, we performed ELDAs (*extreme limiting dilution assays*) in U87 cells. These results are visualized by dose-response

graphs representing the number of cells seeded per well (axis X) *vs.* the logarithm of the fraction of negative wells (non-responding cells) (axis Y). Consequently, the line slope, represented by a continuous line, is directly proportional to the auto-renewal capacity of cells. Discontinuous lines indicate the 95% confidence intervals and dots represent the values for each cell number.

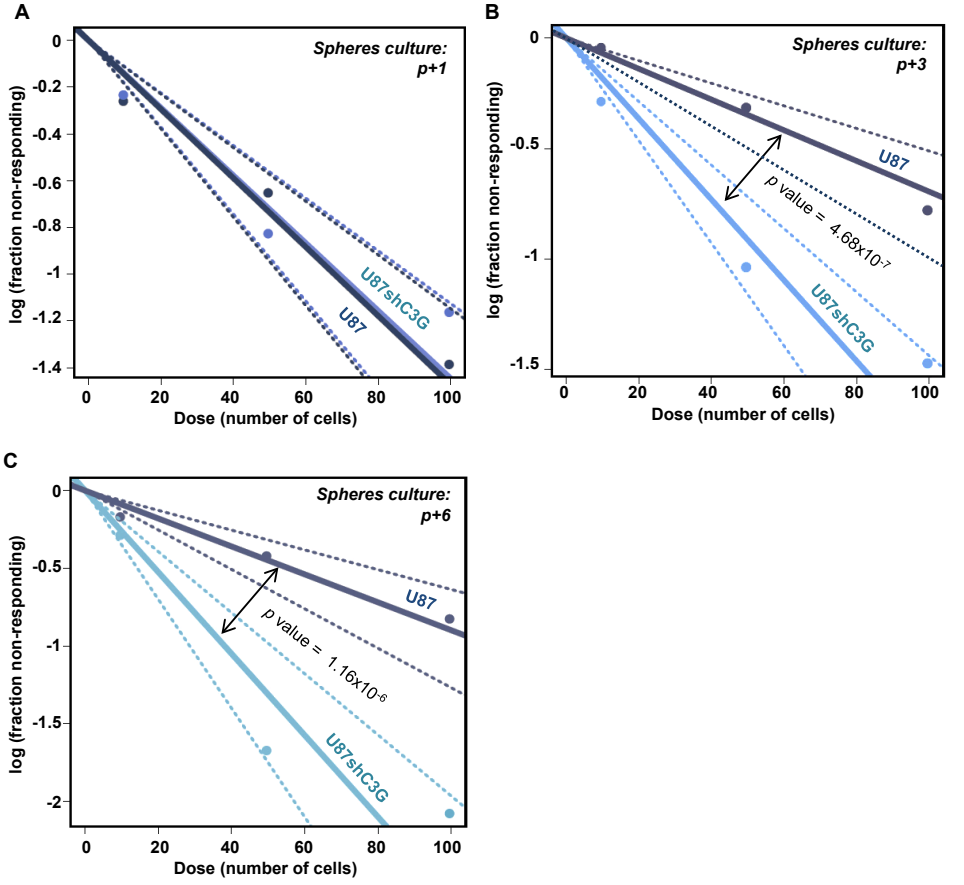

Figure 39 – C3G-silenced U87 cells present a higher GSC-associated sphere-forming capacity in ELDAs. U87 and U87shC3G cells were maintained under conditions promoting GSC phenotype. **(*A-C*)** ELDA results along culture passage: p+1 (*A*), p+3 (*B*) or p+6 (*C*). Statistical analyses: *Appendix 7*.

Using this method, we compared self-renewal capacity of parental and C3G-silenced U87 cells along passages under stem-promoting culture conditions, at p+1 (*Figure 39A*), p+3 (*Figure 39B*) and p+6 (*Figure 39C*). According to the results, C3G downregulation did not affect stemness at the very beginning (p+1), but it clearly increased auto-renewal capacity at p+3 and on. In agreement with this, we observed that, along the passages, from p+1 to p+6, U87shC3G-derived spheres increased their auto-renewal capacity (*p* value=0.0017) in a greater proportion than parental U87-derived spheres (*p* value=0.0204) (*Figure 40*). Moreover, ELDAs results are in

agreement with the increased sphere-forming capacity found in U87shC3G cells, previously shown in *Figure 38B*. Data derived from ELDAs and their statistical analyses are shown in *Appendix 7.*

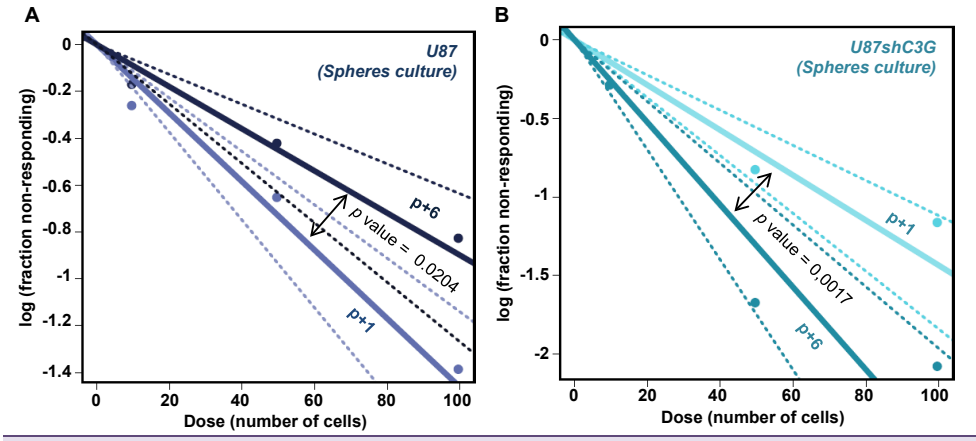

Figure 40 – C3G-silenced U87 cells present a higher GSC-associated sphere-forming capacity in ELDAs. U87 and U87shC3G cells were maintained GSC-promoting conditions. **(*A-B*)** ELDA results in U87 (*A*) and U87shC3G (*B*) cells, comparing p+1 and p+6. Statistical analyses: *Appendix 7*.

6.2. C3G downregulation increases Nestin and Glial fibrillary acidic protein levels, while decreases NeuN, in tumours

The signals governing the GSC-like phenotype in GBM such as BMPs, EGF, FGF or Eph are not specific of stem cell populations. They also control functions in differentiated cells of these tumours. A standard GSC-promoting cell culture medium is supplemented with EGF and FGF-2, whose signalling capacity is conditioned by C3G levels in differentiated GBM cells, as previously shown. Moreover, GSC-like phenotype is directly regulated by cell organization within tumours and their microenvironment. Therefore, we analysed the levels of Nestin by immunofluorescence in CAM-derived tumours generated by parental and C3G silenced U87 cells. Nestin is an intermediate filament protein, which is upregulated in stem-like populations (NSCs and GSCs). As seen in *Figure 41A*, Nestin is upregulated in tumours derived from C3G silenced cells, indicating that these tumours display a more accentuated GSC-like phenotype. This *in vivo* result is in agreement with our previous *in vitro* sphere-forming and ELDAs data. Taking into account the relevance of GFAP as an astrocytic marker, we also evaluated its expression in CAM-derived tumours (*Figure 41B*). Interestingly, tumours formed by U87shC3G presented a higher GFAP staining than those generated by parental U87 cells. On the other hand, the neural marker, NeuN, was slightly downregulated in CAM-tumours generated by C3G-silenced U87 cells (*Figure 41C*).

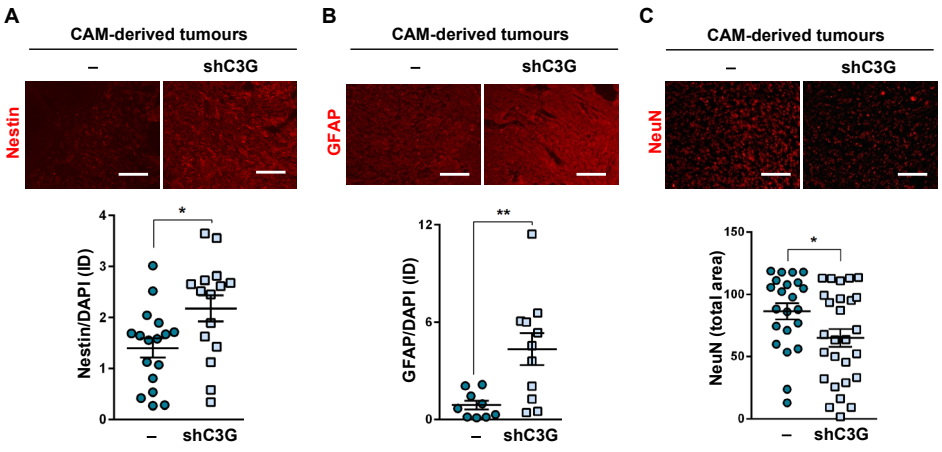

Figure 41 – Nestin and GFAP increase in CAM-derived tumours generated by C3G knock-down U87 cells, while NeuN decreases. (*A-C*) Immunofluorescence microscopy analysis in tumours generated by U87 cells without or with C3G silencing in CAM assays. Nestin (red) (*A*), GFAP (red) (*B*) and NeuN (red) (*C*) were detected using antibodies against these proteins. Representative images (*upper panels*) and graphs (*lower panels*) representing the mean values ± S.E.M. of integrated Density (ID) or total stained area (several sections per tumour, from a total of 3 staining reactions). Scale bars: 100 μm. **p* value <0.05, ***p* value <0.01, as indicated.

Altogether these results may indicate that C3G may play an important role in the control of the acquisition of stemness properties by GBM cells. Hence, C3G downregulation might favour a GSC-like phenotype. However, a further characterization of the expression of CSC/GSC (*cancer/GBM stem cells*)-associated markers is necessary to confirm this idea. In addition, the mechanisms implicated need to be uncovered. Nevertheless, these preliminary data represent an important step, since C3G had never been implicated in CSC regulation before, nor in GBMs, neither in other tumours.

7. C3G downregulation induces changes in the proteomic profile of glioblastoma cells

As previously shown, C3G silencing in GBM cells induced multiple functional effects accompanied by changes in the expression of some proteins and the activation of different signalling pathways. Nevertheless, it would be expected the existence of changes in the expression of more proteins than those previously analysed, which might have specific functions. Hence, to gain further insights into novel functions of C3G in GBM cells, we performed a hypothesis-free proteome-wide analysis. To do it, we compared the proteomic profile of parental and C3G knock-

down U87 cells. Samples were prepared following IACS Proteomics Scientific and Technical Service's indications, which were in charge of performing the proteomic determinations.

To analyse the data, we first classified the proteins in two groups according to whether they were overrepresented in parental U87 (*Appendix 8A*) or U87shC3G cells (*Appendix 8B*). Then, all these proteins (*columns 1 and 2*) were ranked from higher to lower score (*column 3*) taking into account the number of matched peptides (*column 4*) and the fold change between parental and C3G-silenced cells (*column 5*) in each case. As shown in the *Appendix 8* tables, only proteins with statistically significant changes were considered (*column 6*). All keratins were discarded, since they were considered contaminants.

In order to determine the potential biological relevance of these changes in the proteomic-wide profile of GBM cells, we performed several enrichment analyses to determine which GO (*gene ontology*) terms were modulated by C3G levels. To do it, we used the list of proteins overrepresented in C3G-silenced U87 cells (*Appendix 8B*) due to the increased number of proteins detected (70, *vs.* 46 proteins overrepresented in U87 parental cells) and their slightly higher median fold change value (1.45, *vs.* 1.3 for proteins overrepresented in parental U87 cells). Three online software were used for GO terms enrichment analyses: *Panther* (*Figure 42*) (2019), *Cancertool* (*Figure 43*) (2019) and *DAVID* (*Figure 44*) (2019). Statistically significant GOs were represented and compared according to their *p* value. We analysed GOBP (*GO biological processes*), GOCC (*GO cellular component*), GOMF (*GO molecular function*), Reactome (only in *Cancertool* software) and KEGG Pathway (only in *DAVID* software). Only statistically significant GOs (*p* value<0.05 and, consequently, -log10(adjusted *p* value)>1.3) were represented and compared. Additionally, *Panther* software displayed ''fold enrichment'' values, which are indicated in *Figure 42*.

First, it is important to highlight that these proteome-wide analyses revealed data related to our previous results and data from the group. For example, GOCC analysis from *Cancertool* software indicated an enrichment of "Extracellular vesicular exosome" and "Vesicle" GO terms. Moreover, Reactome analysis from *Cancertool* software also pointed to the enrichment in FGFR signalling-related GO terms (e.g. "FGFR2 ligand binding and activation" and "FGFR3b ligand binding and activation") in C3G-silenced cells. These data are in agreement with results shown in previous sections, which demonstrated that C3G regulates RTKs signalling in GBM cells. On one side, C3G was required for EGFR recycling and signalling, while attenuated FGFR1 signalling.

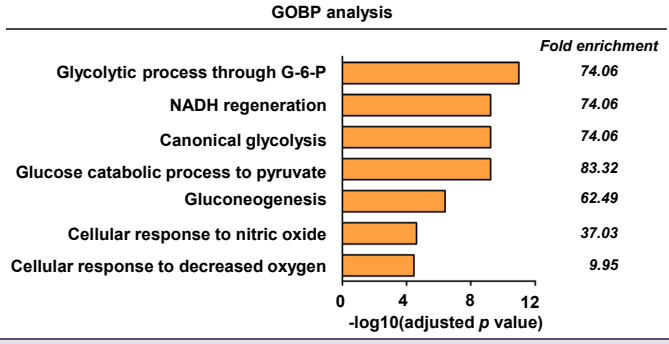

Figure 42 – GO terms enrichment analysis by Panther software of proteins overrepresented in C3G-silenced GBM cells. GOBP (*gene ontology biological processes*) terms determined by Panther software *(*2019) using the list of IDs overrepresented in U87shC3G compared to U87 parental cells according to a proteome-wide analysis.

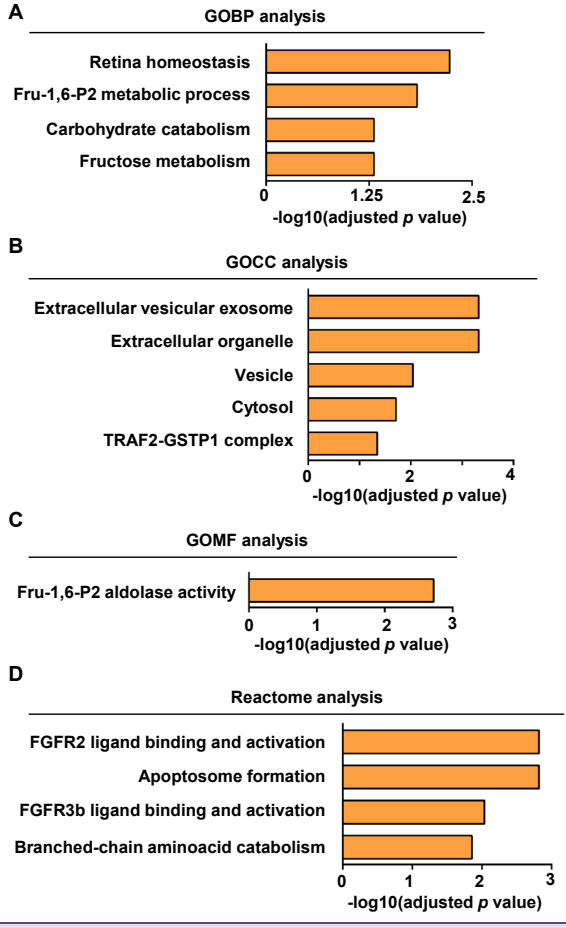

Figure 43 – GO terms enrichment analysis by Cancertool software of proteins overrepresented in C3G-silenced GBM cells. (*A*) GOBP (*gene ontology biological processes*), **(*B*)** GOCC (*GO cellular component*), **(*C*)** GOMF (*GO molecular function*) and **(*D*)** Reactome terms determined by Cancertool software (2019) using the list of IDs overrepresented in U87shC3G compared to parental U87 cells according to a proteome-wide analysis.

Interestingly, diverse metabolism-associated GO terms were detected. In particular, GO terms related to glycolysis were upregulated upon C3G downregulation in GOBP from *Panther* software (e.g. “Glycolytic process through glucose-6-phosphate”, “Canonical glycolysis”, “Glucose catabolic process to pyruvate” or even “Cellular response to decrease oxygen”) (*Figure 42*), in GOBP and GOMF from *Cancertool* software (e.g. “Fructose-1,6-biphosphate metabolic process” or “Fructose-1,6-biphosphate aldolase activity”) (*Figure 43*), and in GOPB and KEGG PATHWAY from *DAVID* software (e.g. “Canonical glycolysis”, “Glycolytic process” or “Glycolysis/Gluconeogenesis”) (*Figure 44*).

These coincidences among the diverse used software add validity to our results and suggest that C3G may act as a regulator of cancer cell metabolism. This potential function of C3G had never been considered before, neither for GBM, nor for other tumours.

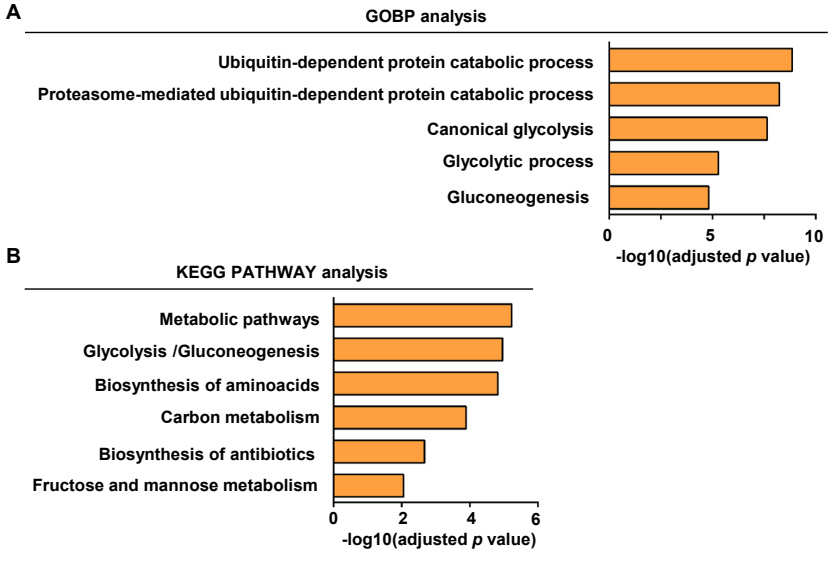

Figure 44 – GO terms enrichment analysis by DAVID software of proteins overrepresented in C3G-silenced GBM cells. (*A*) GOBP (*gene ontology biological processes*) and **(*B*)** KEGG Pathway terms determined by DAVID software (2019) using the list of IDs overrepresented in U87shC3G compared to parental U87cells according to a proteome-wide analysis.

8. C3G inhibits the acquisition of a pro-glycolytic phenotype in U87 cells

8.1. C3G downregulation promotes the expression and/or activity of enzymes and transporters involved in glycolysis and lactate released

Taking into account the potential role of C3G in GBM metabolism revealed by the proteomic-wide assay detailed above, we decided to further characterize the glycolytic status of parental and U87shC3G cells.

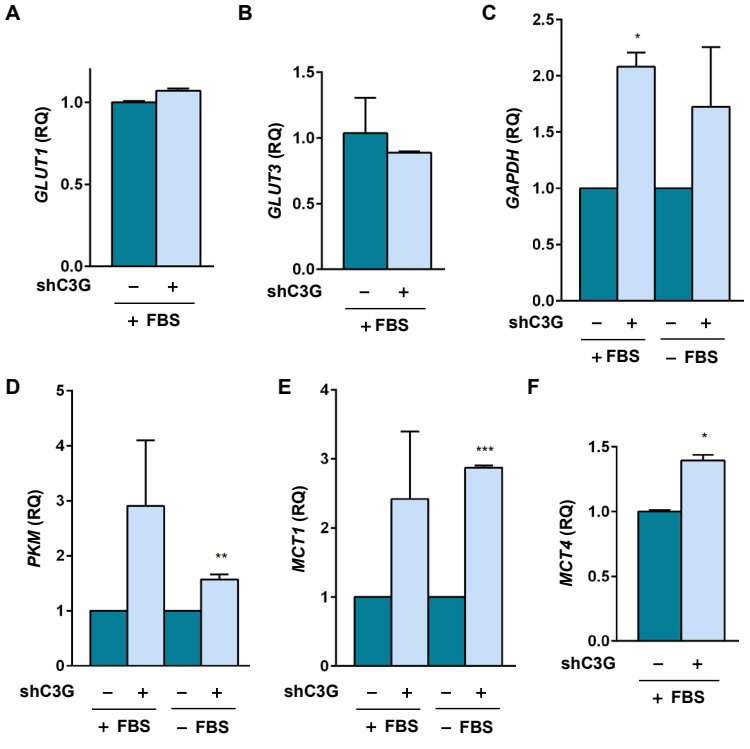

Figure 45 – C3G silencing increases the mRNA levels of enzymes and transporters involved in the final steps of glycolysis. (*A-G*) *GLUT1* (*A*), *GLUT3* (*B*), *GAPDH* (*C*), *PKM* (*D*), *MCT1* (*E*) and *MCT4* (*F*) mRNA levels in U87-/+shC3G cells maintained either in the presence (+) and/or absence (-) (24h) of serum (FBS). Histograms represent RQ mean value ± S.E.M. referred to parental cells (at least, n=3). **p* value <0.05, ****p* value <0.001, versus parental cells.

We first analysed the mRNA expression of several transporters and enzymes relevant for glycolysis by RT-qPCR (*Figure 45*). We observed that *GAPDH*, *PKM*, *MCT1* and *MCT4* genes displayed a tendency (statistically significant or not depending on cell culture conditions) to increase its expression in U87shC3G cells as

compared to non-silenced cells. Nevertheless, *GLUT1* and *GLUT3* mRNA levels remained unaltered. These results were consistent with data derived from the proteomic analysis, indicating an enhancement of a glycolytic-like phenotype in GBM cells when C3G is downregulated. Hence, we decided to study glycolysis at a functional level.

First, we evaluated the glucose uptake capacity of U87 cells using a glucose analogue with fluorescent properties, NBDG (*2-(N-(7-nitrobenz-2-oxa-1,3-diazol-4-yl)amino)-2-deoxyglucose*). Under our experimental conditions, C3G downregulation did not alter glucose uptake capacity of U87 cells, independently of the presence or absence of serum, as shown in *Figures 46A and 46B*, respectively. NBDG is internalized in cells by GLUTs (*glucose transporters*), as glucose does. As seen above, *GLUT1* and *GLUT3* mRNA levels were not regulated by C3G in GBM cells, supporting glucose uptake data. After internalization, glucose is phosphorylated by HK (*hexokinase*) and so it does NBDG, in order to avoid their release. Thus, we determined HK activity in parental and U87shC3G cell lysates (*Figure 46C*), observing that it was not affected by C3G downregulation.

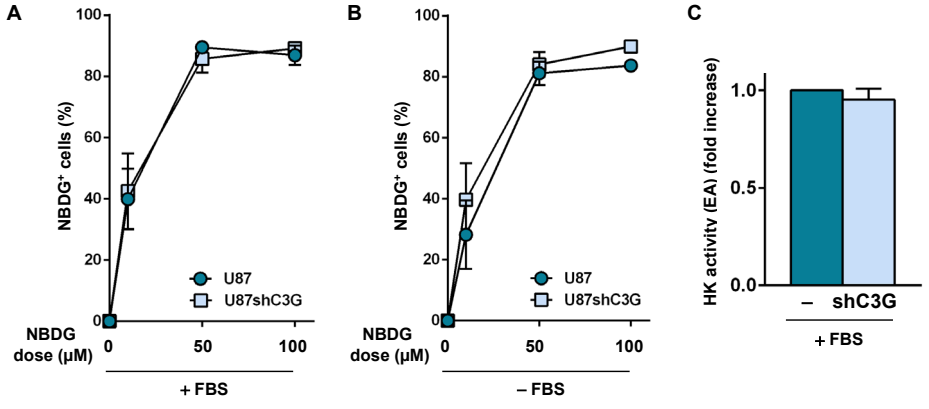

Figure 46 – C3G silencing do not affect either glucose uptake or HK activity in U87 cells. U87 cells without or with C3G silencing were used. **(*A-B*)** NBDG (0-100 μM) dose-response uptake assays of cells maintained in the presence (+) (*A*) or absence (-) (*B*) of serum (FBS). Representation of the percentage of positive cells mean value ± S.E.M. (n=3). **(*C*)** HK activity analysis in cells maintained in a medium supplemented with serum (+FBS); histogram represents the fold increase mean values referred to parental cells ± S.E.M. (n=3).

Once having discarded functional changes at the first steps of glycolysis, we studied the effect of C3G silencing in the final steps of the anaerobic branch of glycolysis: lactate release (*Figures 47A and 47B*) and LDH (*lactate dehydrogenase*) activity (*Figures 47C and 47D*). We measured the amount of lactate in cell culture

media from serum-deprived parental and C3G-silenced U87 cells at different time points (0h, 6h, 18h, 24h and 48h). We observed that lactate release was upregulated in C3G-silenced cells at 48h, while it remained unchanged and at a lower level in parental U87 cells (*Figure 47A*). Lactate release and accumulation in cell culture medium was also higher in the presence of serum in C3G knock-down U87 cells (*Figure 47B*). These results are in agreement with the increased mRNA levels of the lactate transporters, *MCT1* and *MCT4*, detected in U87shC3G cells and previously shown.

Intracellular lactate, which is released to the medium by MCTs (*monocarboxylate transporters*), is generated from pyruvate in a reaction catalysed by LDH enzyme. This reaction is considered the last step of anaerobic glycolysis, opposed to the aerobic branch of glycolysis, in which pyruvate is used to feed the mitochondrial TCA (*tricarboxylic acids*) cycle and respiratory chain. Hence, we determined LDH enzymatic activity in parental and U87shC3G cell lysates (*Figure 47C*). LDH activity was increased in C3G-silenced cells, both when cells are maintained in the presence or absence of serum. We also determined LDH activity in the presence of azide that inhibits Cytochrome C oxidase, an enzyme from the mitochondrial respiratory chain (Bolaños, 2016). Parental U87 cells treated with azide displayed a higher LDH activity when compared to untreated cells, while only a slight tendency to increase (not statistically significant) was observed in U87shC3G (*Figure 47D*). Importantly, LDH activity in all cell culture media, a well-established indicator of cell death due to plasma membrane breakdown, whose variation could be affecting our results, was also measured. It was not altered by either C3G downregulation, or azide treatment. Moreover, we detected a tendency to decrease *LDHB* mRNA levels in U87shC3G cells as compared to parental cells (*Figure 47E*). *LDHB* gene encodes LDH-B subunits, which are responsible for LDH oxidative function by catalysing the conversion of lactate to pyruvate, which is susceptible of entering TCA cycle.

To further characterize if C3G levels condition the catabolism of glucose in GBM cells through anaerobic (via lactate) or mitochondrial (via TCA cycle and respiratory chain) pathways, we measured mRNA levels of some SDH (*succinate dehydrogenase*) subunits by RT-qPCR (*Figure 48*). SDH complex, also known as Complex II of mitochondrial respiratory chain, is formed by four subunits: SDHA (which catalyses the oxidation of succinate to fumarate coupled to FAD (*flavin adenine dinucleotide*) reduction to $FADH_2$), SDHB (which transports the electrons from $FADH_2$ to heme group), SDHC and SDHD (that interact with heme group). Although C3G levels did not regulate *SDHA* mRNA levels (*Figure 48A*), the expression of *SDHB* and *SDHC* mRNAs (*Figures 48B and 48C*) was significantly downregulated in C3G-silenced U87 cells. This suggests that the mitochondrial respiratory activity of U87 cells would be reduced when C3G is downregulated.

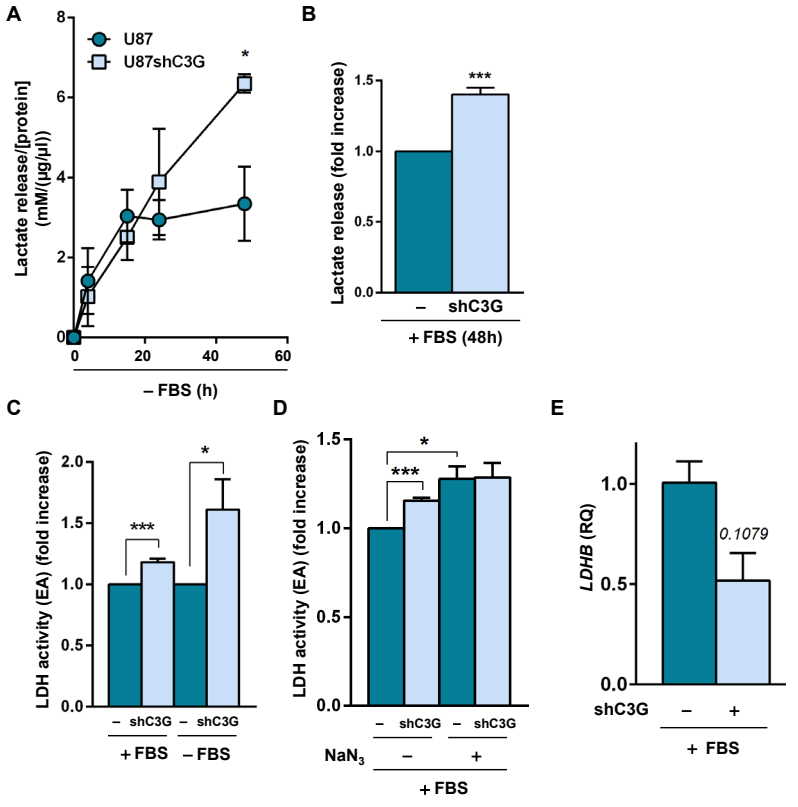

Figure 47 – Increased lactate release and LDH activity in C3G-silenced U87 cells. (*A-B*) Lactate levels were determined in culture media from non-silenced and C3G-silenced U87 cells maintained in the absence (-) (*A*) or presence (+) (*B*) of serum (FBS) for the specified time. Graphs represent the fold increase value referred to parental cells (serum-starved for 0h in case of *A*) ± S.E.M. (n=3). **(*C-D*)** Analysis of LDH activity of U87-/+shC3G cells maintained in medium without (-FBS) (*C*) or with serum (+FBS) (*C, D*). When indicated, cells were treated with azide (10 mM) (NaN_3). Histograms represent the fold increase mean values referred to untreated parental cells ± S.E.M. (n=3). (E) *LDHB* mRNA levels in U87-/+shC3G cells maintained in the presence of serum (FBS). Histograms represent RQ mean value ± S.E.M. referred to parental cells (at least, n=3). **p* value <0.05, ****p* value <0.001, versus parental cells or as indicated.

Therefore, we have confirmed by functional assays that C3G knock-down in GBM cells is associated with an upregulation of glycolysis, directing glucose to its use by anaerobic glycolysis. We have not detected alterations in glucose uptake, indicating that changes upon C3G silencing occur in the final steps of glycolysis. Additionally, we have validated our bioinformatic GO terms analyses.

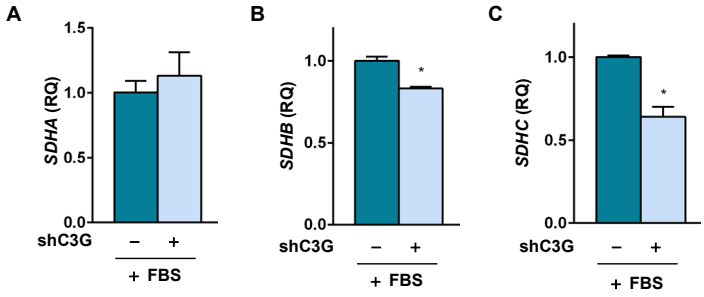

Figure 48 – *SDHB* and *SDHC* mRNA levels are downregulated upon C3G knock-down in GBM cells. (*A-C*) *SDHA* (*A*), *SDHB* (*B*) and *SDHC* (*C*) mRNA levels in U87-/+shC3G cells maintained in the presence of serum (FBS). Histograms represent RQ mean value ± S.E.M. referred to parental cells (at least, n=3). **p* value <0.05, versus parental cells.

8.2. C3G silencing increases Pyruvate kinase activity and the levels of PKM2 isoform in glioblastoma

To further understand this novel role of C3G as a negative regulator of glycolysis in GBM cells, we analysed if C3G controlled other key steps of glycolysis. The reaction catalysed by PK (*pyruvate kinase*) is a highly-regulated, irreversible step from the glycolytic pathway. In addition, PKM2 isoform has been associated to tumour formation and progression. According to the proteomic-wide analysis performed in U87 cells, PKM protein levels were increased in U87shC3G cells as compared to parental cells (*Appendix 8B*). *PKM* mRNA levels were also upregulated in C3G-silenced cells (*Figure 45E*). Thus, we further characterized the regulation of this glycolytic enzyme by C3G.

PK activity is essential for glycolysis and constitutes a rate-limiting step. As it can be seen in *Figure 49A*, PK activity was increased in U87shC3G cells as compared to parental cells. Taking into account that PK activity analysis was performed in the presence of the PKM2 allosteric modulator, fructose-1,6-bifosfate (*Fru-1,6-P2*), it is likely that PKM2 isoform may be increased in C3G-silenced cells. Hence, we determined PKM2 protein levels in CAM-derived tumours. We found an upregulation of PKM2 in CAM-derived tumours generated by C3G knock-down U87 cells as compared to parental cells (*Figure 49B*). Moreover, it was discarded a predominant nuclear localization of PKM2, independently of C3G levels.

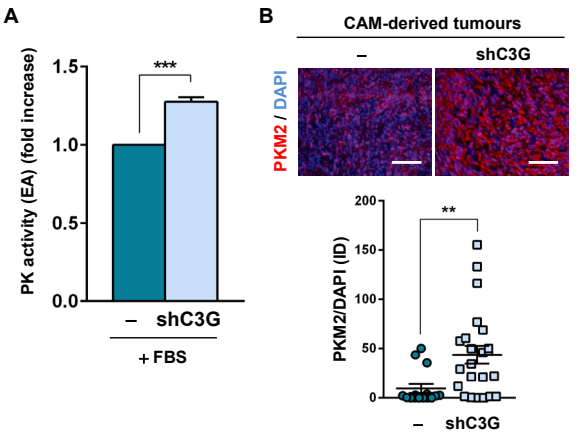

Figure 49 – C3G downregulation in GBM cells leads to an enhanced PK activity and higher levels of PKM2 isoform in CAM-derived tumours. (*A*) Analysis of PK activity of U87-/+shC3G cells maintained in medium containing serum (+ FBS). Histogram represents the fold increase mean values referred to parental cells ± S.E.M. (n=3). **(*B*)** Immunofluorescence microscopy analysis in tumours generated by U87 cells without or with C3G silencing in CAM assays: PKM2 (red) and DAPI (blue). Representative images (*upper panels*) and graphs (*lower panels*) representing Integrated Density (ID) values ± S.E.M. (several sections per tumour, from a total of 3 stainings). Scale bars: 100 μm. ***p* value <0.01, ****p* value <0.001, as indicated.

These data support a function for C3G as a regulator of PK activity and/or the expression of PKM2 isoform. However, further studies are required to fully establish its function in the control of PKM expression and activity, as well as the mechanisms involved and its functional relevance.

8.3. C3G regulates the expression of mRNAs coding for proteins from Pyruvate dehydrogenase complex and Pyruvate dehydrogenase kinase 1

As mentioned above and explained in the Introduction section, pyruvate, the end-product of glycolysis, can be metabolized by LDH or by mitochondrial TCA. In this last case, pyruvate is converted into acetyl-coA by an irreversible reaction catalysed in the mitochondria by PDH (*pyruvate dehydrogenase*) complex. In cancer cells, anaerobic processing of pyruvate is favoured by PDH complex downregulation via PDK (*pyruvate dehydrogenase kinase*)-dependent phosphorylation and/or downregulation of the expression of PDH components.

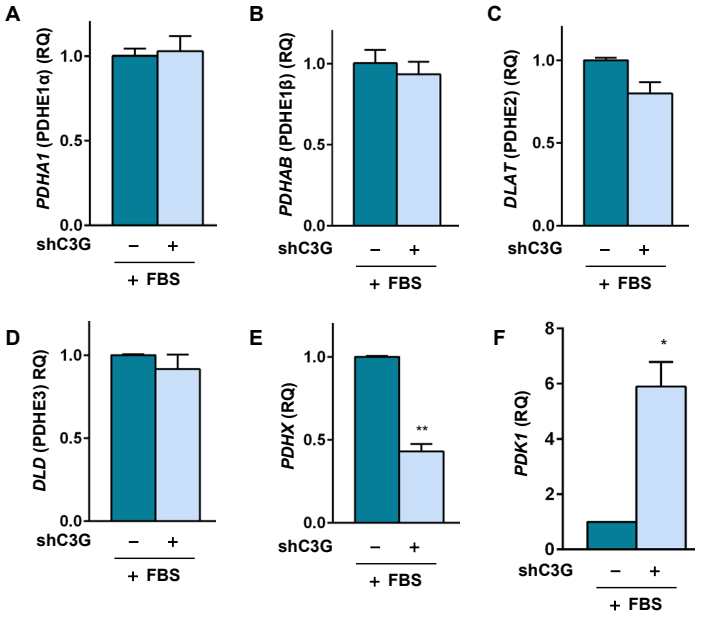

Figure 50 – C3G silencing modifies the mRNA levels of two components of PDH/PDK regulatory axis. (*A-F*) *PDHA1* (*A*), *PDHAB* (*B*), *DLAT* (*C*), *DLD* (*D*), *PDHX* (*E*) and *PDK1* (*F*) mRNA levels of U87-/+shC3G cells maintained in the presence of serum (FBS). Histograms represent RQ mean value ± S.E.M. referred to parental cells (at least, n=3). **p* value <0.05, ***p* value <0.01, versus parental cells.

Hence, we wondered if the upregulation of LDH activity in U87shC3G cells as compared to parental U87 cells was associated to a downregulation of PDH levels. We analysed the mRNA levels of several PDH complex components by RT-qPCR (*Figure 50A-E*). We did not find changes upon C3G silencing in the mRNA levels of *PDHA1* (that encodes PDHE1α subunit), *PDHAB* (that encodes PDHE1β subunit), *DLAT* (that encodes PDHE2 subunit) or *DLD* (that encodes PDHE3 subunit) under our experimental conditions. However, *PDHX* mRNA levels (encoding PDHX subunit) were downregulated in C3G-silenced cells. Interestingly, the absence of PDHX subunit (also called PDHE3-binding protein) is associated with decreased PDH activity and alterations in mitochondrial metabolism.

We also analysed *PDK1* mRNA levels, since PDK1-mediated PDHE1α phosphorylation inhibits PDH complex activity. In agreement with the above referred results, *PDK1* mRNA levels increased in C3G knock-down U87 cells (*Figure 50F*).

These data indicate that C3G may act as a regulator of PDH/PDK1 axis expression in GBM cells and, consequently, C3G downregulation would reduce pyruvate processing via mitochondrial TCA and respiratory chain in these tumours, even under normoxia.

Discussion

1. C3G expression is downregulated in glioblastoma, associated to a mesenchymal phenotype

C3G, encoded by *RAPGEF1* gene, is an important regulator of brain development and homeostasis. C3G expression is higher in fetal and adult brain compared to other tissues (Tanaka et al., 1994) (V. Radha et al., 2011) (Cheerathodi et al., 2015) (*ProteinAtlas database*) and brain-specific isoforms of C3G have been also described (Cheerathodi et al., 2015) (Sriram et al., 2020). C3G regulates differentiation and migration of various neural populations (Voss et al., 2006) (Voss et al., 2008) (Yip et al., 2012) (Shah et al., 2016), being involved not only in Reelin pathway (Ballif et al., 2004) (Park & Curran, 2008) (Voss et al., 2008) (Yip et al., 2012) (Bock & May, 2016), but also in EGFR, Trk and other RTKs signal transduction (Lu et al., 2000) (Kao et al., 2001) (Wu et al., 2001). Despite its relevance, almost nothing is known about the role of C3G in the nervous system under pathological conditions. Moreover, C3G regulates relevant processes involved in tumour progression, including proliferation, apoptosis, adhesion, invasion and angiogenesis, although its function in cancer appears to depend on tumour stage and cell context (Okino et al., 2006) (Martín-Encabo et al., 2007) (Maia et al., 2009) (Gutiérrez-Uzquiza et al., 2010) (Dayma & Radha, 2011) (Maia et al., 2013) (Priego et al., 2016) (Martín-Granado et al., 2017) (Sequera et al., 2018) (Carabias et al., 2020) (Sequera et al., 2020). Taking into account the relevance of C3G in the brain, we hypothesized it could play a role in GBM, which remained undetermined before the initiation of this work. Indeed, Crk, its main interacting protein, is overexpressed in GBM and associated to aggressive progression (Birge et al., 2009). In this work, we uncover a previously unknown function of C3G in human GBM dissemination, tumourigenesis and cell signalling.

First, public databases revealed that *RAPGEF1* mRNA levels are decreased in GBM patients as compared to healthy brain tissue (*Figure 1*), being independent of patient sex/gender and age (*Figure 2*). In contrast, we did not find major changes in the mutational status of C3G in GBM using data from COSMIC and cBioportal webpage. Lack of information in TCGA database prevented us to analyse the correlation between C3G levels and IDH mutational status, a novel molecular entity included by WHO in 2016 to classify GBMs (Louis et al., 2016). Nevertheless, our data suggest that C3G levels could be down-regulated during GBM onset and/or progression and it could have a potential value in clinic. Moreover, we analysed the association between C3G expression and GBM molecular subtypes defined according to markers for classical, proneural, neural or mesenchymal described by *Verhaak et al. (2010)*. This showed that samples with low *RAPGEF1* mRNA levels are linked to classical and mesenchymal subtypes (*Figure 3*). Altogether these data indicate that, although, in general, *RAPGEF1* expression is decreased in GBMs, there

are differences in expression based on the molecular subtype. Thus, C3G would control GBM phenotype, so that C3G downregulation would be associated to the acquisition of a mesenchymal GBM phenotype and a potential enhanced disseminative capacity. Unfortunately, using TCGA information, we did not detect any association between *RAPGEF1* mRNA levels and overall survival of GBM patients using Kaplan-Meier test. Probably, this is due to the very low survival of GBM patients upon diagnosis. In fact, it is rare to observe changes in overall survival, even for well-established genes controlling these tumours. Actually, nowadays first-line treatment (surgical resection followed by adjuvant radiotherapy and treatment with TMZ) is considered effective although it only increases median survival in around 2-3 months.

In agreement with the reduced *RAPGEF1* mRNA levels in samples from GBM patients, C3G protein levels are also downregulated in all GBM cell lines analysed (U87, U118, T98, U251 and A172 cells) as compared to non-tumourigenic HAs (Bejarano et al., 2017) (*Figure 4*). All tested cell lines come from male GBM patients. Although data from TCGA indicate that sex/gender does not affect *RAPGEF1* mRNA levels in GBM patients, further studies should be performed to be able to extrapolate our results to female GBM patients. We have not detected, either in HAs or in GBM cell lines, the novel brain-specific C3G isoform of 175 kDa (Sriram et al., 2020). This is in agreement with their results since they indicate that it is undetectable in cell lines. According to them, this isoform is mainly expressed in postnatal and adult brain by $NeuN^+$ cells (neurons), but not by $GFAP^+$ cells (astrocytes) (Sriram et al., 2020), while 140 kDa isoform seems to be expressed by embryonic precursors. Here, we show that HAs and GBM cell lines ($GFAP^+$ cells) express the 140 kDa C3G isoform. However, GBM cell lines expressing lower C3G protein levels (U87, U251 and A172 cells) present higher levels of GFAP. Importantly, in agreement with patient data, C3G downregulation in GBM cells is accompanied by Vimentin upregulation, a well-established mesenchymal marker associated to poor prognosis in GBM (Ivaska, 2011) (Lin et al., 2016) (Zhao et al., 2018) (Nowicki et al., 2019).

Therefore, according to patient data and GBM cell lines, C3G downregulation is associated to an enhanced expression of mesenchymal markers. This indicates that C3G may be a potential regulator of GBM onset, tumourigenesis and/or dissemination.

2. C3G as a regulator of glioblastoma migration, invasion and adhesion

Regarding motility, the results derived from this study (summarized in *Figure D1*) demonstrate that C3G downregulation/depletion in GBM promotes the acquisition of an enhanced mesenchymal phenotype with increased migratory/invasive capacity and decreased adhesion. This has been demonstrated in a well-established GBM cell line (U87) and in several non-commercial PDCs (12Φ12D and HCO1D cells) using gene silencing and CRISPR/Cas9 technology approaches. This is also supported by overexpression data, which show that C3G inhibits invasion and enhances adhesion of GBM cells. These results are in agreement with the increased migratory properties of C3G-deficient MEFs (Gutiérrez-Uzquiza et al., 2010), C3G-silenced coloncarcinoma (Priego et al., 2016) and HCC cells (Sequera et al., 2020), as well as with the inhibitory effect of C3G overexpression on breast carcinoma cells migration (Dayma & Radha, 2011). However, in HCC, even though C3G downregulation promotes cell dissemination, the growth of these secondary foci is associated to a secondary upregulation of C3G (Sequera et al., 2020). Moreover, in healthy brain, C3G depletion also inhibits differentiation-associated migration of neural precursors in some brain areas during development (Voss et al., 2006), impairing cortical plate formation and a proper organization and attachment of radial glia (Voss et al., 2008).

Interestingly, c-Abl silencing leads to changes in the pro-invasive capacity of GBM cells, similar to those induced by C3G downregulation (Lamballe et al., 2016). Taking into account that c-Abl can regulate and interact with both C3G and Crk (V. Radha et al., 2007) (Birge et al., 2009) (A. Mitra & Radha, 2010) (V. Radha et al., 2011), c-Abl/Crk/C3G axis might be operating in GBM cells, playing a negative role in the control of the acquisition of a mesenchymal/pro-invasive phenotype.

The pro-migratory effect of C3G downregulation in GBM is associated to the decrease in cell-cell contacts determined by the reduction of ZO-1 and β-catenin in cell periphery. ZO-1/2/3 proteins, occludins and claudins, are the main components of tight junctions (Bhat et al., 2019) and β-catenin, through its interaction with E-cadherin, forms part of adherens junctions (Wijnhoven et al., 2000). Cell to cell contacts destabilization followed by β-catenin and/or ZO-1 internalization has also been observed upon C3G downregulation in other cell types. For example, a reciprocal negative regulation between C3G and β-catenin was described in highly invasive breast cancer cells (Dayma et al., 2012). Our group has also described that C3G silencing induces the loss of ZO-1-rich cell-cell contacts in coloncarcinoma cells (Priego et al., 2016) and β-catenin internalization in HCC cells (Sequera et al., 2020). β-catenin internalization could be also occurring in C3G-silenced 12Φ12D cells as a

consequence of the decrease in E-cadherin levels as in coloncarcinoma cells (Priego et al., 2016). Although the decrease in E-cadherin levels has only been observed in 12Φ12D cells due to its epithelial-like phenotype, this mechanism might be acting in other GBM cells. This includes U87 cells, in which E-cadherin is expressed according to the scientific literature (Lamballe et al., 2016), even though we did not detect it. It is known that internalized β-catenin is translocated to the nucleus, where it regulates the expression of pro-metastatic genes, among other genes (Wijnhoven et al., 2000). This mechanism potentially promoted by C3G silencing needs to be further studied in GBM cells.

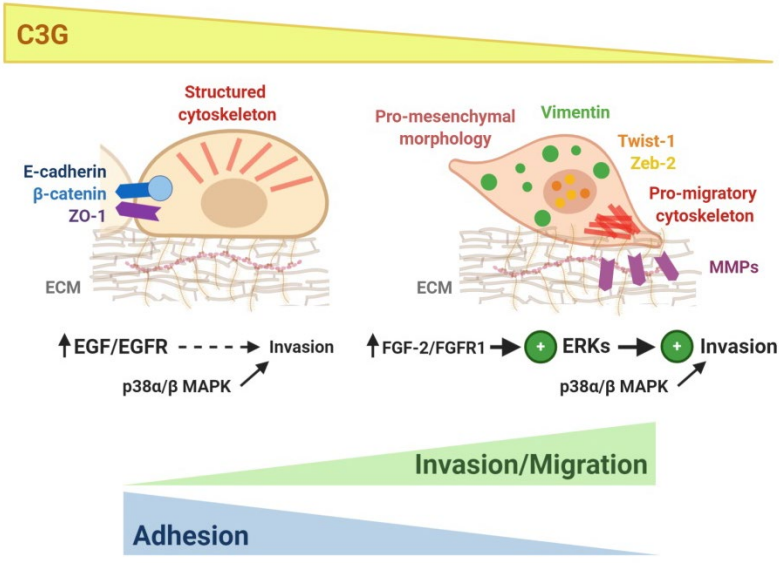

Figure D1 – C3G downregulation in GBM cells induces functional and molecular changes associated to a pro-mesenchymal phenotype. According to our data, C3G silencing/depletion promotes invasion and migration, while decreases adhesion. These functional changes are accompanied by molecular alterations, such as cytoskeleton reorganization, Vimentin upregulation, MMP-2 overactivation and increased *TWIST1* and *ZEB2* mRNA levels, among others. EGF/EGFR signalling is defective in C3G-silenced GBM cells, but FGF-2/FGFR1-dependent ERKs overactivation likely contributes to enhance invasiveness upon C3G knockdown. p38α/β promotes invasion in GBM cells, independently of C3G levels. *ECM: Extracellular matrix; MMP: matrix metalloproteinase.*

In GBM cells with C3G downregulation, the enhanced migration/invasion might be a consequence of an EMT-like process that promotes the acquisition of a more mesenchymal phenotype. This is supported by increased Vimentin levels, MMP2 activity, and *TWIST1* and *ZEB2* mRNA levels and accompanied by actin reorganization. A similar effect is patent in coloncarcinoma cells, in which C3G silencing also induced actin cytoskeleton reorganization, MMP-2 hyperactivation, E-cadherin down-regulation and ZO-1 internalization (Priego et al., 2016). Nevertheless,

the role of EMT in GBM is controversial due to brain plasticity, its non-epithelial characteristics, similarities with astrogliosis and the pro-mesenchymal profile of most GBMs (Tso et al., 2006) (Iser et al., 2017). Despite this, it is accepted that GBM cells can acquire a more mesenchymal phenotype with increased Vimentin levels, associated to invasiveness and poor prognosis (Lin et al., 2016) (Zhao et al., 2018) (Nowicki et al., 2019). This suggests that C3G expression could be used in clinic as a prognosis marker. Moreover, in GBM, changes specifically associated to ‘‘glial to mesenchymal transition’’ (Mahabir et al., 2013) (Matias et al., 2017) (C. Chen & Wang, 2019) or ‘‘proneural to mesenchymal transition’’ (Fedele et al., 2019) have been described, too. As we will discuss in following sections, we could discard that C3G silencing promotes a ‘‘glial to mesenchymal transition’’, while a ‘‘proneural to mesenchymal transition’’ might potentially explain the observed changes in a wider manner.

C3G is a GEF for several G proteins from Ras superfamily, mainly Rap1, but it can also act through GEF–independent mechanisms (Guerrero et al., 1998) (Shivakrupa et al., 2003) (Guerrero et al., 2004) (Gutiérrez-Uzquiza et al., 2010). The role of Rap proteins in GBM is unclear, being different family members associated to diverse, even opposite, functions. For example, Rap1 would control cell death, proliferation and invasion (Moon et al., 2012) (Barrett et al., 2014) (Sayyah et al., 2014), while Rap2A appears to inhibit migration and invasion (Lei Wang et al., 2014). Rap activity is controlled by GEFs and GAPs. Epac2, one of the most predominant RapGEFs in brain, has been recently proposed as a negative regulator of gliomas invasion and MMP-2 activity (Jiang et al., 2019), similarly to that observed for C3G. This suggests that Rap regulators might play a relevant role in GBM through its GEF activity, additionally suggesting that C3G and Epac2 could collaborate to inhibit GBM dissemination acting through Rap. Using complementary strategies based on overexpression of full length C3G (C3G-FL), a C3G mutant lacking CDC25H catalytic region (C3G-ΔCat) (Guerrero et al., 1998) or Rap1A (wildtype or V12 mutant), we have studied the potential contribution of GEF activity of C3G to the regulation of invasion and adhesion. Overexpression of C3G-FL, but not C3G-ΔCat, decreases invasion in U87 cells, suggesting that its GEF activity would be necessary to negatively control invasion. In agreement with this, the overexpression of the constitutively active Rap1A mutant, Rap1AV12, decreases C3G silencing-induced invasiveness, although it has no effect in non-silenced cells. Therefore, the role of C3G as an inhibitor of invasiveness in GBM cells might be dependent on its GEF activity, being Rap1A a potential mediator. However, this remains to be further characterized, since published studies indicate that Rap1 mediates PDGF-induced invasion in GBM via DOCK1 regulation (Barrett et al., 2014) and other small G proteins from Ras superfamily could contribute to mediate C3G effects, too.

In contrast, regulation of adhesion by C3G appears to be independent of its GEF activity in GBM, based on the increased adhesiveness induced by both C3G-FL and C3G-ΔCat overexpression in non-silenced U87 cells. This is in agreement with the lack of effect of either Rap1Awt or Rap1AV12 overexpression on adhesion at 1h. However, the increased adhesion observed at 15min in U87shC3G cells upon Rap1AV12 overexpression is not consistent with these results. Therefore, new complementary studies are required to fully understand whether C3G-induced adhesion of GBM cells is GEF-dependent or independent, and, in case it is GEF-dependent, which small G proteins are the mediators.

As previously mentioned, p38α plays a dual role in cancer, having a pro-migratory/invasive effect (Arechederra et al., 2015) (Priego et al., 2016). In coloncarcinoma cells and in MEFs, C3G downregulation leads to p38α MAPK hyperactivation, which is responsible for the enhanced migration and invasion (Priego et al., 2016). C3G also decreases p38α MAPK activation in other cell types and contexts both under non-pathological (Gutiérrez-Uzquiza et al., 2010) and pathological conditions (e. g. in CML (Maia et al., 2009) (Maia et al., 2013)). However, according to our results, C3G does not play a homogeneous activating or inhibiting effect on p38 MAPK activity in all GBM cell lines used. In C3G-silenced U87 cells, a slight downregulation of p-p38 MAPK levels is produced (*Figure 27A*) in response to serum or EGF stimulation. In contrast, in 12Φ12D cells, serum-induced p38 phosphorylation increases upon C3G downregulation. Independently of the regulation of p38 by C3G, p38α/β MAPK inhibition with SB203580 impairs invasion and enhances adhesion in U87 cells in both non-silenced and C3G-silenced cells. This is in agreement with previous studies indicating that p38α upregulation in GBM correlates with dissemination and bad prognosis (Demuth et al., 2007). Therefore, further studies are required to understand C3G-mediated p38 regulation in this tumour and its potential relationship with specific molecular alterations of GBM cells.

3. C3G differentially regulates receptor tyrosine-kinases signalling in glioblastoma, conditioning ERKs activation and invasiveness

RTKs are essential signalling hubs controlling cancer onset and progression, as well as widely-studied therapeutic targets (Lemmon & Schlessinger, 2010). In almost 90% GBMs, RTKs and their downstream pathways are altered, being EGFR the most predominantly altered, followed by PDGFRα, ErbB2, Met and FGFR1 (TCGA, 2008).

Unfortunately, the prognostic value of EGFR in GBM depends on patient age or the mutational pattern of the tumour (Zahonero & Sánchez-Gómez, 2014). C3G is known to participate in the regulation of different RTKs such as EGFR (Okada & Pessin, 1997) (Lu et al., 2000) (Kao et al., 2001) (Wu et al., 2001), Met (Sakkab et al., 2000) (Sequera et al., 2020), FGFR (Lu et al., 2000), or Alk (Schönherr et al., 2010). In most of them, C3G acts as a Crk-interacting protein that connects RTKs with small GTPases activation and other downstream signalling proteins.

Our data point out that C3G downregulation induces ERKs hyperactivation in U87 and 12Φ12D cells and ERKs inhibition with PD98059 decreases C3G silencing-associated invasiveness. Similarly, C3G-mediated ERKs down-regulation was previously described in different tumours (Carmen Guerrero et al., 2004) (Martín-Encabo et al., 2007) (Maia et al., 2009) (Priego et al., 2016). However, further studies are necessary to characterize this regulatory relationship between C3G and ERKs in GBM. By itself, this C3G/ERKs regulation in GBMs is already interesting, but interpreted together with the results related to RTKs regulation, will become even more powerful.

Our data unveil a novel function of C3G controlling the signalling elicited by RTKs, which represent the most commonly altered molecules in GBMs (TCGA, 2008). According to the presented results, C3G acts as a key mediator of EGFR signalling in GBM. C3G down-regulation in GBM cells reduces the amount of EGFR at the cell surface. This reflects defects in receptor recycling which would explain the defecits in EGFR signalling and in its pro-invasive effect. This may represent an opposite phenotype of that found in GBM cells expressing EGFRvv, an internalization-deficient EGFR truncated form (Zahonero & Sánchez-Gómez, 2014). However, the precise mechanisms involved in C3G-mediated proper EGFR recycling and membrane localization need to be characterized in detail. C3G controls exocytosis of angiogenic factors in platelets and interacts with VAMP7 (Martín-Granado et al., 2017), which is involved in the secretory pathway that regulates EGFR localization in membrane microdomains, endocytosis and signalling (Danglot et al., 2010). Multiple SNAREs, alone or in collaboration with others, also control cell trafficking in general and, particularly, EGFR transport to membrane (Williams & Coppolino, 2014). Consequently, C3G might favour EGFR membrane localization and recycling, acting through VAMP proteins. However, other mechanisms might contribute to the defective EGF/EGFR signalling, such as the reduced formation of EGFR-Crk-C3G complexes (Kao et al., 2001) or the regulation of actin cytoskeleton and/or microtubules organization (van Bergen en Henegouwen et al., 1992).

As indicated in Figure D1, we show here that EGF-induced invasion is higher in the presence of C3G (*Figure 32B*), in agreement with a correct activation of

EGF/EGFR pathway. However, in invasion assays using serum as chemoattractant, GBM cells with low levels of C3G showed an enhanced invasiveness and migration (*Figures 10A-C, 11 and 12*). Therefore, other signals and receptors might be responsible for this increased motility.

According to the results derived from the anti-phospho-RTKs array, an increased phosphorylation of several, but not all RTKs, was observed in C3G-silenced GBM cells. This indicates that C3G seems to differentially regulate signals mediated by distinct RTKs, being likely that some of these RTKs might contribute to increase invasion in C3G-silenced GBM cells. For example, we observed a strong upregulation of FGFR1 phosphorylation, a relevant RTK in GBM (Watcharin Loilome, 2009) (Shirakihara et al., 2011) (Jimenez-Pascual & Siebzehnrubl, 2019). In addition, FGF-2 treatment induced a stronger pro-invasive effect on C3G-silenced GBM cells and the enhanced invasiveness of these cells when using serum as chemoattractant is impaired by Infigratinib, a FGFR inhibitor acting predominantly over FGFR1. This is in agreement with FGFR1-induced expression of EMT-associated genes in GBM (Gouazé-Andersson et al., 2018). Moreover, in C3G-silenced U87 cells, FGF-2 promotes ERKs overactivation and the FGF-2/FGFR1/ERKs axis seems to be responsible for C3G knock-down-associated enhanced invasiveness (as shown in *Figure D1*), as ERKs or FGFR1 inhibition prevents this effect.

Our data also revealed increased phosphorylation of ErbB2, Tie-1/2 and several Eph family members (e.g. EphA6, EphB1, EphB2 or EphB4) upon C3G silencing. EphB2 has been linked to migration and invasion of GBM and GSCs (Nakada et al., 2004) (Wang et al., 2012), and ErbB2 facilitates migration and contributes to anti-EGFR resistance (Wang et al., 2013). Interestingly, EphB4 activation favours FGFR signalling in GBM (Jimenez-Pascual & Siebzehnrubl, 2019). Tie-1/2 phosphorylation is also upregulated in C3G-silenced GBM cells, which suggests that C3G down-regulation might facilitate a pro-endothelial transdifferentiation. GBM cells are able to transdifferentiate into endothelial-like and pericyte-like cells to support tumour-associated vasculature (Liebelt et al., 2016) (Gargini et al., 2019). In fact, some GSC subpopulations express endothelial markers (e.g. Tie2) and they can form tubular networks under endothelial culture conditions (Liebelt et al., 2016). Interestingly, GBMs with EGFR alterations can undergo an EMT-like process, by which they acquire a pericyte-like phenotype, promoting angiogenesis and tumour growth (Gargini et al., 2019). This transdifferentiation has also been linked to therapy resistance (Soda et al., 2011) (Deshors et al., 2019).

Moreover, we detected lower phosphorylation levels upon C3G silencing, not only for EGFR, but also for FGFR3, MCSFR, cRet, ROR1, MusK or DDR1/2. Further studies should be performed to study the relevance of the downregulation of all these

RTKs in GBM onset and/or progression. Importantly, not all analysed RTKs present changes in their activation status based on C3G levels. ErbB4, FGFR4, Alk or RYK did not vary. Taking into account the relevance of MDK/Alk axis in GBM and GSCs (López-Valero et al., 2020) and that C3G regulates Alk in neuroblastoma cells (Schönherr et al., 2010), we have confirmed this result from a functional point of view. Validating the anti-phospho-RTK array result, MDK treatment induced invasion to a similar extent in both parental and C3G-silenced U87 cells. In spite of that, we cannot discard that MDK/Alk axis may be affected by C3G levels in other GBM cell contexts, such as GSCs.

C3G-dependent RTK signalling plasticity may be relevant for anti-EGFR therapy (e.g. erlotinib) resistance (TCGA, 2008) (J. R. D. Pearson & Regad, 2017). For example, cancer cells with impaired EGFR signalling or resistant to anti-EGFR treatment switch to a tumour-specific FGFR (Izumchenko et al., 2014) or ErbB2 (Berezowska et al., 2010) (Clark et al., 2012) upregulation, similarly to that observed in C3G-silenced GBM cells. Treatment approaches based on inhibitors cocktails acting against several RTKs decrease tumour resistance, although they are difficult to implement in clinic. For example, combination of anti-EGFR therapy plus Met inhibitors does not impair resistance in GBM patients due to FGFR autocrine activation, which maintains ERKs upregulation in the absence of EGFR or Met signalling (Day et al., 2020). This partially resembles that observed in C3G-silenced U87 cells. According to *Day et al. (2020)*, Sprouty-2 may be responsible for GBM resistance upon co-treatment with EGFR and Met inhibitors. Interestingly, GBM patients' TCGA data processed by UCSC Xena online software (*UCSC Xena webpage*, 2020) show an inverse correlation between *RAPGEF1* and *SPRY2* (encoding Sprouty-2) mRNA levels. This raises the possibility that Sprouty-2 could be involved in the C3G-dependent regulation of EGFR trafficking and signalling, although other mechanisms might contribute, too.

Even though the role of C3G in RTKs regulation should be further characterized, C3G might be useful to discriminate GBM patients susceptible to respond to specific RTK inhibition protocols. Hence, GBM patients with a low C3G expression might not respond to anti-EGFR therapies, while other inhibitors (e.g. FGFR1 inhibitors) may display higher efficacy in these tumours.

4. C3G down-regulation alters the tumourigenic properties of glioblastoma cells

According to our results (summarized in *Figure D2*), C3G-silenced GBM U87 and 12Φ12D cells form bigger tumors in xenograft and CAM assays, even though proliferation is decreased both *in vitro* and *in vivo*. This correlates with the higher number of foci with less cells/focus formed by C3G knock-down GBM cells in anchorage-dependent and -independent growth assays (*Figures 21 and 22*). Therefore, this lower cell density might be caused by the loss of cell-cell interactions and the higher mobility of GBM cells upon C3G down-regulation, which would lead to increased number of foci and larger tumours. Hence, lower C3G levels would favour cell escape from primary focus, dispersion and potential generation of secondary foci *in vitro*. A similar behaviour is expected to occur *in vivo* to explain why tumours present a higher size. Similarly, *Hoang-Minh et al. (2018)* described that slow-cycling GBM cells show a higher infiltration into brain parenchyma than fast-cycling GBM cells, which generate non-infiltrated tumour masses.

Moreover, tumours originated by C3G-silenced cells in CAM assays present higher levels of α-SMA and MECA32, pointing to an enrichment in stroma and blood vessels, most likely by infiltration of host-niche cells. Previous studies indicate that C3G overexpression in platelets promotes secretion of pro-angiogenic factors (Martín-Granado et al., 2017), although it remains unknown if C3G does so in tumour and/or stromal cells in GBM context. Results obtained in GBM tumours support its potential relevance and it should be further studied. Independently of the mechanism, C3G silencing enhanced stroma infiltration and angiogenesis, likely contributing to increase the size of tumours. This, in addition to the increased disseminative capacity of GBM cells with lower levels of C3G, indicates that C3G downregulation would be globally linked to a higher aggressiveness (Agarwal et al., 2016) (Velásquez et al., 2019).

The generation of larger GBM tumours upon C3G downregulation is surprising when compared to coloncarcinoma (Priego et al., 2016) and HCC (Sequera et al., 2020). In both cases, C3G downregulation reduces *in vivo* tumour size, although C3G silencing reduces cell density within foci in a similar way than in GBM. The latest is explained by the fact that C3G promotes proliferation in GBM, coloncarcinoma and HCC tumors (Sequera et al., 2020) (Priego et al., 2016). Moreover, in HCC cells, C3G silencing leads to an increased number of foci in *in vitro* anchorage-independent growth assays, even though *in vivo* and *in vitro* proliferation is reduced (Sequera et al., 2020). All this resembles the results obtained in GBM.

Although *in vivo* heterotopic xenograft and CAM assays properly reproduce GBM onset and growth (Hagedorn, 2005) (López-Valero et al., 2018) (López-Valero et al., 2020), the effect of brain tumour microenvironment requires additional complementary assays. Taken into account its relevance (Bi et al., 2020) (Klemm et al., 2020), the function of C3G in GBM should be further characterized by *in vivo* orthotopic xenograft assays. These experiments would also allow us to evaluate the effect of GBM cells with or without C3G silencing on the functionality of CNS in mice (e.g. motor and/or behavioural tests depending on inoculation area), as well as their survival. These results would help to further characterize the role of C3G in GBM.

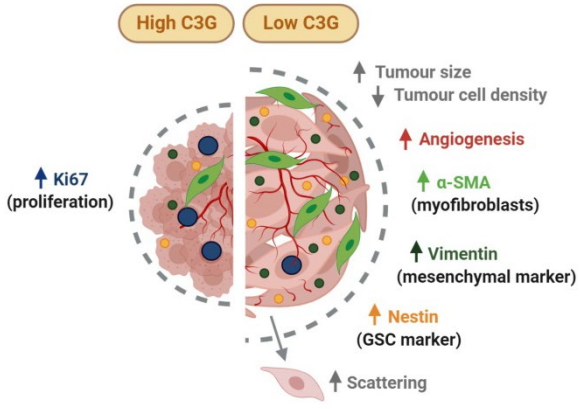

Figure D2 – C3G downregulation increases foci formation in *in vitro* assays and tumour size in *in vivo* assays, although tumour cell density and proliferation are decreased. C3G silencing increases foci formation and tumour size accompanied by lower proliferation (denoted by Ki67 staining). The increased scattering, decreased cell-cell contacts and increased stromal infiltration and angiogenesis would contribute to tumour enlargement. Hence, tumours formed by C3G-silenced cells present higher presence of myofibroblasts (α-SMA+ stromal cells) and blood vessels (MECA32+ cells). Low levels of C3G in GBM also correlate with prompted GSC-like phenotype (e.g. increased Nestin staining). GSC-like phenotype (e.g. increased Nestin staining). *α-SMA: α-smooth muscle actin; GSC: glioblastoma stem cell.*

Differently from U87 and 12Φ12D cells, C3G silencing in HCO1D cells does not increase foci formation, although it promotes the appearance of solitary cells and small colonies that cannot be quantified as foci according to our criteria. This supports the idea that cell scattering plays a key role in foci formation upon C3G silencing, leading to foci with a decreased cell density, as it occurs in all cases: GBM (U87, 12Φ12D and HCO1D), coloncarcinoma (Priego et al., 2016) and HCC cells (Sequera et al., 2020). In HCO1DshC3G cells, the reduction in the number of cells within the foci would be extreme. Primary genetic alterations of HCO1D (e.g. mutations in RTKs, p53 or pRb) could also alter foci formation capacity as compared to U87 and 12Φ12D cells. On the other hand, we cannot discard that the low number of foci formed by HCO1DshC3G cells could be a consequence of non-optimal experimental conditions for these cells, such as insufficient time. Moreover, it is pending the analysis of the effect of C3G silencing on its tumorigenic potential using *in vivo* models.

It is important to mention that the effect of C3G silencing resembles the pro-invasive action of c-Abl down-regulation or inhibition, but not its *in vitro* and *in vivo* anti-tumourigenic effect (Lamballe et al., 2016). However, both c-Abl and C3G downregulation decrease proliferation of GBM cells. These distinct effects of both signalling molecules could reflect the differential impact of c-Abl *vs*. C3G on the expression and/or activity of individual RTKs.

Mechanistically, the hyperactivation of ERKs induced by C3G downregulation in GBM cells would be responsible for the increased foci formation capacity, as demonstrated by the impaired foci formation upon treatment of U87shC3G cells with PD98059. However, ERKs inhibition only decreases proliferation in parental U87 cells, but not in U87shC3G cells. ERKs are usually involved in proliferation, although they can also mediate other cellular functions depending on the magnitude and duration of its activation, and its sub-cellular localization. Hence, ERKs can induce survival, invasiveness or differentiation, among others. For example, in neural precursors, ERKs are activated by EGF in a transient manner, promoting proliferation, while NGF-induced sustained ERKs activation leads to differentiation (Lu et al., 2000) (Kao et al., 2001). In GBM, there are data indicating that ERKs activation is slightly higher in peripheral areas, which suggests that it is mediating tumour dissemination and invasion (Lama et al., 2007). This idea is also supported by the data presented here, showing that ERKs inhibition decreases invasiveness of U87shC3G cells. In addition, our results indicate that foci formation is also impaired by ERKs inhibition, while proliferation remains unaltered. These data support the idea that the enhanced cell scattering would be responsible for the formation of new secondary foci by C3G-silenced GBM cells.

5. C3G downregulation favours the acquisition of glioblastoma stem cell-like properties

GSCs (*glioblastoma stem cells*) are defined as a small subpopulation of cancer cells with glioblastoma-initiating, stem and auto-renewal capacities (Liebelt et al., 2016). They also express neural and stem-associated markers and they can differentiate into non-stem tumour cells or stromal cells, such as endothelial-like and pericyte-like cells (Liebelt et al., 2016). Due to all this, they are directly responsible for therapy inefficiency and resistance, as well as for tumour relapse in apparently cured patients (J. Chen et al., 2012) (Palanichamy et al., 2018). These cells survive anti-GBM treatments due to their low proliferative capacity and their high plasticity, which allows a rapid switching of different signalling pathways (e.g. Notch, BMPs or RTKs

as EGFR, FGFR, Alk or Eph) to better adapt to the microenvironment conditions (Liebelt et al., 2016).

Taking into account the effects of C3G downregulation on GBM dissemination and growth, as well as the pro-mesenchymal and slow-cycling phenotype of these cells, we could expect that reduced C3G levels would facilitate the acquisition of a GSC-like phenotype. Our results revealed that C3G silencing in U87 cells increases the formation of spheres in cell cultures promoting a GSC-like phenotype and enhances self-renewal capacity according to ELDAs assays. These ELDAs assays better reproduce the conditions to evaluate stemness and auto-renewal capacity, because cells are isolated and only the absence or presence of spheres is quantified. Therefore, C3G down-regulation might induce stemness in GBM cells associated to a pro-mesenchymal phenotype. This relationship between EMT-like processes and the acquisition of a GSC phenotype by GBM cells has been previously observed (Mikheeva et al., 2010) (Siebzehnrubl et al., 2013) (Caja et al., 2018) (Kowalski-Chauvel et al., 2019), although it cannot be considered universal (Lamballe et al., 2016). Further experiments are necessary to establish the molecular mechanisms underlying the acquisition of both pro-mesenchymal and pro-GSC phenotypes upon C3G silencing. For example, C3G-mediated regulation of β-catenin or RTKs, among others, may be involved, modifying the expression of transcription factors regulating both processes.

Upon C3G silencing, we observed in CAM-derived tumours increased levels of Nestin (GSC marker), accompanied by the NeuN (neural marker) downregulation. This also indicates that C3G-silenced cells present an enhanced undifferentiated phenotype. High levels of Nestin are usually associated to classical GBM molecular subtype, which is also linked to C3G downregulation, as previously described. However, U87shC3G-derived tumours also present higher levels of GFAP (astrocytic marker), suggesting that this GSC-like phenotype may be partial. Nevertheless, this upregulation of GFAP upon C3G silencing in GBM should not be surprising. As seen in *Figure 3* and previously discussed, C3G downregulation in GBM is linked to classical and mesenchymal molecular subtypes which are enriched in astrocytic and astro-glial markers, respectively (Verhaak et al., 2010). Moreover, this strong inverse correlation between GFAP and C3G in CAM-derived tumours (*Figure 41B*) also agrees with previous results indicating that GBM cell lines with low C3G levels (U87, U251 and A172) present higher levels of GFAP (*Figure 4*). Additionally, NeuN downregulation accompanied by GFAP upregulation upon C3G silencing also agrees with the tendencies observed in healthy brain by *Sriram et al. (2020)*. Therefore, the role of C3G controlling neural precursors and GSCs, as well as their differentiation lineages, could share common mechanisms that need to be further characterized. It

would be also important to determine why C3G downregulation is unable to induce a fully GSC-like phenotype in GBM.

Partial GSC-like phenotypes have been previously observed in GBM. For example, some GSC populations have the capacity to differentiate into endothelial-like cells (Liebelt et al., 2016), particularly those presenting EGFR impairment (Gargini et al., 2019). As explained, C3G downregulation in GBM cells attenuates EGFR signalling, promotes a GSC-like phenotype and upregulates Tie-1/2 activation. Taking all this into account, U87shC3G cells might have the capacity to form tubular vessel networks under endothelial culture conditions, but it needs to be analysed.

Although all these results about the role played by C3G in the regulation of the GSC-like phenotype are promising, they are still very preliminary. Other GSC-associated markers and signalling pathways should be evaluated in GBM cells and CAM-derived tumours. Based on the different regulation of EGFR and FGFR1 by C3G and taking into account that they promote GSC-like growth, it would be interesting to test whether C3G-induced RTK regulation contributes to the acquisition of a GSC-like phenotype. Furthermore, the results derived from GBM studies show the opportunity of analysing the effect of C3G in CSCs from other cancers in which C3G is already known to regulate several processes (e.g. coloncarcinoma or HCC) and other non-tumour stem-like populations.

6. C3G silencing promotes a metabolism reprogramming in glioblastoma cells, increasing their glycolytic capacity

The proteome-wide analysis performed using parental and C3G knock-down U87 cells confirmed C3G functions previously described in GBM or other cell types, but it also uncovered novel roles. Although these data should be experimentally confirmed, the results are interesting. We have identified 70 proteins upregulated by C3G silencing and 46 in parental cells, being related to actin and glycolysis those reaching the highest scores (*Appendix 8*). Surprisingly, Crk seems to be upregulated in cells presenting low levels of C3G, but only one peptide has been detected and it remains undetermined if this overrepresentation of Crk is playing any role in C3G-silenced GBM cells. Moreover, NFH protein (main component of neurofilaments in neurons) is increased in non-silenced U87 cells, in agreement with its more pro-neural phenotype as compared to C3G silenced cells. Additionally, the translation initiation factors, eIF4H and eIF3G, are upregulated in parental cells. In CML, another translation initiation factor, eIF3b, increases C3G levels and promotes proliferation (Huang et al., 2020). eIF3b might be acting through C3G since p87C3G is associated to CML

progression, too (Gutiérrez-Berzal et al., 2006). As eIF3b is also overexpressed in GBM and its knock-down inhibits proliferation (Liang et al., 2012), it may play a similar role in this tumour. Similarly, based on the correlation between eIF4H and eIF3G and C3G protein levels in GBM cells, they can have an analogous function to that of eIF3b in CML.

In addition to the above results, we have performed GO terms analyses to identify additional pathways altered upon C3G silencing. It is important to highlight that GO terms analyses point to the regulation of proteins and functions previously studied, supporting our results. For example, the Reactome analysis from *Cancertool* software showed the enrichment in FGFR signalling-related GO terms (e.g. ‘‘FGFR2 ligand binding and activation’’ and ‘‘FGFR3b ligand binding and activation’’) in C3G-silenced cells. In addition, GOCC analysis from *Cancertool* software indicates an enrichment of ‘‘Vesicle’’ GO terms in C3G-silenced GBM cells, which could be linked to the altered EGFR recycling, being also in agreement with previous data from platelets (Martín-Granado et al., 2017). Moreover, the enrichment in ‘‘Extracellular vesicular exosome’’ and ‘‘Extracellular organelle’’ could be also related to the role of C3G regulating secretion, as observed in platelets (Martín-Granado et al., 2017). However, not all uncovered functions for C3G in GBM are represented in these GO terms. This could be due to the culture conditions chosen or the extraction method employed.

The proteome-wide analysis uncovered a novel role of C3G as a regulator of the metabolism of GBM cells. Almost all software and analyses carried out (*Figures 42-44*) point to a regulation of GBM metabolism by C3G, being glycolysis the main pathway affected. Then, this has been confirmed by different techniques: RT-qPCR, enzymatic activity evaluation and immunofluorescence staining of CAM-derived tumours, which have also allowed determining the impact of C3G silencing on anaerobic glycolysis in GBM (data are summarized in *Figure D3*).

Our results indicate that C3G silencing mainly regulates the final steps of glycolysis, while glucose uptake and HK activity remain unaltered. Aldolase is the first glycolytic enzyme upregulated in C3G-silenced U87 cells, but we have also detected increased expression and/or activity of GAPDH, PGK-1, enolase, PK, LDH and MCTs, in parallel with an increased lactate production and release. In addition, mRNA levels of some components of mitochondrial SDH and PDH complexes are decreased, being *PDK1* expression upregulated. Altogether, these findings indicate that C3G silencing favours glucose catabolism through increasing anaerobic glycolysis, which resembles the Warburg effect, widely associated to cancer (Vander Heiden et al., 2009) (Tennant et al., 2009) (Liberti & Locasale, 2016). However, the effect of C3G regulation on the mitochondria and the respiratory chain activity needs

to be characterized, as well as the mechanisms operating and their impact on *in vivo* GBM tumour growth.

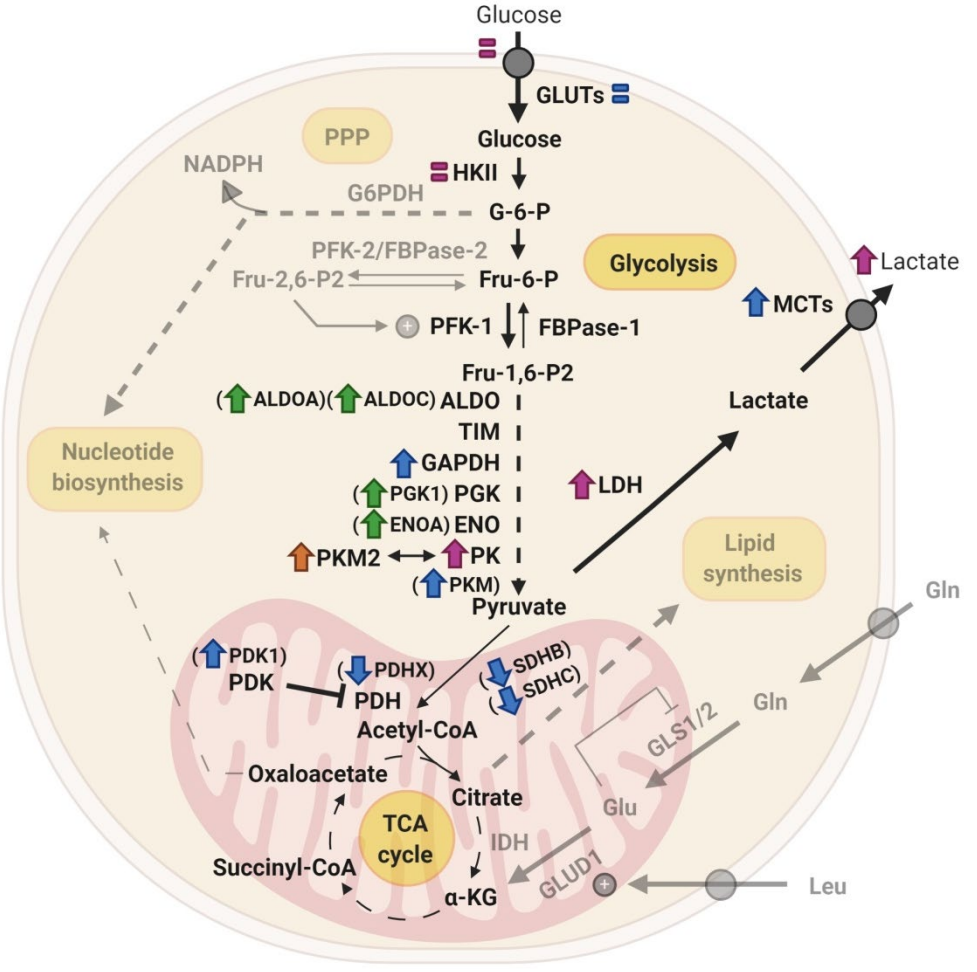

Figure D3 – C3G downregulation promotes a metabolic switching in GBM cells, characterized by the upregulation of the final steps of anaerobic glycolysis, resembling Warburg effect. This scheme is based on data from the proteome-wide screening (green arrows), RT-qPCR (blue arrows), enzymatic activity and uptake/release assays (purple arrows), and protein staining in CAM-derived tumours (orange arrow). *"↑" symbol indicates positive regulation and "↓" symbol indicates negative regulation, in C3G-silenced compared to parental cells; "=" symbol indicates lack of changes. ALDO: Aldolase; ENO: Enolase; G: Glucose; Fru: fructose; P: phosphate; TCA: tricarboxylic acids; α-KG:α-ketoglutarate.*

It is important to mention that although the changes in the enzymatic activity of LDH and PK induced by C3G silencing are not very high, they look meaningful. LDH activity is increased in non-silenced cells upon azide treatment, an inhibitor of mitochondrial respiration (Bolaños, 2016), in a similar extent to that observed in C3G-

silenced cells. This suggests that mitochondrial activity is decreased upon C3G knock-down, favouring LDH activation. However, these data should be confirmed under other experimental conditions and by complementary techniques.

PDH complex is considered the gatekeeper of TCA cycle (Burns & Manda, 2017) and PDK inhibits PDH function. Thus, the decrease in the levels of *PDHX* mRNA levels induced by C3G knock-down, together with the *PDK1* transcriptional upregulation may lead to a reduced PDH and TCA activity as it occurs in other tumours under conditions that enhance Warburg effect (Michelakis et al., 2010) (Woolbright et al., 2019) (Commander et al., 2020).

PKM2 levels are increased in CAM-derived tumours generated by C3G-silenced cells. Importantly, PKM2 dimers and tetramers differ in their pro-glycolytic or pro-oxidative function. PKM2 dimers are considered less glycolytic and they can play non-glycolytic functions in the nucleus. However, in the presence of fructose-1,6-bifosfato, the allosteric activator of PKM2, tetramers are formed increasing glycolysis (Dayton et al., 2016) (Kowalik et al., 2017) (Zahra et al., 2020).Taking into account that several GO terms indicate that fructose-1,6-bifosfato metabolism is enhanced in C3G-silenced cells, we can hypothesize that C3G downregulation might facilitate the existence of the tetrameric PKM2 form, increasing PK activity and contributing to glycolysis.

The increased lactate release in C3G-silenced cells might contribute to favour the infiltration of stromal cells into the tumours, in agreement with the increase presence of MECA-32 and α-SMA positive cells in CAM-derived tumours (*Figure 26*). It has been widely demonstrated that microenvironment acidification due to the increased release of lactate by cancer cells induces changes in the stroma, promoting angiogenesis (De Palma et al., 2017) and immunosuppression, among other effects (Hanahan & Weinberg, 2011) (Bi et al., 2020). Moreover, both, Warburg effect and lactate release, have also been associated to pro-invasive phenotypes and EMT in different cancer types (Commander et al., 2020). For example, in breast and prostate cancer cells, it has been revealed that this switching to glycolytic metabolism is necessary to promote motility and cytoskeleton reorganization (Shiraishi et al., 2014). Additionally, in breast cancer cells, Twist-1 upregulation induces glucose metabolism reprogramming, characterized by increased lactate release, upregulation of glycolytic mediators and decreased mitochondrial mass (Yang et al., 2015). Both studies agree with data presented here, showing that C3G down-regulation enhances invasiveness through the induction of an EMT-like process associated to increased *TWIST1* expression. This correlation between mesenchymal and glycolytic phenotypes might suggest that C3G could reprogram cell metabolism as a secondary or parallel effect of its action on EMT-like processes in GBM. Independently of the mechanism, the

functional consequences of C3G downregulation in GBMs would be the same. However, it needs to be determined whether C3G regulates GSC-like cell metabolism, too.

It is also important to consider the regulatory mechanisms based on cell-cell crosstalk that regulate metabolism specifically in brain. For example, ANLS (*astrocyte to neuron lactate shuttle*) maintains brain homeostasis thanks to the metabolic cooperation between astrocytes, which preferentially use glucose via anaerobic glycolysis, and neurons, which metabolize lactate released by astrocytes via mitochondrial oxidative pathways (Turner & Adamson, 2011). This explains why astrocytes predominantly express LDH-A isoform, GLUT-1 and MCT-1/4 but downregulate mitochondrial mediators, while neurons present higher levels of LDH-B isoform, GLUT-3 and MCT-2 (Bolaños, 2016). Recent studies point to a metabolic crosstalk between GBM subpopulations with different metabolic profiles, mimicking ANLS and other interactions physiologically present in brain (Valvona et al., 2016) (Hoang-Minh et al., 2018) (Bi et al., 2020) (Commander et al., 2020). Regarding this, on the one hand, GBM cells with low levels of C3G present an enhanced mesenchymal phenotype, increased GFAP expression and a glycolytic phenotype characterized by higher LDH activity (associated to low mRNA levels of *LDHB*, the pro-oxidative LDH isoform) and MCT-1/4 expression. On the other hand, GBM cells with higher levels of C3G show a correlation with proneural molecular subtype and present slightly higher levels of NeuN and increased mRNA levels of various components of PDH and SDH complexes. Hence, it would be interesting to determine the potential existence of subpopulations of cells within the GBMs expressing different levels of C3G and whether this subpopulations are able to establish metabolic cooperations to promote tumour progression and dissemination.

According to ANLS, mitochondrial TCA works in astrocytes as a source of intermediates (e.g. glutamate) and, in GBM, multiple metabolic pathways are known to be altered (e.g. IDH mutation, lack of glutaminolysis inhibition or enhanced GLS activity). Thus, the role of C3G in the regulation of these pathways might play a relevant function and it should be further studied.

7. General discussion

In the first part of this study, we have uncovered a downregulation of *RAPGEF1* mRNA levels in GBM tumours from patients and a decrease in C3G protein levels in a panel of human GBM cell lines. Moreover, this *RAPGEF1* downregulation is associated to classical and mesenchymal GBM molecular subtypes, while GBM tumours with higher *RAPGEF1* levels are included in the proneural subtype (Verhaak

et al., 2010). This is also supported by *in vitro* and *in vivo* assays performed with C3G-silenced GBM cells, both standard cell lines (U87) and patient-derived (12Φ12D and HCO1D) cell lines. C3G downregulation enhances invasiveness and a pro-mesenchymal phenotype, while inhibits adhesion of these GBM cells. Moreover, the use of different experimental approaches, as C3G silencing, C3G knock-out by CRISPR/Cas9 technology and transient C3G overexpression, strengthens the results presented here. It is noticeable the role of C3G as a negative regulator of invasiveness of GBM cells, which seems to be a common effect of C3G in several cancer types (Dayma & Radha, 2011) (Priego et al., 2016) (Sequera et al., 2020) and in cells from the nervous system (Voss et al., 2006) (Voss et al., 2008). Although GEF activity of C3G may be involved in the inhibition of invasiveness in GBM cells, a more detailed analysis is necessary to clarify this issue.

We have shown that C3G knock-down induces an EMT-like process in GBM cells responsible for their enhanced migratory capacity, mimicking the features of the ‘‘proneural to mesenchymal transition’’ described by *Fedele et al. (2019)*, in which Zeb-2 plays an essential role. However, the participation of EMT-like processes in GBM dissemination need to be further characterized. Due to the upregulation of astrocytic markers (e.g. GFAP or MTC-1/4) in C3G-silenced cells, we can discard that a ‘‘glial to mesenchymal transition’’ (Mahabir et al., 2013) (Matias et al., 2017) (C. Chen & Wang, 2019) could be taking place. All this should be further studied due to the promising nature of data presented here.

However, the function of C3G in GBM tumourigenesis is more complex. C3G downregulation leads to the generation of bigger tumours even though proliferation is reduced. This differs from other tumours such as coloncarcinoma or HCC, in which C3G downregulation reduces tumour size (Priego et al., 2016) (Sequera et al., 2020). The decreased cell-cell contacts and the increased migratory and invasive capacity of C3G-silenced GBM cells, which favour dispersion, would account for the increased tumour size. In addition, the infiltration of endothelial cells and activated fibroblasts into the tumours would contribute. This could be favoured by the glycolytic phenotype displayed by GBM cells with low levels of C3G. All this should be confirmed under experimental conditions enabling a more physiological context, such as orthotopic xenograft assays.

Results shown also uncover a complex regulation of cell signalling pathways by C3G in GBM cells, where RTKs and ERKs are key players. Although p38 MAPK promotes invasion of GBM cells as described by other authors (Demuth et al., 2007), C3G does not appear to regulate p38 activation in the same way than in other cell types, in which it inhibits p38 activity (Maia et al., 2009) (Gutiérrez-Uzquiza et al., 2010) (Maia et al., 2013) (Priego et al., 2016). Thus, p38 does not mediate the effect

of C3G downregulation on invasion. In contrast, the upregulation of ERKs activity induced by C3G silencing is responsible for the main functional effects of C3G downregulation. Hence, the high ERKs activation mediate migration and invasion of C3G knock-down GBM cells. Moreover, the upregulation of the activation of several RTKs in C3G-silenced cells, such as FGFR1 seems to play a key role in promoting invasion through ERKs activation. This has been demonstrated here for FGF-2/FGFR1 pathway, but other RTKs could have a similar effect contributing to GBM cell dissemination. However, we have also uncovered that C3G regulates other RTKs in a different way. Hence, C3G is required for a full EGFR activation, downstream signalling and functionality in GBM cells. This agrees with previous published data showing the participation of C3G in the signalling elicited by EGFR, among other RTKs, in other cell contexts (Okada & Pessin, 1997) (Lu et al., 2000) (Wu et al., 2001) (Kao et al., 2001). Mechanistically, C3G knock-down impairs EGFR signalling by reducing cell surface EGFR through inhibition of its recycling. This represents a new mechanism used for C3G to regulate EGFR signalling, which might be a more general mechanism involved in the control of the trafficking of other proteins. Further studies are required to clarify the mechanisms by which C3G regulates EGFR recycling and its clinical repercussion, for example, in anti-EGFR therapy resistance. In addition, it would be important to characterize the function of C3G in cell trafficking.

The novel functions of C3G as a negative regulator of stemness and glycolytic metabolism in GBM cells open new perspectives, not only for GBM, but also for other tumours. It is promising the induction of a GSC-like phenotype and self-renewal capacity, as well as the increased glycolytic use of glucose, by C3G downregulation in GBM cells. This last might be also important to establish a crosstalk between tumour cell subpopulations and tumour-microenvironment (Liebelt et al., 2016) (Valvona et al., 2016) (Hoang-Minh et al., 2018) (Bi et al., 2020) (Commander et al., 2020). However, new studies are required to fully understand these roles of C3G and the mechanisms involved.

In conclusion, we have demonstrated for the first time that C3G is downregulated in GBMs, contributing to enhance the disseminative properties of these tumours. Moreover, low levels of C3G also promote the generation of larger tumours even though proliferation is reduced. The enhanced migratory and invasive capacity, accompanied by the infiltration of stromal cells and vessels growth might facilitate tumour enlargement. The promoted glycolytic phenotype induced by C3G downregulation might also favour the increased presence of stromal cells. Furthermore, the defective EGFR signalling might contribute to the resistance to anti-EGFR therapy in patients with low levels of C3G. In contrast, other RTKs and ERKs might represent alternative therapeutic targets in these patients based on the upregulation of their activities. Future studies would allow further characterizing C3G

function in RTKs regulation, which may be also of value for designing novel and personalized therapeutic approaches. In addition, the enhanced GSC-like phenotype induced by C3G downregulation could contribute to generate therapy resistance.

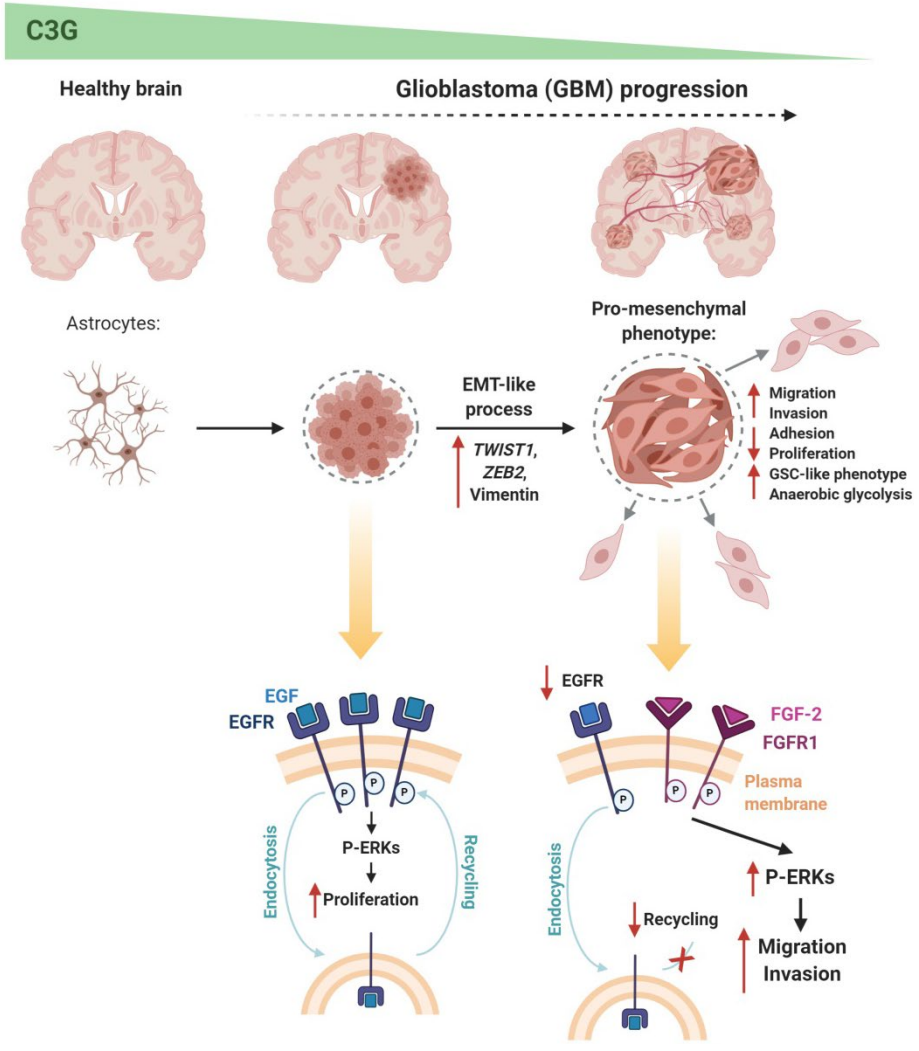

Figure D4 – Graphical abstract showing major discoveries about the function of C3G in glioblastoma. C3G levels are high in healthy brain, decreasing in GBM samples from patients and human cell lines. C3G downregulation promotes foci formation, tumour enlargement and activates cell scattering, while decreases cell density and proliferation. It also increases stromal infiltration and angiogenesis within the tumours, and upregulates GSC-like properties and anaerobic glucose metabolism. C3G knock-down enhances migration/invasion of GBM cells through mechanisms that depend on ERKs overactivation. In particular, FGF-2/FGFR1/ERKs cascade contributes to mediate this enhanced invasion. In contrast, EGFR activity is downregulated in GBM cells with lower levels of C3G, due to its reduced presence at the cell surface as a consequence of EGFR recycling inhibition.

All the above referred effects of C3G downregulation (summarized in *Figure D4*) suggest that C3G levels may be used in clinic. A novel prognostic GBM signature could be generated to evaluate progression and to select an effective therapy, which would include the quantification of C3G and Vimentin levels, ERKs activation and/or the evaluation of the switching from EGFR to FGFR signalling, among others. Nowadays, the use of C3G as a target for GBM treatment remains discouraged.

Conclusions/Conclusiones

1. *RAPGEF1* mRNA levels are decreased in GBM samples from patients compared to healthy brains. Additionally, high *RAPGEF1* mRNA levels correlate with proneural GBM molecular subtype, while low *RAPGEF1* levels are associated to classical and mesenchymal subtypes.
2. C3G protein levels are downregulated in human GBM cell lines compared to human astrocytes, being C3G expression inversely correlated to Vimentin and GFAP protein levels.
3. C3G silencing reduces adhesion, while enhances migration and invasion of U87, 12Φ12D and HCO1D cells, by promoting the acquisition of a pro-mesenchymal phenotype.
4. C3G depletion using CRISPR/Cas9 technology induces a pro-migratory phenotype, decreases adhesion and increases invasion, mimicking the effect observed upon C3G gene silencing.
5. Transient overexpression of C3G favours adhesion and decreases invasion. Its effect on invasiveness is dependent on C3G GEF catalytic domain, CDC25H.
6. Overexpression of the constitutively active Rap1AV12 mutant decreases C3G knock-down- induced invasion, having no major effects on adhesion.
7. In U87 and 12Φ12D GBM cells, C3G silencing promotes *in vitro* foci formation and the generation of larger tumours in *in vivo* heterotopic xenografts and *in ovo* CAM assays. However, foci and tumours generated by C3G-silenced cells present lower cell density and less proliferation.
8. CAM-derived tumours generated by C3G-silenced U87 cells present a higher infiltration of myofibroblasts (identified by α-SMA staining) and blood vessels (identified by MECA32 staining).
9. In HCO1D GBM cells, C3G knock-down decreases foci formation and reduces cell density, generating multiple scattered cells and very small colonies.
10. p38α/β MAPK inhibition with SB203580 promotes adhesion and inhibits invasion through a mechanism not dependent on C3G levels.
11. C3G downregulation induces ERKs hyperactivation in U87 and 12Φ12D cells.
12. C3G silencing-associated high motility is impaired by ERKs inhibition with PD98059 in U87 and 12Φ12D cells.
13. In U87 cells, the higher foci formation induced by C3G silencing is significantly reduced by ERKs inhibition with PD98059, while PD98059 treatment only decreases proliferation in non-silenced cells.
14. C3G knock-down decreases EGFR activation and downstream signalling, as well as EGF-induced invasiveness by impairing EGFR localization at the plasma membrane through inhibition of its recycling.
15. C3G downregulation differentially regulates multiple RTKs, upregulating the phosphorylation of FGFR1 and other RTKs.
16. FGF-2, likely acting through FGFR1, promotes invasion via ERKs upregulation.
17. C3G silencing promotes the acquisition GSC-like properties.

18. C3G knock-down promotes the use of glucose through anaerobic glycolysis by increasing the activity of the last steps of the pathway, including LDH activity and lactate release.

CONCLUDING REMARKS

C3G levels decrease in GBM, the most aggressive tumour of the CNS due to its malignant nature and the lack of effective treatments. This C3G downregulation induces a more mesenchymal phenotype and enhanced invasiveness of GBM cells. Although proliferation is decreased by C3G silencing, it promotes *in vitro* foci formation and *in vivo* tumour enlargement, facilitated by cell scattering. ERKs hyperactivation is responsible for this phenotype. Furthermore, C3G downregulation reduces cell surface EGFR by inhibiting its recycling, leading to attenuated EGFR signalling and functionality. Conversely, the phosphorylation of other RTKs is upregulated upon C3G silencing. The increased activity of FGFR1, likely activated by FGF-2, contributes to enhance invasion of GBM cells with C3G downregulation through a mechanism mediated by ERKs overactivation.

Moving to the clinic, these mechanisms may contribute to define a novel GBM signature associated to tumour progression and dissemination. It would include C3G downregulation associated to Vimentin levels and FGFR1/ERKs activity upregulation, among others. In addition, assessing C3G levels may discriminate, among GBM patients, those likely responding to different RTK inhibition protocols. Hence, GBM patients with tumours presenting low C3G expression might not respond to anti-EGFR therapies.

1. Los niveles del ARNm de *RAPGEF1* están disminuidos en muestras de GBM de pacientes comparado con cerebro sano. Además, mayores niveles de C3G se correlacionan con el subtipo molecular proneural de GBM, mientras que bajos niveles están asociados a los subtipos clásico y mesenquimal.
2. Los niveles proteicos de C3G disminuyen en las líneas celulares humanas de GBM en comparación con los astrocitos humanos, estando la expresión de C3G inversamente relacionada con los niveles proteicos de Vimentina y GFAP.
3. El silenciamiento de C3G reduce la adhesión y aumenta la migración/invasión de células U87, 12Φ12D y HCO1D, promoviendo la adquisición de un fenotipo pro-mesenquimal.
4. La depleción de C3G mediante tecnología CRISPR/Cas9 induce un fenotipo pro-migratorio, disminuye la adhesión y aumenta la invasión, semejante al efecto inducido por silenciamiento génico de C3G.
5. La sobreexpresión transitoria de C3G favorece la adhesión y disminuye la invasión, siendo este último efecto dependiente del dominio catalítico GEF de C3G, CDC25H.
6. La sobreexpresión del mutante constitutivamente activo Rap1AV12 disminuye la invasión inducida por el silenciamiento de C3G, no teniendo efecto sobre la adhesión.
7. El silenciamiento de C3G en las células de GBM U87 y 12Φ12D promueve la formación de focos *in vitro* y la generación de tumores de mayor tamaño *in vivo* en xenotransplantes heterotópicos y en ensayos CAM *in ovo*. Sin embargo, tanto los focos como los tumores generados por las células con silenciamiento de C3G tienen una menor densidad celular y proliferación.
8. Los tumores generados en los ensayos CAM por las células U87 con silenciamiento de C3G presentan una mayor infiltración de miofibroblastos (identificados mediante tinción de α-SMA) y vasos sanguíneos (identificados mediante tinción de MECA32).
9. En las células de GBM HCO1D, el silenciamiento de C3G disminuye la formación de focos y reduce la densidad celular, generando gran cantidad de células dispersas y colonias muy pequeñas.
10. La inhibición de p38α/β MAPK con SB203580 promueve adhesión e inhibe la invasión a través de un mecanismo independiente de C3G.
11. El silenciamiento de C3G induce una hiper-activación de las ERKs en las células U87 y 12Φ12D.
12. La alta motilidad de las células U87 y 12Φ12D asociada al silenciamiento de C3G se reprime al inhibir a las ERKs con PD98059.
13. En las células U87, la alta capacidad de formación de focos inducida por el silenciamiento de C3G se reduce significativamente al inhibir a las ERKs con PD98059, mientras que la proliferación sólo disminuye en células no silenciadas tratadas con PD98059.

14. El silenciamiento de C3G disminuye la activación y señalización del EGFR, así como la invasión inducida por EGF, impidiendo la localización del EGFR en la membrana plasmática mediante la inhibición de su reciclaje.
15. El silenciamiento de C3G regula de manera diferencial la activación de múltiples RTKs, aumentando la activación de FGFR1 y otros RTKs.
16. El FGF-2 actuando probablemente a través de FGFR1 promueve la invasión incrementando la activación de las ERKs.
17. El silenciamiento de C3G promueve la adquisición de propiedades de tipo GSC.
18. El silenciamiento de C3G promueve el uso de glucosa mediante glucolisis anaerobia, incrementando la actividad de sus últimas etapas, incluyendo la actividad de LDH y liberación de lactato.

CONCLUSIONES FINALES

Los niveles de C3G disminuyen en el GBM, considerado el tumor más agresivo del sistema nervioso central por su malignidad y la falta de tratamientos efectivos. Esta disminución de C3G induce un fenotipo más mesenquimal y aumenta la invasividad de las células de GBM. Aunque el silenciamiento de C3G disminuye la proliferación, promueve la formación de focos *in vitro* y el aumento de tamaño de los tumores *in vivo*, ambos facilitados por la alta capacidad de dispersión de estas células. La hiper-activación de las ERKs es responsable de este fenotipo. Además, la disminución de la expresión de C3G también reduce los niveles del EGFR en la superficie celular mediante la inhibición de su reciclaje, dando lugar a una atenuación de la señalización y funcionalidad del EGFR. Por el contrario, la fosforilación de otros RTKs aumenta por efecto del silenciamiento de C3G. El aumento de la actividad del FGFR1, probablemente activado por el FGF-2, contribuye a aumentar la capacidad invasiva de las células de GBM niveles bajos de C3G a través de un mecanismo mediado por la sobre-activación de las ERKs.

Respecto a su relevancia clínica, cabe destacar que estos mecanismos podrían contribuir a definir una nueva firma asociada a la progresión tumoral y diseminación del GBM. Ésta debería incluir la regulación negativa de C3G asociada al incremento de los niveles de Vimentina y el aumento de la actividad de FGFR1/ERKs, entre otros. Además, la determinación de los niveles de C3G en pacientes de GBM podría ayudar a discriminar aquellos con potencial para responder a distintas terapias basadas en la inhibición de RTKs. De esta manera, los pacientes con tumores que presenten baja expresión de C3G, no responderían a tratamientos anti-EGFR.

References

Adrián Martínez-Limón, Manel Joaquin, María Caballero, & and Eulàlia de Nadal. (2020). The p38 Pathway : From Biology to Cancer Therapy. *International Journal of Molecular Sciences*, *21*(1913). https://doi.org/10.3390/ijms21061913

Agarwal, Sane, Oberoi, O. and E. (2016). Delivery of Molecularly Targeted Therapy to Malignant Glioma, a Disease of the Whole Brain. *Expert Rev Mol Med*, *13*.

American Type Culture Collection (ATCC) (glioblastoma cell lines) webpage. (2020). www.atcc.org/~/media/PDFs/Cancer and Normal cell lines tables/Brain cancer and normal cell lines.ashx

American Type Culture Collection (ATCC) (U87MG) webpage. (2020). www.lgcstandards-atcc.org/products/all/HTB-14.aspx?geo_country=es

Arechederra, M., Priego, N., Vázquez-Carballo, A., Sequera, C., Gutiérrez-Uzquiza, Á., Cerezo-Guisado, M. I., Ortiz-Rivero, S., Roncero, C., Cuenda, A., Guerrero, C., & Porras, A. (2015). p38 MAPK down-regulates fibulin 3 expression through methylation of gene regulatory sequences: Role in migration and invasion. *Journal of Biological Chemistry*, *290*(7), 4383–4397. https://doi.org/10.1074/jbc.M114.582239

Arévalo, J. C., Pereira, D. B., Yano, H., Teng, K. K., & Chao, M. V. (2006). Identification of a switch in neurotrophin signaling by selective tyrosine phosphorylation. *Journal of Biological Chemistry*, *281*(2), 1001–1007. https://doi.org/10.1074/jbc.M504163200

Asuri, S., Yan, J., Paranavitana, N. C., & Quilliam, L. A. (2008). E-cadherin dis-engagement activates the Rap1 GTPase. *Journal of Cellular Biochemistry*, *105*(4), 1027–1037. https://doi.org/10.1002/jcb.21902

Augsten, M., Pusch, R., Biskup, C., Rennert, K., Wittig, U., Beyer, K., Blume, A., Wetzker, R., Friedrich, K., & Rubio, I. (2006). Live-cell imaging of endogenous Ras-GTP illustrates predominant Ras activation at the plasma membrane. *EMBO Reports*, *7*(1), 46–51. https://doi.org/10.1038/sj.embor.7400560

Bailey, C. L., Kelly, P., & Casey, P. J. (2009). Activation of Rap1 promotes prostate cancer metastasis. *Cancer Research*, *69*(12), 4962–4968. https://doi.org/10.1158/0008-5472.CAN-08-4269

Balbín, M., Fueyo, A., Tester, A. M., Pendás, A. M., Pitiot, A. S., Astudillo, A., Overall, C. M., Shapiro, S. D., & López-Otín, C. (2003). Loss of collagenase-2 confers increased skin tumor susceptibility to male mice. *Nature Genetics*, *35*(3), 252–257. https://doi.org/10.1038/ng1249

Barrett, A., Evans, I. M., Frolov, A., Britton, G., Pellet-Many, C., Yamaji, M., Mehta, V., Bandopadhyay, R., Li, N., Brandner, S., Zachary, I. C., & Frankel, P. (2014). Correction to A crucial role for DOK1 in PDGF-BB-stimulated glioma cell invasion through p130Cas and Rap1 signalling [J. Cell Sci., 127, 2647-2658]. *Journal of Cell Science*, *127*(15), 3397. https://doi.org/10.1242/jcs.158576

Bejarano, L., Schuhmacher, A. J., Méndez, M., Megías, D., Blanco-Aparicio, C., Martínez, S., Pastor, J., Squatrito, M., & Blasco, M. A. (2017). Inhibition of TRF1 Telomere Protein Impairs Tumor Initiation and Progression in Glioblastoma Mouse Models and Patient-Derived Xenografts. *Cancer Cell*, *32*(5), 590-607.e4. https://doi.org/10.1016/j.ccell.2017.10.006

Berezowska, S., Diermeier-Daucher, S., Brockhoff, G., Busch, R., Duyster, J., Grosu, A.-L., Schlegel, J., & 1Division. (2010). Effect of additional inhibition of human epidermal growth factor receptor 2 with the bispecific tyrosine kinase inhibitor AEE788 on the resistance to specific EGFR inhibition in glioma cells. *International Journal of Molecular Medicine*, *26*, 713–721. https://doi.org/10.3892/ijmm_00000518 Abstract.

Bergers, G., Brekken, R., McMahon, G., Vu, T. H., Itoh, T., Tamaki, K., Tanzawa, K., Thorpe, P., Itohara, S., Werb, Z., & Hanahan, D. (2000). Matrix metalloproteinase-9 triggers the angiogenic switch during carcinogenesis. *Nature Cell Biology*, *2*(10), 737–744. https://doi.org/10.1038/35036374

Bertran, E., Caja, L., Navarro, E., Sancho, P., Mainez, J., Murillo, M. M., Vinyals, A., Fabra, À., & Fabregat, I. (2009). Role of CXCR4/SDF-1α in the migratory phenotype of hepatoma cells that have undergone epithelial-mesenchymal transition in response to the transforming growth factor-β. *Cellular Signalling*, *21*(11), 1595–1606. https://doi.org/10.1016/j.cellsig.2009.06.006

Bhat, A. A., Uppada, S., Achkar, I. W., Hashem, S., Yadav, S. K., Shanmugakonar, M., Al-Naemi, H. A.,

Haris, M., & Uddin, S. (2019). Tight junction proteins and signaling pathways in cancer and inflammation: A functional crosstalk. *Frontiers in Physiology*, *10*(JAN), 1–19. https://doi.org/10.3389/fphys.2018.01942

Bhattacharyya, N., & Fried, M. P. (2002). Nodal metastasis in major salivary gland cancer: Predictive factors and effects on survival. *Archives of Otolaryngology - Head and Neck Surgery*, *128*(8), 904–908. https://doi.org/10.1001/archotol.128.8.904

Bi, J., Chowdhry, S., Wu, S., Zhang, W., Masui, K., & Mischel, P. S. (2020). Altered cellular metabolism in gliomas — an emerging landscape of actionable co-dependency targets. *Nature Reviews Cancer*, *20*(1), 57–70. https://doi.org/10.1038/s41568-019-0226-5

Biddle, A., Liang, X., Gammon, L., Fazil, B., Harper, L. J., Emich, H., Costea, D. E., & Mackenzie, I. C. (2011). Cancer stem cells in squamous cell carcinoma switch between two distinct phenotypes that are preferentially migratory or proliferative. *Cancer Research*, *71*(15), 5317–5326. https://doi.org/10.1158/0008-5472.CAN-11-1059

BioGPS database. (2016). www.biogps.org

Birge, R. B., Kalodimos, C., Inagaki, F., & Tanaka, S. (2009). Crk and CrkL adaptor proteins: Networks for physiological and pathological signaling. *Cell Communication and Signaling*, *7*, 1–23. https://doi.org/10.1186/1478-811X-7-13

Bock, H. H., & May, P. (2016). Canonical and non-canonical reelin signaling. *Frontiers in Cellular Neuroscience*, *10*(Jun), 1–20. https://doi.org/10.3389/fncel.2016.00166

Bolaños, J. P. (2016). Bioenergetics and redox adaptations of astrocytes to neuronal activity. *Journal of Neurochemistry*, *139*, 115–125. https://doi.org/10.1111/jnc.13486

Bragado, Yeriel Estrada, Falguni Parikh, Sarah Krause, Carla Capobianco, Hernan G. Farina, Denis M Schewe, Julio A. Aguirre-Ghiso, P. (2013). TGFβ2 dictates disseminated tumour cell fate in target organs through TGFβ-RIII and p38α/β signalling. *Nat Cell Biol.*, *15*(11), 1351–1361. https://doi.org/doi:10.1038/ncb2861

Bragado, P., Armesilla, A., Silva, A., & Porras, A. (2007). Apoptosis by cisplatin requires p53 mediated p38α MAPK activation through ROS generation. *Apoptosis*, *12*(9), 1733–1742. https://doi.org/10.1007/s10495-007-0082-8

Brodal, P. (2006). *The Central Nervous System*.

Bryan A. Ballif, Lionel Arnaud, William T. Arthur, Deborah Guris, Akira Imamoto & and Jonathan A. Cooper. (2004). *Activation of a Dab1/CrkL/C3G/Rap1 Pathway in Reelin-Stimulated Neurons*. https://doi.org/10.1016/j

Burkhart. (2008). Cellular mechanisms of tumour suppression by the retinoblastoma gene. *Nat Rev Cancer*, *8*(9), 671–682. https://doi.org/10.1038/nrc2399

Burns, J. S., & Manda, G. (2017). Metabolic pathways of thewarburg effect in health and disease: Perspectives of choice, chain or chance. *International Journal of Molecular Sciences*, *18*(12), 1–28. https://doi.org/10.3390/ijms18122755

Caja, L., Tzavlaki, K., Dadras, M. S., Tan, E. J., Hatem, G., Maturi, N. P., Morén, A., Wik, L., Watanabe, Y., Savary, K., Kamali-Moghaddan, M., Uhrbom, L., Heldin, C. H., & Moustakas, A. (2018). Snail regulates BMP and TGFβ pathways to control the differentiation status of glioma-initiating cells. *Oncogene*, *37*(19), 2515–2531. https://doi.org/10.1038/s41388-018-0136-0

Campbell, P. J., Getz, G., Korbel, J. O., Stuart, J. M., Jennings, J. L., Stein, L. D., Perry, M. D., Nahal-Bose, H. K., Ouellette, B. F. F., Li, C. H., Rheinbay, E., Nielsen, G. P., Sgroi, D. C., Wu, C. L., Faquin, W. C., Deshpande, V., Boutros, P. C., Lazar, A. J., Hoadley, K. A., … Zhang, J. (2020). Pan-cancer analysis of whole genomes. *Nature*, *578*(7793), 82–93. https://doi.org/10.1038/s41586-020-1969-6

Cancertool software. (2019). www.genomics.cicbiogune.es/CANCERTOOL

Carabias, A., Gómez-Hernández, M., de Cima, S., Rodríguez-Blázquez, A., Morán-Vaquero, A., González-Sáenz, P., Guerrero, C., & de Pereda, J. M. (2020). Mechanisms of autoregulation of C3G, activator of the GTPase Rap1, and its catalytic deregulation in lymphomas. *Science Signaling*, *13*(647), 1–18. https://doi.org/10.1126/scisignal.abb7075

Cargnello, M., & Roux, P. P. (2011). Activation and Function of the MAPKs and Their Substrates, the MAPK-Activated Protein Kinases. *Microbiology and Molecular Biology Reviews*, *75*(1), 50–83. https://doi.org/10.1128/mmbr.00031-10

Che, Y. L., Luo, S. J., Li, G., Cheng, M., Gao, Y. M., Li, X. M., Dai, J. M., He, H., Wang, J., Peng, H. J., Zhang, Y., Li, W. Y., Wang, H., Liu, B., & Linghu, H. (2015). The C3G/Rap1 pathway promotes secretion of MMP-2 and MMP-9 and is involved in serous ovarian cancer metastasis. *Cancer Letters*, *359*(2), 241–249. https://doi.org/10.1016/j.canlet.2015.01.019

Cheerathodi, James J. Vincenta, and Bryan A. Ballifa, M. (2015). Quantitative Comparison of CrkL-SH3 Binding Proteins from Embryonic Murine Brain and Liver: Implications for Developmental Signaling and the Quantification of Protein Species Variants in Bottom-Up Proteomics. *J Proteomics*, *125*, 104–111. https://doi.org/doi:10.1016/j.jprot.2015.04.033

Chen, C., & Wang, L. (2019). *FOXO1 associated with sensitivity to chemotherapy drugs and glial - mesenchymal transition in glioma*. *January 2018*, 882–893. https://doi.org/10.1002/jcb.27450

Chen, J., Li, Y., Yu, T.-S., McKay, R. M., Burns, D., Kernie, S. G., & Parada, L. F. (2012). A restricted cell population propagates glioblastoma growth following chemotherapy Jian. *Nature*, *488*(7412), 522–526. https://doi.org/10.1038/nature11287.A

Chiang, Christian A. Baumann, Makoto Kanzaki, Debbie C. Thurmond, Robert T. Watson, Cheryl L. Neudauerk, Ian G. Macarak. (2001). *Insulin-stimulated GLUT4 translocation requires the CAP-dependent activation of TC10*. *410*(April).

Clark, M. J., Homer, N., O'Connor, B. D., Chen, Z., Eskin, A., Lee, H., Merriman, B., & Nelson, S. F. (2010). U87MG decoded: The genomic sequence of a cytogenetically aberrant human cancer cell line. *PLoS Genetics*, *6*(1). https://doi.org/10.1371/journal.pgen.1000832

Clark, P. A., Iida, M., Treisman, D. M., Kalluri, H., Ezhilan, S., Zorniak, M., Wheeler, D. L., & Kuo, J. S. (2012). Activation of multiple ERBB family receptors mediates glioblastoma cancer stem-like cell resistance to EGFR-targeted inhibition. *Neoplasia (United States)*, *14*(5), 420–428. https://doi.org/10.1596/neo.12432

Clarke, M. F., Dick, J. E., Dirks, P. B., Eaves, C. J., Jamieson, C. H. M., Jones, D. L., Visvader, J., Weissman, I. L., & Wahl, G. M. (2006). Cancer stem cells - Perspectives on current status and future directions: AACR workshop on cancer stem cells. *Cancer Research*, *66*(19), 9339–9344. https://doi.org/10.1158/0008-5472.CAN-06-3126

Clustal Omega Software. (2020). https://www.ebi.ac.uk/Tools/msa/clustalo/

Commander, R., Wei, C., Sharma, A., Mouw, J. K., Burton, L. J., Summerbell, E., Mahboubi, D., Peterson, R. J., Konen, J., Zhou, W., Du, Y., Fu, H., Shanmugam, M., & Marcus, A. I. (2020). *Subpopulation targeting of pyruvate dehydrogenase and GLUT1 decouples metabolic heterogeneity during collective cancer cell invasion*. 1–17. https://doi.org/10.1038/s41467-020-15219-7

COSMIC Cell Lines webpage. (2020). www.cancer.sanger.ac.uk/cell_lines

Cuadrado, A., & Nebreda, A. R. (2010). Mechanisms and functions of p38 MAPK signalling. *Biochemical Journal*, *429*(3), 403–417. https://doi.org/10.1042/BJ20100323

Daneman. (2015). *The Blood-Brain Barrier*. https://doi.org/10.1111/j.1469-8749.1961.tb10410.x

Danglot, L., Chaineau, M., Dahan, M., Gendron, M. C., Boggetto, N., Perez, F., & Galli, T. (2010). Role of TI-VAMP and CD82 in EGFR cell-surface dynamics and signaling. *Journal of Cell Science*, *123*(5), 723–735. https://doi.org/10.1242/jcs.062497

Dar, M. I., Jan, S., Reddy, G. L., Wani, R., Syed, M., Dar, M. J., Sawant, S. D., Vishwakarma, R. A., & Syed, S. H. (2020). Differentiation of human neuroblastoma cell line IMR-32 by sildenafil and its newly discovered analogue IS00384. *Cellular Signalling*, *65*(November 2019).

https://doi.org/10.1016/j.cellsig.2019.109425

Dasgupta, A., Lim, A. R., & Ghajar, C. M. (2017). Circulating and disseminated tumor cells: harbingers or initiators of metastasis? *Molecular Oncology*, *11*(1), 40–61. https://doi.org/10.1002/1878-0261.12022

Datta, K., Muders, M., Zhang, H., & Tindall, D. J. (2010). Mechanism of lymph node metastasis in prostate cancer. *Future Oncology*, *6*(5), 823–836. https://doi.org/10.2217/fon.10.33

DAVID software. (2019). www.david.ncifcrf.gov

Day, E. K., Sosale, N. G., Xiao, A., Zhong, Q., Purow, B., & Lazzara, M. J. (2020). Glioblastoma Cell Resistance to EGFR and MET Inhibition Can Be Overcome via Blockade of FGFR-SPRY2 Bypass Signaling. *Cell Reports*, *30*(10), 3383-3396.e7. https://doi.org/10.1016/j.celrep.2020.02.014

Dayma, K., & Radha, V. (2011). Cytoskeletal remodeling by C3G to induce neurite-like extensions and inhibit motility in highly invasive breast carcinoma cells. *Biochimica et Biophysica Acta - Molecular Cell Research*, *1813*(3), 456–465. https://doi.org/10.1016/j.bbamcr.2011.01.004

Dayma, K., Ramadhas, A., Sasikumar, K., & Radha, V. (2012). Reciprocal Negative Regulation between the Guanine Nucleotide Exchange Factor C3G and β-Catenin. *Genes and Cancer*, *3*(9–10), 564–577. https://doi.org/10.1177/1947601912471189

Dayton, T. L., Jacks, T., & Vander Heiden, M. G. (2016). PKM 2, cancer metabolism, and the road ahead . *EMBO Reports*, *17*(12), 1721–1730. https://doi.org/10.15252/embr.201643300

De Palma, M., Biziato, D., & Petrova, T. V. (2017). Microenvironmental regulation of tumour angiogenesis. *Nature Reviews Cancer*, *17*(8), 457–474. https://doi.org/10.1038/nrc.2017.51

Demuth, T., Reavie, L. B., Rennert, J. L., Nakada, M., Nakada, S., Hoelzinger, D. B., Beaudry, C. E., Henrichs, A. N., Anderson, E. M., & Berens, M. E. (2007). MAP-ing glioma invasion: Mitogen-activated protein kinase kinase 3 and p38 drive glioma invasion and progression and predict patient survival. *Molecular Cancer Therapeutics*, *6*(4), 1212–1222. https://doi.org/10.1158/1535-7163.MCT-06-0711

Deshors, P., Toulas, C., Arnauduc, F., Malric, L., Siegfried, A., Nicaise, Y., Lemarié, A., Larrieu, D., Tosolini, M., Cohen-Jonathan Moyal, E., Courtade-Saidi, M., & Evrard, S. M. (2019). Ionizing radiation induces endothelial transdifferentiation of glioblastoma stem-like cells through the Tie2 signaling pathway. *Cell Death and Disease*, *10*(11). https://doi.org/10.1038/s41419-019-2055-6

Dinorah Friedmann-Morvinski, Eric A. Bushong, Eugene Ke, Yasushi Soda, Tomotoshi Marumoto, Oded Singer, Mark H. Ellisman, and I. M. V. (2012). *Dedifferentiation of Neurons and Astrocytes by*. *338*(6110), 1080–1084. https://doi.org/10.1126/science.1226929.Dedifferentiation

Dolado, I., Swat, A., Ajenjo, N., De Vita, G., Cuadrado, A., & Nebreda, A. R. (2007). p38α MAP Kinase as a Sensor of Reactive Oxygen Species in Tumorigenesis. *Cancer Cell*, *11*(2), 191–205. https://doi.org/10.1016/j.ccr.2006.12.013

Erwin G. Van Meir, PhD1, Costas G. Hadjipanayis, MD, PhD2, Andrew D. Norden, MD, MPH3, Hui-Kuo Shu, MD4, Patrick Y. Wen, MD5, and Jeffrey J. Olson, M. (2010). Exciting New Advances in Neuro-Oncology: The Avenue to a Cure for Malignant Glioma. *CA Cancer J Clin*, *60*(3), 166–193. https://doi.org/10.3322/caac.20069

Fedele, M., Cerchia, L., Pegoraro, S., Sgarra, R., & Manfioletti, G. (2019). *Proneural-Mesenchymal Transition : Phenotypic Plasticity to Acquire Multitherapy Resistance in Glioblastoma*.

Feng, S., Cai, X., Li, Y., Jian, X., Zhang, L., & Li, B. (2019). Tripartite motif-containing 14 (TRIM14) promotes epithelial-mesenchymal transition via ZEB2 in glioblastoma cells. *Journal of Experimental & Clinical Cancer Research*, *38*(57). https://doi.org/10.1186/s13046-019-1070-x

Fernández-Nogueira, P., Mancino, M., Fuster, G., López-Plana, A., Jauregui, P., Almendro, V., Enreig, E., Menéndez, S., Rojo, F., Noguera-Castells, A., Bill, A., Gaither, L. A., Serrano, L., Recalde-Percaz, L., Moragas, N., Alonso, R., Ametller, E., Rovira, A., Lluch, A., … Bragado, P. (2020). Tumor-Associated Fibroblasts Promote HER2-Targeted Therapy Resistance through FGFR2 Activation. *Clinical Cancer Research : An Official Journal of the American Association for Cancer Research*, *26*(6), 1432–1448. https://doi.org/10.1158/1078-0432.CCR-19-0353

FireBrowse database. (n.d.). www.firebrowse.org/

Freeman, S. A., McLeod, S. J., Dukowski, J., Austin, P., Lee, C. C. Y., Millen-Martin, B., Kubes, P., McCafferty, D. M., Gold, M. R., & Roskelley, C. D. (2010). Preventing the activation or cycling of the Rap1 GTPase alters adhesion and cytoskeletal dynamics and blocks metastatic melanoma cell extravasation into the lungs. *Cancer Research*, *70*(11), 4590–4601. https://doi.org/10.1158/0008-5472.CAN-09-3414

Friedl, P., & Wolf, K. (2003). Tumour-cell invasion and migration: Diversity and escape mechanisms. *Nature Reviews Cancer*, *3*(5), 362–374. https://doi.org/10.1038/nrc1075

Fukai, J., Yokote, H., Yamanaka, R., Arao, T., Nishio, K., & Itakura, T. (2008). *EphA4 promotes cell proliferation and migration through a novel EphA4-FGFR1 signaling pathway in the human glioma U251 cell line*. 2768–2779. https://doi.org/10.1158/1535-7163.MCT-07-2263

Fukuyama, T., Ogita, H., Kawakatsu, T., Fukuhara, T., Yamada, T., Sato, T., Shimizu, K., Nakamura, T., Matsuda, M., & Takai, Y. (2005). Involvement of the c-Src-Crk-C3G-Rap1 signaling in the nectin-induced activation of Cdc42 and formation of adherens junctions. *Journal of Biological Chemistry*, *280*(1), 815–825. https://doi.org/10.1074/jbc.M411099200

Gao, F., Cui, Y., Jiang, H., Sui, D., & Wang, Y. (2016). *Circulating tumor cell is a common property of brain glioma and promotes the monitoring system*. *7*(44).

Gargini, R., Segura-collar, B., Herránz, B., & Garcia-, V. (2019). *Title : IDH-Tau-EGFR triad defines the neovascular landscape of diffuse gliomas by controlling mesenchymal differentiation Running title : Glioma genotype defines the vascular phenotype*. 1–39.

George, J. T., Jolly, M. K., Xu, S., Somarelli, J. A., & Levine, H. (2017). Survival outcomes in cancer patients predicted by a partial EMT gene expression scoring metric. *Cancer Research*, *77*(22), 6415–6428. https://doi.org/10.1158/0008-5472.CAN-16-3521

Gloushankova, N. A., Rubtsova, S. N., & Zhitnyak, I. Y. (2017). Cadherin-mediated cell-cell interactions in normal and cancer cells. *Tissue Barriers*, *5*(3), 1–15. https://doi.org/10.1080/21688370.2017.1356900

Gotoh, T, Hattori, S., Nakamura, S., Kitayama, H., Noda, M., Takai, Y., Kaibuchi, K., Matsui, H., Hatase, O., & Takahashi, H. (1995). Identification of Rap1 as a target for the Crk SH3 domain-binding guanine nucleotide-releasing factor C3G. *Molecular and Cellular Biology*, *15*(12), 6746–6753. https://doi.org/10.1128/mcb.15.12.6746

Gotoh, Takaya, Niino, Y., Tokuda, M., Hatase, O., Nakamura, S., Matsuda, M., & Hattori, S. (1997). *Activation of R-Ras by Ras-Guanine Nucleotide-releasing Factor *. 272*(30), 18602–18607.

Gouazé-Andersson, V., Ghérardi, M. J., Lemarié, A., Gilhodes, J., Lubrano, V., Arnauduc, F., Moyal, E. C. J., & Toulas, C. (2018). FGFR1/FOXM1 pathway: A key regulator of glioblastoma stem cells radioresistance and a prognosis biomarker. *Oncotarget*, *9*(60), 31637–31649. https://doi.org/10.18632/oncotarget.25827

Gravina, G. L., Mancini, A., Colapietro, A., Vitale, F., Vetuschi, A., Pompili, S., Rossi, G., Marampon, F., Richardson, P. J., Patient, L., Patient, L., Burbidge, S., & Festuccia, C. (2017). The novel CXCR4 antagonist, PRX177561, reduces tumor cell proliferation and accelerates cancer stem cell differentiation in glioblastoma preclinical models. *Tumor Biology*, *39*(6). https://doi.org/10.1177/1010428317695528

GTExPortal database. (2016). www.gtexportal.org

Guan, J., & Chen, J. (2013). Mesenchymal stem cells in the tumor microenvironment. *Biomedical Reports*, *1*(4), 517–521. https://doi.org/10.3892/br.2013.103

Guerrero, C., Fernandez-Medarde, A., Rojas, J. M., Font De Mora, J., Esteban, L. M., & Santos, E. (1998). Transformation suppressor activity of C3G is independent of its CDC25-homology domain. *Oncogene*, *16*(5), 613–624. https://doi.org/10.1038/sj.onc.1201569

Guerrero, Carmen, Martín-Encabo, S., Fernández-Medarde, A., & Santos, E. (2004). C3G-mediated suppression of oncogene-induced focus formation in fibroblasts involves inhibition of ERK activation,

cyclin a expression and alterations of anchorage-independent growth. *Oncogene*, *23*(28), 4885–4893. https://doi.org/10.1038/sj.onc.1207622

Gui, A., Kobayashi, A., Motoyama, H., Kitazawa, M., Takeoka, M., & Miyagawa, S. (2012). Impaired degradation followed by enhanced recycling of epidermal growth factor receptor caused by hypo-phosphorylation of tyrosine 1045 in RBE cells. *BMC Cancer*, *12*. https://doi.org/10.1186/1471-2407-12-179

Guo, G., Yao, W., Zhang, Q., & Bo, Y. (2013). Oleanolic Acid Suppresses Migration and Invasion of Malignant Glioma Cells by Inactivating MAPK/ERK Signaling Pathway. *PLoS ONE*, *8*(8), 2–9. https://doi.org/10.1371/journal.pone.0072079

Guo, X. X., An, S., Yang, Y., Liu, Y., Hao, Q., & Xu, T. R. (2016). Rap-Interacting Proteins are Key Players in the Rap Symphony Orchestra. *Cellular Physiology and Biochemistry*, *39*(1), 137–156. https://doi.org/10.1159/000445612

Gutiérrez-Berzal, J., Castellano, E., Martín-Encabo, S., Gutiérrez-Cianca, N., Hernández, J. M., Santos, E., & Guerrero, C. (2006). Characterization of p87C3G, a novel, truncated C3G isoform that is overexpressed in chronic myeloid leukemia and interacts with Bcr-Abl. *Experimental Cell Research*, *312*(6), 938–948. https://doi.org/10.1016/j.yexcr.2005.12.007

Gutiérrez-Herrero, S., Maia, V., Gutiérrez-Berzal, J., Calzada, N., Sanz, M., González-Manchón, C., Pericacho, M., Ortiz-Rivero, S., González-Porras, J. R., Arechederra, M., Porras, A., & Guerrero, C. (2012). C3G transgenic mouse models with specific expression in platelets reveal a new role for C3G in platelet clotting through its GEF activity. *Biochimica et Biophysica Acta - Molecular Cell Research*, *1823*(8), 1366–1377. https://doi.org/10.1016/j.bbamcr.2012.05.021

Gutiérrez-Uzquiza, Á., Arechederra, M., Bragado, P., Aguirre-Ghiso, J. A., & Porras, A. (2012). p38α mediates cell survival in response to oxidative stress via induction of antioxidant genes: Effect on the p70S6K pathway. *Journal of Biological Chemistry*, *287*(4), 2632–2642. https://doi.org/10.1074/jbc.M111.323709

Gutiérrez-Uzquiza, Á., Arechederra, M., Molina, I., Baños, R., Maia, V., Benito, M., Guerrero, C., & Porras, A. (2010). C3G down-regulates p38 MAPK activity in response to stress by Rap-1 independent mechanisms: Involvement in cell death. *Cellular Signalling*, *22*(3), 533–542. https://doi.org/10.1016/j.cellsig.2009.11.008

Guvakova, M. A., Lee, W. S. Y., Furstenau, D. K., Prabakaran, I., Li, D. C., Hung, R., & Kushnir, N. (2014). The small GTPase Rap1 promotes cell movement rather than stabilizes adhesion in epithelial cells responding to insulin-like growth factor I. *Biochemical Journal*, *463*(2), 257–270. https://doi.org/10.1042/BJ20131638

Hagedorn. (2005). *Accessing key steps of human tumor progression in vivo by using an avian embryo model*.

Hanahan, D., & Weinberg, R. A. (2000). The Hallmarks of Cancer. *Cell*, *100*(7), 57–70. https://doi.org/10.1007/s00262-010-0968-0

Hanahan, D., & Weinberg, R. A. (2011). Hallmarks of cancer: The next generation. *Cell*, *144*(5), 646–674. https://doi.org/10.1016/j.cell.2011.02.013

He, Y., Kapoor, A., Cook, S., Liu, S., Xiang, Y., Rao, C. V., Kenis, P. J. A., & Wang, F. (2011). The non-receptor tyrosine kinase Lyn controls neutrophil adhesion by recruiting the CrkL-C3G complex and activating Rap1 at the leading edge. *Journal of Cell Science*, *124*(13), 2153–2164. https://doi.org/10.1242/jcs.078535

Hegi, M. E., Liu, L., Herman, J. G., Stupp, R., Wick, W., Weller, M., Mehta, M. P., & Gilbert, M. R. (2008). Correlation of O6-methylguanine methyltransferase (MGMT) promoter methylation with clinical outcomes in glioblastoma and clinical strategies to modulate MGMT activity. *Journal of Clinical Oncology*, *26*(25), 4189–4199. https://doi.org/10.1200/JCO.2007.11.5964

Hirata, T., Nagai, H., Koizumi, K., Okino, K., Harada, A., Onda, M., Nagahata, T., Mikami, I., Hirai, K., Haraguchi, S., Jin, E., Kawanami, O., Shimizu, K., & Emi, M. (2004). Amplification, up-regulation and over-expression of C3G (CRK SH3 domain-binding guanine nucleotide-releasing factor) in non-small cell lung cancers. *Journal of Human Genetics*, *49*(6), 290–295. https://doi.org/10.1007/s10038-004-

0148-1

Hoang-Minh, L. B., Siebzehnrubl, F. A., Yang, C., Suzuki-Hatano, S., Dajac, K., Loche, T., Andrews, N., Schmoll Massari, M., Patel, J., Amin, K., Vuong, A., Jimenez-Pascual, A., Kubilis, P., Garrett, T. J., Moneypenny, C., Pacak, C. A., Huang, J., Sayour, E. J., Mitchell, D. A., … Deleyrolle, L. P. (2018). Infiltrative and drug-resistant slow-cycling cells support metabolic heterogeneity in glioblastoma. *The EMBO Journal*, *37*(23), 1–21. https://doi.org/10.15252/embj.201798772

Hobbs; Der; and Rossman. (2016). Ras isoforms and mutations in cancer at a glance. *J Cell Sci*, *129*(7), 1287–1292.

Hogan, C., Serpente, N., Cogram, P., Hosking, C. R., Bialucha, C. U., Feller, S. M., Braga, V. M. M., Birchmeier, W., & Fujita, Y. (2004). Rap1 Regulates the Formation of E-Cadherin-Based Cell-Cell Contacts. *Molecular and Cellular Biology*, *24*(15), 6690–6700. https://doi.org/10.1128/mcb.24.15.6690-6700.2004

Horiuchi, A., Imai, T., Wang, C., Ohira, S., Feng, Y., Nikaido, T., & Konishi, I. (2003). Up-regulation of small GTPases, RhoA and RhoC, is associated with tumor progression in ovarian carcinoma. *Laboratory Investigation*, *83*(6), 861–870. https://doi.org/10.1097/01.LAB.0000073128.16098.31

Horton, E. R., Byron, A., Askari, J. A., Ng, D. H. J., Millon-Frémillon, A., Robertson, J., Koper, E. J., Paul, N. R., Warwood, S., Knight, D., Humphries, J. D., & Humphries, M. J. (2015). Definition of a consensus integrin adhesome and its dynamics during adhesion complex assembly and disassembly. *Nature Cell Biology*, *17*(12), 1577–1587. https://doi.org/10.1038/ncb3257

Hosseini, H., Obradovic, M. M. S., Hoffmann, M., Harper, K. L., Sosa, M. S., Werner-Klein, M., Nanduri, L. K., Werno, C., Ehrl, C., Maneck, M., Patwary, N., Haunschild, G., Guzvic, M., Reimelt, C., Grauvogl, M., Eichner, N., Weber, F., Hartkopf, A. D., Taran, F. A., … Klein, C. A. (2016). Early dissemination seeds metastasis in breast cancer. *Nature*, *540*(7634), 552–558. https://doi.org/10.1038/nature20785

Hu, Y., & Smyth, G. K. (2009). ELDA: Extreme limiting dilution analysis for comparing depleted and enriched populations in stem cell and other assays. *Journal of Immunological Methods*, *347*(1–2), 70–78. https://doi.org/10.1016/j.jim.2009.06.008

Huang, L., Wei, Z., Chang, X., Zheng, X., Yan, J., Huang, J., Zhang, J., & Sheng, L. (2020). eIF3b regulates the cell proliferation and apoptosis processes in chronic myelogenous leukemia cell lines via regulating the expression of C3G. *Biotechnology Letters*, *1*. https://doi.org/10.1007/s10529-020-02878-1

Ichiba, T., Hashimoto, Y., Nakaya, M., Kuraishi, Y., Tanaka, S., Kurata, T., Mochizuki, N., & Matsuda, M. (1999). Activation of C3G guanine nucleotide exchange factor for Rap1 by phosphorylation of tyrosine 504. *Journal of Biological Chemistry*, *274*(20), 14376–14381. https://doi.org/10.1074/jbc.274.20.14376

Iser, I. C., Pereira, M. B., Lenz, G., & Wink, R. (2017). The Epithelial-to-Mesenchymal Transition-Like Process in Glioblastoma : An Updated Systematic Review and In Silico Investigation. *Medicinal Research Reviews*, *37*(2), 271–313. https://doi.org/10.1002/med.21408

Ivaska, J. (2011). Vimentin: Central hub in EMT induction? *Small GTPases*, *2*(1), 1–4. https://doi.org/10.4161/sgtp.2.1.15114

Izumchenko, E., Chang, X., Michailidi, C., Kagohara, L., Ravi, R., Paz, K., Brait, M., Hoque, M., Ling, S., Bedi, A., & Sidransky, D. (2014). The TGFβ-miR200-MIG6 pathway orchestrates the EMT-associated kinase switch that induces resistance to EGFR inhibitors. *Cancer Research*, *74*(14), 3995–4005. https://doi.org/10.1158/0008-5472.CAN-14-0110

Jeong, H. H., Smith, C. A., Salhia, B., & Rutka, J. T. (2008). The role of fascin in the migration and invasiveness of malignant glioma cells. *Neoplasia*, *10*(2), 149–159. https://doi.org/10.1593/neo.07909

Jiang, M., Zhuang, Y., Zu, W., Jiao, L., Richard, S. A., & Zhang, S. (2019). Overexpression of epac2 reduces the invasion of glioma cells via mmp-2. *Oncology Letters*, *17*(6), 5080–5086. https://doi.org/10.3892/ol.2019.10200

Jimenez-Pascual, A., & Siebzehnrubl, F. A. (2019). Fibroblast Growth Factor Receptor Functions in Glioblastoma. *Cells*, *8*(715).

Jobling, P., Pundavela, J., Oliveira, S. M. R., Roselli, S., Walker, M. M., & Hondermarck, H. (2015). Nerve-cancer cell cross-talk: A novel promoter of tumor progression. *Cancer Research*, *75*(9), 1777–1781. https://doi.org/10.1158/0008-5472.CAN-14-3180

Joerger, A. C., & Fersht, A. R. (2016). The p53 Pathway: Origins, Inactivation in Cancer, and Emerging Therapeutic Approaches. *Annual Review of Biochemistry*, *85*(1), 375–404. https://doi.org/10.1146/annurev-biochem-060815-014710

Joseph, J. V., Conroy, S., Tomar, T., Eggens-Meijer, E., Bhat, K., Copray, S., Walenkamp, A. M. E., Boddeke, E., Balasubramanyian, V., Wagemakers, M., Den Dunnen, W. F. A., & Kruyt, F. A. E. (2014). TGF-β is an inducer of ZEB1-dependent mesenchymal transdifferentiation in glioblastoma that is associated with tumor invasion. *Cell Death and Disease*, *5*(10), e1443-14. https://doi.org/10.1038/cddis.2014.395

Kao, S. C., Jaiswal, R. K., Kolch, W., & Landreth, G. E. (2001). Identification of the Mechanisms Regulating the Differential Activation of the MAPK Cascade by Epidermal Growth Factor and Nerve Growth Factor in PC12 Cells. *Journal of Biological Chemistry*, *276*(21), 18169–18177. https://doi.org/10.1074/jbc.M008870200

Karen D. Cowden Dahl, Jaime Symowicz, Yan Ning, Elisa Gutierrez, David A. Fishman, Brian P. Adley, M. Sharon Stack, and L. G. H. (2008). Matrix metalloproteinase (MMP)-9 is a mediator of epidermal growth factor dependent E-cadherin loss in ovarian carcinoma cells. *Cancer Res.*, *15*(68), 4606–4613. https://doi.org/10.1158/0008-5472.CAN-07-5046

Kaushik, I., Ramachandran, S., & Srivastava, S. K. (2019). CRISPR-Cas9: A multifaceted therapeutic strategy for cancer treatment. *Seminars in Cell and Developmental Biology*, *96*(April), 4–12. https://doi.org/10.1016/j.semcdb.2019.04.018

Kessenbrock, K., Plaks, V., & Werb, Z. (2010). Matrix Metalloproteinases: Regulators of the tumor. *Cell*, *141*(1), 52–67. https://doi.org/10.1038/jid.2014.371

Klemm, F., Maas, R. R., Bowman, R. L., Kornete, M., Soukup, K., Nassiri, S., Brouland, J. P., Iacobuzio-Donahue, C. A., Brennan, C., Tabar, V., Gutin, P. H., Daniel, R. T., Hegi, M. E., & Joyce, J. A. (2020). Interrogation of the Microenvironmental Landscape in Brain Tumors Reveals Disease-Specific Alterations of Immune Cells. *Cell*, *181*(7), 1643-1660.e17. https://doi.org/10.1016/j.cell.2020.05.007

Knudsen, B. S., Feller, S. M., & Hanafusa, H. (1994). Four proline-rich sequences of the guanine-nucleotide exchange factor C3G bind with unique specificity to the first Src homology 3 domain of Crk. *Journal of Biological Chemistry*, *269*(52), 32781–32787.

Kowalik, M. A., Columbano, A., & Perra, A. (2017). Emerging role of the pentose phosphate pathway in hepatocellular carcinoma. *Frontiers in Oncology*, *7*(MAY). https://doi.org/10.3389/fonc.2017.00087

Kowalski-Chauvel, A., Gouaze-Andersson, V., Baricault, L., Martin, E., Delmas, C., Toulas, C., Cohen-Jonathan-Moyal, E., & Seva, C. (2019). Alpha6-integrin regulates FGFR1 expression through the ZEB1/YAP1 transcription complex in glioblastoma stem cells resulting in enhanced proliferation and stemness. *Cancers*, *11*(3), 1–15. https://doi.org/10.3390/cancers11030406

Lama, G., Mangiola, A., Anile, C., Sabatino, G., Bonis, P. D. E., Lauriola, L., Giannitelli, C., Torre, G. L. A., Jhanwar-uniyal, M., Sica, G., & Maira, G. (2007). *Activated ERK1 / 2 expression in glioblastoma multiforme and in peritumor tissue*. 1333–1342.

Lamballe, F., Toscano, S., Conti, F., Arechederra, M., Baeza, N., Figarella-Branger, D., Helmbacher, F., & Maina, F. (2016). Coordination of signalling networks and tumorigenic properties by ABL in glioblastoma cells. *Oncotarget*, *7*(46), 74747–74767. https://doi.org/10.18632/oncotarget.12546

Lamouille, S., Xu, J., & Derynck, R. (2014). Molecular mechanisms of epithelial-mesenchymal transition. *Nature Reviews Molecular Cell Biology*, *15*(3), 178–196. https://doi.org/10.1038/nrm3758

Lathia, J. D., Mack, S. C., Mulkearns-hubert, E. E., Valentim, C. L. L., & Rich, J. N. (2015). Cancer stem cells in glioblastoma. *GENES & DEVELOPMENT*, *29*, 1203–1217.

Lee, J., Kotliarova, S., Kotliarov, Y., Li, A., Su, Q., Donin, N. M., Pastorino, S., Purow, B. W., Christopher, N., Zhang, W., Park, J. K., & Fine, H. A. (2006). Tumor stem cells derived from glioblastomas cultured in bFGF and EGF more closely mirror the phenotype and genotype of primary tumors than do serum-cultured cell lines. *Cancer Cell*, *9*(5), 391–403. https://doi.org/10.1016/j.ccr.2006.03.030

Lemmon, M. A., & Schlessinger, J. (2010). Cell signaling by receptor-tyrosine kinases Mark. *Cell*, *141*(7), 1117–1134. https://doi.org/10.1016/j.cell.2010.06.011.Cell

Lenting, K., Verhaak, R., ter Laan, M., Wesseling, P., & Leenders, W. (2017). Glioma: experimental models and reality. *Acta Neuropathologica*, *133*(2), 263–282. https://doi.org/10.1007/s00401-017-1671-4

Liang, H., Ding, X., Zhou, C., Zhang, Y., Xu, M., Zhang, C., & Xu, L. (2012). Knockdown of eukaryotic translation initiation factors 3B (EIF3B) inhibits proliferation and promotes apoptosis in glioblastoma cells. *Neurological Sciences*, *33*(5), 1057–1062. https://doi.org/10.1007/s10072-011-0894-8

Liberti, M. V, & Locasale, J. W. (2016). The Warburg Effect: How Does it Benefit Cancer Cells? (vol 41, pg 211, 2016). *Trends in Biochemical Sciences*, *41*(3, SI), 287. https://doi.org/10.1016/j.tibs.2016.01.004

Liebelt, B. D., Shingu, T., Zhou, X., Ren, J., Shin, S. A., & Hu, J. (2016). Glioma Stem Cells : Signaling , Microenvironment and Therapy. *Stem Cells International*. https://doi.org/10.1155/2016/7849890

Lin, L., Wang, G., Ming, J., Meng, X., Han, B., Sun, B., Cai, J., & Jiang, C. (2016). Analysis of expression and prognostic significance of vimentin and the response to temozolomide in glioma patients. *Tumor Biology*, *37*(11), 15333–15339. https://doi.org/10.1007/s13277-016-5462-7

López-Valero, I., Dávila, D., González-Martínez, J., Salvador-Tormo, N., Lorente, M., Saiz-Ladera, C., Torres, S., Gabicagogeascoa, E., Hernández-Tiedra, S., García-Taboada, E., Mendiburu-Eliçabe, M., Rodríguez-Fornés, F., Sánchez-Domínguez, R., Segovia, J. C., Sánchez-Gómez, P., Matheu, A., Sepúlveda, J. M., & Velasco, G. (2020). Midkine signaling maintains the self-renewal and tumorigenic capacity of glioma initiating cells. *Theranostics*, *10*(11), 5120–5136. https://doi.org/10.7150/thno.41450

López-Valero, I., Torres, S., Salazar-Roa, M., García-Taboada, E., Hernández-Tiedra, S., Guzmán, M., Sepúlveda, J. M., Velasco, G., & Lorente, M. (2018). Optimization of a preclinical therapy of cannabinoids in combination with temozolomide against glioma. *Biochemical Pharmacology*, *157*(August), 275–284. https://doi.org/10.1016/j.bcp.2018.08.023

Louis, D. N., Ohgaki, H., Wiestler, O. D., Cavenee, W. K., Burger, P. C., Jouvet, A., Scheithauer, B. W., & Kleihues, P. (2007). The 2007 WHO classification of tumours of the central nervous system. *Acta Neuropathologica*, *114*(2), 97–109. https://doi.org/10.1007/s00401-007-0243-4

Louis, D. N., Perry, A., Reifenberger, G., von Deimling, A., Figarella-Branger, D., Cavenee, W. K., Ohgaki, H., Wiestler, O. D., Kleihues, P., & Ellison, D. W. (2016). The 2016 World Health Organization Classification of Tumors of the Central Nervous System: a summary. *Acta Neuropathologica*, *131*(6), 803–820. https://doi.org/10.1007/s00401-016-1545-1

Lu, L., Annerén, C., Reedquist, K. A., Bos, J. L., & Welsh, M. (2000). NGF-dependent neurite outgrowth in PC12 cells overexpressing the Src homology 2-domain protein Shb requires activation of the Rap1 pathway. *Experimental Cell Research*, *259*(2), 370–377. https://doi.org/10.1006/excr.2000.4984

Lun, M., Lok, E., Gautam, S., Wu, E., & Wong, E. T. (2011). The natural history of extracranial metastasis from glioblastoma multiforme. *Journal of Neuro-Oncology*, *105*(2), 261–273. https://doi.org/10.1007/s11060-011-0575-8

Maia, V., Ortiz-Rivero, S., Sanz, M., Gutierrez-Berzal, J., Álvarez-Fernández, I., Gutierrez-Herrero, S., De Pereda, J. M., Porras, A., & Guerrero, C. (2013). C3G forms complexes with Bcr-Abl and p38α MAPK at the focal adhesions in chronic myeloid leukemia cells: Implication in the regulation of leukemic cell adhesion. *Cell Communication and Signaling*, *11*(1), 1–17. https://doi.org/10.1186/1478-811X-11-9

Maia, V., Sanz, M., Gutierrez-Berzal, J., de Luis, A., Gutierrez-Uzquiza, A., Porras, A., & Guerrero, C. (2009). C3G silencing enhances STI-571-induced apoptosis in CML cells through p38 MAPK activation, but it antagonizes STI-571 inhibitory effect on survival. *Cellular Signalling*, *21*(7), 1229–1235. https://doi.org/10.1016/j.cellsig.2009.03.015

Mani, S. A., Guo, W., Liao, M., Eaton, E. N., Zhou, A. Y., Brooks, M., Reinhard, F., Zhang, C. C., Campbell, L. L., Polyak, K., Brisken, C., Yang, J., & Weinberg, R. A. (2008). EMT creates cells with the properties of stem cells. *Cell*, *133*(4), 704–715. https://doi.org/10.1016/j.cell.2008.03.027.The

Marampon, F., Ciccarelli, C., & Zani, B. M. (2019). Biological Rationale for Targeting MEK / ERK Pathways in Anti-Cancer Therapy and to Potentiate Tumour Responses to Radiation. *International Journal of Molecular Sciences*, *20*(2530). https://doi.org/10.3390/ijms20102530

Martín-Encabo, S., Santos, E., & Guerrero, C. (2007). C3G mediated suppression of malignant transformation involves activation of PP2A phosphatases at the subcortical actin cytoskeleton. *Experimental Cell Research*, *313*(18), 3881–3891. https://doi.org/10.1016/j.yexcr.2007.07.036

Martín-Granado, V., Ortiz-Rivero, S., Carmona, R., Herrero, S. G., Barrera, M., San-Segundo, L., Sequera, C., Perdiguero, P., Lozano, F., Martín-Herrero, F., González-Porras, J. R., Muñoz-Chápuli, R., Porras, A., & Guerrero, C. (2017). C3G promotes a selective release of angiogenic factors from activated mouse platelets to regulate angiogenesis and tumor metastasis. *Oncotarget*, *8*(67), 110994–111011. https://doi.org/10.18632/oncotarget.22339

Mathupala, S. P., Ko, Y. H., & Pedersen, P. L. (2010). The pivotal roles of mitochondria in cancer: Warburg and beyond and encouraging prospects for effective therapies. *Biochimica et Biophysica Acta - Bioenergetics*, *1797*(6–7), 1225–1230. https://doi.org/10.1016/j.bbabio.2010.03.025

Matias, D., Balça-silva, J., Dubois, L. G., & Pontes, B. (2017). Dual treatment with shikonin and temozolomide reduces glioblastoma tumor growth, migration and glial-to-mesenchymal transition. *Cell Oncol.* https://doi.org/10.1007/s13402-017-0320-1

Meng, J., Li, P., Zhang, Q., Yang, Z., & Fu, S. (2014). A radiosensitivity gene signature in predicting glioma prognostic via EMT pathway. *Oncotarget*, *5*(13), 4683–4693. https://doi.org/10.18632/oncotarget.2088

Michelakis, E. D., Sutendra, G., Dromparis, P., Webster, L., Haromy, A., Niven, E., Maguire, C., Gammer, T. L., Mackey, J. R., Fulton, D., Abdulkarim, B., McMurtry, M. S., & Petruk, K. C. (2010). Metabolic modulation of glioblastoma with dichloroacetate. *Science Translational Medicine*, *2*(31). https://doi.org/10.1126/scitranslmed.3000677

Mikheeva, S. A., Mikheev, A. M., Petit, A., Beyer, R., Oxford, R. G., Khorasani, L., Maxwell, J., Glackin, C. A., Wakimoto, H., González-herrero, I., Sánchez-garcía, I., Silber, J. R., Horner, P. J., & Rostomily, R. C. (2010). *TWIST1 promotes invasion through mesenchymal change in human glioblastoma*. 1–18.

Mitra, A., & Radha, V. (2010). F-actin-binding domain of c-Abl regulates localized phosphorylation of C3G: Role of C3G in c-Abl-mediated cell death. *Oncogene*, *29*(32), 4528–4542. https://doi.org/10.1038/onc.2010.113

Mitra, Aninda, Kalayarasan, S., Gupta, V., & Radha, V. (2011). TC-PTP dephosphorylates the guanine nucleotide exchange factor C3G (RapGEF1) and negatively regulates differentiation of human neuroblastoma cells. *PLoS ONE*, *6*(8), 1–13. https://doi.org/10.1371/journal.pone.0023681

Moon, E. Y., Lee, G. H., Lee, M. S., Kim, H. M., & Lee, J. W. (2012). Phosphodiesterase inhibitors control A172 human glioblastoma cell death through cAMP-mediated activation of protein kinase A and Epac1/Rap1 pathways. *Life Sciences*, *90*(9–10), 373–380. https://doi.org/10.1016/j.lfs.2011.12.010

Nagano, M., Hoshino, D., Koshikawa, N., Akizawa, T., & Seiki, M. (2012). Turnover of focal adhesions and cancer cell migration. *International Journal of Cell Biology*, *2012*. https://doi.org/10.1155/2012/310616

Nakada, M., Niska, J. A., Miyamori, H., McDonough, W. S., Wu, J., Sato, H., & Berens, M. E. (2004). The Phosphorylation of EphB2 Receptor Regulates Migration and Invasion of Human Glioma Cells. *Cancer Research*, *64*(9), 3179–3185. https://doi.org/10.1158/0008-5472.CAN-03-3667

Nieto, M. A., Huang, R. Y. Y. J., Jackson, R. A. A., & Thiery, J. P. P. (2016). Emt: 2016. *Cell*, *166*(1), 21–45. https://doi.org/10.1016/j.cell.2016.06.028

NIH - National Cancer Institute (Colorectal cancer) webpage. (2020). www.cancer.gov/types/colorectal

Nishimura, Y., & Itoh, K. (2019). Involvement of SNX1 in regulating EGFR endocytosis in a gefitinib-resistant NSCLC cell lines. *Cancer Drug Resistance*, 539–549. https://doi.org/10.20517/cdr.2019.15

Nishimura, Y., Takiguchi, S., Ito, S., & Itoh, K. (2015). EGF-stimulated AKT activation is mediated by EGFR recycling via an early endocytic pathway in a gefitinib-resistant human lung cancer cell line. *International Journal of Oncology*, *46*(4), 1721–1729. https://doi.org/10.3892/ijo.2015.2871

Nowicki, M. O., Hayes, J. L., Chiocca, E. A., & Lawler, S. E. (2019). Proteomic analysis implicates Vimentin in Glioblastoma cell migration. *Cancers*, *11*(4). https://doi.org/10.3390/cancers11040466

Obenauf, A. C., & Massagué, J. (2015). Surviving at a Distance: Organ-Specific Metastasis. *Trends in Cancer*, *1*(1), 76–91. https://doi.org/10.1016/j.trecan.2015.07.009

Ohba, Y., Ikuta, K., Ogura, A., Matsuda, J., Mochizuki, N., Nagashima, K., Kurokawa, K., Mayer, B. J., Maki, K., Miyazaki, J. I., & Matsuda, M. (2001). Requirement for C3G-dependent Rap1 activation for cell adhesion and embryogenesis. *EMBO Journal*, *20*(13), 3333–3341. https://doi.org/10.1093/emboj/20.13.3333

Ohba, Y., Mochizuki, N., Yamashita, S., Chan, A. M., Schrader, J. W., Hattori, S., Nagashima, K., & Matsuda, M. (2000). Regulatory proteins of R-Ras, TC21/R-Ras2, and M-Ras/R-Ras3. *Journal of Biological Chemistry*, *275*(26), 20020–20026. https://doi.org/10.1074/jbc.M000981200

Ohgaki, H., & Kleihues, P. (2013). The definition of primary and secondary glioblastoma. *Clinical Cancer Research*, *19*(4), 764–772. https://doi.org/10.1158/1078-0432.CCR-12-3002

Okada, S., Matsuda, M., Anafi, M., Pawson, T., & Pessin, J. E. (1998). Insulin regulates the dynamic balance between Ras and Rap1 signaling by coordinating the assembly states of the Grb2-SOS and CrkII-C3G complexes. *EMBO Journal*, *17*(9), 2554–2565. https://doi.org/10.1093/emboj/17.9.2554

Okada, S., & Pessin, J. E. (1997). Insulin and epidermal growth factor stimulate a conformational change in Rap1 and dissociation of the CrkII-C3G complex. *Journal of Biological Chemistry*, *272*(45), 28179–28182. https://doi.org/10.1074/jbc.272.45.28179

Okino, K., Nagai, H., Nakayama, H., Doi, D., Yoneyama, K., Konishi, H., & Takeshita, T. (2006). Inactivation of Crk SH3 domain-binding guanine nucleotide-releasing factor (C3G) in cervical squamous cell carcinoma. *International Journal of Gynecological Cancer*, *16*(2), 763–771. https://doi.org/10.1111/j.1525-1438.2006.00352.x

Ophir Shalem, Neville E. Sanjana, Ella Hartenian, Xi Shi, David A. Scott, Tarjei S. Mikkelsen, Dirk Heckl, Benjamin L. Ebert, David E. Root, John G. Doench, Feng Zhang. (2014). Genome-Scale CRISPR-Cas9 Knockout Screening in Human Cells. *Science*, *314*, 84–87.

Ortiz-Rivero, S., Baquero, C., Hernández-Cano, L., Roldán-Etcheverry, J. J., Gutiérrez-Herrero, S., Fernández-Infante, C., Martín-Granado, V., Anguita, E., De Pereda, J. M., Porras, A., & Guerrero, C. (2018). C3G, through its GEF activity, induces megakaryocytic differentiation and proplatelet formation. *Cell Communication and Signaling*, *16*(1), 1–17. https://doi.org/10.1186/s12964-018-0311-5

Ostrom, Q. T., Bauchet, L., Davis, F. G., Deltour, I., Fisher, J. L., Langer, C. E., Pekmezci, M., Schwartzbaum, J. A., Turner, M. C., Walsh, K. M., Wrensch, M. R., & Barnholtz-Sloan, J. S. (2014). The epidemiology of glioma in adults: A state of the science review. *Neuro-Oncology*, *16*(7), 896–913. https://doi.org/10.1093/neuonc/nou087

Palanichamy, K., Jacob, J. R., Litzenberg, K. T., Ray-Chaudhury, A., & Chakravarti, A. (2018). Cells isolated from residual intracranial tumors after treatment express iPSC genes and possess neural lineage differentiation plasticity. *EBioMedicine*, *36*, 281–292. https://doi.org/10.1016/j.ebiom.2018.09.019

Panther software. (2019). www.pantherdb.org

Park, T. J., & Curran, T. (2008). Crk and Crk-like play essential overlapping roles downstream of disabled-1 in the reelin pathway. *Journal of Neuroscience*, *28*(50), 13551–13562. https://doi.org/10.1523/JNEUROSCI.4323-08.2008

Pearson, G. W. (2019). Control of Invasion by Epithelial-to-Mesenchymal Transition Programs during

Metastasis. *Journal of Clinical Medicine*, *8*(5), 646. https://doi.org/10.3390/jcm8050646

Pearson, J. R. D., & Regad, T. (2017). Targeting cellular pathways in glioblastoma multiforme. *Signal Transduction and Targeted Therapy*, *2*(February), 1–11. https://doi.org/10.1038/sigtrans.2017.40

Peinado, H., Olmeda, D., & Cano, A. (2007). Snail, ZEB and bHLH factors in tumour progression: An alliance against the epithelial phenotype? *Nature Reviews Cancer*, *7*(6), 415–428. https://doi.org/10.1038/nrc2131

Porras, Zuluaga, Black, Valladares, Álvarez, Ambrosino, Benito, Nebreda, A. (2004). p38␣ Mitogen-activated Protein Kinase Sensitizes Cells to Apoptosis Induced by Different Stimuli. *Molecular Biology of the Cell*, *15*, 922–933. https://doi.org/10.1091/mbc.E03

Priego, N., Arechederra, M., Sequera, C., Bragado, P., Vázquez-Carballo, A., Gutiérrez-Uzquiza, Á., Martín-Granado, V., Ventura, J. J., Kazanietz, M. G., Guerrero, C., & Porras, A. (2016). C3G knock-down enhances migration and invasion by increasing Rap1-mediated p38α activation, while it impairs tumor growth through p38α-independent mechanisms. *Oncotarget*, *7*(29), 45060–45078. https://doi.org/10.18632/oncotarget.9911

Priego, N., Zhu, L., Monteiro, C., Mulders, M., Wasilewski, D., Bindeman, W., Doglio, L., Martínez, L., Martínez-Saez, E., Cajal, S. R. Y., Megías, D., Hernández-Encinas, E., Blanco-Aparicio, C., Martínez, L., Zarzuela, E., Muñoz, J., Fustero-Torre, C., Piñeiro-Yáñez, E., Hernández-Laín, A., … Valiente, M. (2018). STAT3 labels a subpopulation of reactive astrocytes required for brain metastasis article. *Nature Medicine*, *24*(7), 1024–1035. https://doi.org/10.1038/s41591-018-0044-4

Prolo, L. M., Li, A., Owen, S. F., Parker, J. J., Foshay, K., Nitta, R. T., Morgens, D. W., Bolin, S., Wilson, C. M., Vega L, J. C. M., Luo, E. J., Nwagbo, G., Waziri, A., Li, G., Reimer, R. J., Bassik, M. C., & Grant, G. A. (2019). Targeted genomic CRISPR-Cas9 screen identifies MAP4K4 as essential for glioblastoma invasion. *Scientific Reports*, *9*(1), 1–12. https://doi.org/10.1038/s41598-019-50160-w

ProteinAtlas database. (2016). www.proteinatlas.org/

Pye, D. S., Rubio, I., Pusch, R., Lin, K., Pettitt, A. R., & Till, K. J. (2013). Chemokine Unresponsiveness of Chronic Lymphocytic Leukemia Cells Results from Impaired Endosomal Recycling of Rap1 and Is Associated with a Distinctive Type of Immunological Anergy. *The Journal of Immunology*, *191*(3), 1496–1504. https://doi.org/10.4049/jimmunol.1203484

Radha, S. C. N. and V. (2019). *Running title: C3G (RapGEF1) localizes to the mother centriole and regulates centriole division and primary cilia dynamics*.

Radha, V., Mitra, A., Dayma, K., & Sasikumar, K. (2011). Signalling to actin: Role of C3G, a multitasking guanine-nucleotide- exchange factor. *Bioscience Reports*, *31*(4), 231–244. https://doi.org/10.1042/BSR20100094

Radha, V., Rajanna, A., Gupta, R. K., Dayma, K., & Raman, T. (2008). The guanine nucleotide exchange factor, C3G regulates differentiation and survival of human neuroblastoma cells. *Journal of Neurochemistry*, *107*(5), 1424–1435. https://doi.org/10.1111/j.1471-4159.2008.05710.x

Radha, V., Rajanna, A., Mitra, A., Rangaraj, N., & Swarup, G. (2007). C3G is required for c-Abl-induced filopodia and its overexpression promotes filopodia formation. *Experimental Cell Research*, *313*(11), 2476–2492. https://doi.org/10.1016/j.yexcr.2007.03.019

Radha, V., Rajanna, A., & Swarup, G. (2004). Phosphorylated guanine nucleotide exchange factor C3G, induced by pervanadate and Src family kinases localizes to the Golgi and subcortical actin cytoskeleton. *BMC Cell Biology*, *5*, 1–15. https://doi.org/10.1186/1471-2121-5-31

Ramachandran, S., Coffin, S. L., Tang, T. Y., Jobaliya, C. D., Spengler, R. M., & Davidson, B. L. (2016). Cis-acting single nucleotide polymorphisms alter MicroRNA-mediated regulation of human brainexpressed transcripts. *Human Molecular Genetics*, *25*(22), 4939–4950. https://doi.org/10.1093/hmg/ddw317

Raza, A., Franklin, M. J., & Dudek, A. Z. (2010). Pericytes and vessel maturation during tumor angiogenesis and metastasis. *American Journal of Hematology*, *85*(8), 593–598. https://doi.org/10.1002/ajh.21745

Roger Stupp, M.D., Warren P. Mason, M.D., Martin J. van den Bent, M.D., Michael Weller, M.D., Barbara Fisher, M.D., Martin J.B. Taphoorn, M.D., Karl Belanger, M.D., Alba A. Brandes, M.D., Christine Marosi, M.D., Ulrich Bogdahn, M.D., Jürgen Curschmann, M., M. . (2005). Radiotherapy plus Concomitant and Adjuvant Temozolomide for Glioblastoma. *The New England Journal of Medicine*, *352*(10), 987–996.

Roshan Mahabir, Mishie Tanino, Aiman Elmansuri, Lei Wang, Taichi Kimura, Tamio Itoh, Yusuke Ohba, Hiroshi Nishihara, Hiroki Shirato, Masumi Tsuda, and S. T. (2013). Sustained elevation of Snail promotes glial-mesenchymal transition after irradiation in malignant glioma. *Neuro-Oncology*, *16*(5), 671–685. https://doi.org/10.1093/neuonc/not239

Ryan J. Sullivan 1 , Jeffrey R. Infante 2 , Filip Janku 3 , Deborah Jean Lee Wong 4 , Jeffrey A. Sosman 5 , Vicki Keedy 5 , Manish R. Patel 6 , Geoffrey I. Shapiro 7 , James W. Mier 8 , Anthony W. Tolcher 9 , Andrea Wang-Gillam 10 , Mario Sznol 11 , Keith, and B. T. L. 12. (2018). First-in-Class ERK1 / 2 Inhibitor Ulixertinib (BVD-523) in Patients with MAPK Mutant Advanced Solid Tumors : Results of a Phase I Dose-Escalation and Expansion Study. *Cancer Discov.*, 185–195. https://doi.org/10.1158/2159-8290.CD-17-1119

Sakkab, D., Lewitzky, M., Posern, G., Schaeper, U., Sachs, M., Birchmeier, W., & Feller, S. M. (2000). Signaling of hepatocyte growth factor/scatter factor (HGF) to the small GTPase Rap1 via the large docking protein Gab1 and the adapter protein CRKL. *Journal of Biological Chemistry*, *275*(15), 10772–10778. https://doi.org/10.1074/jbc.275.15.10772

Samuelsson, J., Alonso, S., Ruiz-Larroya, T., Cheung, T. H., Wong, Y. F., & Perucho, M. (2011). Frequent somatic demethylation of RAPGEF1/C3G intronic sequences in gastrointestinal and gynecological cancer. *International Journal of Oncology*, *38*(6), 1575–1577. https://doi.org/10.3892/ijo.2011.972

Sasi Kumar, K., Ramadhas, A., Nayak, S. C., Kaniyappan, S., Dayma, K., & Radha, V. (2015). C3G (RapGEF1), a regulator of actin dynamics promotes survival and myogenic differentiation of mouse mesenchymal cells. *Biochimica et Biophysica Acta - Molecular Cell Research*, *1853*(10), 2629–2639. https://doi.org/10.1016/j.bbamcr.2015.06.015

Sato, A., Okada, M., Shibuya, K., Watanabe, E., Seino, S., Narita, Y., Shibui, S., Kayama, T., & Kitanaka, C. (2014). Pivotal role for ROS activation of p38 MAPK in the control of differentiation and tumor-initiating capacity of glioma-initiating cells. *Stem Cell Research*, *12*(1), 119–131. https://doi.org/10.1016/j.scr.2013.09.012

Sayyah, J., Bartakova, A., Nogal, N., Quilliam, L. A., Stupack, D. G., & Brown, J. H. (2014). The Ras-related protein, Rap1A, mediates thrombin-stimulated, integrin-dependent glioblastoma cell proliferation and tumor growth. *Journal of Biological Chemistry*, *289*(25), 17689–17698. https://doi.org/10.1074/jbc.M113.536227

Schönherr, C., Yang, H. L., Vigny, M., Palmer, R. H., & Hallberg, B. (2010). Anaplastic lymphoma kinase activates the small GTPase Rap1 via the Rap1-specific GEF C3G in both neuroblastoma and PC12 cells. *Oncogene*, *29*(19), 2817–2830. https://doi.org/10.1038/onc.2010.27

Sequera, C., Bragado, P., Manzano, S., & Arechederra, M. (2020). C3G Is Upregulated in Hepatocarcinoma, Contributing to Tumor Growth and Progression and to HGF/MET Pathway Activation. *Cancers*, *12*, 2282.

Sequera, C., Manzano, S., Guerrero, C., & Porras, A. (2018). How Rap and its GEFs control liver physiology and cancer development. C3G alterations in human hepatocarcinoma. *Hepatic Oncology*, *5*(1), HEP05. https://doi.org/10.2217/hep-2017-0026

Shah, B., Lutter, D., Bochenek, M. L., Kato, K., Tsytsyura, Y., Glyvuk, N., Sakakibara, A., Klingauf, J., Adams, R. H., & Püschel, A. W. (2016). C3G/Rapgef1 is required in multipolar neurons for the transition to a bipolar morphology during cortical development. *PLoS ONE*, *11*(4), 1–22. https://doi.org/10.1371/journal.pone.0154174

Shakyawar, D. K., Dayma, K., Ramadhas, A., Varalakshmi, C., & Radha, V. (2017). C3G shows regulated nucleocytoplasmic exchange and represses histone modifcations associated with euchromatin. *Molecular Biology of the Cell*, *28*(7), 984–995. https://doi.org/10.1091/mbc.E16-09-0660

Shakyawar, D. K., Muralikrishna, B., & Radha, V. (2018). C3G dynamically associates with nuclear speckles and regulates mRNA splicing. *Molecular Biology of the Cell*, *29*(9), 1111–1124.

https://doi.org/10.1091/mbc.E17-07-0442

Shamir, E. R., Coutinho, K., Georgess, D., Auer, M., & Ewald, A. J. (2016). Twist1-positive epithelial cells retain adhesive and proliferative capacity throughout dissemination. *Biology Open*, *5*(9), 1216–1228. https://doi.org/10.1242/bio.019703

Shipitsin, M., Campbell, L. L., Argani, P., Weremowicz, S., Bloushtain-Qimron, N., Yao, J., Nikolskaya, T., Serebryiskaya, T., Beroukhim, R., Hu, M., Halushka, M. K., Sukumar, S., Parker, L. M., Anderson, K. S., Harris, L. N., Garber, J. E., Richardson, A. L., Schnitt, S. J., Nikolsky, Y., … Polyak, K. (2007). Molecular Definition of Breast Tumor Heterogeneity. *Cancer Cell*, *11*(3), 259–273. https://doi.org/10.1016/j.ccr.2007.01.013

Shiraishi, T., Verdone, J. E., Huang, J., Kahlert, U. D., James, R., Torga, G., Zarif, J., Epstein, T., Gatenby, R., McCartney, A., Elisseeff, J., Mooney, S., An, S., & Pienta, K. (2014). Glycolysis is the primary bioenergetic pathway for cell motility and cytoskeletal remodeling in human prostate and breast cancer cells. *Oncotarget*, *6*(1), 130–143. https://doi.org/10.18632/oncotarget.2766

Shirakihara, T., Horiguchi, K., Miyazawa, K., Ehata, S., Shibata, T., Morita, I., Miyazono, K., & Saitoh, M. (2011). TGF-β regulates isoform switching of FGF receptors and epithelial-mesenchymal transition. *EMBO Journal*, *30*(4), 783–795. https://doi.org/10.1038/emboj.2010.351

Shivakrupa, R., Radha, V., Sudhakar, C., & Swarup, G. (2003). Physical and Functional Interaction between Hck Tyrosine Kinase and Guanine Nucleotide Exchange Factor C3G Results in Apoptosis, Which Is Independent of C3G Catalytic Domain. *Journal of Biological Chemistry*, *278*(52), 52188–52194. https://doi.org/10.1074/jbc.M310656200

Siebzehnrubl, F. A., Silver, D. J., Tugertimur, B., Deleyrolle, L. P., Siebzehnrubl, D., Sarkisian, M. R., Devers, K. G., Yachnis, A. T., Kupper, M. D., Neal, D., Nabilsi, N. H., Kladde, M. P., Suslov, O., Brabletz, S., Brabletz, T., Reynolds, B. A., & Steindler, D. A. (2013). The ZEB1 pathway links glioblastoma initiation , invasion and chemoresistance. *EMBO Molecular Medicine*, *5*, 1196–1212.

Silantyev, A. S., Falzone, L., Libra, M., Gurina, O. I., Sutton, C. W., Mitsias, P. D., & Tsatsakis, A. (2019). Current and Future Trends on Diagnosis and Prognosis of Glioblastoma : From Molecular Biology to Proteomics. *Cells*, *8*(863). https://doi.org/10.3390/cells8080863

Soda, Y., Marumoto, T., Friedmann-Morvinski, D., Soda, M., Liu, F., Michiue, H., Pastorino, S., Yang, M., Hoffman, R. M., Kesari, S., & Verma, I. M. (2011). Transdifferentiation of glioblastoma cells into vascular endothelial cells. *Proceedings of the National Academy of Sciences of the United States of America*, *108*(11), 4274–4280. https://doi.org/10.1073/pnas.1016030108

Soledad Sosa, Paloma Bragado, and Julio A. Aguirre-Ghiso, M. (2014). Mechanisms of disseminated cancer cell dormancy: an awakening field. *Nat Rev Cancer.*, *14*(9), 611–612. https://doi.org/doi:10.1038/nrc3793

Sriram, D., Chintala, R., Parthasaradhi, B. V. V., Nayak, S. C., Mariappan, I., & Radha, V. (2020). Expression of a novel brain specific isoform of C3G is regulated during development. *Scientific Reports*, *10*(1), 1–17. https://doi.org/10.1038/s41598-020-75813-z

Stankic, M., Pavlovic, S., Chin, Y., Brogi, E., Padua, D., Norton, L., Massagué, J., & Benezra, R. (2013). TGF-β-Id1 signaling opposes twist1 and promotes metastatic colonization via a mesenchymal-to-epithelial transition. *Cell Reports*, *5*(5), 1228–1242. https://doi.org/10.1016/j.celrep.2013.11.014

Sternlicht, M. D., & Werb, Z. (2001). How Matrix Metalloproteinases Regulate Cell Behavior. *Annual Review of Cell and Developmental Biology*, *17*(1), 463–516. https://doi.org/10.1146/annurev.cellbio.17.1.463

Strickland, M., & Stoll, E. A. (2017). Metabolic reprogramming in glioma. *Frontiers in Cell and Developmental Biology*, *5*(APR). https://doi.org/10.3389/fcell.2017.00043

Sun, T., Plutynski, A., Ward, S., & Rubin, J. B. (2015). An integrative view on sex differences in brain tumors. *Cellular and Molecular Life Sciences*, *72*(17), 3323–3342. https://doi.org/10.1007/s00018-015-1930-2

Takahashi, M., Rikitake, Y., Nagamatsu, Y., Hara, T., Ikeda, W., Hirata, K. I., & Takai, Y. (2008). Sequential activation of Rap1 and Rac1 small G proteins by PDGF locally at leading edges of NIH3T3 cells.

Genes to Cells, *13*(6), 549–569. https://doi.org/10.1111/j.1365-2443.2008.01187.x

Takai, S., Tanaka, M., Sugimura, H., Yamada, K., Naito, Y., Kino, I., & Matsuda, M. (1994). Mapping of the human C3G gene coding a guanine nucleotide releasing protein for Ras family to 9q34.3 by fluorescence in situ hybridization. *Human Genetics*, *94*(5), 549–550. https://doi.org/10.1007/BF00211024

Tanaka, S., Morishita, T., Hashimoto, Y., Hattori, S., Nakamura, S., Shibuya, M., Matuoka, K., Takenawa, T., Kurata, T., Nagashima, K., & Matsuda, M. (1994). C3G, a guanine nucleotide-releasing protein expressed ubiquitously, binds to the Src homology 3 domains of CRK and GRB2/ASH proteins. *Proceedings of the National Academy of Sciences of the United States of America*, *91*(8), 3443–3447. https://doi.org/10.1073/pnas.91.8.3443

Tardito, S., Oudin, A., Ahmed, S. U., Fack, F., Keunen, O., Zheng, L., Miletic, H., Sakariassen, P. Ø., Weinstock, A., Wagner, A., Lindsay, S. L., Hock, A. K., Barnett, S. C., Ruppin, E., Harald MØrkve, S., Lund-Johansen, M., Chalmers, A. J., Bjerkvig, R., Niclou, S. P., & Gottlieb, E. (2015). Glutamine synthetase activity fuels nucleotide biosynthesis and supports growth of glutamine-restricted glioblastoma. *Nature Cell Biology*, *17*(12), 1556–1568. https://doi.org/10.1038/ncb3272

TCGA. (2008). Comprehensive genomic characterization defines human glioblastoma genes and core pathways The. *Genomics*, *455*(7216), 1061–1068. https://doi.org/10.1038/nature07385.Comprehensive

Tennant, D. A., Durán, R. V., Boulahbel, H., & Gottlieb, E. (2009). Metabolic transformation in cancer. *Carcinogenesis*, *30*(8), 1269–1280. https://doi.org/10.1093/carcin/bgp070

Teslaa, T., & Teitell, M. A. (2014). Techniques to monitor glycolysis. *Methods in Enzymology*, *542*, 91–114. https://doi.org/10.1016/B978-0-12-416618-9.00005-4

Thiery, J. P., Acloque, H., Huang, R. Y. J., & Nieto, M. A. (2009). Epithelial-Mesenchymal Transitions in Development and Disease. *Cell*, *139*(5), 871–890. https://doi.org/10.1016/j.cell.2009.11.007

Tian, M., Ma, W., Chen, Y., Yu, Y., Zhu, D., Shi, J., & Zhang, Y. (2018). Impact of gender on the survival of patients with glioblastoma. *Bioscience Reports*, *38*(6), 1–9. https://doi.org/10.1042/BSR20180752

Tomas; Clare E. Futter; Eden, A. (2014). EGF receptor trafficking: consequences for signaling and cancer. *Trends Cell Biol.*, *24*(1), 26–34. https://doi.org/10.1016/j.tcb.2013.11.002

Tong, L., Yi, L. I., Liu, P., Abeysekera, I. R., & Hai, L. (2018). Tumour cell dormancy as a contributor to the reduced survival of GBM patients who received standard therapy. *Oncology Reports*, *40*, 463–471.

Toni Celià-Terrassa, Óscar Meca-Cortés, Francesca Mateo, Alexia Martínez de Paz, Nuria Rubio, Anna Arnal-Estapé, Brian J. Ell, Raquel Bermudo, Alba Díaz, Marta Guerra-Rebollo, Juan José Lozano, Conchi Estarás, Catalina Ulloa, Marian Martínez-Balbás, Antonio García de Herreros, Roger R. Gomis, Yibin Kang, Jerónimo Blanco, Pedro L. Fernández and Timothy M. Thomson. (2012). Epithelial-mesenchymal transition can suppress major attributes of human epithelial tumor-initiating cells. *The Journal of Clinical Investigation*, *122*(5), 1849–1868. https://doi.org/10.1172/JCI59218.ity

Tsai, J. H., Donaher, J. L., Murphy, D. A., Chau, S., & Yang, J. (2012). Spatiotemporal regulation of EMT is Essential for Squamous Cell Carcinoma Metastasis. *Changes*, *29*(6), 997–1003. https://doi.org/10.1016/j.biotechadv.2011.08.021.Secreted

Tso, C., Shintaku, P., Chen, J., Liu, Q., Liu, J., Chen, Z., Yoshimoto, K., Mischel, P. S., Cloughesy, T. F., Liau, L. M., & Nelson, S. F. (2006). *Primary Glioblastomas Express Mesenchymal Stem-Like Properties*. *4*(September), 607–620. https://doi.org/10.1158/1541-7786.MCR-06-0005

Turner, D. A., & Adamson, D. C. (2011). Neuronal-astrocyte metabolic interactions: Understanding the transition into abnormal astrocytoma metabolism. *Journal of Neuropathology and Experimental Neurology*, *70*(3), 167–176. https://doi.org/10.1097/NEN.0b013e31820e1152

UCSC Xena webpage. (2020). www.xena.ucsc.edu/welcome-to-ucsc-xena/

Utreras, E., Henriquez, D., Contreras-vallejos, E., Olmos, C., Di, A., Maass, A., Kulkarni, A. B., & Gonzalez-billault, C. (2013). CDK5 REGULATES RAP1 ACTIVITY. *Neurochem Int.*, *62*(6), 848–853. https://doi.org/10.1016/j.neuint.2013.02.011.CDK5

Uttamsingh, S., Bao, X., Nguyen, K. T., Bhanot, M., Gong, J., Chan, J. L. K., Liu, F., Chu, T. T., & Wang, L. H. (2008). Synergistic effect between EGF and TGF-β1 in inducing oncogenic properties of intestinal epithelial cells. *Oncogene*, *27*(18), 2626–2634. https://doi.org/10.1038/sj.onc.1210915

Valvona, C. J., Fillmore, H. L., Nunn, P. B., & Pilkington, G. J. (2016). The Regulation and Function of Lactate Dehydrogenase A: Therapeutic Potential in Brain Tumor. *Brain Pathology*, *26*(1), 3–17. https://doi.org/10.1111/bpa.12299

van Bergen en Henegouwen, P. M. P., den Hartigh, J. C., Romeyn, P., Verkleij, A. J., & Boonstra, J. (1992). The epidermal growth factor receptor is associated with actin filaments. *Experimental Cell Research*, *199*(1), 90–97. https://doi.org/10.1016/0014-4827(92)90465-K

Van Den Berghe, N., Cool, R. H., Horn, G., & Wittinghofer, A. (1997). Biochemical characterization of C3G: An exchange factor that discriminates between Rap1 and Rap2 and is not inhibited by Rap1A(S17N). *Oncogene*, *15*(7), 845–850. https://doi.org/10.1038/sj.onc.1201407

Vander Heiden, M., Cantley, L., & Thompson, C. (2009). The Metabolic Requirements of Cell Proliferation. *Science*, *324*(5930), 1029–1033. https://doi.org/10.1126/science.1160809.Understanding

Velásquez, C., Mansouri, S., Mora, C., Nassiri, F., Suppiah, S., Martino, J., Zadeh, G., & Fernández-Luna, J. L. (2019). Molecular and Clinical Insights into the Invasive Capacity of Glioblastoma Cells. *Journal of Oncology*, *2019*. https://doi.org/10.1155/2019/1740763

Verhaak, R. G. W., Hoadley, K. A., Purdom, E., Wang, V., Qi, Y., Wilkerson, M. D., Miller, C. R., Ding, L., Golub, T., Mesirov, J. P., Alexe, G., Lawrence, M., O'Kelly, M., Tamayo, P., Weir, B. A., Gabriel, S., Winckler, W., Gupta, S., Jakkula, L., … Hayes, D. N. (2010). Integrated Genomic Analysis Identifies Clinically Relevant Subtypes of Glioblastoma Characterized by Abnormalities in PDGFRA, IDH1, EGFR, and NF1. *Cancer Cell*, *17*(1), 98–110. https://doi.org/10.1016/j.ccr.2009.12.020

Villar, V. H., Merhi, F., Djavaheri-Mergny, M., & Durán, R. V. (2015). Glutaminolysis and autophagy in cancer. *Autophagy*, *11*(8), 1198–1208. https://doi.org/10.1080/15548627.2015.1053680

Voss, A. K., Britto, J. M., Dixon, M. P., Sheikh, B. N., Collin, C., Tan, S. S., & Thomas, T. (2008). C3G regulates cortical neuron migration, preplate splitting and radial glial cell attachment. *Development*, *135*(12), 2139–2149. https://doi.org/10.1242/dev.016725

Voss, A. K., Gruss, P., & Thomas, T. (2003). The guanine nucleotide exchange factor C3G is necessary for the formation of focal adhesions and vascular maturation. *Development*, *130*(2), 355–367. https://doi.org/10.1242/dev.00217

Voss, A. K., Krebs, D. L., & Thomas, T. (2006). C3G regulates the size of the cerebral cortex neural precursor population. *EMBO Journal*, *25*(15), 3652–3663. https://doi.org/10.1038/sj.emboj.7601234

Walker, C., Mojares, E., & Del Río Hernández, A. (2018). Role of extracellular matrix in development and cancer progression. In *International Journal of Molecular Sciences* (Vol. 19, Issue 10). https://doi.org/10.3390/ijms19103028

Wang, J., Sakariassen, P. Ø., Tsinkalovsky, O., Immervoll, H., Bøe, S. O., & Svendsen, A. (2008). *CD133 negative glioma cells form tumors in nude rats and give rise to CD133 positive cells*. *768*, 761–768. https://doi.org/10.1002/ijc.23130

Wang, Lei, Zhan, W., Xie, S., Hu, J., Shi, Q., Zhou, X., Wu, Y., Wang, S., Fei, Z., & Yu, R. (2014). Over-expression of Rap2a inhibits glioma migration and invasion by down-regulating p-AKT. *Cell Biology International*, *38*(3), 326–334. https://doi.org/10.1002/cbin.10213

Wang, Lulu, Liu, Q., Zhao, H., Cui, K., Yao, L., Nie, F., Jin, G., Hao, A., & Wong, S. T. C. (2013). Differential effects of low- and high-dose GW2974, a dual epidermal growth factor receptor and HER2 kinase inhibitor, on glioblastoma multiforme invasion. *Journal of Neuroscience Research*, *91*(1), 128–137. https://doi.org/10.1002/jnr.23140

Wang, S. D., Rath, P., Lal, B., Richard, J. P., Li, Y., Goodwin, C. R., Laterra, J., & Xia, S. (2012). EphB2 receptor controls proliferation/migration dichotomy of glioblastoma by interacting with focal adhesion kinase. *Oncogene*, *31*(50), 5132–5143. https://doi.org/10.1038/onc.2012.16

Wang, X., Wang, S., Li, X., Jin, S., Xiong, F., & Wang, X. (2017). The critical role of EGF-β-catenin

signaling in the epithelial-mesenchymal transition in human glioblastoma. *OncoTargets and Therapy*, *10*, 2781–2789. https://doi.org/10.2147/OTT.S138908

Wang, Y., Yang, J., Zheng, H., Tomasek, G. J., Zhang, P., Paul, E., Lee, E. Y. P., & Zhu, Y. (2009). Expression of mutant p53 proteins implicates a lineage relationship between neural stem cells and malignant astrocytic glioma in a murine model. *Cancer Cell*, *15*(6), 514–526.

Watcharin Loilome. (2009). Glioblastoma cell growth is suppressed by disruption of fibroblast growth factor pathway signaling. *J Neurooncol*, *94*, 359–366. https://doi.org/10.1007/s11060-009-9885-5

Wertheimer, E., Gutierrez-Uzquiza, A., Rosemblit, C., Lopez-Haber, C., Sosa, S., Kazanietz, M. G., & Sosa, M. S. (2012). Rac signaling in breast cancer: A tale of GEFs and GAPs. *Cellular Signalling*, *24*(2), 353–362. https://doi.org/10.1016/j.cellsig.2011.08.011.Rac

Wheelock, M. J., Shintani, Y., Maeda, M., Fukumoto, Y., & Johnson, K. R. (2008). Cadherin switching. *Journal of Cell Science*, *121*(6), 727–735. https://doi.org/10.1242/jcs.000455

Wijnhoven, B. P. L., Dinjens, W. N. M., & Pignatelli, M. (2000). E-cadherin-catenin cell-cell adhesion complex and human cancer. *British Journal of Surgery*, *87*(8), 992–1005. https://doi.org/10.1046/j.1365-2168.2000.01513.x

Williams, K. C., & Coppolino, M. G. (2014). SNARE-dependent interaction of Src, EGFR and ß1 integrin regulates invadopodia formation and tumor cell invasion. *Journal of Cell Science*, *127*(8), 1712–1725. https://doi.org/10.1242/jcs.134734

Woolbright, B. L., Rajendran, G., Harris, R. A., & Iii, J. A. T. (2019). *Metabolic Flexibility in Cancer : Targeting the Pyruvate Dehydrogenase Kinase : Pyruvate Dehydrogenase Axis*. 1673–1682. https://doi.org/10.1158/1535-7163.MCT-19-0079

World Cancer Research Fund webpage. (2020). www.wcrf.org

World Health Organization (WHO) webpage. (2020). www.who.int/health-topics/cancer

Wu, Chun-Fai Lai and William C. Mobley, C. (2001). Nerve growth factor activates persistent Rap1 signaling in endosomes. *Journal of Neuroscience*, *21*(15), 5406–5416. https://doi.org/10.1523/jneurosci.21-15-05406.2001

Yadi Wu, Jiong Deng, Piotr G. Rychahou, Suimin Qiu, B. Mark Evers, and Binhua P. Zhou. (2009). Stabilization of Snail by NF-κB Is Required for Inflammation- Induced Cell Migration and Invasion. *Cancer Cell*, *15*(5), 416–428. https://doi.org/10.1161/CIRCULATIONAHA.110.956839

Yang, D., Zhang, L., Zhang, Z., Hu, S., Fu, Y., Laukkanen, J. A., & Li, G. (2019). Silencing of C3G increases cardiomyocyte survival inhibition and apoptosis via regulation of p-ERK1/2 and bax. *Clinical and Experimental Pharmacology and Physiology*, *46*(3), 237–245. https://doi.org/10.1111/1440-1681.13027

Yang, L., Hou, Y., Yuan, J., Tang, S., Zhang, H., Zhu, Q., Du, Y. e., Zhou, M., Wen, S., Xu, L., Tang, X., Cui, X., & Liu, M. (2015). Twist promotes reprogramming of glucose metabolism in breast cancer cells through PI3K/AKT and p53 signaling pathways. *Oncotarget*, *6*(28), 25755–25769. https://doi.org/10.18632/oncotarget.4697

Yip, Y. P., Thomas, T., Voss, A. K., & Yip, J. W. (2012). Migration of sympathetic preganglionic neurons in the spinal cord of a C3G-deficient mouse suggests that C3G acts in the reelin signaling pathway. *Journal of Comparative Neurology*, *520*(14), 3194–3202. https://doi.org/10.1002/cne.23086

Zahonero, C., & Sánchez-Gómez, P. (2014). EGFR-dependent mechanisms in glioblastoma: Towards a better therapeutic strategy. *Cellular and Molecular Life Sciences*, *71*(18), 3465–3488. https://doi.org/10.1007/s00018-014-1608-1

Zahra, K., Dey, T., Mishra, S. P., & Pandey, U. (2020). *Pyruvate Kinase M2 and Cancer : The Role of PKM2 in Promoting Tumorigenesis*. *10*(March), 1–9. https://doi.org/10.3389/fonc.2020.00159

Zeisberg, M., Yang, C., Martino, M., Duncan, M. B., Rieder, F., Tanjore, H., & Kalluri, R. (2007). Fibroblasts derive from hepatocytes in liver fibrosis via epithelial to mesenchymal transition. *Journal of Biological*

Chemistry, *282*(32), 23337–23347. https://doi.org/10.1074/jbc.M700194200

Zhang, L. Y., Guo, Q., Guan, G. F., Cheng, W., Cheng, P., & Wu, A. H. (2019). Integrin Beta 5 Is a Prognostic Biomarker and Potential Therapeutic Target in Glioblastoma. *Frontiers in Oncology*, *9*(September), 1–12. https://doi.org/10.3389/fonc.2019.00904

Zhao, J., Zhang, L., Dong, X., Liu, L., Huo, L., & Chen, H. (2018). High Expression of Vimentin is Associated with Progression and a Poor Outcome in Glioblastoma. *Applied Immunohistochemistry and Molecular Morphology*, *26*(5), 337–344. https://doi.org/10.1097/PAI.0000000000000420

Zhou, N., Gutierrez-Uzquiza, A., Zheng, X. Y., Chang, R., Vogl, D. T., Garfall, A. L., Bernabei, L., Saraf, A., Florens, L., Washburn, M. P., Illendula, A., Bushweller, J. H., & Busino, L. (2019). RUNX proteins desensitize multiple myeloma to lenalidomide via protecting IKZFs from degradation. *Leukemia*, *33*(8), 2006–2021. https://doi.org/10.1038/s41375-019-0403-2

Zuluaga, S., Gutiérrez-Uzquiza, A., Bragado, P., Álvarez-Barrientos, A., Benito, M., Nebreda, A. R., & Porras, A. (2007). p38α MAPK can positively or negatively regulate Rac-1 activity depending on the presence of serum. *FEBS Letters*, *581*(20), 3819–3825. https://doi.org/10.1016/j.febslet.2007.06.078

Appendixes

APPENDIX 1 – C3G knock-out using CRISPR/Cas9 technology: Generation of U87-Cas9^{+} cells and alteration in genomic DNA in LG3 pool of cells

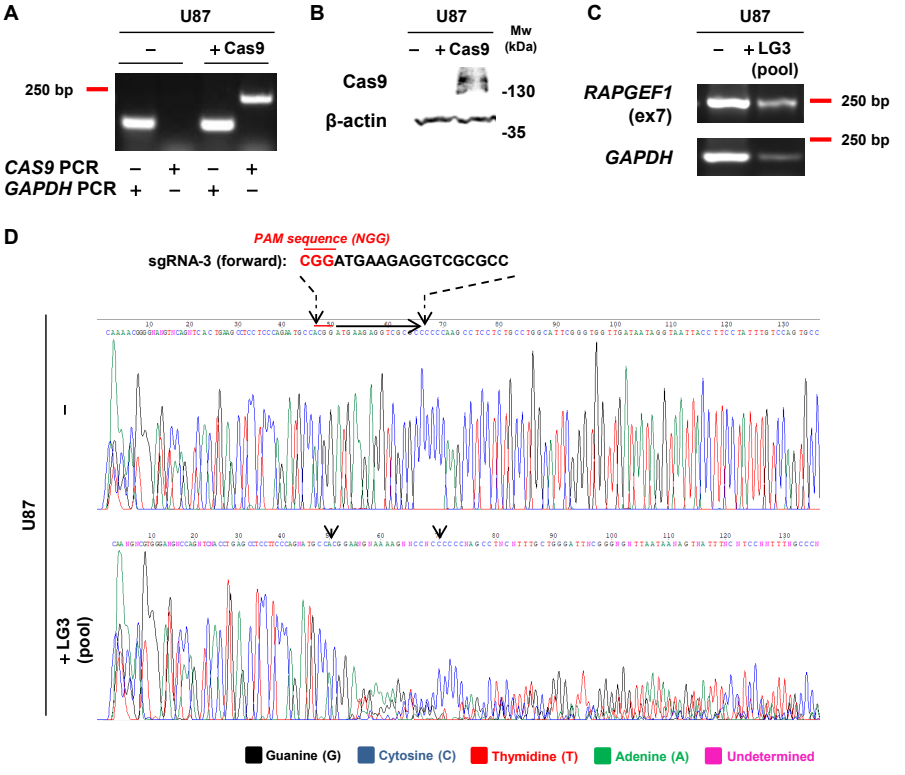

(***A-B***) Parental U87 cells were infected with lentiCas9-Blast lentiviral particles, generating U87-Cas9^{+} pool of cells. *CAS9* gene incorporation in genomic DNA was detected by PCR using specific primers (250 bp fragment) and GAPDH as a control (*A*) and Cas9 protein expression was checked by western blot analysis using β-actin as a loading control (*B*). (***C***) PCR amplification of genomic region targeted by pLentiguide-hC3G-KO-3 plasmid from exon 7 (ex7) of *RAPGEF1* gene (250 bp), using GAPDH as a control. (***D***) Sanger sequencing of the amplified sequence from *RAPGEF1* gene (exon 7) and detection of genomic alterations generated by Cas9 action guided by sgRNA-3, inserted in pLentiguide-hC3G-KO-3 construct.

APPENDIX 2 – C3G knock-out using CRISPR/Cas9 technology: Generation of pLentiguide-hC3G-KO-#1/2/3/5 constructs

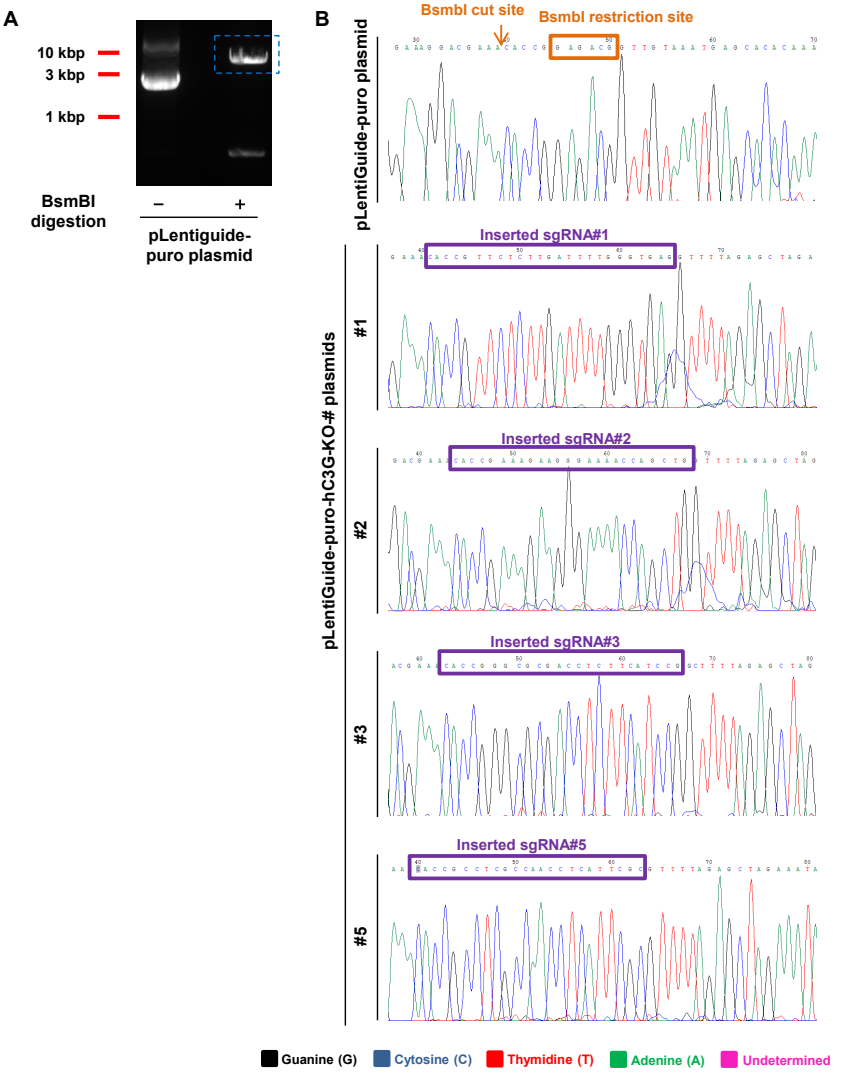

(*A*) pLentiGuide-puro plasmid (from *Addgene*) was digested with BsmBI and the corresponding fragment (around 8kb, marked in the figure by a blue square) was gel-extracted. **(*B*)** Sanger sequencing of pLentiGuide-puro and pLentiGuide-puro-#1/2/3/5 constructs to detect the incorporation of the corresponding sgRNA in each.

APPENDIX 3 – C3G full-length (*FL*) overexpression: Generation of pCDNA3-C3G-FL construct and overexpression in 293T cells

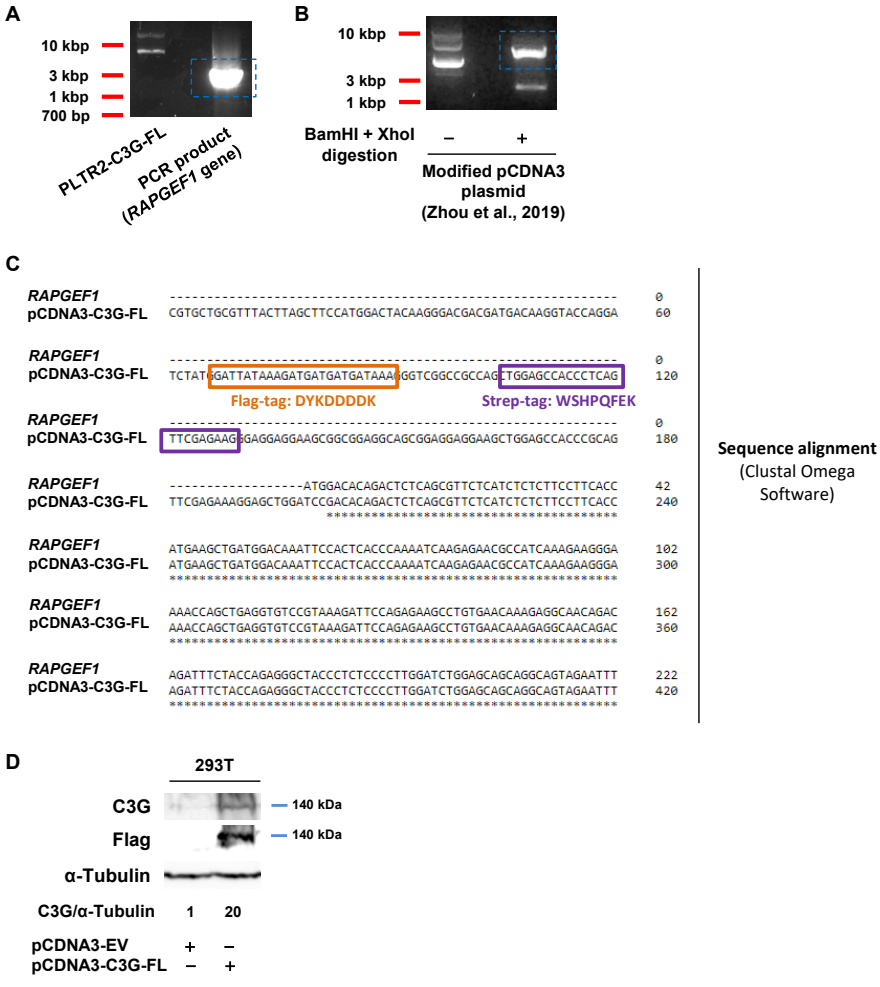

(***A***) Amplification of *RAPGEF1* sequence (around 3kb, marked in the figure by a blue square) from PLTR2-C3G-FL plasmid by PCR using specific primers. (***B***) Digestion of modified pCDNA3 plasmid (generated by *Zhou et al., 2019*) with BamHI and XhoI, generating the fragment of interest (around 6kb, marked in the figure by a blue square). (***C***) Sequence alignment using *Clustal Omega Software* comparing *RAPGEF1* sequence and that inserted in pCDNA3-C3G-FL. Sequence from pCDNA3-C3G-FL plasmid was determined by Sanger sequencing. Flag-tag (orange) and Strep-tag (purple) included in pCDNA3 are also indicated. (***D***) Western blot analysis of C3G and Flag, normalized to α-Tubulin, in 293T cells transfected with pCDNA3-EV or pCDNA3-C3G-FL (around 140 kDa) constructs. Densitometric quantification of C3G/α-Tubulin ratio is expressed as the fold increase of cells transfected with pCDNA3-EV plasmid.

APPENDIX 4 – Overexpression of a C3G mutant lacking CDC25H domain (C3G-ΔCat): Generation of pCDNA3-C3G-ΔCat construct and overexpression in 293T cells

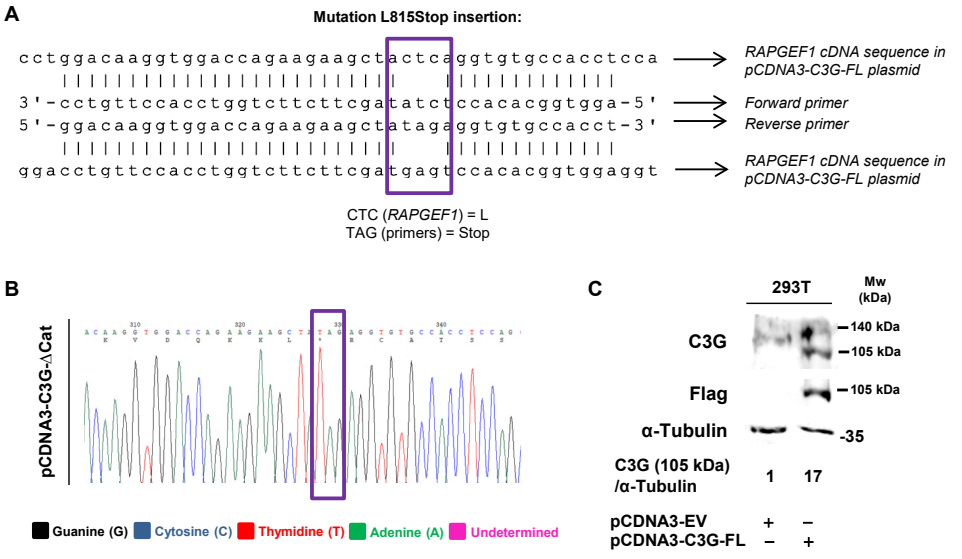

(***A***) Site-directed mutagenesis scheme generated by Quickchange Agilent software. This shows the original sequence present in pCDNA-C3G-FL plasmid and the specific primers designed to insert L815Stop mutation (purple square), in order to obtain pCDNA3-ΔCat plasmid to overexpress a C3G mutant lacking CDC25H domain (ΔCat). (***B***) Sanger sequencing demonstrating the mutation incorporation (purple square). (***C***) Western blot analysis of C3G and Flag, normalized to α-Tubulin, in 293T cells transfected with pCDNA3-EV or pCDNA3-C3G-ΔCat (around 105 kDa) constructs. Endogenous C3G (140 kDa) is also detected. Densitometric quantification of C3G/α-Tubulin ratio is expressed as the fold increase of cells transfected with pCDNA3-EV plasmid.

APPENDIX 5 – Restriction maps of pCDNA3-FFSS plasmids: pCDNA3-EV, pCDNA3-C3G-FL and pCDNA3-C3G-ΔCat

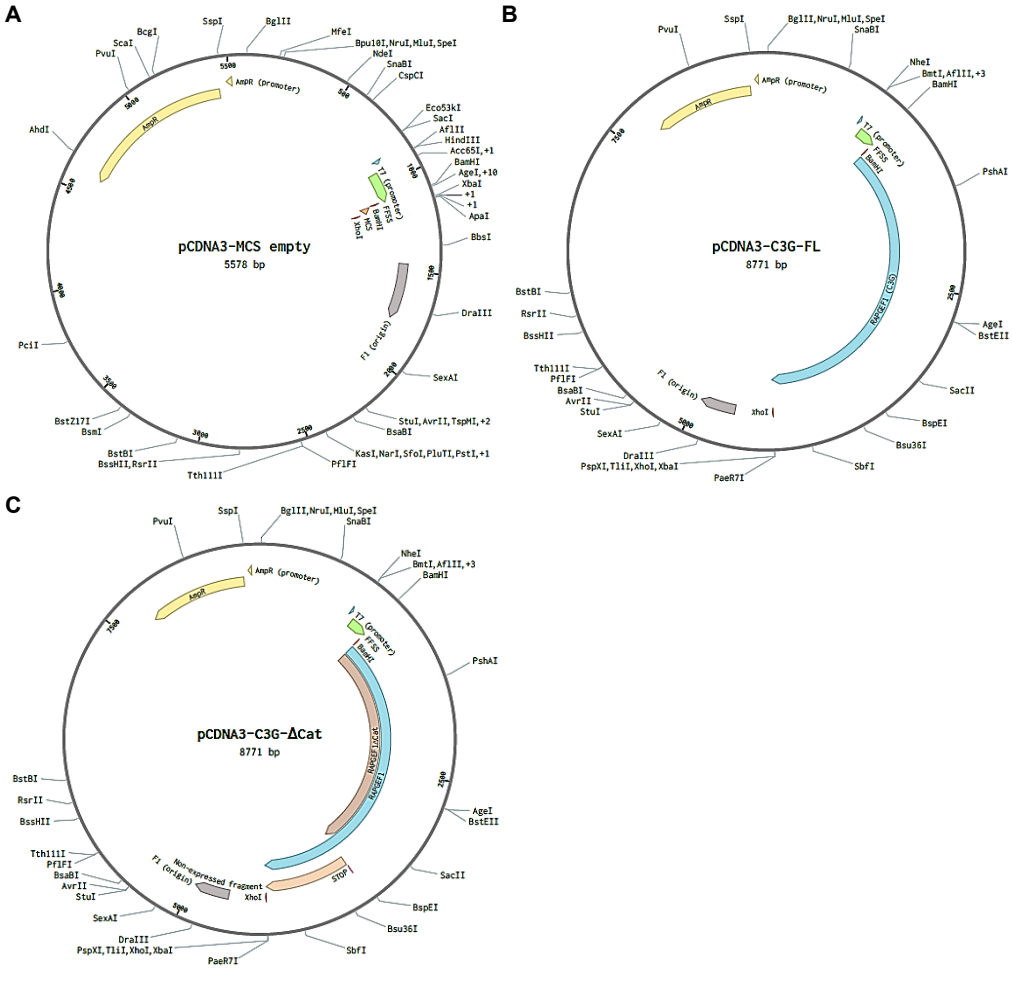

(*A-C*) Restriction maps of pCDNA-EV (also named pCDNA-MCS empty) (*A*), pCDNA3-C3G-FL (*B*) and pCDNA3-C3G-ΔCat (*C*) plasmids, indicating the most relevant sites for restriction enzymes, F1 origin of replication (purple), elements for Ampicillin resistance in bacteria (*AmpR*) (promoter and gene), T7 promoter and flag-flag-strep-strep (*FFSS*) tag sequence (green). BamHI and XhoI sites are highlighted (red) because they are essential for the cloning protocol designed. In *B* and *C*, inserted *RAPGEF1* cDNA sequence is also indicated. Additionally, in *C*, L815Stop mutation (*STOP*) and the non-expressed fragment are shown (orange). *MCS*: *Multi-cloning site.*

APPENDIX 6 – Phosphorylation of RTKs using a proteome profiler human phospho-RTK array

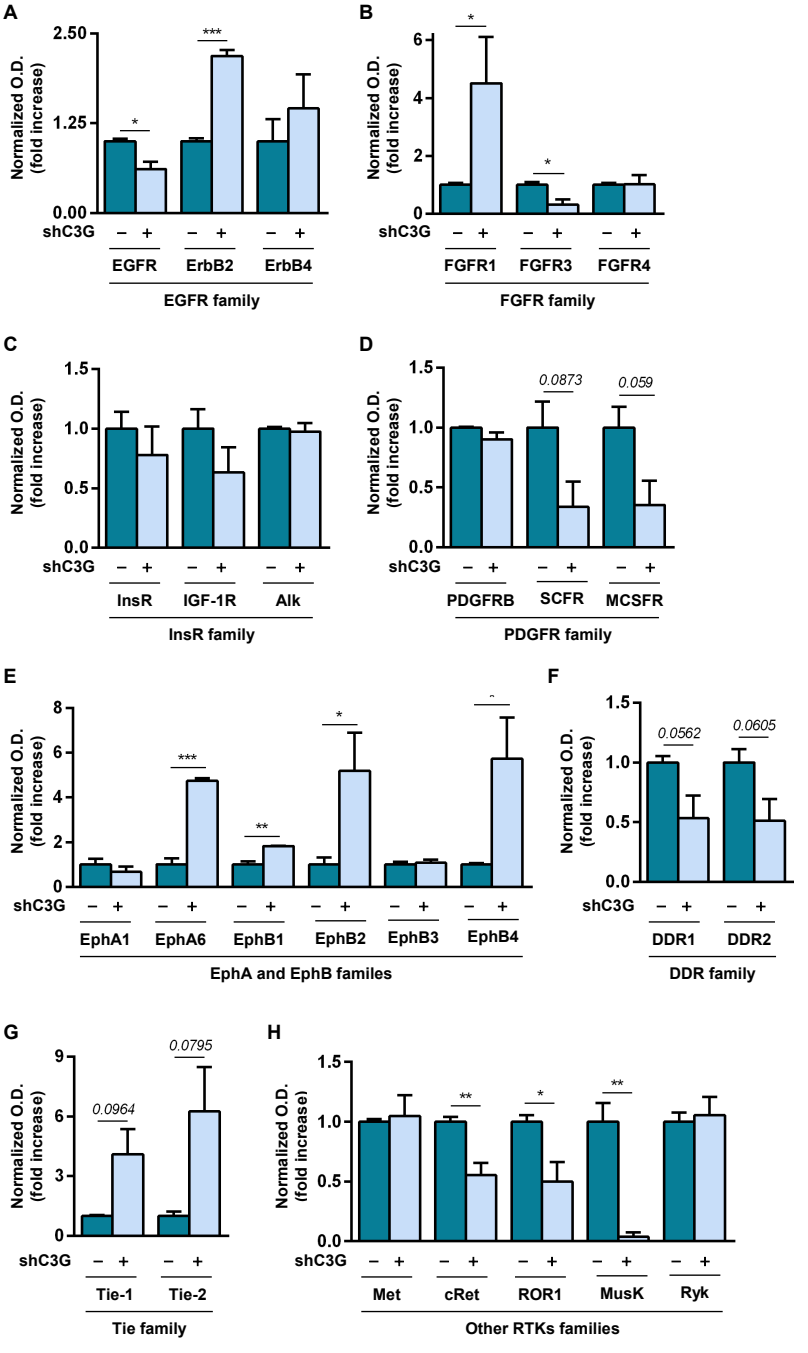

(***A-H***) Densitometric quantification of P-*RTK* referred to the positive control from the array is expressed as the fold increase of parental cells. Data are divided into RTK families: EGFR (*A*), FGFR (*B*), Insulin Receptor (*InsR*) (*C*), PDGFR (*D*), EphA/B (*E*), DDR (*F*), Tie (*G*) and others (*H*). **p* value <0.05, ***p* value <0.01, ****p* value <0.001, as indicated. Additionally, p values < 0.1 are also shown. *O.D.: Optic density*.

APPENDIX 7 – Summary of ELDAs statistics, indicating the statistical significance by comparison (chiq or χ^2 and p value) between the analysed groups and figure references to which they correspond

Figure	Group 1	Group 2	χ^2	DF	*p* value
39A	U87 (p+1)	U87shC3G (p+1)	0.0103	1	0.92 (*ns*)
39B	U87 (p+3)	U87shC3G (p+3)	25.4	1	4.68×10^{-7} (***)
39C	U87 (p+6)	U87shC3G (p+6)	23.6	1	1.16×10^{-6} (***)
40A	U87 (p+1)	U87 (p+6)	5.38	1	0.0204 (*)
40B	U87shC3G (p+1)	U87shC3G (p+6)	9.85	1	0.0017 (**)

DF: Degree of Freedom

**p* value <0.05, ***p* value <0.01, ****p* value <0.001

ns: not significant (*p* value >0.05)

APPENDIX 8A – Results from proteome-wide analysis: proteins over-represented in parental U87 cells compared to U87shC3G cells

ID (gene)	Protein name	Score	Matches (peptides)	Fold change(*)	*p* value
ACTB	Actin, cytoplasmic 1	228	24	1.3	**
ACTB	Actin, cytoplasmic 1	177	15	1.2	**
ACTA	Actin, aortic smooth muscle	175	14	1.3	**
POTEE	POTE ankyrin domain family member E	109	9	1.3	**
AHSA1	Activator of 90 kDa heat shock protein ATPase homolog 1	100	6	1.2	**
POTEE	POTE ankyrin domain family member E	89	6	1.2	**
RSSA	40S ribosomal protein SA	89	6	1.2	**
ACTBL	Beta-actin-like protein 2	79	6	1.3	**
CATD	Cathepsin D	79	6	1.3	**
IF4H	Eukaryotic translation initiation factor 4H	62	3	1.5	*
ACTBL	Beta-actin-like protein 2	51	8	1.2	**
TADBP	TAR DNA-binding protein 43	46	1	1.3	**
PGK1	Phosphoglycerate kinase 1	44	3	1.3	**
TBCA	Tubulin-specific chaperone A	43	3	1.3	**
COTL1	Coactosin-like protein	41	1	1.3	**
EFTU	Elongation factor Tu, mitochondrial	41	2	1.3	**
EIF3G	Eukaryotic translation initiation factor 3 subunit G	41	3	1.3	**
NFH	Neurofilament heavy polypeptide	38	3	1.5	*
ASAP2	Arf-GAP with SH3 domain, ANK repeat and PH domain-containing protein 2	37	1	1.3	**
GLP2R	Glucagon-like peptide 2 receptor	37	3	1.2	**
ENOA	Alpha-enolase	36	2	1.3	**
MED16	Mediator of RNA polymerase II transcription subunit 16	36	1	1.3	**

CXCL5	C-X-C motif chemokine 5	35	1	1.5	*
CENPF	Centromere protein F	34	1	1.3	**
PEX1	Peroxisome biogenesis factor 1	31	3	1.5	*
BD1L1	Biorientation of chromosomes in cell division protein 1-like 1	29	3	1.5	*
BD1L1	Biorientation of chromosomes in cell division protein 1-like 1	28	3	1.2	**
CATD	Cathepsin D OS=Homo sapiens	28	2	1.2	**
O2T35	Olfactory receptor 2T35	28	2	1.3	**
4ET	Eukaryotic translation initiation factor 4E transporter	27	1	1.5	*
AL4A1	Delta-1-pyrroline-5-carboxylate dehydrogenase, mitochondrial	27	1	1.5	*
HCD2	3-hydroxyacyl-CoA dehydrogenase type-2	26	4	1.5	*
SI1L3	Signal-induced proliferation-associated 1-like protein 3	26	1	1.5	*
SOX5	Transcription factor SOX-5	26	1	1.5	*
AT1A4	Sodium/potassium-transporting ATPase subunit alpha-4	22	2	1.2	**
PTPRQ	Phosphatidylinositol phosphatase PTPRQ	20	1	1.2	**
RHBT3	Rho-related BTB domain-containing protein 3	20	1	1.3	**
MIER1	Mesoderm induction early response protein 1	17	1	1.5	*
OCTC	Peroxisomal carnitine O-octanoyltransferase	16	1	1.2	**
RBM46	Probable RNA-binding protein 46	16	1	1.2	**
YD286	Glutaredoxin-like protein C5orf63	16	1	1.2	**
AGRF5	Adhesion G protein-coupled receptor F5	14	1	1.2	**
LC7L2	Putative RNA-binding protein Luc7-like 2	14	1	1.2	**
LIPB1	Liprin-beta-1	14	1	1.2	**
SDHF2	Succinate dehydrogenase assembly factor 2, mitochondrial	14	1	1.2	**
VATD	V-type proton ATPase subunit D	14	1	1.2	**

*(*) **Fold change:** levels detected in parental U87 cells vs. levels in U87shC3G.*

APPENDIX 8B – Results from proteome-wide analysis: proteins over-represented in U87shC3G cells compared to parental U87 cells

ID (gene)	Protein name	Score	Matches (peptides)	Fold change(*)	*p* value
LMNA	Prelamin-A/C	213	22	1.4	*
PCBP1	Poly(rC)-binding protein 1	192	14	1.3	*
STIP1	Stress-induced-phosphoprotein 1	171	19	1.4	*
ALDOA	Fructose-bisphosphate aldolase A	147	9	1.3	*
CAPG	Macrophage-capping protein	132	7	1.4	*
TPIS	Triosephosphate isomerase	126	7	1.2	**
ACTB	Actin, cytoplasmic 1	125	7	1.3	*
PGK1	Phosphoglycerate kinase 1	110	20	1.3	*
POTEE	POTE ankyrin domain family member E	83	4	1.3	*
POTEI	POTE ankyrin domain family member I	74	3	1.3	*
ALDOA	Fructose-bisphosphate aldolase A	64	3	1.4	*
GALK1	Galactokinase	54	1	1.4	*
PRS10	26S protease regulatory subunit 10B	46	4	1.3	*
AIFM1	Apoptosis-inducing factor 1, mitochondrial	43	2	1.4	*
ASAP2	Arf-GAP with SH3 domain, ANK repeat and PH domain-containing protein 2	42	2	2.1	**
HNRDL	Heterogeneous nuclear ribonucleoprotein D-like	42	2	1.4	*
HNRPD	Heterogeneous nuclear ribonucleoprotein D0	42	2	1.4	*
CC181	Coiled-coil domain-containing protein 181	41	1	1.3	*
CTCFL	Transcriptional repressor CTCFL	41	1	1.3	*
ENOA	Alpha-enolase	41	1	1.3	*

ISK5	Serine protease inhibitor Kazal-type 5	41	1	1.3	*
PERI	Peripherin	41	1	1.3	*
KPYM	Pyruvate kinase PKM	40	3	1.4	*
HSPB1	Heat shock protein beta-1	37	3	1.2	**
SNED1	Sushi, nidogen and EGF-like domain-containing protein 1	37	1	2.1	**
ANKY2	Ankyrin repeat and MYND domain-containing protein 2	36	2	1.4	*
MAK16	Protein MAK16 homolog	36	2	1.4	*
AIFM1	Apoptosis-inducing factor 1, mitochondrial	35	1	1.3	*
ALDOA	Fructose-bisphosphate aldolase A	35	2	1.3	*
FMN1	Formin-1	35	1	1.3	*
MA7D3	MAP7 domain-containing protein 3	34	2	1.3	*
ACTBL	Beta-actin-like protein 2 OS=Homo sapiens GN=ACTBL2 PE=1 SV=2	33	3	1.3	*
QRIC2	Glutamine-rich protein 2	33	1	2.1	**
ERI1	3'-5' exoribonuclease 1	31	1	1.4	*
CCDC6	Coiled-coil domain-containing protein 6	30	1	1.4	*
PSD13	26S proteasome non-ATPase regulatory subunit 13	30	1	1.4	*
QCR2	Cytochrome b-c1 complex subunit 2, mitochondrial	30	2	1.3	*
CRK	Adapter molecule crk	29	1	2.1	**
PPR36	Protein phosphatase 1 regulatory subunit 36	29	1	2.1	**
RGSL	Regulator of G-protein signalling protein-like	29	1	1.3	*
RGSL	Regulator of G-protein signalling protein-like	29	1	1.4	*
TERA	Transitional endoplasmic reticulum ATPase	29	1	1.4	*
ALDOC	Fructose-bisphosphate aldolase C	28	2	1.3	*
APOP1	Apoptogenic protein 1, mitochondrial	28	1	1.3	*
ENOA	Alpha-enolase	28	3	1.3	*
RAD50	DNA repair protein RAD50	28	2	1.3	*
FANCB	Fanconi anemia group B protein	27	1	1.3	*

SPIN3	Spindlin-3	27	1	1.3	*
DOCK6	Dedicator of cytokinesis protein 6	24	1	1.2	**
ARI4B	AT-rich interactive domain-containing protein 4B	23	5	1.3	*
DDX53	Probable ATP-dependent RNA helicase DDX53	23	1	1.3	*
FACR1	Fatty acyl-CoA reductase 1	23	1	1.3	*
GSTP1	Glutathione S-transferase P	23	1	2.1	**
NSF	Vesicle-fusing ATPase	23	1	1.3	*
PLXC1	Plexin-C1	23	1	1.3	*
RFIP3	Rab11 family-interacting protein 3	23	2	1.2	**
RFIP3	Rab11 family-interacting protein 3	23	1	1.3	*
RFIP3	Rab11 family-interacting protein 3	21	3	2.1	**
RIOK3	Serine/threonine-protein kinase RIO3	21	1	1.2	**
AT1A4	Sodium/potassium-transporting ATPase subunit alpha-4	20	2	1.4	*
CTRO	Citron Rho-interacting kinase	20	2	1.3	*
ERO1A	ERO1-like protein alpha	20	1	1.3	*
KCC4	Calcium/calmodulin-dependent protein kinase type IV	20	1	2.1	**
Z518B	Zinc finger protein 518B	20	2	2.1	**
B3GA2	Galactosylgalactosylxylosyl protein 3-beta-glucuronosyltransferase 2	19	1	2.1	**
DEN1C	DENN domain-containing protein 1C	19	1	1.3	*
CO6A3	Collagen alpha-3(VI) chain	18	2	1.4	*
JCAD	Junctional protein associated with coronary artery disease	17	1	1.2	**
C102A	Coiled-coil domain-containing protein 102A O	16	1	1.2	**
MINT	Msx2-interacting protein	16	3	1.4	*

(*) Fold change: *levels detected in U87shC3G cells vs. levels in parental U87 cells.*